SCHOOL OF BIOLOGICAL SCIENCES

SUMOylation Regulates Focal Adhesion Dynamics in Cancer Cell Migration

THESIS SUBMITTED TO THE SCHOOL OF BIOLOGICAL SCIENCES AT THE UNIVERSITY OF READING FOR THE DEGREE OF DOCTOR OF PHILOSOPHY

By

Salem Hussain Alharethi

Supervisor: Professor Phil Dash

Ph.D. Thesis

19/12/2019

Declaration

I confirm that this is my own work and the use of all materials from other sources has been properly and fully acknowledged.

Signature: ……

Date: ……

Acknowledgment

When I accepted the job offer from Najran University in 2009, I have not seriously thought that I would be spending the next ten years studying in different places in another language. Today after completing writing my Ph.D. thesis, I believe it was a great journey that expand my knowledge and experience despite the circumstances surrounding me. This achievement would not have been completed without the help and support I received throughout my career.

Firstly, I would like to express my sincere gratitude to my supervisor Prof. Phil Dash for the continuous support during my Ph.D. study and related research, for his patience, motivation and kindness. His guidance helped me in all the time of research and writing of this thesis. I could not have imagined having a better advisor and mentor for my study. Beside my supervisor, I would like to thank my thesis committee: Prof. Jon Gibbins and Dr. Michael Fry, for their insightful comments and support during my study. I would like to thank my lab meeting members and colleagues for the valuable discussion and all the fun we had in the last four years. I also thank my colleagues from different labs for useful advice and to the laboratory staff for their help.

I thank my family: my parents for believing in me and to my brothers and sisters for supporting me spiritually during my study as always. Special thanks to my wife, and to my sons: Hussain and Naif for being beside me through these difficult years. I would not have finished this project without their love, great support and understanding. No more homesick, it is time to go back home. I also thank my friends for their support and encouragement during my writing.

Last but not least, I would like to express my gratitude to Najran University for their financial sponsorship. A special thanks to Reading University for providing me with the opportunity to complete my Ph.D., for the great campus, state of the art technology and friendly staff.

Abstract

Cell migration is a key cellular function involved in normal conditions such as embryonic development and immune cell travelling and in diseases such as in cancer metastasis. Cell migration is a tightly regulated process that requires the coordinated activity of different cellular structures including cytoskeletal networks and focal adhesions. Focal adhesions connect cells to the extracellular environments and are critical in cell migration by transmitting the force generated by cytoskeletal networks to the extracellular matrix allowing cells to move through these matrices. During cell migration, existing focal adhesions are disassembled, and new focal adhesions are formed at new sites allowing cells to detach from the matrix and continue migration. SUMOylation has been recently suggested to be involved in the regulation of these adhesion structures. However, previous studies lack the evidence of a direct role of SUMOylation at focal adhesion sites.

The aims of this project are to investigate the role of SUMOylation in the regulation of focal adhesions and cancer cell migration. Treating MDA-MB-231 breast cancer cells with SUMOylation inhibitors significantly reduced their migration. These inhibitors also increased the size and turnover time of focal adhesions suggesting that SUMOylation is likely to facilitate cancer cell migration by enhancing focal adhesion turnover. In addition, bioinformatic analysis predicted the presence of SUMOylation consensus and SUMOylation interacting motifs in various focal adhesion proteins indicating a possible role of this post-translation modification in the regulation of focal adhesions. SUMO specific proteases (SENPs) are critical in cancer metastasis by deSUMOylating associated proteins. Here, SENP2 was found to interact with major FA proteins including talin, vinculin, FAK and paxillin. This interaction could indicate a possible role of this protease in the regulation of SUMOylation levels of focal adhesion proteins. Knocking down SENP2 significantly reduced MDA-MB-231 cancer cell migration. It also increased the size and turnover time of focal adhesions suggesting that the reduction in cell migration of these cells was caused by impairment in FA dynamics.

In order to investigate the direct role of SUMOylation in the regulation of focal adhesion dynamics, one of the main aims of this project is to investigate the effects of preventing SUMOylation of vinculin on Focal dynamics and cancer cell migration. This was achieved by replacing lysine residues with arginine in highly scored SUMOylation motifs in vinculin using mutagenesis. This way of investigation provides the opportunity to investigate the consequences of preventing SUMOylation of specific targets without influencing global SUMOylation that may affect many important cellular mechanisms. Replacing lysine at position 80 in the amino acid sequence in vinculin reduced its interaction with SUMO2 indicating that this site is a major SUMOylation acceptor site in vinculin. Expressing the K80R mutated vinculin in different cancer cells caused a significant increase in focal adhesion size and turnover time and significantly reduced their migration speed. As one of the main

functions of SUMOylation is mediating protein-protein interaction, the last aim of this project is to investigate the consequences of K80R mutation on talin-vinculin interaction. Talin is one of the early recruited focal adhesion proteins and its interaction with vinculin enhances the stability of focal adhesions. Photobleaching FRET assay revealed that the K80R mutation enhances talin-vinculin interaction. This finding indicates that SUMO2 attachment to vinculin at K80 disassociates talin-vinculin interaction and mutating this site to prevent SUMO2 attachment allowed their interaction to last longer.

Taken together, the finding in this project provides novel evidence that indicate a direct role of SUMOylation in the regulation of focal adhesion dynamics and consequently cell migration. It clearly suggests that SUMOylation regulates the disassembly of focal adhesions by SUMO2 conjugation to vinculin at K80 to disassociate its interaction with talin. The disassociation of talin-vinculin interaction induces the disassembly of existing focal adhesions, a critical requirement during cell migration. The prediction of several potential SUMO substrates in focal adhesions indicates a wider role of SUMOylation in the regulation of different functions of focal adhesions. Small molecule inhibitors against specific SUMO substrates could be promising therapeutic strategy for the development of anticancer drugs for cancer intervention.

Table of Abbreviations

2-D08	2’,3’,4’-trihydroxyflavone
ADP	Adenosine diphosphate
Akt	Serine/threonine-specific protein kinase
ANOVA	Analysis of variance
Arp2/3 complex	Actin-related protein-2/3
ATP	Adenosine triphosphate
BSA	Bovine serum albumin
BRCA1	Breast cancer type 1 susceptibility protein
Cdc42	Cell division control protein 42 homolog
Co-IP	Co-immunoprecipitation
D2S	Distance to start
DMEM	Dulbecco’s Modified Eagle’s Medium
DMSO	Dimethyl Sulphoxide
DNA	Deoxyribonucleic acid
ECL	Enhanced chemiluminescence
ECM	Extracellular matrix
EDTA	Ethylenediaminetetraacetic acid
EGFR	Epidermal growth factor receptor
EMT	Epithelial-to-mesenchymal transitions
ERK1/ERK2	Extracellular signal-regulated kinase 1/2
FAK	Focal adhesion kinase
FAs	Focal adhesions
F-actin	Actin filaments, microfilaments
FBS	Feotal bovine serum
GBD	GTPase-binding domain
GEFs	Guanine nucleotide exchange factors
GFP	Green fluorescence protein
Gka	Ginkgolic acid
GPS-SUMO	Group-based prediction system algorithm SUMO
Gossypetin	3-B08, Goss 3,5,7,8,3’,4’-hexahydroxyflavone
HA-tag	Hemagglutinin tag
HEK293	Human Embryonic Kidney cells
HRP	Horseradish Peroxidase
HDAC	Histone deacetylase
HGF	Hepatocyte growth factor
IHC	Immunocytochemistry
LB medium	Luria-Bertani medium
MAPK	Mitogen-activated protein kinase
MEF2A	Myocyte-specific enhancer factor 2A
MTs	Microtubules
NEM	N-Ethylmaleimide
PAGE	Polyacrylamide gel electrophoresis
PBS	Phosphate Buffered Saline
PDK1	3-phosphoinositide-dependent protein kinase-1

PI3K	Phosphatidylinositol 3-kinase
PIC	Protease Inhibitors Cocktail
PIP3	Phosphatidylinositol 3,4,5-triphosphate
PKC	Protein kinase C
p130Cas	p130 CRK-associated substrate
PVDF	Polyvinylidene difluoride membrane
Penstrep	Penicillin/Streptomycin
PFA	Paraformaldehyde
PIAS1	Protein inhibitor of activated STAT1
PDSM	Phosphorylation dependent SUMOylation motif, ψKxExxSP
PIP2	Phosphatidylinositol-4,5-bisphosphate
PIP3	Phosphatidylinositol (3,4,5)-trisphosphate
PTMs	Post-translational modifications
RanGAP1	RanGTPase-activating protein
RIPA buffer	Radioimmunoprecipitation assay buffer
SAE1/2	SUMO-activating enzyme subunit ½ (E1)
SDS	Sodium dodecyl sulphate
SEM	Standard error of the mean
Ser/Thr	serine/threonine
SIM	SUMO-interaction motif
Smt3	Suppressor of Mif2
siRNA	small interfering RNA
Src	Proto-oncogene tyrosine-protein kinase
SUMO	small ubiquitin-related modifier
TBS	Tris buffer saline
TBST	Tris Buffer Saline Tween
TEA	Triethanolamine
TEMED	Tetramethylenediamine
TGFβ	Transforming growth factor beta
TGFβR	Transforming Growth Factor Beta Receptor
TRF1/TRF2	Telomeric repeat-binding factor 1 or 2
TNF	Tumour necrosis factor receptors
Tyr	Tyrosine
Ubc9	SUMO-conjugating enzyme (E2)
VASP	Vasodilator-stimulated phosphoprotein
WB	Western blot
WHO	World health organisation
MMP	Matrix Metalloproteases
PML	Promyelocytic leukaemia

Table of Contents

List of Figures

Chapter 1

Chapter 2

Chapter 3

Chapter 4

Chapter 5

List of Tables

1. Introduction

1.1 Introduction

1.1.1 Cancer Metastasis

Cancer is the second leading cause of human mortality, and according to the world health organisation (WHO), 17.03 million new cancer cases (20.78% increase compared 2012) were reported, and 9.6 million cancer-related deaths (17% increase) occurred in 2018 (Ferlay et al., 2015; Bray et al., 2018). In this latest report, lung cancer has the highest occurrence (2.09 million cases, 12.3% of all cancer new cases) followed by breast cancer (2.08 million new cases, 12.3% off all cancer new cases). Colorectal and prostate cancers represent 10.9% and 7.5% of new cancer cases, respectively. Furthermore, according to WHO, 18.6% (1.76 million) of cancer associated deaths occurring in 2018 were caused by lung cancer. Colorectal and breast cancers represent 9.3% and 6.6% of cancer deaths respectively (WHO, 2018). Taken together, these reports indicate the major impact of cancer on human health and economy and the requirement to identify potential therapeutic targets for cancer intervention.

There are more than 100 types of cancer; it is a complex disease with cancers varying even within the same organ. Thus, researchers have tried to identify the common features shared by these different cancer types to gain a better understanding of its mechanisms. Six features have been suggested by Hanahan and Weinberg (2000) as essential for the survival and proliferation of all cancer types (Figure 1.1). Cancer cell proliferation is one of these hallmarks and is characterised by the uncontrolled proliferation of cancer cells. They

stimulate their proliferation by producing growth factor ligands that promote proliferation or by sending signals to tumour microenvironment to produce growth factor signals (Cheng et al., 2008). Alternatively, they could also sustain proliferation by altering structures of growth factor ligand receptors to activate them without the requirement of growth factor signalling ligands. The second feature common to all different cancer types is their ability to circumvent growth suppressers. There are many growth suppressors that regulate the fate of cells including RB protein, which integrates extracellular signals, and p53 protein that integrate intracellular stress and abnormality signals. Both proteins functions like gatekeepers that control cell proliferation and induce apoptosis upon damage and abnormality (Burkhart and Sage, 2008). Cancer cells circumvent these antiproliferation processes by inactivating these proteins through mutations or changes in their signalling pathways. The tumour suppressor p53 is reported to be inactivated in different cancer types by mutations (Feki and Irminger-Finger, 2004) or by interacting with oncoproteins that attenuate its functions (Manfredi, 2010). In addition, TGF-β is a known cell proliferation suppressor and cancer cells were reported to alter its function from antiproliferation effects to enhancing the activation of epithelial-to-mesenchymal transition (EMT) that promote tumour malignancy. Another hallmark of cancer cells is their ability to evade cell death, which is a natural barrier to tumorigenesis (Lowe et al., 2004). Apoptosis is triggered by external or internal signals that activate the proapoptotic proteins such as Bax and Bak, which are located in the outer membrane of the mitochondria. Upon their activation, these proteins induce the release more proapoptotic such as proteins cytochrome c, which in turn activate proteolytic activity of caspases leading to the disassembly of cells and consumption by its neighbouring cells or phagocytes. Cancer cells resist cell death by overexpressing

antiapoptotic proteins such as Bcl-2 that binds to the proapoptotic proteins Bax and Bak and supress their functions (Adams and Cory, 2007). Limitless replicative potential is another common feature of cancer cells. It is mediated by maintaining the length of telomeres which are located at the end of every chromosome. Normally, telomeres are shortened after each cell cycle until they reach a length at which they could protect the 3' end of chromosomes and thus stop replicating. Cancer cells sustain limitless replication by maintaining the telomere length by upregulating the telomerase enzyme (Blasco, 2005). Sustained angiogenesis is another feature of cancer cells as it is important to supply them with oxygen and nutrients, which is supported by the ability to induce the formation of new blood vessels in tumours to maintain their supply with oxygen and nutrients and evacuate metabolic waste and carbon dioxide (Baeriswyl and Christofori, 2009). In 2011, four more hallmarks common to all cancer types were suggested by Hanahan and Weinberg including avoiding immune system, genomic instability, tumour promoting and inflammation and deregulation of cellular energies (Hanahan and Weinberg, 2011).

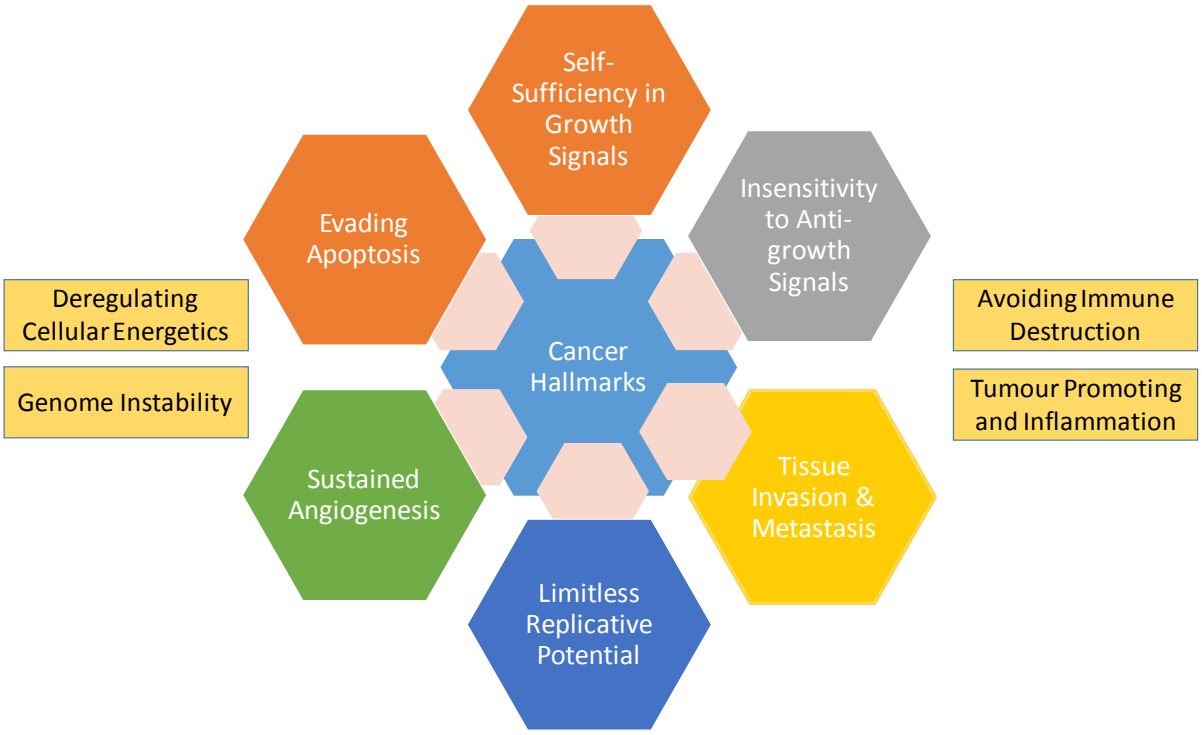

Figure 1.1 Cancer hallmarks. The six hallmarks of cancer cells that facilitate their survival and proliferation are in hexagon boxes (Hanahan and Weinberg, 2000). New emerged cancer hallmarks suggested by Hanahan and Weinberg in 2011 are in square boxes. This diagram was adapted from (Hanahan and Weinberg, 2011).

Metastasis is one of the main hallmarks of cancer cells and is the main cause of cancer mortality as well as the main challenge in cancer treatment (Steeg, 2016). Metastasis is a multistep process that requires the activity of multiple cellular functions (Figure 1.2) (Gupta and Massagué, 2006). The initial step of metastasis is the local invasion of tumour into surrounding tissue and this step requires changes in cytoskeleton and extracellular matrix (ECM) dynamics and loss of adhesion (Friedl and Alexander, 2011). Following that cancer cells detach from the original tumour site and enzymatically degrade the surrounding tissue and the ECM before reaching the blood/lymph vessels, where they then penetrate (intravasate) and circulate, spreading to potential metastatic sites. When these migrating cancer cells arrive at their preferred sites, they adhere to the endothelial cells of the blood

vessel and extravasate to these sites, where they proliferate and form colonies (Gómez-Cuadrado et al., 2017). Matrix metalloproteases (MMPs) are essential in metastasis as they degrade the ECM to facilitate blood vessel intravasation. Researchers have developed small molecular compounds to inhibit the function of these proteases but failed clinically as tumour cells evade MMPs inhibition by travelling through the ECM via protease-independent mechanisms (Wolf et al., 2003, Wyckoff et al., 2006). Therefore, understanding the different molecular pathways involved in metastasis will potentially identify promising cancer therapeutic targets.

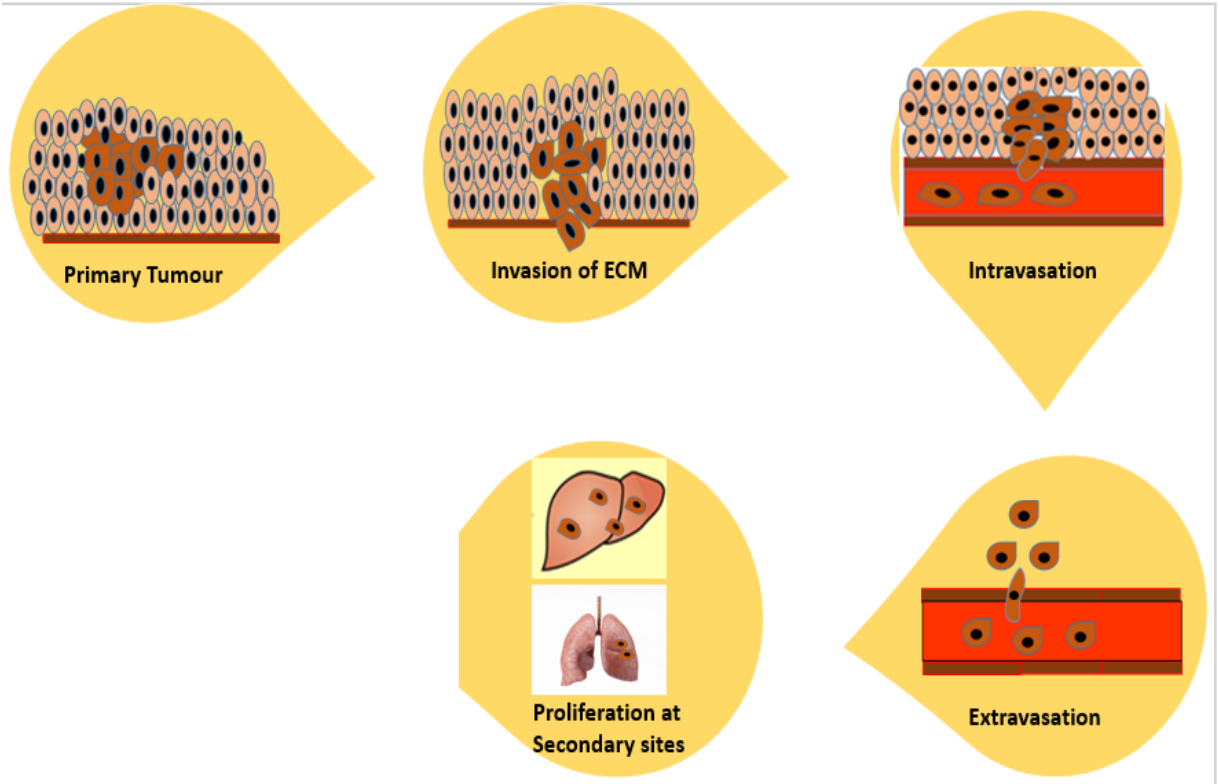

Figure 1.2 Different processes involved in cancer metastasis. Tumour cells de-attach from the primary tissue and invade surrounding tissue. After intravasation to lymph/blood vessels, they circulate through these systems until they reach secondary sites, where they extravasate from these vessels and proliferate in these new sites. This diagram was adapted from (Fidler, 2003).

1.1.2 Cell Migration

Cell migration processes facilitate cellular movement within the same tissue or between various organs, which is essential in many cellular processes, including embryonic development, immune cell trafficking and tissue repair (Keller, 2005, Friedl and Weigelin, 2008). However, cell migration is also involved in serious human illnesses such as cancer, in which cancer cells detach from the original tumour site and migrate to different locations within the body, thus initiating secondary tumours.

Cells use three different migratory strategies: proteolytic migration, a slow migration characterised by proteases breaking down the ECM (Sabeh et al., 2004); non-proteolytic integrin-dependent migration (Wolf et al., 2003), which has intermediate speed; and non-proteolytic integrin-independent strategy, which has a higher speed than the aforementioned two (Lammermann et al., 2008). The migration strategy adapted by cells depends on extracellular and intracellular factors and is not entirely understood. When cells migrate, they are exposed to various environments with dissimilar biochemical properties and diverse ranges of topology (Wolf and Friedl, 2011). In addition, the intracellular biochemical properties of the migrating cell itself, such as protein expression and the activity of signalling pathways, also affects cell migration strategy. As cells vary in their biochemical properties, they can migrate differently even within the same ECM. For instance, the velocity of fibroblast cell movement on the collagen matrix is few microns per hour, whereas the velocity of dendritic and T cells on the same matrix is more than 10 microns per minute (Madsen and Sahai, 2010). Although cells differ in migratory behaviours and velocity properties, cell motility is derived from the force generated by the different structures of the actin cytoskeletal filaments (such as blebs, filopodia and lamellipodia) and

by actomyosin contraction. The force generated by the actomyosin contraction can change the shape of the migrating cells (Keren et al., 2008), which allows these cells to have directional polarity with a leading edge and cell rear.

Cell migration is divided into two main types: single and collective cell migration (Friedl et al., 2001, Friedl and Wolf, 2010). Single cell migration is subdivided into two main movement types with different features: amoeboid and mesenchymal. Amoeboid single cell movement is characterised by rounded cells moving without the involvement of cell adhesion to the ECM, and this type of movement is supported by the force generated by bleb propulsion (Fackler and Grosse, 2008, Charras and Paluch, 2008). This is referred to as blebby amoeboid movement and is seen in embryonic cells, leukocytes and cancer cells. Amoeboid migration is also supported by the formation of the actin-cytoskeletal filopodia with weak adhesion, which can be seen in dendritic cells, neutrophils and tumour cells (Smith et al., 2007, Gadea et al., 2008).

Unlike the amoeboid single cell migration, mesenchymal migration is strongly dependent on adhesion to substrates (Grinnell, 2003). This type of movement is seen in fibroblasts, sarcoma cells and highly de-differentiated tumour cells that undergo epithelial to mesenchymal transition (EMT) (Thiery, 2002), which is associated with increased malignancy and intensified invasive potential of tumours (Morel et al., 2008). Collective migration is characterised by the movement of a group of cells that are attached to each other (Vaughan and Trinkaus, 1966) and have leading cells that move invasively through the ECM and

following cells that follow in their tracks. This type of movement is seen in mammary glands and cancer cell invasion (Alexander et al., 2008, Hegerfeldt et al., 2002).

Cell migration requires the organised regulation of many cellular components including continuous formation and disassembly of cytoskeletal structures and focal adhesions, protease-dependent remodelling of the ECM, contraction of the cell body and retraction of the cell tail (Lauffenburger and Horwitz, 1996).

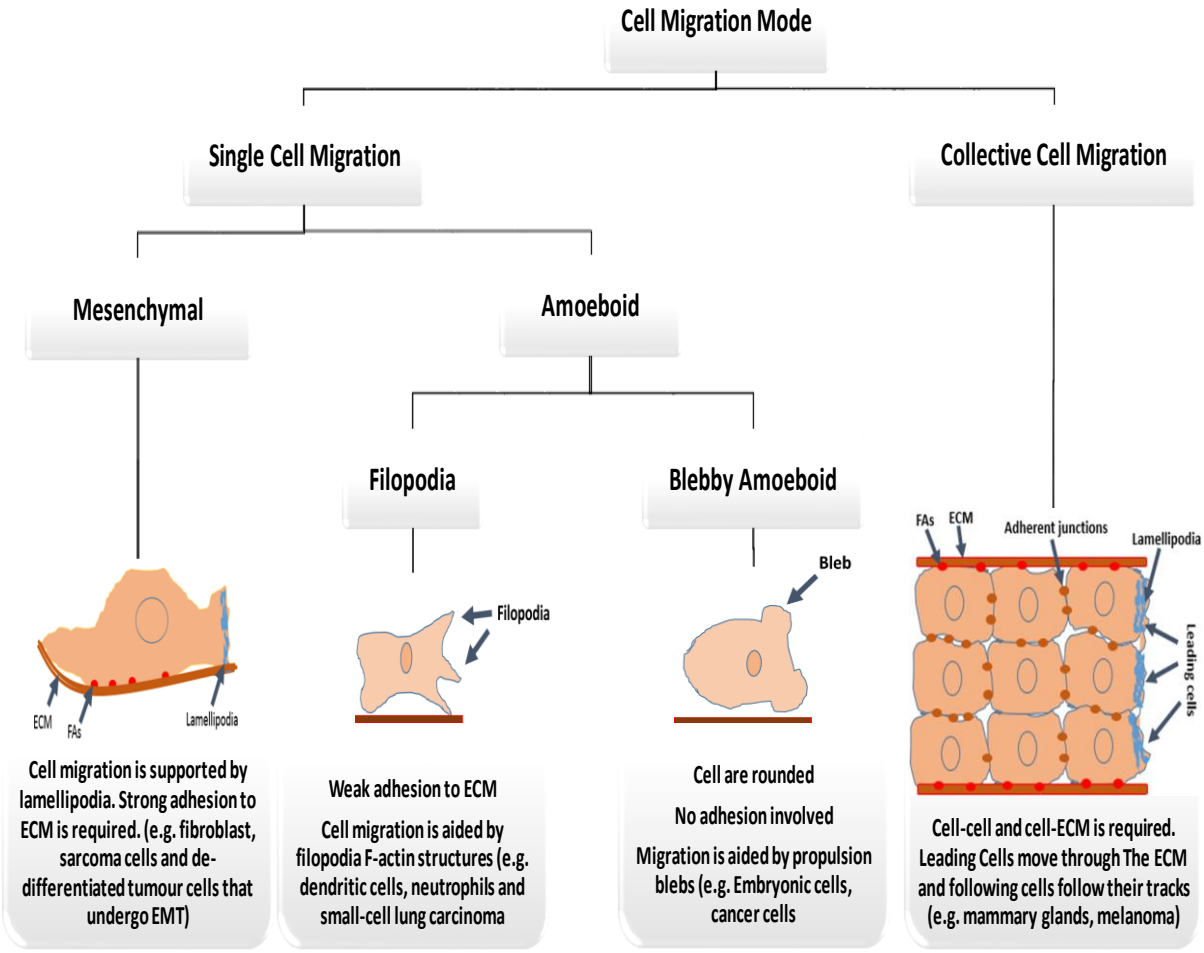

Figure 1.3 Diagram shows different cell migration types. Single cell movement is divided into two types. Mesenchymal, which requires strong adhesion to the ECM; and amoeboid cell migration, which includes blebby adhesion that does not require adhesion to the ECM, and Filopodia cell migration, which requires weak adhesion. Collective cell migration is the movement of groups of cells with leading cells that move invasively through the ECM and following cells that follow their tracks, adapted from (Schmidt and Friedl, 2009).

1.1.3 Cytoskeleton

The cytoskeleton networks are composed of various protein fibres and are critical in maintaining cell shape and structure, allowing cells to resist different types of force and in transportation of cellular components. There are three major components of the cytoskeleton network including actin filaments (also called microfilaments), intermediate filaments and microtubules, and these various cytoskeletal protein fibres have different roles in cells.

Actin filaments, the first type of these cytoskeletal structures, are composed of actin polymers that extend towards the plasma membrane to create tension that maintains cell shape and stability. These filaments are also one of the basic units alongside myosin, which are involved in muscle contraction and are essential requirements of other processes, including cell motility, transportation of cellular cargos within cells and cytokinesis in cell division (Stossel, 1993, Mitchison and Cramer, 1996, Soldati and Schliwa, 2006). Three main F-actin types are implicated in cell movement: filopodium, lamellipodium and contractile bundles. Filopodium filaments are unbranched F-actin and are mainly used in sensing the extracellular environment, such as the rigidity of the surrounding environments (Hoffmann and Schäfer, 2010). Lamellipodia filaments are branched F-actin found at the edges of migrating cells, and the formation of these filaments at their edges promotes cell migration by generating a force that pushes the membrane forward. Contractile bundles of F-actin and myosin are found at a cell's rear, and their contraction generates a contractile force that pushes cells forward.

Long chains of tubulin α and β proteins are organised into a hollow tube shape to form microtubules (MT), which are the largest cytoskeletal components (Valiron et al., 2001). The hollow shape of these filaments increases their force-resistance strength, which enables cells to resist compression forces. Microtubules play an important role in cell division as they facilitate chromosome separation by forming mitotic spindles and targeting these filaments has prevented cell division (Jaspersen and Winey, 2004). In addition to their role in maintaining cell shape, microtubules and F-actin are critical transportation systems within cells that enable cells, via motor proteins, to move different cargo along these filaments to their destinations (Conde and Caceres, 2009).

Unlike F-actin and microtubules, intermediate filaments are composed of various protein subunits; they are less dynamic and are not involved in cellular transportation. Instead, they contribute to maintaining cell shape by anchoring organelles, such as the nucleus, that do not move. These filaments also provide structural support for tissues as they connect by extending through cell junctions called desmosomes and join the intermediate filaments of adjacent cells. Thus, intermediate filaments are cell type-specific and are classified into four different groups depending on their protein subunits and their presence in different cell types (Eriksson et al., 2009). For example, the protein subunits of intermediate filaments found in epithelial cells are keratins (Fuchs, 1995); whereas the subunits of these filaments in connective tissue are vimentin and vimentin-related proteins (Franke et al., 1978). Laminin intermediate filaments are found in the nuclear envelope, giving it its rigidity, and neurofilaments are found in nerve cells (Eriksson et al., 2009).

1.1.4 Focal adhesions (FAs)

Many cellular functions including cell survival, morphology, migration and proliferation require the cell adhesion to the ECM via integrins (Gumbiner, 1996, Geiger and Yamada, 2011). Through adhesive structures, cells can sense variable microenvironments and signals can be sent towards the inside of cells to trigger the appropriate cellular response. Deregulation of adhesion to the ECM has been implicated in human diseases including cancer (Okegawa et al., 2004); therefore, understanding its mechanisms and effects on cellular behaviour will increase our understanding of its roles in these diseases and consequently increases the chances of improving their treatment. In recent years, many studies have investigated this field and have identified key factors implicated in adhesion to the ECM.

Integrins, heterodimers composed of α and β subunits, are the major transmembrane receptors that mediate adhesion to the components of the ECM (Martin et al., 2002, Takada et al., 2007). These transmembrane receptors contain two domains: a large extracellular domain that binds to the components of the ECM and a cytoplasmic tail that recruits multiple adaptor and signalling proteins to connect the ECM to the intracellular cytoskeleton filaments (Parsons et al., 2010). There are more than 18 α subunits and 8 β subunits that have been identified, and these form more than 24 types of integrins with different specificity to the various ECM components (van der Flier and Sonnenberg, 2001). Integrins are important in inside-out and outside-in signalling and they are activated by two different ways. For the inside-out activation, FA proteins that contain the FERM domain such as talin and kindlin bind to the intracellular domain of integrins leading to structural

changes in this receptor and these changes activate integrins and induce their attachment to extracellular ligands (Moser et al., 2009). For the outside-in activation, binding of the extracellular domain of integrin to extracellular ligands including collagen, laminin, vitronectin or fibronectin leads to the recruitment of various cytosolic proteins, forming structures called focal adhesions (Figure 1.4). These recruited proteins provide a linkage between the ECM and actin cytoskeleton (Liu et al., 2000) and are referred to collectively as the adhesome (Whittaker et al., 2006). Beside their role in the formation of FAs, integrins are critical in the development and maturation of FAs by transmitting the force generated by the ECM to FA proteins leading to alterations in their conformation revealing binding sites for various proteins. Therefore, additional adaptor and signalling proteins are recruited to FAs to strengthen the ECM-cytoskeleton linkage (Moore et al., 2010). This linkage to the ECM allows cells to generate and transduce tension and traction forces required for cells to modify their morphology and movement during migration. In addition to transmitting these forces, and after their recruitment to FAs, signalling proteins also transmit signals from the extracellular microenvironment to many essential cellular pathways involved in cell survival, proliferation and migration, and these signals control their functions (Mitra et al., 2005, Geiger and Yamada, 2011).

1.1.5 Formation of focal adhesions

There are more than 200 FA proteins with various cellular functions making FAs important signalling hubs for the regulation of diverse cellular mechanisms (Horton et al., 2015). Focal adhesions components and structure have been reported in the literature. Although they have many diverse proteins, FAs were found to be structurally organised and proteins were

found localised at different nanoscale layers of FAs. Focal adhesions were found to be organised into three different layers (Fig 1.4). The first layer is called integrin signalling layer (ISL) and is located within <20 nm of the plasma membrane and contains integrin, paxillin, FAK and talin head domain. On top of this layer is the force transduction layer (FTL), which is located within 20-40 nm of the plasma membrane and contains proteins that provide mechanical support for the ECM-actin linkage including talin and vinculin. The third layer is actin regulatory layer (ARL) that is located within 50-60 nm of the plasma membrane and contain proteins that regulate the dynamic of F-actin including vasodilator-stimulated phosphoprotein (VASP), zyxin and α-actinin (Kanchanawong et al., 2010).

Focal adhesions are formed and developed through protein-protein interactions and talin, paxillin, vinculin and FAK play key roles in the formation of nascent FAs. The early formed focal adhesions are called nascent focal adhesions (also called focal complexes) and are characterised by the small size, low protein composition and fast turnover (Nobes and Hall, 1995). Some of these nascent FAs are maturated into larger and more stable FAs by recruitment of multiple adaptor and signalling proteins and mechanical force generated by cytoskeleton network induces FAs maturation by promoting protein-protein interaction (Pasapera et al., 2010). These later focal adhesion can develop into fibrillar adhesions that are involved in ECM remodelling (Pankov et al., 2000; Geiger and Yamada, 2011). Talin plays an important role in the formation of early focal adhesions by binding to the cytoplasmic domain of integrins with its head domain, whereas its tail domain contains binding sites for actin (Ziegler et al., 2008, Bois et al., 2006). By binding to integrins with its head domain and to F-actin with its tail domain, talin links the ECM to the cytoskeleton network. Besides its

binding to integrins and actin filaments, talin interacts with PIP2, α-actinin, paxillin and has multiple binding sites for vinculin making it a critical adaptor protein for the recruitment of important FA proteins (Atherton et al., 2019).

Paxillin is one of the early recruited proteins to FAs, where it functions as a critical adaptor protein that recruits various proteins which have different functions at FA complexes including signalling proteins such as kinases and phosphatases and structural proteins such as vinculin (Laukaitis et al., 2001). The activity and localisation of paxillin at FAs was reported to be regulated by its phosphorylation at different tyrosine residues (27, 39-41), which can be triggered by the attachment of integrins to ECM (Bellis et al., 1995, Hu et al., 2014). One of the main binding partners of paxillin at FAs is the tyrosine kinase FAK and preventing their interaction was reported to decrease the localisation of this kinase to FAs, which in turn reduces the phosphorylation of different FAs proteins leading to changes in cell migration (Deramaudt et al., 2014). Tension force derived from actomyosin contraction was also shown to induce the phosphorylation of paxillin at tyrosine residues 31 and 118 by FAK/Src kinases. Its phosphorylation at these sites promotes its interaction with vinculin leading to the recruitment of the latter protein to FAs. Expressing the mutated version of paxillin that mimic its phosphorylation at these sites was found to be adequate for the localisation of vinculin to these adhesion sites (Pasapera et al., 2010).

Another important FA protein is α-actinin, which is involved in re-organisation of F-actin via cross-linking individual filaments, a crucial function that allow cells to modify their morphology and to provide mechanical force that drive cell migration (Ciobanasu et al.,

2014). This actin binding protein is a dimer composed of two identical monomers that have anti-parallel organisation allowing the existence of the N-terminal actin binding domains at each end of the dimer enabling its function (Borrego-Diaz et al., 2006). Beside its role in cross-linking actin-filaments, α-actinin interacts with FAs proteins including integrins, talin and vinculin indicating its importance in linking cytoskeleton to FAs (Sjöblom et al., 2008).

Vinculin is a 117-kDa cytosolic protein involved in anchoring FAs to actin filaments by binding to talin and actin (Carisey et al., 2013). It contains an acidic N-terminus head (90-kDa) domain and a basic C-terminus tail domain (30-kDa) separated by a proline-rich segment. The vinculin head domain has binding sites for talin and α-actinin, whereas the tail domain has binding sites for paxillin, actin and lipids (Wood et al., 1994, McGregor et al., 1994). Cytoplasmic vinculin is in an auto-inhibitory state caused by the interaction between its head and tail domains preventing its interaction with other proteins (Chorev et al., 2018). Once nascent FAs are formed, vinculin is recruited to FAs, and paxillin was shown to be required for the recruitment of vinculin to FAs, whereas talin was shown to be necessary for its activation at FAs (Case et al., 2015). The loss of vinculin in cancer cells was shown to reduce the strength of cell adhesion and cell spreading and to enhance cell migration (Coll et al., 1995, Saunders et al., 2006).

Vinculin is important in transmission of force generated by cytoskeleton network to ECM to facilitate cell movement. Vinculin binding to talin and actin increases the stability of FAs allowing them to transmit traction force to the ECM (Case et al., 2015). Force traction was significantly reduced in fibroblasts that lack vinculin (Diez et al., 2011) and vinculin

interaction with actin was suggested to be required for force transmission from cytoskeleton to the ECM (Dumbauld et al., 2010). Beside its role in FAs maturation, vinculin also plays important role in sensing the rigidity of the ECM. Physical properties of the ECM affect various cellular functions such as proliferation and migration and FAs play an important role in sensing and interpreting the ECM physical cues into biochemical signalling, a process called mechanotransduction, to trigger the appropriate cellular function (Geiger et al., 2009; Hoffman et al., 2011; Humphrey et al., 2014). Vinculin was shown to be involved in mechanotransduction by interaction with phosphorylated-paxillin (Pasapera et al., 2010). In addition, rigidity of substrates was suggested to influence the number and size of FAs. Cells on more rigid substrates form more FAs with increased size compared to cells on soft substrates. Vinculin was found to be essential in sensing ECM rigidity by interaction with vinexin-α and preventing their interaction affects the rigidity influences on cell movement (Yamashita et al., 2014). Vinculin was also reported to regulate the dynamics of F-actins by interacting with the actin binding protein α-actinin. Each monomer of this latter protein contains a single vinculin binding site buried in its central rod domain, which contains 4 spectrin-like repeats (SR) (Bois et al., 2005), and subjecting this domain to mechanical force leads to unfolding these repeats exposing vinculin binding sites in SR4. Unlike the rest of SRs in this domain, once unfold, vinculin binds to these sites and prevents SR4 from refolding again after releasing force. Vinculin enhances the α-actinin-actin linkage by binding to both proteins enhancing the overall cross-linking of actin filaments (Le et al., 2017).

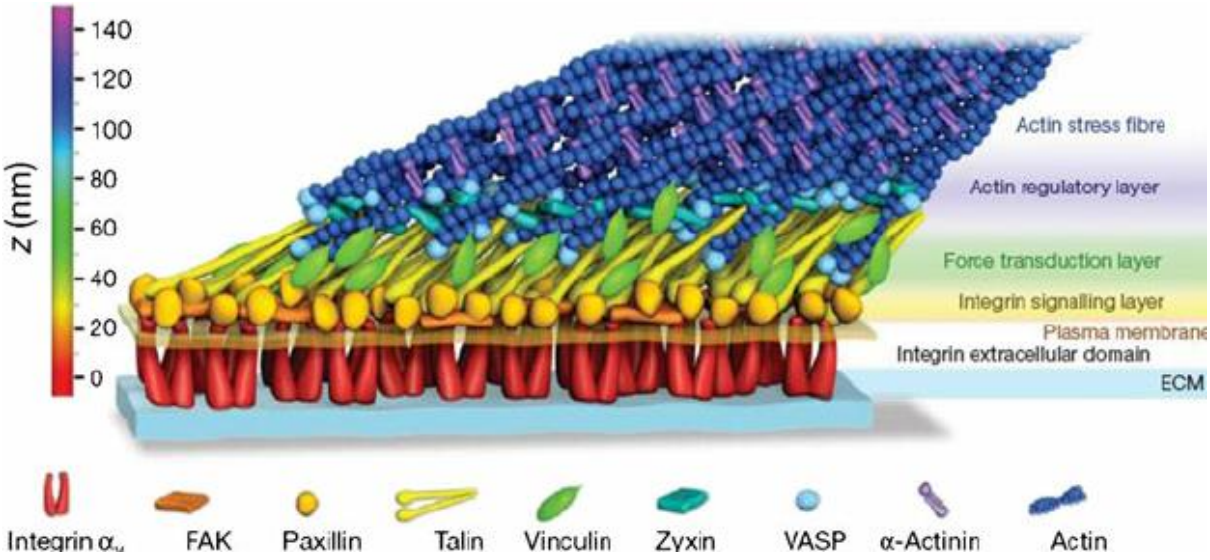

Figure 1.4 Focal adhesion structure and protein components. The extracellular domain of integrins binds to the ECM components, and this interaction stimulates integrins. When activated, the cytoplasmic domain integrins recruit multiple proteins leading to the formation of FAs (Kanchanawong et al., 2010).

For cells to migrate, they must be able to detach from the ECM regularly, but it remains poorly understood how attachment and detachment of adhesion structures are controlled. When cells are migrating, FAs are formed allowing the transmission of the traction force to ECM enabling cells to move along matrices. The FAs must then disassemble to release adhesion to the ECM to continue migration. Thus, assembly and disassembly of FAs must be regulated continuously for efficient cell migration (Webb et al., 2002, Broussard et al., 2008).

1.1.6 Regulation of Focal adhesion dynamics

Understanding the dynamics of these adhesion structures will increase our understanding of their cellular functions. Different mechanisms have been reported to regulate the dynamics of these structures including the cytoskeleton networks, protease-mediated cleavage of their associated proteins and phosphorylation. The Rho GTPase family member, Rac1, which can be activated by integrins, is a key player in initiating the assembly of nascent focal complexes, although the molecular mechanism of its function in inducing this formation still needs to be determined (Burridge and Wennerberg, 2004). Activated Rac1 can directly bind and interact with different proteins, and these interactions promote membrane protrusions. This enhances the formation of actin filaments, which generate the required force for the formation of focal complexes.

1.1.6.1 Microtubules

Microtubules (MTs) are one of the major regulators of focal adhesion disassembly as demonstrated by de-polymerizing MTs using nocodazole (Kaverina et al., 1999, Ezratty et al., 2005). After nocodazole treatment, the disassembly of FAs was inhibited, and their stability was increased, which enhanced adhesion to the extracellular environment. Treating cells with nocodazole increased FA-associated protein phosphorylation, and there was a reduction in this phosphorylation after its removal, suggesting that MTs might deliver signals that de-phosphorylate these proteins to trigger FAs disassembly and promote migration (Ezratty et al., 2005).

Another FA disassembly effector is the motor protein kinesin-1, which is essential for transporting multiple proteins along microtubules towards the plus end (Hirokawa et al., 2009). Reduced expression of this motor protein prevented FA disassembly and increased their size and stability in a manner similar to de-polymerizing MTs by nocodazole, although it did not affect MT polymerisation, suggesting that the activity of this motor protein is required for FAs turnover (Krylyshkina et al., 2002).

1.1.6.2 Proteases

Focal adhesion dynamics are also regulated by the protease calpain2, which proteolyses key protein components in the focal adhesions including talin, FAK and paxillin (Cortesio et al., 2011). In a previous study, the role of calpain-2-mediated proteolysis of paxillin in the dynamics of focal adhesions and cell migration was investigated. This protease was found to cleave paxillin, resulting in the production of a C-terminal fragment similar to paxillin delta, which is an alternative splice of paxillin (Cortesio et al., 2011). In this study, they found that this alternative calpain-mediated product of paxillin impaired focal adhesion disassembly and cell migration, whereas non-cleaved paxillin enhanced them. By introducing a single mutant in paxillin (S95G), which prevented calpain from cleaving it, focal adhesion turnover and cell migration were enhanced, indicating the negative regulation of this protease in focal adhesion dynamics and cell migration. On the other hand, calpain-mediated cleavage of talin and FAK was shown to enhance the disassembly of these adhesion sites and consequently cell migration. Calpain-2 was shown to cleave talin between its head and tail domains promoting its disassembly from adhesion sites (Franco et al., 2004). In this study, they introduced mutants into talin to prevent its calpain-mediated proteolysis, and found

that these mutations impaired the turnover of other components in focal adhesion structures, such as zyxin and vinculin, indicating the role of calpain-mediated proteolysis of talin in the regulation of the dynamic of these adhesion structures. Like other focal adhesion proteins, FAK is a known substrate of calpain, and calpain-mediated proteolysis of FAK regulates the dynamics of talin thereby regulating the dynamics of talin-containing focal adhesions (Chan et al., 2010).

1.1.6.3 Phosphorylation

Focal adhesions are rich in post-translational modifications such as phosphorylation, which is a key regulator in the assembly and disassembly of these structures (Webb et al., 2004). ECM-mediated activation of integrins leads to the phosphorylation at tyrosine residues of key proteins involved in focal adhesions, including FAK, paxillin and p130Cas, etc. (Schaller et al., 1999). Consequently, phosphorylation regulates these adhesion structures by regulating the catalytic activity of target proteins. The phosphorylation and activation of these proteins leads to the recruitment of further signalling proteins or to the initiation of their downstream signalling pathways, such as the Ras and MAP kinase signalling pathways. Knocking down FAK in the fibroblasts increased the number and size of focal adhesions and decreased their migration indicating the importance of this kinase in focal adhesion turnover in migrating cells (Ilic et al., 1995). To be activated sufficiently, FAK is phosphorylated at six different tyrosine residues located at positions 397, 407, 576, 577, 861 and 925 (Calalb et al., 1995). Phosphorylating FAK at Tyr397 was believed to be a key step in its activation, and phosphorylation of this site is induced upon integrin attachment to components of the ECM (Kornberg et al., 1992). After its phosphorylation at this site, the

binding affinity towards other proteins such as members of Src family kinases, phosphatidylinositol 3-kinase (PI3K), Grb7 or phospholipase Cγ is increased (Xing et al., 1994). Src kinase binding to Tyr397- phosphorylated FAK promotes the phosphorylation of FAK at other phospho-acceptor tyrosine residues, which in turn enhances FAK activity and is shown to be required for Src kinases activation, thereby increasing their signalling (Leu and Maa, 2002). Phosphorylation of these different sites in FAK has different effects on its function as its phosphorylation at its kinase domain (tyrosine 576 and 577) is required for its full activity, whereas phosphorylation at tyrosine 861 enhances its binding affinity towards paxillin and talin (Mitra et al., 2005). In addition, Src-mediated phosphorylation of FAK of the tyrosine residue at 925 within its FAT domain induced its interaction with Grb2, which is required for recruiting dynamin to FAs. Dynamin has been implicated in the internalisation of integrins and thereby promoting the turnover of focal adhesions (Ezratty et al., 2005). However, it has been shown that when microtubules extend towards FAs, they result in the de-phosphorylation of FAK at tyrosine 397, and this step is required for efficient disassembly of FAs. Another study conducted by Hamadi et al., 2005 investigated the importance of FAK in focal adhesion disassembly and found that its phosphorylation at Tyr397 and subsequently at Tyr576 is required for their disassembly. Introducing a mutant in FAK that prevented its phosphorylation at Tyr397 decreased its residency time at FAs and impaired their disassembly. These findings indicate that FAK phosphorylation is required for enhancing its existence at FAs, which in turn promotes their disassembly facilitating cell migration (Hamadi et al., 2005). From these findings, it can be concluded that phosphorylation is a key regulator of FA turnover by regulating critical proteins associated with FAs.

1.1.7 SUMOylation

1.1.7.1 SUMOylation history

Ubiquitin was first reported to covalently modify proteins by Avram Hershko and his student Aaron Ciechanover in the late 1970s (Ciehanover et al., 1978). Modifying proteins by ubiquitin was shown in following studies to target them to the proteasome for degradation in the presence of ATP (Ciechanover et al., 1980). This new post-translational modification opened the gate for a new field in cellular and biological research, as it was shown to be implicated in most cellular functions. Researchers investigated this field for two decades to reveal its mechanisms and impacts on cell functions before the discovery of small ubiquitin-related modifiers (SUMO proteins) in 1995 by different research groups. Investigation of the latter proteins was facilitated by applying strategies developed for studying ubiquitin. SUMO proteins were found to modify proteins via a similar mechanism to that of ubiquitin, and that SUMOylation is involved in many essential cellular functions reviewed in Geiss-Friedlander and Melchior (2007). The identification of SUMO proteins was first revealed by analysing the role of Mif2 protein in chromosome segregation in yeast (Meluh and Koshland, 1995). It was demonstrated that Mif2 has a critical role in chromosome segregation and was localised in the centromere. Several high-copy suppressors of Mif2 were revealed in this study, and one of them was the suppressor of Mif2, clone 3 (smt3), which codes for the yeast ortholog in human SUMO1. This study did not show if SUMO modifies Mif2 or other centromere-related proteins or if it has a role in chromosome segregation. However, in future studies, SUMO proteins were found to modify various centromere-associated proteins, and this modification is critical in chromosome

segregation(Eifler and Vertegaal, 2015). The human cDNA coding for SUMO1 was first identified using yeast two-hybrid screening in 1996. SUMO1 was found to interact with the promyelocytic leukaemia (PML) protein, and it was named PIC1 (PML-interacting clone 1) (Boddy et al., 1996). Although SUMO1 was found to interact with PML, no evidence of covalent modification of SUMO1 to PML was revealed in this study. However, it is now recognised that SUMO1 is conjugated to PML, and this modification of PML is essential in the formation of PML nuclear bodies (Sahin et al., 2014). In addition, early studies of SUMOylation revealed the interaction between SUMO1 and Fas/APO-1 receptor (Okura et al., 1996). Ligands targeting this receptor were found to induce apoptosis and overexpressing SUMO1 inhibited this pathway, thereby protecting cells from apoptosis. Given its importance in protecting cells from death, it was referred as Sentrin (after sentry). DNA recombinase (RAD51), which is involved in DNA damage repair, was found to be the third SUMO1-interacting protein in early SUMO studies (Shen et al., 1996). This finding was the first to indicate the significance of SUMOylation in DNA damage repair alongside its role in chromosome segregation. Later studies revealed that SUMOylation is a vital regulatory mechanism for all aspects of DNA repair and its interaction with ubiquitination is required for maintaining genome integrity (Jackson and Durocher, 2013). RAD51 was later identified to interact with SUMO1 non-covalently, and this interaction is necessary for recruiting RAD51 to DNA double-strand damages(Shima et al., 2013).

Although the previous early studies linked SUMO1 to critical cellular functions by interacting with different proteins, they lack the evidence that SUMO proteins covalently attach to their substrates and therefore function as a post-translational modification system. It was not

until the late 1990s when SUMO1 was identified to covalently attach to Ran GTPase-activating protein, RanGAP1, and this modification was suggested to be reversible (Mahajan et al., 1997, Matunis et al., 1996). In both studies, RanGAP1 antibodies detected the presence of different forms of RanGAP1 with different molecular masses. A unique peptide was found to be attached to the higher in molecular mass form of RanGAP1 and this peptide was reported to have molecular weight of 11.5 kDa and share some sequence similarity with ubiquitin. These two groups investigated the association between this unique peptide and RanGAP1 differently. The Mahajan group recognised an ATP-dependent interconversion between the different forms of RanGAP1 indicating the requirement of ATP in SUMOylation (Mahajan et al., 1997). The other group showed that the larger form of RanGAP1 was converted to the lower one when treating rat liver with DTT during the extraction of the nuclear envelope. This conversion was inhibited when using N-ethylmaleimide (NEM), which inhibits all cysteine peptidases, indicating the presence of cysteine-dependent SUMO isopeptidases (Matunis et al., 1996). Both groups revealed that the SUMOylation of RanGAP1 leads to its interaction with RanBP2 at these nuclear complexes. The finding from these studies suggests that SUMOylation is a reversible post-translational modification that modifies proteins by similar mechanisms to that of ubiquitination. In addition, it was shown that SUMOylation alters protein interactions and was required for the formation of protein complexes beside its roles in chromosome segregation and DNA damage repair.

1.1.7.2 SUMOylation pathway

SUMOylation has since been recognised as a major post-translational modification mechanism of proteins by the covalent attachment of the 12 kDa small ubiquitin-like modifier (SUMO) proteins. The attachment of SUMO proteins results in alterations in the function, localisation, activity or binding affinity of their substrates (Geiss-Friedlander and Melchior, 2007). SUMO substrates were shown to be involved in different cellular processes including nuclear-cytosolic transport, apoptosis, DNA damage response and transcription (Tang et al., 2008, Bettermann et al., 2012) indicating the importance of this modification system in the regulation of various cellular functions. While the yeast genome encodes a single SUMO protein called suppressor of MIF2 mutation 3 (SMT3), which significantly impaired growth when depleted (Tanaka et al., 1999), there are four SUMO genes in humans encoding the four SUMO proteins (SUMO1-SUMO4). The first member of this family, SUMO1, shares less than 50% sequence identity with other members. In addition, this SUMO isoform was reported to modify most of the identified SUMO substrates (Saitoh and Hinchey, 2000). On the other hand, the SUMO-family protein isoforms, SUMO2 & SUMO3, are referred collectively as SUMO2/3 as they share more than 97% sequence similarity, differing only in three amino acid residues situated N-terminally. The last member of this family, SUMO4, shares more sequence similarity to SUMO2/3 (87%) than SUMO1 (Wei et al., 2008).

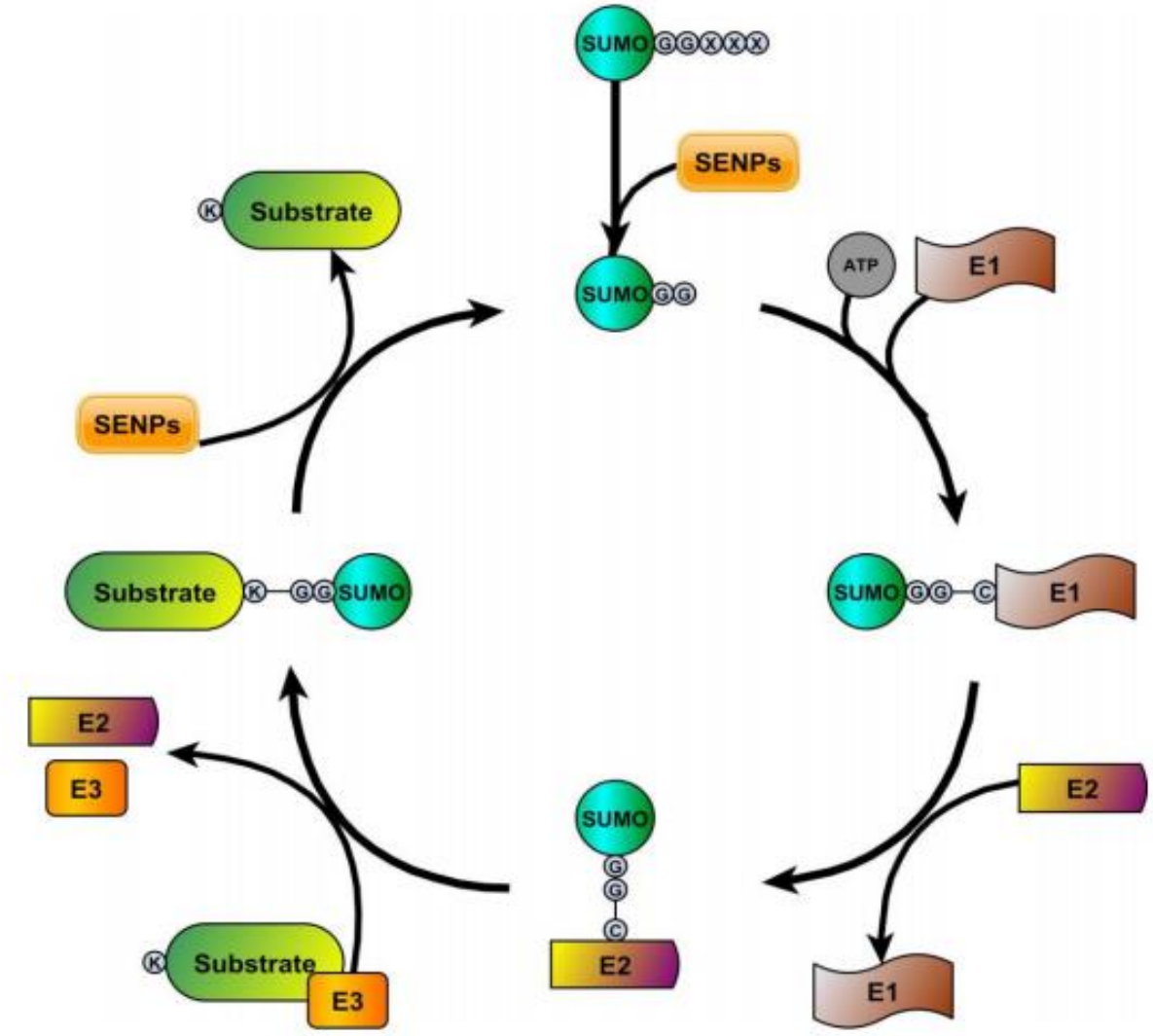

Figure 1.5 The enzymatic cascade of SUMOylation. SENPs cleave the C-termini of SUMO proteins revealing a di-glycine motif. Cleaved SUMO proteins are activated by SUMO E1 enzyme, SAE1/2, and after their binding SUMOs are transferred to SUMO E2 conjugating enzyme, Ubc9. This enzyme attaches SUMOs to their substrates. E3 SUMO ligases enhance the efficiency of this attachment by binding to E2-SUMO complex and substrates. This diagram was adapted from (Alonso et al., 2015).

SUMO proteins form an isopeptide bond between their di-glycine motif located within the C-terminal and the ε-amino group of lysine residues in their substrate. This binding requires the catalytic activity of an enzymatic cascade involving an activating enzyme E1, a conjugating enzyme E2 and a ligase E3 (Gareau and Lima, 2010). As the precursor forms of SUMO proteins are in their inactive state after being synthesised, and to become mature,

SUMO-specific proteases (SENPs) cleave their C-termini exposing this motif (Guo et al., 2014). The enzymatic cascade is initiated after the SENPs-cleaved ATP-binding SUMO proteins are catalysed by their SUMO-activating enzymes (E1), which is a heterodimer of two subunits: SAE1 (SUMO-activating enzyme E1) and SAE2 (Schulman and Harper, 2009). This enzyme hydrolyses ATP and adenylates SUMO proteins at their C-termini. These alterations promote the association between the Cys173 residue in this enzyme and the di-glycine residues at the C-terminus of adenylated SUMO protein (Olsen et al., 2010). This interaction induces the formation of a thioester bond between these sites, which results in the transformation of these proteins to their E1 activating enzymes (Lu et al., 2010, Lois and Lima, 2005). After transferring SUMO proteins to this activating enzyme, they are transferred to their E2 conjugating enzyme, ubiquitin-conjugating 9 (Ubc9). A thioester bond is formed between the same C-terminal glycine residues in SUMO proteins and the catalytic cysteine residue (Cys 93) within this enzyme (Bernier-Villamor et al., 2002, Wilkinson and Henley, 2010). Following the binding of SUMO proteins to this enzyme, it covalently attaches them to the lysine residue of their substrates (Geiss-Friedlander and Melchior, 2007). The role of SUMO-E3 ligases in SUMOylation is to improve its efficiency by interacting with both Ubc9-SUMO complexes and their substrates (Tozluoglu et al., 2010).

Knockout mice models of SUMO proteins and the enzymes involved in the SUMOylation pathway revealed different effects upon silencing these proteins. For example, silencing either SUMO1 or SUMO3 in mice has no effect on their development (Evdokimov et al., 2008), whereas SUMO2 has a greater impact on the development of mice when knocked out as it causes embryonic lethality (Wang et al., 2014). In addition, knocking out the SUMO

E2 conjugating enzyme Ubc9 impaired the segregation of chromosomes that leads to the death mice during embryonic development (Nacerddine et al., 2005).

1.1.7.3 SUMO E3 ligases

In ubiquitination, which targets proteins for degradation, the role of the E3 ligases is more critical than that of the SUMO-E3 ligases. These ubiquitin-ligases are divided into two groups: the first group members, which contain the HECT (homologous with E6-associated protein C-terminus) domain, are able to form a thioester bond with ubiquitin after interacting with ubiquitin-conjugating enzymes (E2). This interaction leads to the transfer of ubiquitin to these ligases before targeting substrates. The other group contains proteins that contain a RING domain and members of this group are not able to bind to ubiquitin directly. Instead, they bind to ubiquitin-E2s complex and bind at the same time with substrates to allow efficient ubiquitination (Pickart, 2001). Unlike ubiquitination, the SUMO-E2 conjugating enzyme Ubc9 is able to attach SUMO proteins to their substrates containing the SUMO consensus motif (Bernier-Villamor et al., 2002, Gareau and Lima, 2010). The role of SUMO E3 ligases was suggested to improve the efficiency of SUMOylation as they can bind to both Ubc9-SUMO complex and substrates, resembling the function of RING-domain-containing ubiquitin ligases and for recognising substrates that do not contain this motif. More than 600 human genes have been identified to encode proteins that possess E3 ligase activity in the ubiquitination pathway, whereas few numbers of proteins that possess E3 ligase activity in the SUMOylation pathway have been reported (Deshaies and Joazeiro, 2009).

The first proteins identified to have ligase activity in the SUMOylation system were the Siz proteins in yeast and knocking down these proteins prevented SUMOylation in yeast (Johnson and Gupta, 2001). The PIAS [protein inhibitor of activated STAT (signal transducer and activator of transcription)] protein family, which contains five SUMO E3 ligases, is analogous to the mammalian homologue of Siz proteins (Sachdev et al., 2001, Müller et al., 1998). This Siz/PIAS group contains the so-called SP (Siz/PIAS)-RING domain, which is a zinc finger domain with a similar structure to that of the RING domain present in ubiquitin E3 ligases. As they contain this RING-domain like domain, their ligation activity is similar to that of RING-domain-containing ubiquitin ligases by binding to both Ubc9-SUMO intermediate and substrate, but they can also bind to SUMO proteins non-covalently. These Siz/PIAS ligases have been implicated in the regulation of multiple cellular processes such as DNA damage response and regulation of cell-cycle and transcription (Schmidt and Müller, 2002, Flotho and Melchior, 2013).

A member of the Polycomb (Pc) protein family, Pc2, was identified as a SUMO E3 ligase (Kagey et al., 2003) that lacks the SP-RING domain. Unlike the Siz/PIAS ligases, this ligase binds directly to SUMO proteins, Ubc9, and to its substrate, CtBP (C-terminal-binding protein) (Merrill et al., 2010). Other proteins have been reported to lack this RING-domain-like domain and possess SUMO E3 ligase activity include histone deacetylase 4 and 7 (Grégoire and Yang, 2005, Gao et al., 2008) and tumour necrosis-factor-associated protein 7 (TRAF7) (Morita et al., 2005). The tumour suppressor p14Arf (Zhao and Blobel, 2005) and the G-protein Rhes (Subramaniam et al., 2009) have also been reported to possess SUMO E3 ligase activity, both of which also lack the RING-domain.

Another type of SUMO E3 ligase is Ran-binding protein 2 (RanBP2) (Pichler et al., 2002). This ligase has been implicated in the SUMOylation of many substrates including SP100, topoisomerase Iiα, HDAC4 and promyelocytic leukaemia (PML) (Dawlaty et al., 2008). This ligase has been shown to facilitate the SUMOylation of substrates by binding to the SUMOylation moiety, Ubc9-SUMO. By binding to this complex, it promotes conformational changes in this SUMO moiety to facilitate the transfer of SUMO proteins to their targets without binding to these substrates itself, indicating that it functions differently from other SUMO E3 ligases. In addition, this ligase was shown to be critical in nucleoplasmic transportation by stabilising the SUMOylation complex (Ubc9- SUMO) of its binding partner Ran GTPases-activating protein 1 (Ran GAP1) (Werner et al., 2012). This stabilisation of the SUMOylation complex targeting RanGAP1, which regulates the activity of the central regulator of nuclear transport, Ran GTPase, indicates the importance of both this ligase and SUMOylation in the regulation of cytosolic-nuclear trafficking. The Fanconi anaemia protein SLX4 is another SUMO ligating protein that has been identified recently. This ligase is involved in the global replication stress response, and it was revealed that this ligase is SUMOylated itself, and therefore promotes the SUMOylation of the DNA repair factor XPF (Guervilly et al., 2015, Ouyang et al., 2015). Although it lacks the SUMO consensus motif, SLX4 has a SUMO interaction motif (SIM) (Guervilly et al., 2015). This motif is characterised by the presence of large hydrophobic residues flanked by unstructured regions and was shown to enhance SUMOylation of proteins even in the absence of the SUMO consensus region (Knipscheer et al., 2008). This motif has been reported in many SUMO-modification

substrates, and bioinformatic analysis is being developed to detect both motifs (Zhao et al., 2014).

1.1.7.4 SUMOylation motifs

The majority of SUMO substrates contain the consensus SUMOylation motif ψKxD/E (where ψ is a large hydrophobic residue, D/E is an acidic residue) (Rodriguez et al., 2001, Yang et al., 2017). However, it is worth mentioning that not all SUMO substrates contain this motif. Additionally, the presence of this motif on proteins cannot confirm if a protein is a SUMO substrate as some proteins containing this motif are not SUMOylated, whereas some lysine residues lying outside this motif are SUMOylated (Xu et al., 2008). Following studies described different residues surrounding this core motif and the described motifs were shown to increase the probability of a protein to be SUMOylated. Phosphorylation-dependent SUMOylation motif (PDSM) was identified in 2006 by Hietakeangas and colleagues to be present in different SUMO substrates. This motif is composed of the core SUMOylation motif and an adjacent phosphorylation site followed by a proline residue. Phosphorylation of this motif was shown to enhance SUMOylation of PDSM-containing targets (Hietakangas et al., 2006). Negatively charged amino acid-dependent SUMOylation motif (NDSM) is another SUMO motif that was shown to compensate the absence of phosphorylation site by a cluster of acidic amino acids located in the vicinity of the SUMO core consensus motif (ψKxD/E-x-[2 out 6 must be acidic residues]). These acidic amino acids were suggested to enhance the binding of substrates to the E2 SUMO conjugating enzyme (Yang et al., 2006). Furthermore, a cluster of hydrophobic residues were found to proceed the core SUMOylation sequence and this motif is called hydrophobic cluster SUMOylation

motif (HCSM). The core SUMOylation consensus motif was also found to be inverted in some SUMO targets (Matic et al., 2010).

Although they were described to covalently modify a broad range of substrates, SUMO proteins were reported to interact non-covalently with many proteins that have SUMO-interacting motifs (SIMs). This non-covalent interaction influences various cellular functions and expands SUMOylation functions in various cellular mechanisms. Two-hybrid assays have been used to distinguish between the covalent and non-covalent interactions of SUMO proteins with their substrates. By utilising these assays, many proteins have been identified to interact non-covalently with SUMO proteins via SIMs (Hannich et al., 2005, Hecker et al., 2006).

The first SUMO-interacting motif was discovered by Minty and his colleagues in 2000 (Minty et al., 2000). In this study, they demonstrated that SUMO-modified p73 interacts with specific proteins that have a conserved SXS sequence with an adjacent hydrophobic core on one side and acidic residues on the other. The SXS motif alongside the hydrophobic core was found to be critical in this non-covalent interaction with SUMO proteins. However, a further study performed by Song and his team in 2004 contradicted this finding. In this study, the SXS sequence was not shown to be critical for this interaction. Instead, the hydrophobic core consisting of the [V/I-X-V/I-V/I] motif was found to facilitate the interaction of SIM-containing proteins with SUMOs. This hydrophobic sequence was later reported to be present in many SUMO associated proteins including proteins involved in

SUMO pathway, such as the SAE2 subunit of the SUMO activating enzyme E1 and SUMO E3 ligases PIASx and RanPB2 (Song et al., 2004).

In the structure of SUMO proteins, a SIM-binding groove is formed between the α-1 and the β-2. Peptides containing SIMs were found to be embedded in this groove, which contain critical hydrophobic residues involved in the interaction with SIMs. Although residues forming the hydrophobic core are conserved among all SUMO isoforms, their positions within the groove varied from one isoform to another. The hydrophobic core consists of H35, F36, and V38 in SUMO1 or Q31, F32 and I34 in SUMO2 (Baba et al., 2005, Hecker et al., 2006). Introducing mutations in these sites prevented the interaction with SIMs (Zhu et al., 2008). Negatively charged acidic amino acids, aspartic and glutamic acid, were shown to cluster around this hydrophobic core and to be critical in effective interaction (Hecker et al., 2006). In addition, serine and threonine residues that reside closed to SIMs can compensate for the loss of acidic residues. Phosphorylation of these residues was indicated to alter their charge to negative, thereby mimicking the acidic residues and inducing the interaction between SIMs and SUMO molecules (Chang et al., 2011, Cappadocia et al., 2015). These negatively charged residues within SIMs interact with positively charged basic residues in the hydrophobic groove of SUMO. These basic residues are K37, K39 and K46 in SUMO1 or K33, K35 and K42 in SUMO2 (Husnjak et al., 2016, Chupreta et al., 2005). As the hydrophobic and basic residues are found in different positions in the SIM-interacting groove in different SUMO isoforms, they may contribute to the orientation of SIM domains and to the preference of SUMO substrates towards interacting with a specific isoform of SUMO (Husnjak et al., 2016).

The influence of a non-covalent interaction of SUMO proteins with SIM-containing proteins have been of research interest since the discovery of these motifs. One example to illustrate the importance of this interaction is the regulation of thymine DNA glycosylase (TDG) by SUMO proteins. TDG hydrolyses mismatched thymine, thereby creating an abasic site in double-stranded DNA to prevent mutations. To release it from the abasic site to repair it, TDG is covalently modified by SUMO proteins. TDG has both a SUMO consensus motif and a SUMO-interacting motif, and both motifs are critical for its disassociation from DNA. Introducing SUMO and TDG proteins to a DNA substrate was shown to induce conformational changes in the latter protein, which in turn disrupts its binding to the DNA substrate (Baba et al., 2005).

Both motifs within TDG are located adjacent to each other suggesting that both motifs are necessary for altering its structure by SUMO interactions. The adjacent position of these motifs to each other in this SUMO substrate indicates a possible interaction between the covalently-bound SUMO proteins with the SIM. This interaction probably stabilises the altered structure of TDG to release it from the DNA substrate. Covalent modification of TDG by SUMOs was inhibited when deleting its SIM, although the SUMO consensus motif was still present. In addition to releasing TDG from double-stranded DNA, SUMOylation was implicated in its localisation to PML nuclear bodies. Deleting one of these motifs alone did not affect its localisation to these complexes, but deleting both motifs prevented its localisation (Takahashi et al., 2005). It can be concluded from these findings, that the noncovalent interaction of SUMO with TDG is a prerequisite for its covalent modification and both interactions are necessary for its recruitment to the PML nuclear complexes.

1.1.7.5 Function of SUMOylation

Proteins vary in their response to SUMOylation. The interaction of some substrates with their binding partners could be altered by the attachment of SUMO proteins to their specific binding sites. One of these proteins is the ubiquitin E2 conjugating enzyme, 25k. When SUMOylated, this enzyme's interaction with ubiquitin-activating enzymes is inhibited and thus prevents the ubiquitination of its substrates (Pichler et al., 2005). On the other hand, SUMOylation of other proteins enhances their binding affinity towards new partners, and this interaction could lead to different functions including translocating these proteins within cells and/or promoting their degradation. One example to demonstrate these subsets of SUMO-modified proteins is the SUMO modification of RanGAP1, which leads to the translocation of this protein from the cytosol to the nuclear pore by inducing its association with RanBP2 (Mahajan et al., 1997). Another example is the poly-SUMOylation-mediated degradation of PML by ubiquitination by promoting its association with the ubiquitin E3 ligase RNF4 (ring finger protein 4), which binds to the SUMO chains on PML and degrades the whole complex (Lallemand-Breitenbach et al., 2008). In addition, SUMOylation could regulate the function of its targets by altering their structures, which in turn regulates their activity. For example, SUMOylation of the enzyme thymine-DNA glycosylase (TDG) induces conformational changes that release it from DNA damaged sites (Baba et al., 2005). The previous examples indicate that this post-translational modification is implicated in many cellular processes and regulates an extensive range of proteins differently.

Several studies demonstrated that certain SUMOylation substrates are modified by only a single member of SUMO proteins while others are regulated by a combination of both isoforms, SUMO1 and SUMO2/3. For instance, SUMO1 has been implicated in the SUMOylation of RanGAP1 facilitating its transportation from the cytosol to the nuclear pore, whereas SUMO2/3 was shown to modify sp100 (Saitoh and Hinchey, 2000). One example of the substrates that can be SUMOylated by both isoforms, SUMO1 and SUMO2/3, is PML. SUMOylation of PML by SUMO1 leads to its translocation within the nuclear domains PML nuclear bodies (Müller et al., 1998), while modifying this protein by SUMO2/3 and the consequent SUMO-chain formation promotes its degradation by ubiquitination (Lallemand-Breitenbach et al., 2008).

Previous studies have reported that different cellular stress stimuli lead to a global increase in SUMOylation. Under normal conditions, most SUMO1 isoforms were conjugated to their substrates, whereas there is a considerable amount of unconjugated SUMO2/3 isoforms in COS-7 cells (Saitoh and Hinchey, 2000). On the other hand, subjecting these cells to heat shock, oxidative, ethanol and osmotic stresses resulted in a significant increase in conjugated SUMO2/3 isoforms without affecting the level of conjugated SUMO1 (Golebiowski et al., 2009). This increase in the levels of conjugated SUMO2/3 proteins was also observed in cells when challenged with deprivation in oxygen/glucose and hypothermia in neurones (Yang et al., 2008, Loftus et al., 2009). These findings indicate the critical role of SUMOylation in rapid adaption to different types of stress.

Despite the fact that cellular stresses cause a rapid increase in global SUMOylation, various SUMO substrates are modified differently. While the SUMO modification of some substrates in response to cellular stress increases, the levels of SUMOylation of others were not affected and/or decreased in other proteins. The stability of the SUMO-specific protease SENP3, which is degraded by ubiquitination in resting conditions, is increased in response to oxidative stress. Consequently, this protease deSUMOylates p300 leading to the activation of HIF1α (hypoxia-inducible factor 1α), which in turn induces the transcription of stress-responsive genes (Huang et al., 2009).

SUMO2/3 are the major stress response-dependent SUMO proteins, to increase their SUMOylation efficiency they are subjected to the attachment of SUMO proteins themselves. These SUMO isoforms were shown to contain the SUMO consensus motif at their N-termini (K11) facilitating the formation of SUMO chains (Tatham et al., 2001), like the poly-SUMOylation of PML that leads to its degradation by ubiquitination. This motif is not present in SUMO1, preventing it from forming chains, and it was suggested that the interaction between it and SUMO2/3 formed chains results in the disassembly of these chains (Matic et al., 2008). However, recent studies have identified lysine residues within both SUMO1 and SUMO2/3 located outside the consensus motif that can be SUMOylated, increasing the complexity of SUMO chain forming (Bruderer et al., 2011, Hendriks et al., 2014).

1.1.7.6 SUMO-Targeted Ubiquitin Ligases (STUbLs)

To maintain homoeostasis of SUMOylation levels on substrates, SUMO modified proteins are either de-SUMOylated by SUMO proteases or targeted to the proteasome for degradation (Prudden et al., 2007). SUMOylation and ubiquitination are thought to be different modification systems and are thought to have a competitive relationship as they compete for the same lysine residue on their targets (Ulrich, 2005). SUMOylation of some substrates was shown to prevent their degradation by ubiquitination (Desterro et al., 1998). Another type of relationship between these two types of modification has emerged, in which SUMOylation of some substrates promotes ubiquitination of the same substrates leading to their degradation (Huang and Reichardt, 2003). Ubiquitination of SUMOylated proteins are facilitated by a set of enzymes called SUMO-targeted ubiquitin ligases (STUbLs) (Uzunova et al., 2007, Sun et al., 2007). These enzymes have ubiquitin E3 ligase activity and were identified to specifically recognise SUMOylated proteins and poly-ubiquitinate them leading to their degradation. Three of these enzymes have been reported including Uls1p-Nis1p, Slx5pSlx8p/RNF4 and Rad18p (Yang et al., 2006). Several targets for the UIs1p enzyme have been identified including Pac1p, a microtubule-associated protein, and the DNA-binding protein Rap1p (Jain and Cooper, 2010, Alonso et al., 2012).

1.1.7.7 De-SUMOylation

SUMOylation can be rapidly reversed by a specific group of proteases called SUMO-specific proteases (SENPs) (Hickey et al., 2012, Guo et al., 2014). In addition to their role in activating the precursor form of SUMO proteins, SENPs have the ability to de-conjugate SUMO proteins from their target proteins. They cleave the isopeptide bond formed between the C-

terminal glycine motif on SUMO proteins and the ε-amino group of lysine on their target protein to release SUMO proteins (Mukhopadhyay and Dasso, 2007, Yeh, 2009).

In mammalians, the SENP protease family contains of six members that have a different affinity towards cleaving and de-conjugating SUMO proteins. These members have been divided into three sub-groups according to several factors, including sequence similarity, their distribution within the cells and target specificity. The first subgroup members, SENP1 and SENP2, have a broad specificity towards SUMO isoforms as they are involved in the maturation and de-conjugation of both SUMO1 and SUMO2/3 (Gong et al., 2000, Reverter and Lima, 2006). The second subgroup members, SENP3 and SENP5, prefer processing and de-conjugating monomer SUMO2/3 over SUMO1 (Di Bacco et al., 2006, Sharma et al., 2013). The final subgroup proteases, SENP6 and SENP7, have been implicated in the disassembly of SUMO chains formed by SUMO2/3, but not in the maturation of SUMO proteins or in the de-conjugation of monomer SUMO2/3 from their substrates (Drag et al., 2008, Shen et al., 2009). All different isoforms of SENPs contain at their C-termini a 250-amino acid long conserved cysteine protease catalytic functioning domain (Hickey et al., 2012).

On the other hand, these isoforms have a large and non-conserved N-terminal domain. This domain has minimal or no homology to that of other isoforms and was suggested to contribute to their subcellular distribution and substrate specificity (Bailey and O'Hare, 2004). As they vary in their N-terminal domain, different SENP isoforms vary in their subcellular localisation. SENP1 was shown to localise at the nucleoplasm(Gong et al., 2000), SENP2 was found at the nuclear pore (Zhang et al., 2002), SENP3 and SENP5 were reported

to be in the nucleolus (Nishida et al., 2000), whereas SENP6 was reported to localise in the cytoplasm (Kim et al., 2000). In a different study, SENP2 was found to shuttle between the nucleus and the cytoplasm as it contains a nuclear localisation signal (NLS) sequence and a nuclear export signal (NES) sequence (Itahana et al., 2006). The NLS sequence presents at its N-terminal domain and was shown to be essential for its recruitment to the nuclear pore complex (Zhang et al., 2002). In addition, the NES sequence was reported to be in the central domain of this protease. These signals presented in the non-conserved region of this protease and were not found in other members of this family. Introducing mutations in the NES prevented its shuttling between the nucleus and the cytoplasm (Itahana et al., 2006).

1.1.7.8 SUMOylation in cancer

Although it has been implicated in the regulation of critical cellular mechanisms in normal cells, SUMOylation has been shown to be deregulated in serious human diseases including cancer (Bawa-Khalfe and Yeh, 2010), heart failure and neurodegenerative diseases (Droescher et al., 2013, Kho et al., 2011). SUMOylation has been reported to support different aspects of cancer progression(Seeler and Dejean, 2017). SUMO1 conjugation to p53 was shown to stabilise its activity and consequently induce apoptosis in human non-small cell lung carcinoma (Ivanschitz et al., 2015). In addition, Akt protein kinase is an important regulator of several cellular mechanisms including cell proliferation, cell migration and apoptosis and activation of this kinase has been reported to be deregulated in cancer (Brazil et al., 2002). Different post-translational modifications including phosphorylation, ubiquitination and acetylation have been suggested to regulate Akt stability and activity (Manning and Cantley, 2007, Li and Yang, 2010). A recent study

identified a critical role of SUMOylation in the kinase activity of Akt where residue K276 was found to be the major SUMOylation acceptor. Introducing a mutation at this site completely inhibited Akt SUMOylation and kinase activity, whereas overexpressing SUMO1 or the SUMO E3 ligase PIAS1 increased its activity. SUMOylation of this kinase was shown to enhance Akt-mediated tumorigenesis and cancer cell proliferation in different cancer cells (Li et al., 2013b).

SUMOylation levels were reported to be increased in tumours compared to surrounding tissues(Liang et al., 2017) indicating the importance of SUMOylation for cancer progression. The expression of enzymes involved in the SUMOylation pathway has shown to be deregulated in different cancer types. The SUMO E1 activating enzyme (SAE) is upregulated in different cancer types including Hepatocellular carcinoma (Lee and Thorgeirsson, 2004), breast cancer (Kessler et al., 2012) and small cell lung cancer (Inamura et al., 2007, Liu et al., 2015). The overexpression of SAE in small cell lung cancer was shown to be associated with tumorigenesis and reducing expression of this enzyme has led to a reduction in cell growth and increased levels of apoptosis. In addition, migration of these cancer cells was prevented and their sensitivity to chemotherapy was enhanced by knocking it down (Liu et al., 2015). In addition, Myc is an oncogenic protein that is overexpressed in about 25% of breast cancer cells and its overexpression is associated with increased malignancy (Adler et al., 2006). The upregulation of SAE in these breast cancer subsets was shown to enhance Myc-dependent tumour growth and inhibiting this enzyme supressed Myc activity (Kessler et al., 2012). In the same study, the expression levels of SAE were found to contribute to the malignancy stage and survival rate of patients with this subtype of breast cancer. The low expression

levels of this SUMO enzyme were shown to be associated with improved survival rate low occurrence of metastasis, whereas high levels are associated with increased malignancy and high metastasis occurrence (Kessler et al., 2012).

The deregulation of the SUMO conjugating enzyme (Ubc9) was reported in various cancer types and its overexpression was suggested to aid tumour growth and metastasis (Li et al., 2013a, Seeler and Dejean, 2017). This enzyme was shown to be upregulated in breast cancer tumours compared to normal tissues and its overexpression is associated with tumour growth and metastasis. In addition, the low expression levels of Ubc9 were associated with enhanced survival rate and sensitivity to chemotherapy of patients with breast cancer (Chen et al., 2011). In another study, Ubc9 expression was shown to be elevated in Hepatocellular carcinoma (HCC) compared to surrounding tissues and its overexpression is associated with tumour growth and resistance to chemotherapy (Fang et al., 2017).

SUMO-specific proteases (SENPs) are important in cellular physiology as they maintain the balance between SUMO-modified and non-modified proteins. Deficiency of SENP1 and SENP2 in mice resulted in death during embryonic development (Shen et al., 2006). The expression of SENPs is deregulated in different types of cancer. These changes in the expression of SENPs disrupt the balance between SUMOylated and un-SUMOylated levels of proteins, thereby enhancing cancer malignancy and metastasis (Ma et al., 2014, Xu et al., 2011).

The androgen receptor (AR) is an essential protein in the tumorigenesis of prostate cancer. It has been shown that both SENP1 and 2 de-SUMOylate this protein and that overexpression of SENP1 increased its transcriptional activity (Kaikkonen et al., 2009, Cheng et al., 2004). In 2013, Wang and colleagues reported that expression of SENP1 in prostate cancer is associated with its malignancy and metastasis, whereas silencing this protease impaired these metastatic properties (Wang et al., 2013). Furthermore, in more than 50% of prostate cancer samples, SENP1 was overexpressed indicating its role in prostate tumorigenesis (Cheng et al., 2006). In another study, SENP1 upregulation was shown to induce colon cancer cell growth by inducing the expression of CDK inhibitors (Xu et al., 2011). In a different 2014 study, Ma, Chenchao and colleagues demonstrated that SENP1 overexpression is associated with progress and metastasis of pancreatic cancer. In their study, they found that in pancreatic ductal adenocarcinoma (PDAC), the expression of this SUMO protease was higher than in surrounding tissues. In addition, knockdown studies in these cells indicated that silencing SENP1 by siRNAs inhibited essential cellular functions including proliferation, migration and invasion. In this study, knocking down SENP1 was found to cause the downregulation of MMP-9, a member of metalloproteases involved in cell migration by degrading the extracellular matrix (Ma et al., 2014). In prostate cancer, hypoxia-inducible factor 1α (HIF-1α) regulates the expression of the many genes involved angiogenesis (Semenza, 2003). Several groups have reported the importance of SUMOylation on the activity of HIF 1-α (Bae et al., 2004, Berta et al., 2007). Polycomb chromobox 4 (CBX4) and RWD-containing SUMOylation enhancer (RSUME) increased the transcriptional activity of HIF-1α by accumulating its SUMOylation and stability (Carbia-Nagashima et al., 2007, Li et al., 2014). In addition, in the absence of SENP1, HIF-1α was

actively SUMOylated, and its SUMOylation resulted in its degradation by ubiquitination, indicating the importance of SENP1 on the stability of this factor (Cheng et al., 2007). In a 2011 study, Xu and colleagues examined how SENP1 regulates colon cancer cell growth and found that it was overexpressed in most sample tissues. Knocking down this protease inhibited cancer growth in nude mice and colony formation in colon cancer cell lines DLD-1 (Xu et al., 2011).

Unlike most SENPs, SENP2 is downregulated in different cancer types including bladder cancer (Tan et al., 2013) and Hepatocellular carcinoma (Shen et al., 2012). SENP2 was found to be down regulated in bladder cancer tissues compared to surrounding tissue (Tan et al., 2013). In this study, they found that overexpression of this protease significantly decreased the migration and invasion of these cells by specifically down regulating the expression of the metalloprotease MMP13, which normally enhances metastases when upregulated. In bladder cancer, β-catenin was found to translocate to the nucleus and to target the promoter of MMP13 in order to activate it, thereby promoting metastases. WNT signalling promotes the SUMOylation of the complex TBL1/TBLR1, which when SUMOylated, forms a complex with β-catenin facilitating its transport to the nucleus. To prevent the expression of MMP13, SENP2 de-SUMOylates TBL1/TBLR1, thus, preventing TBL1/TBLR1 from binding to β-catenin and consequently preventing its nuclear translocation and the activation of MMP13 (Tan et al., 2015). In addition, SENP2 has been implicated in regulating the SUMOylation levels of the oncoprotein MDM2. SUMOylation of this ligase was found to be essential for its binding to tumour suppressor p53, which in turn reduces the activity of the latter protein. Overexpression of SENP2 leads to deSUMOylation MDM2 and consequently

disrupts MDM2-p53 interaction increasing the p53 tumour suppressor activity (Chiu et al., 2008, Jiang et al., 2011).

Overexpression of SENP3 in gastric cancer cells is correlated with enhanced epithelial-to-mesenchymal transition (EMT). EMT is a cellular process, in which an epithelial cell is changed into a mesenchymal one, thereby losing its epithelial phenotype and acquiring a mesenchymal one. In this transition, epithelial markers such as E-cadherin are reduced, and mesenchymal markers such as N-cadherin, fibronectin and vimentin are increased. These markers are used to determine whether an epithelial cell is in transit to a mesenchymal cell or not. By changing their phenotype from epithelial to mesenchymal, EMT enhances the ability of epithelial cancer cells to migrate, therefore promoting metastasis (Kalluri and Weinberg, 2009). This phenotype alteration is the result of an alteration in gene expression, and some transcription factors including Snail, Twist and Zeb protein families regulate these genotype alterations. Some of these transcription factors repress the epithelial marker's expression, whereas others induce the expression of mesenchymal markers (Tam and Weinberg, 2013). Cellular stresses have a great impact on EMT, and TGF-β was shown to promote this transition (Gal et al., 2008). An increased amount of ROS is generated upon the stimulation of TGF-β, and the growing amount of ROS induces EMT by activating the EMT-involved signalling pathways (Giannoni et al., 2011). According to these findings, Ren and colleagues (2014) suggested that redox regulates EMT; therefore, it is essential to identify redox-sensitive proteins and one of these proteins was SENP3. The overexpression of this protease was noticed in different types of cancer and was shown to promote cancer cell malignancy, proliferation and metastasis (Han et al., 2010). In their study, Ren group tried to identify the role of SENP3 in EMT in gastric cancer cells, and found that ROS stimulates the

expression of SENP3. Activated SENP3 was found to deSUMOylate the transcription factor FOXC2, which in turn induces the expression of mesenchymal genes, thereby facilitating EMT and cancer metastasis (Ren et al., 2014). Increased transcriptional activity of FOXC2 is correlated with the expression of mesenchymal markers and was highly upregulated in invasive breast cancer (Hollier et al., 2013) and other cancers (Nishida et al., 2011, Yu et al., 2013).

In 2014, Cashman and colleagues used gene expression datasets from 1363 patients to determine the relationship between breast cancer patient survival and the expression of SENP5. They found that high expression levels of this protease were associated with poor prognosis and vice versa. Silencing this protease in breast cancer cell lines inhibited different cellular functions including proliferation and cell migration. When this protease is silenced, the SUMOylation levels of TGFβRI are enhanced leading to the down regulation of the matrix metalloprotease-9 (MMP9) (Cashman et al., 2014).

1.1.7.9 SUMOylation in cell migration

SUMOylation has been implicated in cell migration as it regulates cytoskeletal networks by targeting the basic subunits of actin filaments (F-actin) and microtubules (MT), actin and tubulin, respectively (Panse et al., 2004). It also modifies cytoskeletal regulatory proteins such as members of the Ras GTPase superfamily, including the Rho and Rac1-GTPase (Castillo-Lluva et al., 2010). The building block for F-actins, actin, was found to be SUMOylated at lysine 68 and 284 by SUMO2/3, and its SUMOylation was found to regulate its nuclear localisation (Hofmann et al., 2009). In addition, a proteomic study revealed that tubulin α and β, which are the building blocks of microtubules, were found to be SUMO1

and SUMO3 substrates and their SUMOylation was suggested to facilitate their assembly by preventing their binding with other proteins (Rosas-Acosta et al., 2005).

Rho-family GTPases are critical regulators implicated in many cellular processes, including cell adhesion, cell migration and cell morphology as they promote the formation of different types of actin filament structures (Paterson et al., 1990, Ridley and Hall, 1992). The cytoskeletal actin is regulated by members of the Rho family GTPases, and some of these small GTPases are modified by SUMO proteins. Rac1 and RhoA are critical regulators of actin filaments as they induce the formation of different actin filament structures such as lamellipodia, filopodia, stress fibres and membrane ruffles (Nobes and Hall, 1995). The activity of Rho family GTPases is dependent on their binding to GTP to be active, or to GDP to be inactive. Their binding to GTP, and thus their activity, is regulated by different sets of proteins. GTPase-activating proteins (GAPs) inactivate the target GTPase by promoting hydrolysis of GTP to GDP, while guanine-nucleotide exchange factors (GEFs) activate GTPases by enhancing the exchange of GDP to GTP.

RhoGDIs (Rho GDP-dissociation inhibitor) are another group of proteins that have been implicated in the regulation of subcellular localisation of Rho family GTPases. They bind to their target GTPases and this binding releases these GTPases from the plasma membrane and/or prevents their attachment to it (Dovas and Couchman, 2005). Post-translational modifications have been linked to the regulation of RhoGDIs. For example, phosphorylation of these proteins causes their dissociation from their Rho GTPases (DerMardirossian et al., 2006, Price et al., 2003). Recent studies revealed that SUMOylation is also involved in the

regulation of RhoGDIs. The SUMO-modified lysine residue in RhoGDI is localised at position 138 and SUMOylation of this protein was found to activate it, thus inhibiting Rho-GTPase activity (Liu et al., 2011, Yu et al., 2012). By inhibiting the activity of Rho-GTPases, the formation of F-actin structures is reduced due to the impaired recruitment of the actin-nucleating protein complex Arp2/3, which consequently reduces cell motility (Yu et al., 2012). X-linked inhibitor of apoptosis protein (XIAP) was shown to regulate the SUMO modification of RhoGDI, in which the RING domain of XIAP binds to RhoGDI, and this binding blocks the SUMOylation site within RhoGDI. Thus, the activity of RhoGDI is inhibited and the recruitment of Arp2/3 complex to the cytoplasm is enhanced, which in turn increases the formation of F-actin structures that promote cell migration (Yu et al., 2012).

Arp2/3 complex is another critical regulator of actin, and it functions by binding to previous actin filaments at the leading edge of the membrane and initiating new branches of these filaments. These newly formed actin filaments push the plasma membrane forward, facilitating cell motility. This complex is composed of Arp2 and Arp3 proteins and five smaller proteins called Arcs (Goley and Welch, 2006). Proteomic studies identified that some components of Arp2/3 complex, particularly Arc35p and Arc40p, can be SUMO modified (Sung et al., 2013).

The Rho-family GTPase, Rac1, is essential to cell migration as it regulates the rearrangement of cytoskeletal protein fibres. In epithelial cells, hepatocyte growth factor (HGF) stimulates cell migration as it promotes cell colony spreading by forming the cytoskeletal structures, lamellipodia and membrane ruffles, and disrupting cell-cell

adhesions. Rac1 GTPase was involved in both processes (Ridley and Hall, 1992). SUMOylation was reported to be required for stabilising this GTPase in its active state, and this stable active form is required for cell migration and invasion (Castillo-Lluva et al., 2010). Hepatocyte growth factor, a ligand for the growth factor receptor c-Met and a migration stimulus, promoted the interaction of Rac1 with the SUMO ligase PIAS3 and SUMO1. This interaction enhances the activity of this GTPase and consequently increases cell migration. SUMOylating this GTPase was found to improve its binding affinity to GTP, which increased its active levels and lead to the formation of cell motility-associated structures, lamellipodia and membrane ruffles (Castillo-Lluva et al., 2010). Silencing the SUMO ligase, PIAS3, was found in the same study to be associated with reduction in the formation of lamellipodia and membrane ruffles and cell migration. Therefore, this group hypothesised that this ligase causes these effects by regulating the levels of active Rac1. To test this hypothesis, they compared levels of Rac1-GTP in PIAS3-deficient cells or control in response to HGF treatment. There was no increase in Rac1-GTP levels PIAS3-deficient cells compared to high levels in control, suggesting that PIAS3 was required for its activation. In addition, the phosphorylation and activation of the Rac-signalling mediator, p38, downstream of this GTPase, was reduced in PIAS3- deficient cells. Furthermore, the epidermal growth factor (EGF)-mediated activation of Rac1 was reduced when silencing this ligase, suggesting that SUMOylation of this GTPase occurs in response to various stimuli and is not restricted to HGF only (Castillo-Lluva et al., 2010).

On the other hand, overexpressing PIAS3 increased GTP-binding Rac1 levels compared to control when treated with HGF. However, downregulation of PIAS3 did not affect the levels

of other Rho family GTPases, including Cdc42-GTP, indicating that PIAS3 is a Rac1-specific ligase. Furthermore, PIAS3 efficiently interacted with Rac1-GTP or Rac1V12 (constitutively activated Rac1) rather than GDP-binding Rac1. In addition to regulation of cytoplasmic Rac1 activity, this study also revealed that PIAS3 was co-localised with Rac1 at the leading edge of cells in response to HGF treatment, indicating that this ligase is involved in both regulating the activity of Rac1 in the cytoplasm and in membrane protrusions, revealing the importance of SUMOylation in Rac1-mediated cell migration. The expression of a nonSUMOylatable active form of Rac1 in Rac1-deficient mouse embryonic fibroblasts (MEFs) rescued 45% of defects in lamellipodia and ruffles formation compared to wild type (WT) which rescued up to 85%. However, defects in migration and invasiveness in Rac1-deficient MEFs were not rescued when expressing non-SUMOylated active Rac1 compared to WT. Finally, membrane ruffling and cell migration were not rescued when expressing WT Rac1 in Rac1-deficient MEFs upon silencing PIAS3, indicating that PIAS3 is essential for WT Rac1-mediated rescue of cell migration and membrane ruffles in these cells (Castillo-Lluva et al., 2010).

SUMOylation has been implicated in the regulation of focal adhesions by modifying key proteins involved in their turnover. SUMOylation of FAK was shown to enhance its auto-phosphorylation at Tyr397, which is a critical step in its activation (Kadaré et al., 2003). In a different study, the SUMO E3 ligase PIAS1 was found to interact with FAK in non-small cell lung cancer (NSCLC) cells in the nuclear periphery or within the nucleus. This interaction did not affect the total level of FAK or p-FAK; instead, it changes its subcellular localisation independently from its phosphorylation. Overexpression of PIAS1 and SUMO1 produce a

lower molecular weight form (87 kDa) of FAK, a calpain-mediated cleavage of FAK (Constanzo et al., 2016). Because of the negative regulation of this cleavage product at FAs, they assumed that PIAS1 might be involved in regulating the dynamic of focal adhesions. Reduced expression of PIAS1 decreased the turnover of FAs and increased the sensitivity of cells to apoptosis by increasing pro-apoptosis proteins. In addition, silencing this ligase in NSCLC cells reduced the polymerisation of actin filaments and decreased the localisation of vinculin at focal adhesions. On the other hand, overexpressing PIAS1 induced the localisation of FAK at the nucleus and rescued the loss of vinculin at focal adhesions and polymerisation of F-actins (Constanzo et al., 2016). Additionally, Talin and Vinculin were identified in a recent screening study for SUMO substrates during mouse spermatogenesis to be targets of SUMOylation (Xiao et al., 2016). From these findings, it can be concluded that SUMOylation is critical in cell migration by regulating cytoskeletal network dynamics and FAs turnover. Both functions are necessary for efficient cancer cell migration.

Overall, SUMOylation has been implicated in the modification of proteins involved in both normal and pathological cellular processes. SUMOylation has been associated with regulation of cancer cell migration by regulating the dynamics of F-actin structures (Castillo-Lluva et al., 2010) and the activity of MMPs (Lao et al., 2019). Overexpression of SUMO and SUMO-associated proteins was shown to enhance the turnover of FAs and cell migration (Constanzo et al., 2016). In addition, the SUMOylation of FAK indicates the involvement of SUMOylation in the regulation of FA dynamics although the SUMOylation of this kinase was found to take place in the nucleus (Constanzo et al., 2016). Furthermore, the FA proteins talin and vinculin were identified in a proteomic study to be among SUMO substrates (Xiao

et al., 2016). SUMOylation was also shown to regulate the activity of other FAs regulators such as phosphorylation and protease-mediated cleavage of focal adhesion proteins (Kadaré et al., 2003, Constanzo et al., 2016). However, the exact role of SUMOylation in the regulation of FAs and cell migration remains poorly understood. Moreover, since SUMOylation has been discovered, more and more SUMO substrates are being identified consciously. More than 200 proteins with different functions have been identified in FAs (Horton et al., 2015). Some of these proteins could be regulated by SUMOylation and investigating the role of SUMOylation in the regulation of these adhesion structures will increase our understanding of the regulation of FAs adhesions in cancer cells. It could also facilitate the identification of promising therapeutic targets, which can then be developed to intervene with cancer metastasis.

1.2 Aims

The hypothesis of this project is that SUMOylation contributes to cancer metastasis by regulating focal adhesions. To test this hypothesis several approaches were taken. The first aim of this project is to accomplish in vitro investigations of the role of SUMOylation in the regulation of FA dynamics and consequently cancer cell migration. SUMOylation inhibitors were used to inhibit SUMOylation in MDA-MB-231 cells, and the effects of its inhibition on their migration were assessed using the cell migration assays, wound healing and cell tracking. These inhibitors were also used to evaluate the effects of inhibiting SUMOylation on the dynamics of focal adhesions. The second aim of this project is to investigate the involvement of SUMOylation in the regulation of FA dynamics and cell migration using a different approach, down regulating the SUMO specific proteases SENP2 and SENP5. siRNA

transfection was used to knockdown SENP2 or SENP5 and cell migration assays and confocal microscopy were used to evaluate the effects of silencing these proteases on MDA-MB-231 cancer cell migration and FA dynamics. Another approach was to investigate the effects of preventing SUMOylation of an individual FA protein on FA dynamics and cancer cell migration without affecting global SUMOylation. Site-directed mutagenesis was used to replace lysine residues in SUMOylation motifs in vinculin. Confocal microscopy was used to monitor the dynamics of FAs and cell migration of cancer cells expressing the mutated version of vinculin. The final aim of this project was to investigate the effects of these mutations on vinculin-talin interaction using Co-IP and FRET assay.

2. Materials and Methods

2.1 Materials

2.1.1 Tissue culture

Table 2-1 List of reagents used in tissue culture

Reagent	Catalog No.	Supplier
Dulbecco's Modified Eagle's Medium (DMEM)	11880-028 and A14430-01	Gibco
Dulbecco's Phosphate Buffered Saline (PBS)	10010-023	Gibco
Eagle's Minimum Essential Medium (EMEM)	30-2003™	ATCC
Fetal Bovine Serum (FBS)	10500-064	Gibco
L-Glutamine	25030-081	Gibco
Penicillin /Streptomycin	15140-122	Gibco
Trypsin-EDTA 0.05%	25300-054	Gibco

2.1.2 SUMOylation effects on FA dynamics and cell migration

Table 2-2 List of reagents used for studying SUMOylation effects on FA dynamics and cell migration

Reagent	Catalog No.	Supplier	Usage
Collagen type 1	2561888	Millipore	Surface coating
DMSO (Dimethyl Sulphoxide)	D8418-1L	Sigma Aldrich	Vehicle control
Fibronectin	F0162-.5MG	Sigma Aldrich	Surface coating
Gelatine	G-6650	Sigma Aldrich	Surface coating
Ginkgolic acid C15:1	75741-5MG	Sigma Aldrich	SUMOylation inhibitor
Gossypetin (3,5,7,8,3',4'-Hexahydroxyflavone)	G500	INDOFINE Chemical Company	SUMOylation inhibitor

2.1.3 Immunoprecipitation and western blot

Table 2-3 List of reagents used in protein lysis, immunoprecipitation and western blot (WB)

Reagent	Catalog No.	Supplier	Usage
30% ProtoGel	EC-890	National diagnostics	SDS-PAGE gel cast
Ammonium persulfate	17874	Thermo Scientific	SDS-PAGE gel cast
Bradford	B6916-500 ml	Sigma Aldrich	Bradford assay
Clarity Western ECL Blotting Substrate	1705060	BIO-RAD	WB
RIPA buffer 250 ml	89901	Thermo Scientific	Total protein harvesting
ReBlot Plus Mild Antibody Stripping Solution (10X)	2502	Millipore	WB
Protease Inhibitor Cocktail	539131	Millipore	Total protein harvesting
Protein A/G Agarose	sc-2003	Santa Cruz	Immunoprecipitation
Phosphate Buffered Saline (PBS) Tablets	1282-1680	Fisher Scientific	WB
Glycine	10061073	Fisher Scientific	SDS-PAGE gel cast/ WB
Methanol	10653963	Fisher Scientific	WB/immunostaining
Polyvinylidene Difluoride (PVDF) membrane	10600023	GE Healthcare Life Sciences	WB
Precision Plus ProteinTM Dual Colour Standards	161-0374	BIO-RAD	WB
Skimmed Milk Powder	70166-500G	Sigma Aldrich	WB
Sodium Dodecyl Sulphate (SDS)	10593335	Fisher Scientific	SDS-PAGE gel cast
Tris-base	10103203	Fisher Scientific	SDS-PAGE gel cast/ WB
Tetramethylenediamine (TEMED)	T9281-25 ml	Sigma Aldrich	SDS-PAGE gel cast

Sodium Chloride (NaCl)	10428420	Fisher Scientific	SDS-PAGE gel cast/ WB
Tween 20	P1379-500ML	Sigma Aldrich	WB
Potassium Chloride (KCl)	10375810	Fisher Scientific	SDS-PAGE gel cast/ WB
Bovine Serum Albumin Powder (BSA)	11413164	Fisher Scientific	WB

2.1.4 Immunostaining

Table 2-4 List of reagents used in immunocytochemistry

Reagents	**Catalog No.**	**Supplier**
Goat Serum	16210-064	Gibco
Paraformaldehyde, 96%, ACROS Organics™	AC416785000	Fisher Scientific
Triton 100X	T-8787	Sigma Aldrich
VECTASHIELD® Antifade Mounting Medium with DAPI	H-1200	Vector laboratories
VECTASHIELD® Antifade Mounting Medium	H-1000	Vector laboratories

Table 2-5 List of primary antibodies used in immunocytochemistry and WB

Primary Antibody	**Dilution**	**Host species**	**Catalog No.**	**Supplier**
Anti-Actin	1:2000 WB 1:100 IHC	Mouse monoclonal	Ab3280	Abcam
Anti-FAK	1:1000 WB 1:100 IP	Mouse monoclonal	611722	BD Bioscience
Anti-GAPDH	1:1000 WB	Mouse monoclonal	Ab8245	Abcam
Anti-GFP	1:2000 WB 1: 100 IP	Rabbit polyclonal	A11122	Thermo Scientific
Anti-Ha	1:5000 WB 1:300 IP	Mouse monoclonal	26183	Thermo Scientific

Rabbit IgG	1:100 IP	Rabbit	I-1000	Vectorlabs
Anti-Paxillin	1:1000 WB 1:100 IP	Mouse monoclonal	Ab23510	Abcam
Anti-SENP2	1:1000 WB 1:100 IP 1:100 IHC	Rabbit polyclonal	Ab58418	Abcam
Anti-SENP2	1:1000 WB 1:100 IP 1:100 IHC	Rabbit polyclonal	Ab96865	Abcam
Anti-SENP5	1:1000 WB 1:100 IHC	Rabbit polyclonal	Ab58420	Abcam
Anti-SUMO2/3	25:1000 WB 5:100 IP 1:100 IHC	Mouse monoclonal	Sc-393144	Santa Cruz
Anti-SUMO2/3	1:1000 WB 1: 100 IP 1:200 IHC	Rabbit polyclonal	Ab109005	Abcam
Anti-Ubc9	1:100 IHC	Mouse monoclonal	Sc-271057	Santa Cruz
Anti-Talin	20:1000 WB 5:100 IP	Rabbit polyclonal	Sc-15336	Santa Cruz
Anti-Talin	1:1000 WB 1:100 IP	Mouse monoclonal	MAB1676	Millipore
Anti-Vinculin	1:100 IHC 1:1000 WB	Mouse monoclonal	Ab18085	Abcam

Table 2-6 List of secondary antibodies used in WB and immunocytochemistry

Secondary antibody	Catalog No.	Supplier
Alexa FluorTM 488 Goat anti-mouse IgG	A11001	Invitrogen
Alexa FluorTM 488 Goat anti-rabbit IgG	A11034	Invitrogen
Alexa Fluor® 546 Goat anti-mouse IgG	A11003	Life Technologies
Alexa Fluor® 546 Goat anti-rabbit IgG	A11010	Life Technologies
Goat anti mouse HRP	7076S	Cell signalling
Goat anti rabbit HRP	7074S	Cell signalling
Cell lightTMTalin GFP	C10611	Thermo Scientific

2.1.5 Construction of pZsYellow1-vinculin and pAmCyan1-SUMO2 or SENP2

Table 2-7 List of reagents used in construction of plasmids

Reagent	Catalog No.	Supplier	Usage
2-Propanol (isopropanol)	I9516	Sigma Aldrich	DNA Extraction
BamHI restriction enzyme	R6021	Promega	Digestion
EcoRI restriction enzyme	R6011	Promega	Digestion
EZ-10 Column and collection tube	SD5005	Bio Basic	DNA Extraction
FastAP Thermosensitive Alkaline Phosphatase (1 U/µL)	EF0651	Thermo Scientific	Dephosphorylation
FastDigest EcoRI restriction enzyme	FD0274	Thermo Scientific	Digestion
FastDigest SalI restriction enzyme	FD0644	Thermo Scientific	Digestion
GeneRuler 1 kb Plus DNA Ladder, ready-to-use	SM1333	Thermo Scientific	Gel Electrophoresis
Glycerol	G7893	Sigma Aldrich	Glycerol stock
HindIII restriction enzyme	R6041	Promega	Digestion
LB Broth (Miller)	L3522	Sigma Aldrich	Growth Medium
LB Broth with agar (Miller)	L3147	Sigma Aldrich	Growth Plates
pAmCyan1-C1 Vector	632441	Clontech	Expression Vector
Phusion Green Hot Start II High-Fidelity PCR Master Mix	F566L	Thermo Scientific	PCR
pZsYellow1-C1 Vector	632444	Clontech	Expression Vector
QIAprep Spin Miniprep Kit	27104	QIAGEN	DNA Extraction
QIAquick Gel Extraction Kit	28115	QIAGEN	DNA Extraction
QIAquick PCR Purification Kit	28104	QIAGEN	DNA Extraction
RevertAid H Minus First Strand cDNA Synthesis Kit	K1631	Thermo Scientific	cDNA Synthesis

RNeasy Mini Kit	74104	QIAGEN	RNA Extraction
SmaI restriction enzyme	R6121	Promega	Digestion
SalI restriction enzyme	R6051	Promega	Digestion
SYBR™ Safe DNA Gel Stain	S33102	Thermo Scientific	Gel Electrophoresis
DNA Gel Loading Dye (6X)	R0611	Thermo Scientific	Gel Electrophoresis
T4 DNA Ligase (1 U/µL)	15224017	Thermo Scientific	Ligation
TAE Buffer (Tris-acetate-EDTA) (50X)	B49	Thermo Scientific	Gel Electrophoresis
TurboFect plasmid Transfection Reagent	R0531	Thermo Scientific	Transfection Reagent
UltraPure™ Agarose	16500500	Thermo Scientific	Gel Electrophoresis

2.2 Methods

2.2.1 Cell culture

2.2.1.1 Cell growth

In this project, three cell lines from the American Type Culture Collection (ATCC) were used.

Cell line	Cancer type
MDA-MB-231	Human breast cancer
HT1080	Human fibrosarcoma
ACHN	renal cell adenocarcinoma

Reagents were prewarmed in a 37°C water bath before use and cell culturing was performed in a sterilised culture hood. MDA-MB-231 or HT1080 cells were cultured in 75 cm^2 or 25 cm^2 flasks in Dulbecco's Modified Eagle Medium (DMEM), while ACHN cells were cultured in Eagle's Minimum Essential Medium (EMEM). Both media were supplemented with 1% streptomycin (100 IU/ml)/penicillin (100 µg/ml) and 10% Fetal Bovine Serum (FBS). Cells were maintained in 37°C in 5% CO_2 and were allowed to grow until they reached ~90% confluency (2-3 days). Then, media were discarded, and cells were washed with phosphate-buffered Saline (PBS) before trypsinising them with 1-3 ml of 1x trypsin-EDTA 0.05% for 3-5 minutes to detach them from flasks. Next, cells were resuspended in a fresh medium (3-6 ml) to deactivate trypsin and 20% of cells were transferred to a new flask containing 20 ml of fresh DMEM medium.

2.2.1.2 Freezing and thawing

In order to store cells for longer periods, media of 80-90% confluent flasks were discarded before washing cells with PBS. Then, cells were detached from the flask by adding 1-3 ml of 0.05% trypsin-EDTA and incubating at 37°C in 5% CO_2 for 3-5 minutes. Following deactivation of trypsin by resuspending cells in 3-6 ml fresh media, cells were transferred into a 15 ml falcon tube and centrifuged at 1000 g for 5 minutes. The supernatant was discarded and the pellet was washed with PBS and centrifuged again, and the supernatant was discarded. Then, the pellet was resuspended in 5 ml FBS containing 10% DMSO and the mixture was aliquoted into cryo vials (1 ml in each vial). Vials were placed in a Mr Frosty container with 100% isopropyl alcohol and stored at -80°C overnight. The next day, vials were transferred to liquid nitrogen.

For culturing stored cells, cell vials were thawed in a 37°C water bath for 1-3 minutes. Then, 1 ml of cells was transferred into a 15 ml falcon tube containing 5 ml PBS and centrifuged at 1000 g for 5 minutes to remove DMSO. The supernatant was then discarded, and the pellet was resuspended in 2 ml of fresh medium and the mixture was transferred to a 75 cm^2 or 25 cm^2 flask and incubated at 37°C in 5% CO_2. The next day, the medium was removed and replaced with fresh medium and cells were grown until they reach 80-90% confluency (2-3 days) before splitting.

2.2.1.3 Cell counting

Cell counting was performed using a haemocytometer slide and an inverted light microscope (Leitz Labovert). After resuspending trypsinised cells in medium, cell suspension was vortex briefly and 10 µl of it was loaded into the chambers in the space between the slide and the coverslip. The haemocytometer was placed under a 10X objective lens and cells in the 4 squares at slide corners were counted and the number of cells/ml was calculated according to the following equation:

Number of cells/ml = (total number of cells counted/ number of squares) X 10^4 X dilution factor

2.2.1.4 Preparation of ECM components' coated surfaces

Collagen Type I, Rat Tail was purchased from Merck Millipore at a concentration of 3.9 mg/ml and stored at 4°C and kept on ice during preparation. Collagen mixture was prepared using 100 µl of 10X DMEM (Gibco), 512 µl of collagen type I and 20 µl of 1 M of Sodium Hydroxide (NaOH) to give pH 8; it was completed to 1 ml by normal media to give a final concentration of 2mg/ml collagen. These components were mixed properly and were added

to wells of tissue culture on 6, 12 or 24 well plates, incubated for 5 minutes at 37°C in 5% CO_2 before seeding cells.

Fibronectin was purchased from Sigma, dissolved in sterile PBS to make a stock solution of 150 µg/ml and stored at -20°C and kept on ice during preparation. For fibronectin coating, 15 µg/ml of fibronectin was prepared, by diluting stock solution in PBS, and applied to each well in the 6-well, 12-well or 24-well plates. Then, the plates were kept in the hood for 1 hour before discarding the solution and washing with PBS three times. Next, the cells were seeded on wells and incubated at 37°C in 5% CO_2 until the next step.

Gelatin was purchased from Sigma and 0.1% gelatin in ddH_2O was prepared, autoclaved and stored at 4°C. The solution was prewarmed at 37°C and coating was performed in a sterile hood. For the 6-well or 12-well plate coating, 2 ml or 1 ml of 0.1% gelatin were added to each well respectively and incubated for 30 minutes at room temperature. Following that, gelatin was aspirated and plates were left to dry for 1 hour at room temperature or 30 minutes at 37°C before seeding cells.

2.2.2 Cell migration assays

2.2.2.1 Wound healing assay

After the cells were trypsinised and re-suspended in 4 ml of media to de-activate the trypsin, the cells were counted using a haemocytometer. For 12-well plates, $2x10^5$ cells were seeded in each well and were allowed to grow at 37°C in 5% CO_2 until they reach 90-100% confluency (2-3 days). Then, the cells were treated with different concentrations (10,

25, 50 and 100 µM) of SUMOylation inhibitors, Ginkgolic acid or Gossypetin, or vehicle control (DMSO, 1 µl/ml) for 2 hours. Next, the cells were wounded using 200 µl tips, a medium containing either inhibitor or DMOS was aspirated, cells were washed with PBS and 1.5 ml of fresh medium was added to each well. Wounds were visualised using an inverted microscope using a 10x objective lens. Three random wound spots for each well were photographed at time points, 0 and 24 hours. Image J (Fiji) software was used to calculate the percentage of wound closure area for each group. A polygon selection tool in image J was used to select the wound area and an analysis/measuring tool was used to measure this area at different time points. The wound closure was calculated according to the following equation:

% wound closure = (wound area at 0 hours – wound area at 24 hours) / wound area at 0 hours X 100.

A GraphPad Prism was used to compare the % wound closure of the inhibitor treated cells to those of the three independent experimental controls. One-way ANOVA with Tukey's Multiple comparison test was used to evaluate any significant differences between groups.

2.2.2.2 Single cell tracking

Cells were seeded in non-coated, 1% gelatin or 2 mg/ml collagen-coated wells in a 12-well plate with a density of $1x10^4$/well and allowed to grow and adhere at 37°C in 5% CO_2. After incubating overnight, cells were treated with inhibitors, Ginkgolic acid (25 µM) or Gossypetin (100 µM), or DMSO (1 µl/ml) and incubated for 2 hours before changing the medium for fresh medium. A Nikon Eclipse TiE Time lapse microscope running NIS elements AR4.10 software was used to capture images using a 10x objective lens for random spots of

cells every 15 minutes for 24 hours. MtrackJ plugin tool in Image J (Fiji) software was used to track single cells and measure their speed and travelled distance. At least forty cells were tracked randomly for each group. GraphPad Prism was used to compare the mean speed measurements of inhibitor treated cells to that of control in the three independent experimental. One-way ANOVA with Tukey's Multiple comparison test was used to evaluate any significant differences between groups.

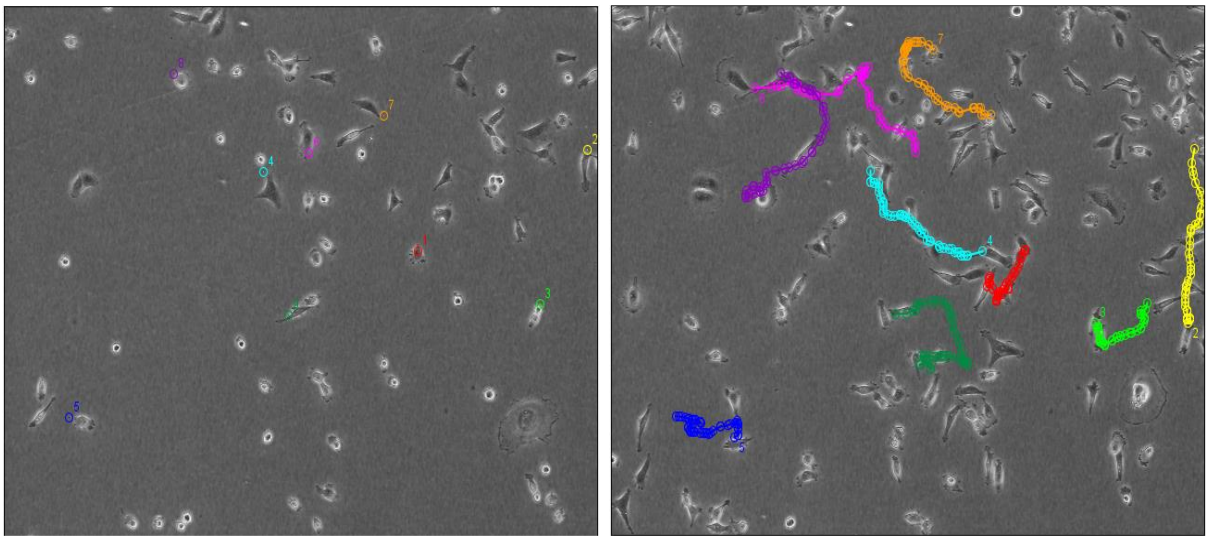

Figure 2.1 Representative images showing Manuel cell tracking using MtrackJ ImageJ plugin. Each cell was tracked in a stepwise manner and denoted with a coloured number. Track measurements were generated and saved in Excel format. Cell speed was calculated by dividing the travelled distance by time.

2.2.3 Immunostaining

Sterilised cover slips were placed in a 6-well plate and 2 ml of 100% methanol was added to each well for 20 minutes to further sterilise them. After that, methanol was aspirated and wells were allowed to stand to dry for 30 minutes in a sterilised culture hood before coating with 0.1% gelatin. Then, the gelatin was discarded and the wells were left to dry in the hood for 1 hour and washed with PBS before seeding $2x10^5$ cells in each well and growing them

overnight. The next day, cells with 80-90% confluency were washed with PBS and fixed with 2 ml/well of 4% (w/v) paraformaldehyde (PFA) for 15 minutes. PFA was aspirated and cells were washed three times with PBS, for 10 minutes each time. Two ml of 0.2% (v/v) Triton-X100 - PBS was added to each well for 15 minutes before repeating the washing steps. The cells were then blocked with 10% (v/v) goat serum – PBS for 1 hour and primary antibodies were incubated with cells overnight at 4°C (1:100 v/v diluted in 2% goat serum - PBS). After washing three times, fluorescent secondary antibodies were incubated with cells for 1 hour in light protected champers (1:100 v/v in 2% goat serum - PBS). Cover slips were then washed three times with PBS and mounted onto glass slides using VECTASHIELD Mounting Medium with DAPI before sealing cover slip edges with nail polish. Slides were visualised and imaged using confocal microscopy or stored at 4°C. Image J (Fiji) software was used to analyse the distribution and localisation of proteins of interest within cells.

2.2.4 Immunoprecipitation and western blot

2.2.4.1 Preparation of cell lysate

Cells were grown in 25 cm^2 or 75 cm^2 flasks until they reach a confluency of more than 90% to extract the total protein lysates. After washing the cells with chilled PBS, they were collected by scraping into 3-5 ml PBS and transferred into 15 ml falcon tubes. Cells were then centrifuged at 4°C at 1500 g for 15 minutes and supernatants were discarded. the pellets were resuspended in 400 µl of lysis solution buffer composed of RIPA buffer (25 mM Tris-HCl pH 7.6, 150 mM NaCl, 1% NP-40, 1% sodium deoxycholate and 0.1% SDS) and 1% protein inhibitor cocktail (Sigma) and passed through 21 gauge needles several times to shear DNA. Later, the suspension was incubated on ice for 30 minutes before transferring to

1.5 ml Eppendorf tubes and centrifuging at 13000 g for 15 minutes. Supernatants were collected in a fresh tube and were used the same day or stored at -20°C.

2.2.4.2 Bradford assay

Bradford protein assay was used to measure the quantity of total protein concentration in the cell lysates. Coomassie Brilliant Blue G-250, a component of the Bradford reagent, interacts with proteins and consequently a blue solution is formed. The intensity of this solution depends on the protein concentration in the samples; a higher protein concentration increases the intensity of the blue solution.

A 96-well plate was used to perform this experiment. In the first column, 195 µL of Bradford reagent was applied to each well (A-H). In the second and third columns, 195 µL of Bradford reagent and 5 µL of ascending concentrations of bovine serum albumin (25-2000 µg/ml) were added to each well to produce a standard curve. The remaining wells were used to mix 5 µL of lysates with 195 µL of Bradford reagent, three replicates for each lysate. A plate reader, the E max Molecular Device, was used to read the absorbance at 600 nm. This reader determines the protein concentration of each well and calculates the mean of total protein concentration (µg/ml) in each lysate.

2.2.4.3 SDS-PAGE /western blot analysis

2.2.4.3.1 Preparation of SDS-PAGE

Two glass plates separated by a 1.5 mm spacer were used to cast SDS gels, which are composed of two layers; 10% resolving gel and 5% stacking gel. Resolving and stacking gels were prepared as described below:

Solution	Components
Preparation of 25 ml of 10% Resolving gel	9.9 ml ddH2O 8.3 ml of 30% Acrylamide mix 6.3 ml of 1.5 M Tris (pH 8.8) 0.25 ml of 10% SDS 0.25 ml of 10% ammonium persulfate 0.01 ml of TEMED
Preparation of 8 ml of 5% Stocking gel	5.5 ml ddH2O 1.3 ml of 30% Acrylamide mix 1.0 ml of 1 M Tris (pH 6.8) 0.08 ml of 10% SDS 0.08 ml of 10% ammonium persulfate 0.008 ml of TEMED

The resolving gel was then added to the cassette and left to polymerise for 30 minutes before adding the stacking gel on top of the resolving gel. A comb of 2.5 cm depth with 10 wells was placed into the stacking gel immediately after adding it. Gels were then left to polymerise for 1-2 hours before being used or they can be stored at 4 °C for 2-4 days until the next step.

2.2.4.3.2 SDS-PAGE buffers

Solution buffers used in WB were prepared as described below:

Solution	Components
500 ml of 10X SDS	50g of SDS in 450 ml ddH2O

1L of 5X Running buffer (Tris –Glycine electrophoresis)	15.1 g of Tris base, 72.1 g of glycine, 50 ml of 10X SDS in 950 ml ddH2O
1L of 1X Running buffer	200 ml of 5X Running buffer and 800 ml ddH2O
1L of 1X transfer buffer	2.8 g of Tris base, 2.9 g of Glycine, 200 ml of methanol in 800 ml ddH2O
1L of 10X Tris Buffer Saline (TBS)	30 g of Tris base, 80 g of NaCl, 2g of KCl in 800 ml ddH2O. pH was adjusted to 7.4 using HCL before completing to 1 L with ddH2O
1L of 1X TBS Tween (TBST)	100 ml of 10 TBS, 900 ml ddH2O and 1 ml of Tween 20

2.2.4.3.3 SDS-PAGE gel running/western blot

Cell lysates were prepared as previously described in 2.2.4.2 and SDS-PAGE was used to separate proteins depending on their size. 25 µl of 5X (v/v) loading buffer was mixed with 100 µl of sample, boiled for 4-5 minutes at 95°C to denature proteins and stored at -20°C until needed. To separate proteins depending on their size, 20-60 µg of protein concentration from each lysate was loaded into 10% hand cast SDS-PAGE gel after filling it with 1X running buffer. A molecular weight marker (Precision Plus Protein™ Prestained Standard (Bio-Rad)) was used to gauge bands. Electrical current was applied to the running tank (3 mA/180 V for one gel and 6 mA/180 V for two gels) for 1-1.30 hours depending on the spreading of the molecular weight marker on the gel. After that, the gel was removed from the running tank and incubated for 20 minutes in 1X transfer buffer. Three filtered papers (8*8 cm) were submerged in 1X transfer buffer and put on the Trans-Blot® SD semi-dry transfer cell (Bio-Rad). The Polyvinylidene difluoride (PVDF) Membrane (8*8 cm), which has a 0.45 mm pore size, was submerged in methanol for 30 seconds and then washed in

ddH_2O and put on top of these filter papers. The gel was then placed over the membrane and three further filter papers were placed on top of the gel. Electrical current was applied for 2 hours at 5 mA/250 V. Later, the membrane was blocked with 5% w/v low fat milk, dissolved in Tris-buffered Saline Tween (TBST), for one hour with agitation. Then, the membrane was washed three times with TBST before incubating with primary antibody (1:1000 in 5% w/v low fat milk-TBST) overnight at 4°C on shaker. The next day, the membrane was washed with TBST three times (10 minutes each) and incubated with secondary antibody (1:3000 in 1% w/v low fat milk-TBST) for one hour at room temperature with agitation and then washed three times with TBST. Clarity TM Western ECL Blotting Substrate reagents A and B. One ml of ECL plus reagent A was mixed with 1 ml of reagent B for 10 minutes and 1 ml of the mixture was added to each membrane before putting it in the detection machine. The bands on the membrane were visualised using an Image Quant LAS 4000 mini-GE Healthcare machine and quantified using Image Quant TL 8.1 software.

2.2.4.4 Co-immunoprecipitation (Co-IP)

A Co-IP approach was used to investigate protein-protein interaction using antibodies and A/G PLUS-Agarose beads (Santa Cruz Biotechnology). It was used in this study to study the interaction between SUMO and SUMO-associated proteins and FA proteins. After measuring the total protein in extracted lysates, 250-500 µg of protein concentration from the cell lysates was mixed with 2 µg of antibodies and incubated overnight at 4 °C with agitation. Protein A/G PLUS-Agarose beads were used to precipitate the antibody-antigen complex (20 µl of beads for each IP sample). Beads were pelleted and washed three times with 300 µl of RIPA buffer and centrifuged after each wash step at 2000 g for 1 minute. Next, the beads pellet was re-suspended in 500 µl RIPA buffer and 100 µl of beads solution was added to

each sample and incubated at 4°C for 2 hours with rotation. Following that, samples were centrifuged at 2000 g for 1 minute and the supernatants were discarded. Bead pellets were washed and centrifuged three times in the same conditions. Then, the pellets were resuspended in 60 µl of 5X (v/v) loading buffer and mixtures were boiled at 95°C for 5 minutes to detach proteins from agarose beads. Finally, samples were centrifuged, supernatants were collected and stored at -20°C until the next step and beads were discarded. Samples were run on SDS-PAGE gel and WB was used to detect the presence of protein of interest in IP samples.

2.2.5 Construction of pZsYellow1-tagged vinculin and pAmCyan1-C1-tagged SUMO2 or SENP2 plasmids

2.2.5.1 RNA extraction

RNA extraction was performed as described in the RNeasy Mini kit (Qiagen) Handbook. MDA-MB-231 cells were grown in 75 cm^2 and incubated at 37°C at 5% CO_2 until the confluency became 80-90%. Then, the cells were washed with PBS and trypsinised and 3 ml of fresh medium was added to cells before centrifuging at 300 g for 5 minutes. The pellet was resuspended in 600 µl of Buffer RLT and the lysate was homogenised by passing it the through a 20-gauge needle several times. After that, 600 µl of 70% ethanol was added to the homogenised lysate and mixed by pipetting. 700 µl of this mixture was applied to the RNeasy spin column before centrifuging for 15 sec at 8000 g. The flow-through was discarded and the rest of the lysate was added to the column and centrifuged again in the same conditions. Then, 350 µl of RW1 buffer was added to the column and centrifuged for 15 sec. 80 µl of DNase incubation mix (10 µl of DNase I stock solution + 70 µl of RDD buffer)

was added to the column and incubated for 15 min at room temperature. 350 µl of RW1 buffer was added to the column before centrifuging again in the same conditions. 500 µl of RPE buffer was added to the column to wash it and centrifuged for 15 sec. The same amount of this buffer was applied to the column before centrifuging for 2 minutes. The column was centrifuged again for 1 min to remove any remaining residual wash buffer. Finally, the column was placed on a sterile Eppendorf collection tube and 40 µl of RNase-free water was added to the column before centrifuging for 1 minute to elute RNA. A nano drop device was used to measure the concentration of RNA in the lysate. Extracted RNA was stored at -20°C until the following step or stored at -80°C for a longer period.

2.2.5.2 cDNA synthesis

First strand cDNA synthesis was carried out according to the handbook of Revert Aid H minus standard cDNA synthesis kit protocols. One µg of total RNA was incubated with a 0.50 µg mixture of oligo $(dT)_{18}$ primer (0.25 µg) and random hexamer primer (0.25 µg) and ddH_2O was added to a total volume of 12 µl. Then, the reagents described in the following table were added to this mixture to a final volume of 20 µl.

Table 2.8 List of reagents used in cDNA synthesis

Reagent	Volume
5X Reaction buffer (250 mM Tris-HCl (pH 8.3), 250 mM KCl, 20 mM $MgCl_2$, 50 mM DTT)	4 µl
RiboLock RNase inhibitor (20 U/µl)	1 µl
10 mM dNTP Mix	2 µl
RevertAid H minus M-Mul V Reverse Transcriptase (200 U/µl)	1 µl
Total volume	20 µl

The mixture was incubated for 5 minutes at room temperature before incubating at 42°C for 1 hour to synthesise the first strand of cDNA. Then, the reaction was incubated at 70°C for 5 minutes to inactivate the reverse transcriptase. Then, the synthesised cDNA was used as a direct templet in a polymerase chain reaction (PCR) to amplify genes of interest or stored at -20°C.

2.2.5.3 Polymerase chain reaction (PCR)

Primers were designed using Primer3Plus server (http://www.bioinformatics.nl/cgi-bin/primer3plus/primer3plus.cgi) and synthesised by the Sigma Aldrich company. Primers were designed to include random buffering nucleotides proceeding restriction enzyme sites at the 5' of primers. Restriction enzymes were selected according to their presence in vector plasmid and absence in genes of interest to avoid unwanted cuts in the gene sequence. Several restriction enzymes have single cut sites in vector plasmids (Figure 2.2).

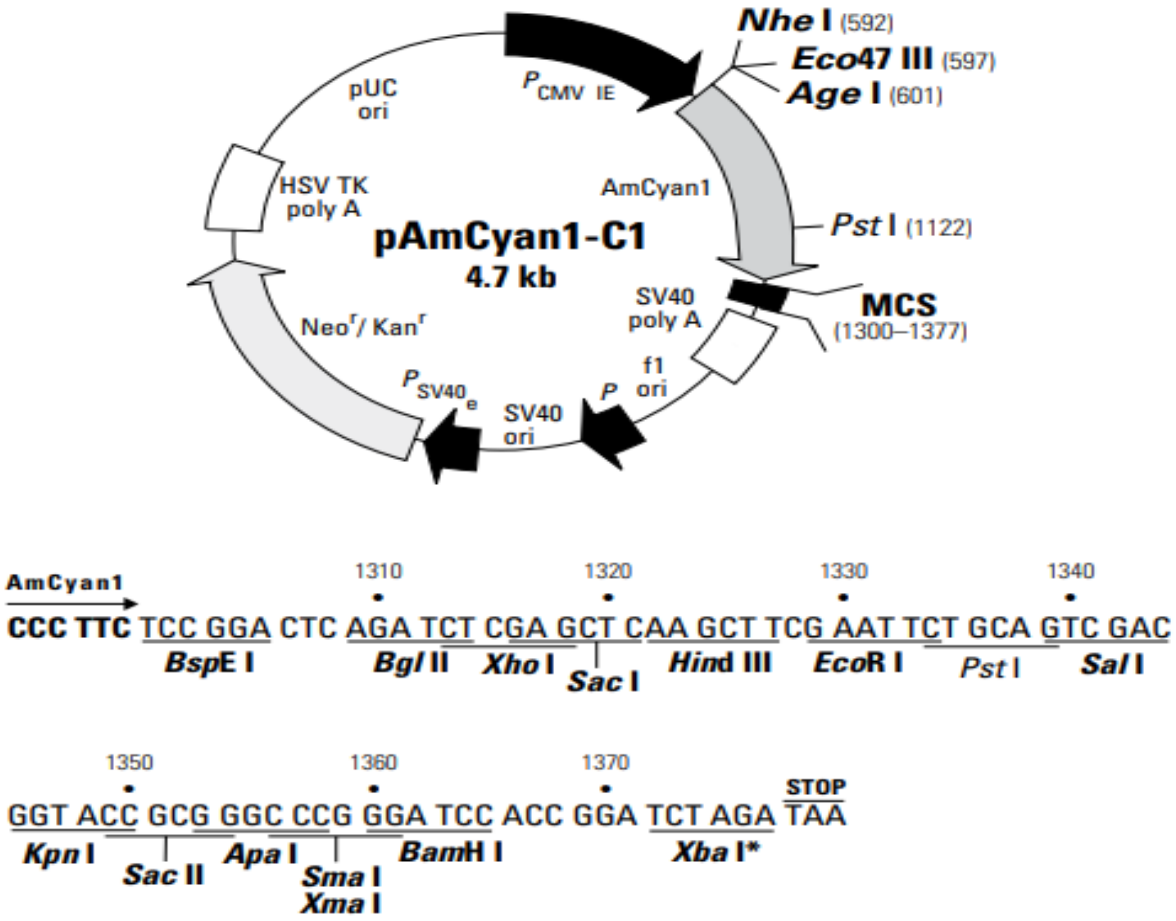

Figure 2.2 Map of pAmCyan1-C1 expression vector. The diagram is showing the available restriction enzyme sites in a multiple cloning site (MCS). A single site for each restriction enzyme was designed (provided by Clontech).

A NEBcutter V2.0 tool (http://nc2.neb.com/NEBcutter2/) was used to screen gene sequences for restriction sites of restriction enzymes that have sties in vectors. Two different restriction enzymes that do not have sites in gene sequences were selected for each gene. Cutting sites for those enzymes were added to the 5' end of gene primers.

Table 2.9 showing primers used in PCR to amplify SUMO2, SENP2 or vinculin. Gene primers are highlighted with cyan; restriction enzyme sites are highlighted with green and buffering random nucleotides are highlighted with yellow.

Gene	Forward primer 5'-3'	Reverse primer 5'-3'	Product size (bp)
SUMO2	TCTAGAATTCTACCTCTTTTGTGAAGCGGC	TAGACCCGGGAGTCAGGATGTGGTGGAACC	400
SENP2	GCGAAGCTTGGTGGTTAAGACGGCGAAG	CGCGAATTCGCGTTTGTTCTTGTGTGGGT	2000
Vinculin	CGCGTCGACGTCGCTGCACAGTCTGTCT	GCGCCCGGGTTCAGCTCCCAGCAACTCTG	3400

The synthesised cDNA was used as a direct templet in a polymerase chain reaction (PCR) to amplify SENP2, SUMO2 or vinculin genes with their specific primers (Table 2.9). The PCR reaction was prepared according to the Phusion Hot Start II High-Fidelity PCR Master Mix manual (Thermo Scientific). Reaction components were prepared as described below.

2X Phusion HS II HF Master Mix	10 µl
Forward Primer (10 µM)	1 µl
Reverse Primer (10 µM)	1 µl
cDNA	2 µl
Distilled Water	6 µl
Total Volume	20 µl

Cycling instructions were programmed as described below:

Step	Temp. °C	Time	Cycles
Initial Denaturation	98°C	1 minute	1
Denaturation	98°C	10 sec	39
Annealing	63°C	30 sec	
Extension	72°C	30 sec/kb	
Final extension	72°C	7-10 minutes	1
Hold	4°C	Hold	1

PCR products were separated by size using gel electrophoresis. 1% agarose gel matrix was prepared in a 1x TAE buffer and heated until it dissolved. After the solution cooled to ¬60°C, SYBR® Safe DNA gel stain was added to the mixture (1µ per 10 ml). DNA was loaded to the gel and was subjected to electrophoresis at 60 V for 1 hour. DNA bands were visualised using U:Genius3 (SYNGENE). Bands were gauged using the GeneRuler 1 kb Plus DNA Ladder, ready-to-use (Thermo Scientific).

2.2.5.4 Digestion

pAmCyan1-C1 and pZsYellow1-C1 expression vectors were purchased from Clontech. PCR products of SUMO2, SENP2 and vinculin were extracted and purified from agarose gel. Selected restriction enzymes were used to linearise vectors and cut the ends of genes leaving sticky ends for insertion into vectors. Extracted PCR products were digested alongside pZsYellow1-C1 and pAmCyan1-C1 expression vectors with a single restriction enzyme. The reaction was prepared as stated below:

Sterile H_2O	10.3 µl
Restriction Enzyme 10X buffer	2 µl
Acetylated BSA, 10 µg/ µl	0.2 µl
DNA 100 ng/ µl	7 µl
This mixture was mixed well by pipetting and the following reagents were added	
Restriction enzyme 10 U/ µl	0.5 µl
Total volume	20 µl

The reaction was mixed gently and incubated for 2 hours at 37°C. Then, digested DNA was purified and digested with the other restriction enzyme following the same procedure. After purification of digested PCR products or expression vectors with both enzymes, 4 µl of 6X DNA loading buffer (Thermo Scientific) was added to one replicate to visualise in agarose gel electrophoreses. The rest of the samples (4 replicates for each gene or vector) were purified using a PCR purification kit (Qiagen) and used directly in ligation or stored at -20 °C.

2.2.5.5 Ligation

Ligation of the expression vector and insert was performed using a 1:3 ratio per reaction. For example, ligation of a 4.7 kb vector and 2 kb SENP2 1:3 ratio was calculated according to the following equation:

$$\frac{20\ ng\ of\ plasmid\ x\ 3.3\ kb\ insert\ (vinculin)}{4.7\ kb\ vector}\ x\ \frac{3}{1} = 42.12\ ng\ SENP2$$

$$\frac{20\ ng\ of\ plasmid\ x\ 0.4\ kb\ insert\ (SUMO2)}{4.7\ kb\ vector}\ x\ \frac{3}{1} = 5.10\ ng\ SUMO2$$

The ligation reaction was prepared as following:

Expression Vector	20 ng
Insert DNA	42.12 ng (vinculin) or 5.10 ng (SUMO2)
Ligase 10X buffer	1 µl
T4 DNA ligase (5 U/ul)	1 ul
Nuclease-free water	To final volume of 10 µl

The reaction was incubated at 14°C for 18 hours and heated at 65°C for 5 minutes to stop the ligase. Then, 5 µl of the reaction was visualised in 1% agarose gel to check the success of the ligation and the rest of the reaction was stored at -20°C until transformation to E. coli.

2.2.5.6 Transformation

Mach1™ T1R competent cells (kindly given by Dr. Andrew Bicknell's lab) were thawed slowly on ice and 3 µl of the ligation reaction was added to 50 µl of competent cells before incubating on ice for 30 minutes. Then, the cells were incubated at 42°C in a water bath for 50 seconds and placed immediately on ice for one minute to achieve heat shock. After that, 400 µl of LB broth media was added to each sample and samples were incubated at 37°C with shaking at 115 rpm for 1 hour. Then, 250 µl of culture was inoculated on LB medium agar plates containing 50 µg/ml Kanamycin and incubated overnight at 37 °C. The next day, colonies were screened using colony PCR and positive colonies were inoculated in 10 ml LB broth media containing 50µg/ml kanamycin and incubated overnight at 37°C with shaking. 0.5 ml of the growth was mixed with 0.5 ml of 50% glycerol and stored at -80°C. The rest of the culture growth was used to extract plasmids using a QIAprep® Miniprep kit (Qiagen).

2.2.5.7 Gel extraction

DNA extraction from agarose gel was performed using a QIAquick Gel Extraction Kit (QIAGEN) according to the manufacturer's procedure. DNA fragments were excised from agarose gel using a sterilised scalpel. Then, fragments were weighed and 3 volumes of buffer QG were added to 1 volume of gel fragments (e.g. for 100 mg weigh of gel fragments = 100 µl volume and for adding three volumes of QG buffer add 300 µl buffer QG). The mixture was then incubated at 50 °C for 10 minutes or until the gel slice was dissolved completely with vortex every 2 minutes. Following that, 1 volume of isopropanol was added to the mixture, mixed and applied to the QIAprep spin columns and centrifuged for 1 minute at 17200 g. The flow-through was discarded and columns were washed by adding 750 µl of Buffer PE, allowing it to stand for 2-4 minutes and centrifuging again in the same conditions.

Columns were then centrifuged again to remove residual wash buffer and DNA was eluted by adding 30-50 µl of buffer EB and allowing it to stand for 2-4 minutes before centrifuging for 1 minute at 17200 g. DNA concentration was measured using a NANO-DROP device.

2.2.5.8 PCR purification

Purification of PCR products was performed using a QIAquick PCR Purification Kit (QIAGEN) according to the manufacturer's procedure. Five volumes of buffer PB were added to PCR samples, mixed thoroughly and applied to the QIAprep spin columns and centrifuged for 30-60 seconds at 17200 g. The flow-through was discarded and columns were washed by adding 750 µl of Buffer PE and centrifuging again in the same conditions. Columns were then centrifuged again to remove residual wash buffer and DNA was eluted by adding 30-50 µl of buffer EB and allowing it to stand for 1-2 minutes before centrifuging for 1 minute at 17200 g. DNA concentration was measured using a NANO-DROP device.

2.2.5.9 Plasmid purification

Plasmid purification was performed using a QIAprep® Miniprep kit (QIAGEN) according to the manufacturer's procedure. Successful colonies were inoculated in a 10 ml LB broth media containing 50µg/ml kanamycin and incubated for 12-16 hours at 37°C with 200 rpm shaking. Then, bacteria were harvested by centrifuging at 8000 rpm (6800 g) for 3 minutes. Each pellet was resuspended in 250 µl buffer P1 and 250 µl of buffer P2 was added to the suspension and mixed gently by inverting several times. Following that, 350 µl of buffer N3 was added to each sample and mixed by inverting 4-6 times before centrifuging at 13000 rpm (17,200 g) for 10 minutes. The supernatants were collected and applied to the QIAprep spin columns and centrifuged for 1 minute at 17200 g. The columns were then washed, by

adding 500 µl of buffer PB, and centrifuged for 1 minute. Then, 750 µl of buffer PE was added to the columns and centrifuged for 1 minute. Then, the columns were centrifuged again to remove any remnant of the washing buffer. Finally, plasmids were eluted by adding 40 µl of buffer EB and allowing it to stand for 2-4 minutes before centrifuging for 1 minute at 17200 g. DNA concentration was measured using a NANO-DROP device.

Plasmids were screened for successful inserts by repeating the PCR and digestion steps using plasmids as templats. Positive colonies were sent for sequencing to further confirm the correct insertion of genes to expression vectors.

2.2.5.10 Construction of pZsYellow1-tagged mutated vinculin

Mutagenic primers were used to create single mutations in predicted SUMO sites in vinculin. Primers were designed using the PrimerX website (https://www.bioinformatics.org/primerx/cgi-bin/DNA_1.cgi) and PCR was used to create mutations. Two individual mutations were created, K80R and K496R, and a combined mutation of both sites was created. Mutagenic primers where designed to replace lysine with arginine by changing a single nucleotide in the lysine codon (AAG) to arginine codon (AGG). Beside mutagenesis primers, vinculin full length primers containing restriction enzyme sites for the amplification of full-length vinculin were used. pZsYellow1-tagged vinculin plasmid at a concentration of 10 ng was used as a templet to amplify two products of vinculin using these different sets of enzymes. In order to replace lysine at position 80 with arginine in vinculin, two steps were performed. The first step was the PCR amplification of two products of vinculin using the original and mutagenic primers. The forward original primer was used with the reverse mutagenic primer to amplify ~ 318 bp of vinculin starting

from the start codon and ending at nucleotide 360. In addition, the forward mutagenic primer was used with the reverse original primer to amplify ~ 3000 bp of vinculin starting from nucleotide 345 and ending with the stop codon. The second step was to mix these products and use them as a templet to amplify the full-length vinculin (~3300 bp). The same procedure was followed to replace lysine at 496 with arginine. For the production of combined mutation (K80R/K496R), pZsYellow1-tagged vinculin with K80R mutation was used as a templet and mutagenic primers were used alongside full length vinculin primers to introduce the K496R mutation.

Reactions and cycling conditions of PCR were as used as described in 2.2.5.3 except for the fact that cycles were reduced from 35 to 25 to avoid unwanted alternations in the vinculin nucleotide sequence. Digestion, ligation, transformation and plasmid purification were used as described previously. Plasmids were screened for successful inserts by repeating the PCR and digestion steps using plasmids as templats. Positive colonies were sent for sequencing to further confirm the correct insertion of genes to expression vectors.

Table 2.10 showing original and mutagenic primers used in PCR to amplify vinculin. Gene primers are highlighted in cyan; restriction enzyme sites are highlighted in green and buffering random nucleotides are highlighted in yellow. Altered nucleotides in mutagenic primers are highlighted in red.

product	Forward primer 5'-3'	Reverse primer 5'-3'	Product size (bp)
Start codon-360 (K80R)	**CGCGTCGACGTCGCTGCACAGTCTGTCT**	**CAAGCATTCTCAACCCTAATAAATGCTGGTGG**	318
345 – Stop codon (K80R)	CCACCAGCATTTATTAGGGTTGAGAATGCTTG	**GCGCCCGGGTTCAGCTCCCAGCAACTCTG**	3000
Full length (K80R)	**CGCGTCGACGTCGCTGCACAGTCTGTCT**	**GCGCCCGGGTTCAGCTCCCAGCAACTCTG**	3400
Start codon-1690 (K496R)	**CGCGTCGACGTCGCTGCACAGTCTGTCT**	CTGTGCTTGCTCAATCCTGCCCTCAAGGTGTAC	1650
1680- Stop codon	**GTACACCTTGAGGGCAGGATTGAGCAAGCACAG**	**GCGCCCGGGTTCAGCTCCCAGCAACTCTG**	1820
Full length	**CGCGTCGACGTCGCTGCACAGTCTGTCT**	**GCGCCCGGGTTCAGCTCCCAGCAACTCTG**	3400

2.2.5.11 Live cell imaging using a confocal microscope

Cells were grown in a µ-Slide 8 Well (ibidi) until 70% confluency before transfection. The cells were then incubated for 24-48 hours before imaging. A confocal microscope was used to take live cell imaging timelapse movies using a 100x oil-immersion objective lens for 5-10 minutes at intervals of 10 seconds for the turnover of FAs. For monitoring FA dynamics, cells were seeded in an µ-Slide 8 Well (ibidi) and were grown until 70% before transfection with pZsYellow1-vinculin. Then, 24-48 hours post-transfection, the plate was placed on the stage of the confocal microscope. The stage of the microscope was heated to 37°C and supplied with 5% CO_2 to maintain normal growth conditions. Image J (Fiji) software was used to determine the turnover time of FAs. The turnover time was calculated from appearance to

disappearance. The turnover of 40 FAs at least was calculated for each group in each replicate.

For cell tracking, 12-well plates were used. After placing the plate on the confocal stage, a 10x objective lens was used to capture fluorescence images of spots of pZsYellow1-vinculin transfected cells. Then, fluorescence was turned off to avoid bleaching and cells were imaged every 15 minutes for 24 hours using optical light. MtrackJ plugin tool in Image J (Fiji) software was used to track single cells and measure their speed and travelled distance. A Graph Prism was used to compare the mean speed measurements of different groups of three independent experiments. One-way ANOVA with Tukey's Multiple comparison test was used to evaluate any significant differences between groups.

2.2.5.12 Analysis of FA size and number

Transfected cells were fixed and a confocal microscope using a 100x oil-immersion objective lens was used to take images of vinculin-containing FAs with a resolution of 1024 x 1024 pixels. Image J (Fiji) software was used to calculate the number and measure the size of FAs. A subtract background image tool with sliding paraboloid option and rolling ball of 50 pixels in Image J (Fiji) software was used to subtract the background in the images. Following that, a CLAHE (Contrast Limited Adaptive Histogram Equalization) tool was used to enhance the image's local contrast with values: block size=19, Histogram bins=256, Maximum slope=6, no mask and fast. To further reduce the background, an EXP tool was applied to the images. Then, a threshold tool was applied to images with two-pixel values, 255 (white) and 0 (black). Following that, FAs were selected using a Polygon selection tool and the 'analyse particles' command (parameters: size between 0.5-infinity and circularity between 0.00-

0.99) was applied to the images to calculate the FA number and to measure their size. The size and number of FAs in at least twenty cells were analysed for each group in each replicate.

2.2.5.13 Co-localisation analysis

Transfected cells were fixed and a confocal microscope using a 100x oil-immersion objective lens was used to take images of fluorescent-tagged proteins with a resolution of 1024 x 1024 pixels and 400Hz using GALVANO mode. To avoid crosstalk between different channels, sequential imaging was used. Channels were split in Image J and a Polygon selection tool was used to select an ROI in one channel. The Coloc2 analysis command was used to calculate co-localisation between two proteins in ROI using the spearman rank correlation value with 0 meaning no co-localisation, and 1 meaning high co-localisation.

2.2.5.14 Statistical analysis

Data observed by Image J (Fiji) software analysis was stored in Excel sheets and graphs were generated using GraphPad Prism, where data were presented as mean ± SEM of three independent experiments. Different statistical tests were used to observe any significant differences between groups ($P < 0.05$) including two-tailed unpaired student's t-test, one-way analysis of variance (ANOVA) with Tukey as the post-test or two-way ANOVA with Bonferroni as a post-test. (*, ** and *** represent $P < 0.05$, 0.01 and 0.001 respectively).

3. SUMOylation is involved in the regulation of focal adhesions and cancer cell migration.

3.1 Introduction and Hypothesis

This chapter explores the effects of SUMOylation on cell migration and focal adhesion (FA) dynamics in MDA-MB-231 cells. SUMOylation was reported in several studies to be deregulated in different cancer types and the deregulation of SUMO and SUMO-related proteins is associated with cancer progress and metastasis (Wang et al., 2013, Ma et al., 2014). Since SUMOylation has been discovered, researchers have focused on its roles on nuclear activities such as chromosome segregation, DNA damage repair, nuclear-cytosolic transport, apoptosis and transcription (Tang et al., 2008, Eifler and Vertegaal, 2015). Recent studies, however, have identified an essential role of this protein modification mechanism in the regulation of a wide range of cytoplasmic proteins involved in critical cellular functions such as cell migration (Hendriks and Vertegaal, 2016). SUMOylation has been suggested to modulate cell migration by regulating the polymerisation of cytoskeleton structures (Castillo-Lluva et al., 2010) and the activity of MMPs (Lao et al., 2019). However, its roles in cell migration remain poorly understood due to the continued identification or prediction of cell migration-associated SUMO targets. Focal adhesions play essential roles in cell migration and SUMOylation was shown to be involved in the regulation of FA proteins. Focal adhesion kinase (FAK), a critical focal adhesion protein, was found previously to be modified by SUMO1 in the nucleus and its modification was shown to promote cancer progression and cell migration (Kadaré et al., 2003). In addition, other important FA proteins have been identified in a proteomic study as SUMO substrates including talin and vinculin (Xiao et al., 2016). The impacts of SUMOylating FAK on cancer cell migration and the possibilities of

targeting other FA proteins encourages investigating of the role of this protein regulatory system on the dynamics of these adhesion complexes and cancer cell migration.

In addition, as key FA proteins were suggested to be SUMO substrates, DeSUMOylation by SUMO specific proteases (SENPs) could be involved in their regulation. Due to the importance of DeSUMOylation in cancer migration, investigating its roles in the dynamics of these adhesion sites is important for understanding the whole picture of the role of SUMOylation in the regulation of FAs.

Hypothesis

Previous studies suggest a possible role of SUMOylation in cancer metastasis and in the regulation of FAK, therefore the hypothesis of this chapter is that SUMOylation modulates cell migration by regulating FA dynamics. In order to test this hypothesis, different approaches have been employed. Two different SUMOylation inhibitors, Ginkgolic acid (Gka) and Gossypetin, were used to investigate the impact of SUMOylation on the migration of MDA-MB-231 cancer cells using cell migration assays, wound healing and cell tracking. These inhibitors were also used to study the effects of inhibiting SUMOylation on the dynamics of FAs using a confocal microscope.

To investigate the involvement of SUMOylation in the regulation of FAs and cancer cell migration using a different approach, siRNA transfection targeting the SUMO specific proteases, SENP2 or SENP5, was applied to assess the effects of their silencing on FA dynamics and cancer cell migration. As SENPs de-SUMOylate proteins, they could be important regulators of FAs turnover and cancer cell migration.

3.2 Material and Methods

3.2.1 Materials

Table 3.1 List of reagents used in siRNA transfection

Reagent	Catalog No.	Supplier
5X siRNA Buffer	B-002000-UB-100	Horizon discovery
DharmaFECT 1 siRNA Transfection Reagent	T-2001-01	Horizon discovery
ON-TARGET plus Non-targeting control siRNA	D-001810-01-05	Horizon discovery
ON-TARGET plus SMART pool SENP2 siRNA	L-006033-00-0005	Horizon discovery
ON-TARGET plus SMART pool SENP5 siRNA	L-005946-00-0005	Horizon discovery

3.2.2 Methods

3.2.2.1 Gene Knockdown with siRNA

MDA-MB-231 cells were seeded in 12-well plate (1 X 10^5 cells/well) or 6-well plate (3 X 10^5 cells/well) and were grown until 70% confluency. Subsequently, cells were transfected with 35 nM of Non-target siRNA, SENP2 siRNA or SENP5 siRNA. Transfection mixture was prepared in a sterile hood according to the manufacturer's protocol (DharmaFECT Transfection protocol). DharmaFECT 1 transfection reagent and 35 nM of siRNA were diluted in serum free medium in separate Eppendorf tubes (Table 3.2). Mixtures were

incubated at room temperature for 5 minutes before mixing them carefully by pipetting and incubating for 20 minutes at room temperature. Then, antibiotic-free media containing 10% FBS was used to complete the final volume of final siRNA concentration of 35 nM.

Table 3.2 procedure of siRNA transfection

	Tube 1 Diluted siRNA		**Tube 2** Diluted DharmaFECT				
Type of siRNA	Volume (µl) of siRNA	Serum free medium (µl)	Volume of DharmaFECT Reagent (µl)	Serum free medium (µl)	T1 and T 2 mixed (µl)	Complete medium (no antibiotic) (µl)	Total Transfection volume (µl/well)
Non-target siRNA (10µM)	3.5 µL	96.6	1.5 µl	98.5	200	800	1000
SENP2 siRNA (10µM)	3.5 µL	96.5	1.5 µl	98.5	200	800	1000
SENP5 siRNA (10µM)	3.5 µL	96.5	1.5 µl	98.5	200	800	1000

Transfection solution was applied to cells depending on the surface area of dishes or flasks. For 6-well plate, a total transfection volume of 1 ml was added to each well, for 12-well plate, a total transfection volume of 500 µl was added to each well, or for 25 cm^2 flasks, a total transfection volume of 4 ml was applied to each flask. Cells were incubated at 37 °C in 5% CO_2 for 24-96 hours. The transfection medium was replaced after 12 hours with antibiotic-free fresh media.

For western blot analysis, 25 cm^2 flasks were used and after incubating cells for 24-96 hours, cell lysates were collected and anti-SENP2 or anti-SENP5 antibodies were used to detect the expression of these proteases in lysates of transfected cells at the different time points of

24, 48 and 96 hours. For cell migration assays, 6-well or 12-well plates were used and for monitoring FA dynamics, µ-Slide 8 Well (ibidi) was used. For monitoring FA dynamics, 24 hours post siRNA transfection, cells were transfected with pZsYellow1-tagged vinculin, incubated for 24 hours and confocal microscopy was used take short timelapse movies of vinculin-containing FAs.

3.3 Effects of inhibiting SUMOylation on cell migration of MDA-MB-231 cancer cells.

To investigate the association between SUMOylation and cancer cell migration, two different SUMOylation-inhibitors were utilized. The first inhibitor, Ginkgolic acid was reported to disrupt the SUMOylation cycle by binding to the SUMO E1 activating enzyme, therefore, preventing its binding to SUMO proteins (Fukuda et al., 2009). To evaluate the effects of this inhibitor on cell migration, MDA-MB-231 cells were treated with vehicle control (DMSO) or 10, 25, 50 or 100 µM of Ginkgolic acid and incubated for 2 hours at 37°C in 5% CO_2 atmosphere before introducing a wound. An inverted microscope was used to take photographs of the wounds at 0 and 24 hours (Figure 3.1 (A)). ImageJ (Fiji) software was used to calculate the wound closure for each group. Results revealed a significant decrease in wound closure in 25, 50 or 100 µM Ginkgolic acid treated cells compared to control (Figure 3.1 (B)). In control cells, the covered area of wound after 24 hours was 51 ± 1.93% compared to 27.16 ± 1.34% in 25 µM treated cells ($p<0.01$), 29.48 ± 4.81% in 50 µM treated cells ($p<0.01$) and 30.02 ± 3.98% in 100 µM treated cells ($p<0.01$). There were no significant changes in covered area between cells treated 25, 50 or 100 µM Ginkgolic acid. On the other hand, there were no significance changes between control and 10 µM Gka treated cells.

To confirm this finding, another SUMOylation inhibitor, Gossypetin, was used to further examine the influences of inhibiting SUMOylation on the migration of MDA-MB-231 cells. Cells were treated with vehicle control or 10, 25, 50 or 100 µM of this inhibitor and incubated for 2 hours at 37°C in 5% CO2 atmosphere before introducing a wound. Results showed a significance reduction in wound coverage in 100 µM Gossypetin treated cells compared to control (Figure 3.1 (C)). The covered area of the wound in control cells was 92.03 ± 0.02%, while in 100 µM Gossypetin treated cells only 60.73 ± 0.05% of the wound was covered after 24 hours ($p<0.01$). No significant changes observed in cells treated with 10, 25 or 50 µM compared to control.

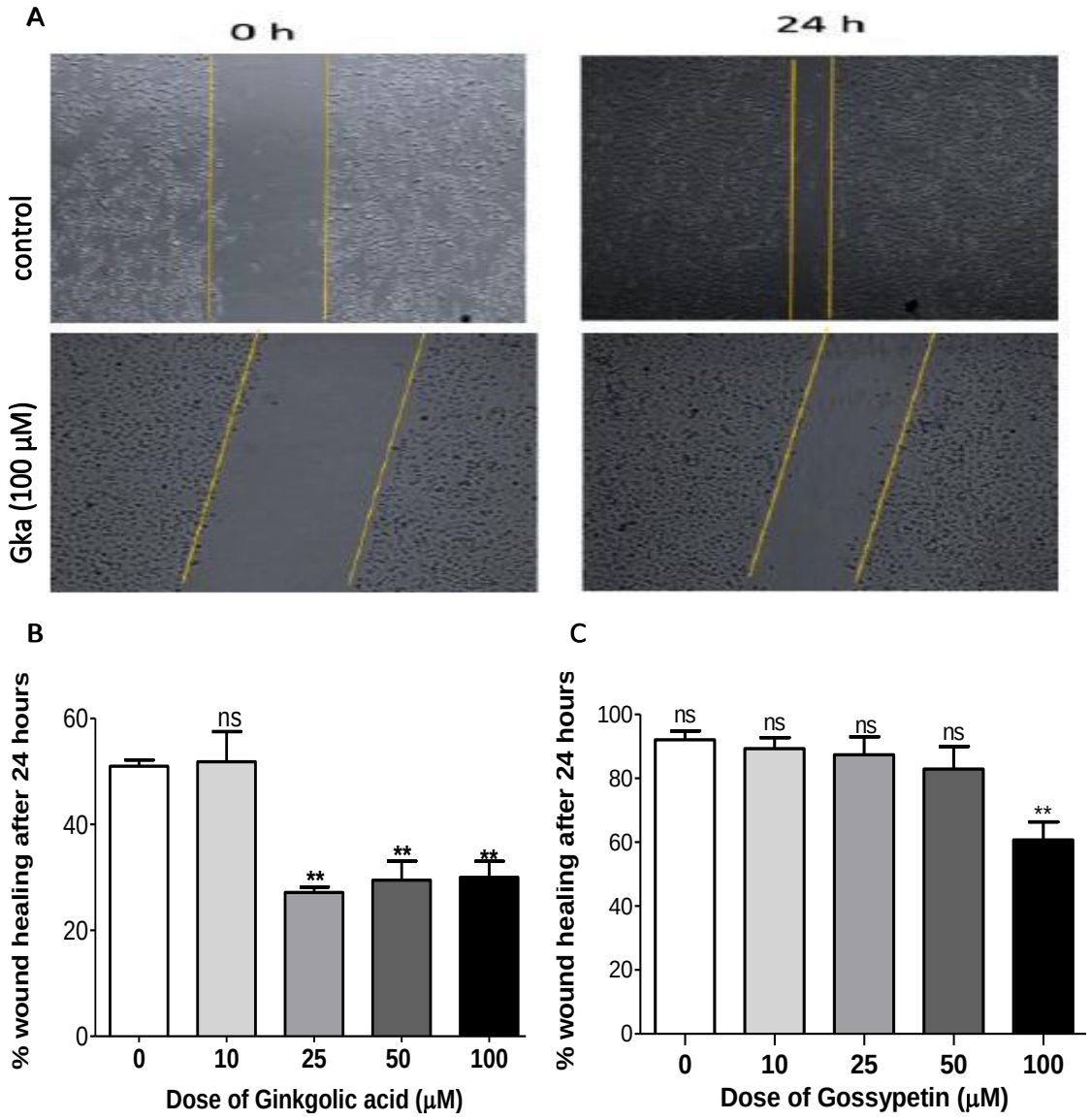

Figure 3.1 Effect of inhibiting SUMOylation on the closure area of wound healing in MDA-MB-231 cells. Cells were incubated with DMSO (control) or different concentrations of Ginkgolic acid or Gossypetin for 2 hours before introducing the wound. Photos of wound area in each group were taken using an inverted microscope and analysed using ImageJ (Fiji) software. A) Photographs showing the wound area at 0 time point and after 24 hours in control cells compared to 100 µM Ginkgolic acid treated cells. B) Quantification analysis showing the mean wound healing measurements in control cells compared to 10, 25, 50, 100 µM Gka treated cells. C) Showing of the quantification analysis of the mean closure area in control compared to 10, 25, 50 or 100 µM Gossypetin treated cells. Data was presented as mean ± SEM of three independent experiments. One-way ANOVA with Tukey's Multiple comparison test was used to evaluate any significance differences between groups (*, ** and *** represent P <0.05, 0.01 and 0.001 respectively).

To further confirm the previous finding from wound healing assays, time lapse cell tracking was used to evaluate the influence of SUMOylation inhibitors on the migration of MDA-MB-231 cells. Treating these cells with 25 µM of Ginkgolic acid was shown to reduce their speed significantly. In the control, the average speed of cells was 22.43 ± 1.57 µm/h compared to 10.85 ± 1.64 µm/h in 25 µM Gka treated cells ($p<0.001$) and 7.333 ± 1.155 µm/h in 100 µM Gossypetin treated cells ($p<0.001$) (Figure 3.2).

Similar effects were shown when seeding cells on 1% gelatin or 2 mg/ml collagen coated wells. The average speed of control cells on gelatin was 21.92 ± 1.80 µm/h compared to 12.48 ± 1.70 µm/h in cells treated with 25 µM Gka ($p<0.01$) and 7.7 ± 1.64 µm/h in cells treated with 100 µM Gossypetin ($p<0.001$). This reduction in their speed was also observed in cells seeded on collagen. In control cells, the average speed of cells was 23.34 ± 3.38 µm/h compared to 13.74 ± 1.33 µm/h in cells treated with 25 µM Gka ($p<0.01$) and 9.49 ± 1.66 µm/h in cells treated with 100 µM Gossypetin ($P<0.001$) (Figure 3.2).

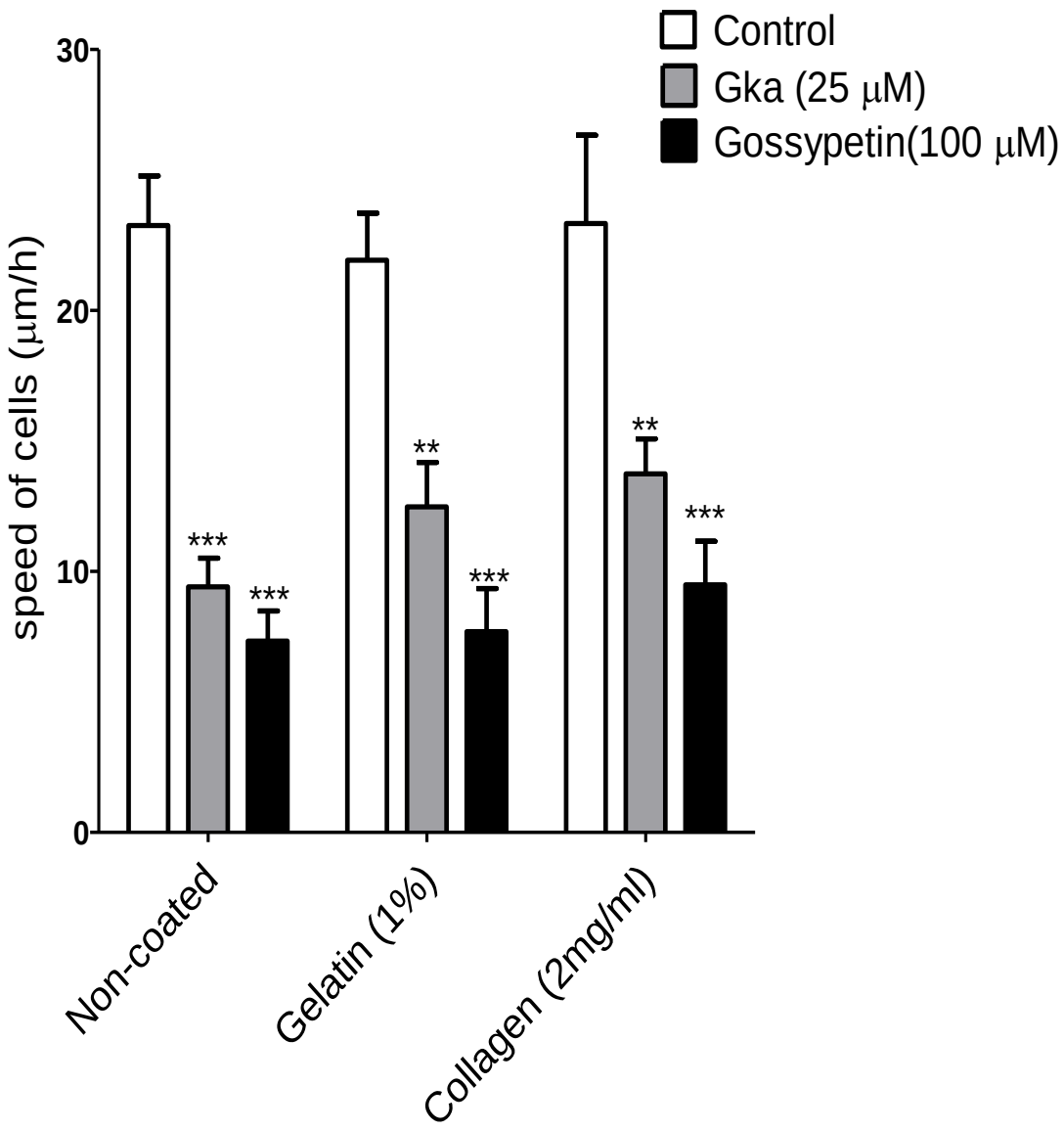

Figure 3.2 Effect of inhibiting SUMOylation on the speed of MDA-MB-231 cells on different surfaces. Cells were seeded on plastic (non-coated), Gelatin or collagen and grown over night. Then, cells were treated with 1 µl/ml DMSO (control), 25 µM Ginkgolic acid or 100 µM Gossypetin for 2 hours. Timelapse microscopy was used to take images every 15 minutes for 24 hours. The graph shows the quantification analysis of the mean speed measurements in control cells compared to 25 µM Ginkgolic acid or 100 µM Gossypetin treated cells migrating on different surface matrices. Data was presented as mean ± SEM of three independent experiments, in each experiment at least 45 cells were analysed for each group. Two-way ANOVA with Bonferroni's Multiple comparison test was used to evaluate any significance differences between groups (*, ** and *** represent P <0.05, 0.01 and 0.001 respectively).

3.4 Inhibiting SUMOylation significantly increases the size and turnover time of focal adhesions.

As focal adhesions are one of the main requirements of cell migration, this part of this chapter focuses on the effects of SUMOylation inhibitors on their dynamics. MDA-MB-231 cells were transfected with YFP-vinculin and confocal microscopy was used to monitor the turnover of FAs after treating cells for 2 hours with SUMOylation inhibitors, Gka or Gossypetin. The results showed that the turnover of vinculin-containing FAs was significantly slower in cells treated with 25 µM Gka (Figure 3.3 (B)) or 100 µM Gossypetin compared to control (Figure 3.3 (A)). In control cells, the average turnover of FAs was 33.80 ± 1.10 seconds compared to 47.82 ± 2.49 seconds in cells treated with 25 µM Gka ($p<0.01$) and 55.14 ± 2.63 seconds in cells treated with 100 µM Gossypetin ($p<0.05$). No significant changes were observed between 25 µM Gka or 100 µM Gossypetin treated cells (Figure 3.3 (C)).

The size of FAs was also affected by these inhibitors. Results in figure 3.4 show a significant increase in the size of FAs from 0.94 ± 0.02 μm^2 in control cells to 1.46 ± 0.07 μm^2 in 25 µM Gka treated cells ($p<0.03$) or 1.42 ± 0.11 μm^2 in 100 µM Gossypetin treated cells ($p<0.03$). No significant changes in the size of FAs were observed between 25 µM Gka and 100 µM Gossypetin treated cells (Figure 3.4 (B)).

However, there were no significant effects of SUMOylation inhibitors on the number of vinculin-containing FAs in these cells. The average number of FAs in control cells was 38.5 ± 19.53 compared to 42.79 ± 7.44 in 25 µM Gka treated cells ($p<0.847$) and 39.88 ± 4.63 in 100 µM Gossypetin treated cells ($p<0.94$) (Figure 3.4 (C)).

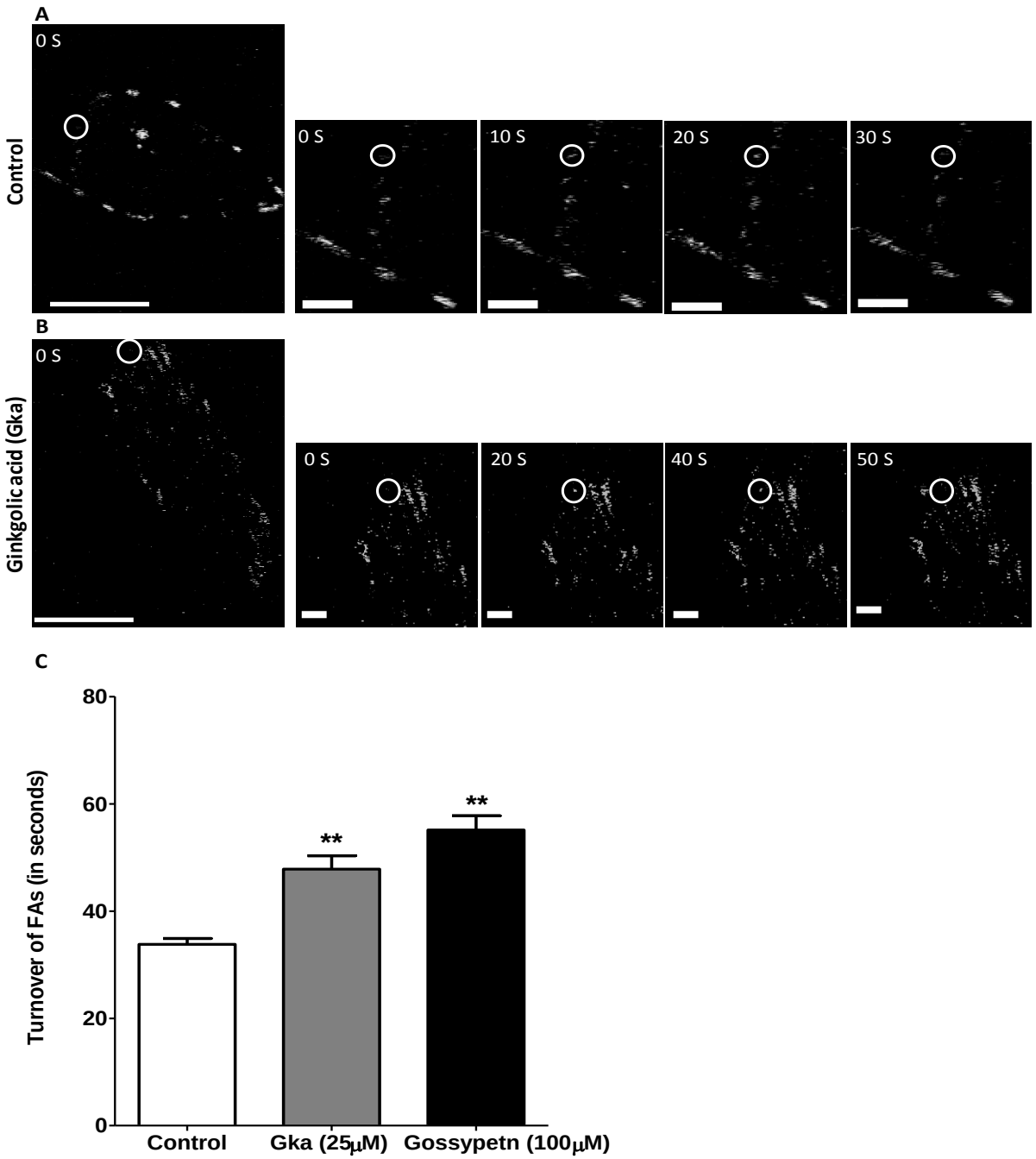

Figure 3.3 Effects of inhibiting SUMOylation on the turnover of vinculin-containing FAs in MDA-MB-231 cells. A) Representation of the turnover of vinculin-containing FAs in control cells and (B) 25 µM Ginkgolic acid treated cells. Cells were transfected with YFP-vinculin, treated with DMSO for 2 hours and live cells imaging were performed using confocal microscopy. Images were captured every 10 seconds for 5 minutes, scale bar = 5 µm. The white circles demonstrate the turnover of a single vinculin-containing FA starting from appearing to disappearing. C) Quantification analysis showing the mean FA turnover measurements in control cells compared to 25 µM Ginkgolic acid or 100 µM Gossypetin treated cells. Data was presented as mean ± SEM of three independent experiments, in each experiment a total number of 210 focal adhesions (24 cells) were analysed. One-way ANOVA with Tukey's Multiple comparison test was used to evaluate any significance differences between groups (*, ** and *** represent P <0.05, 0.01 and 0.001 respectively).

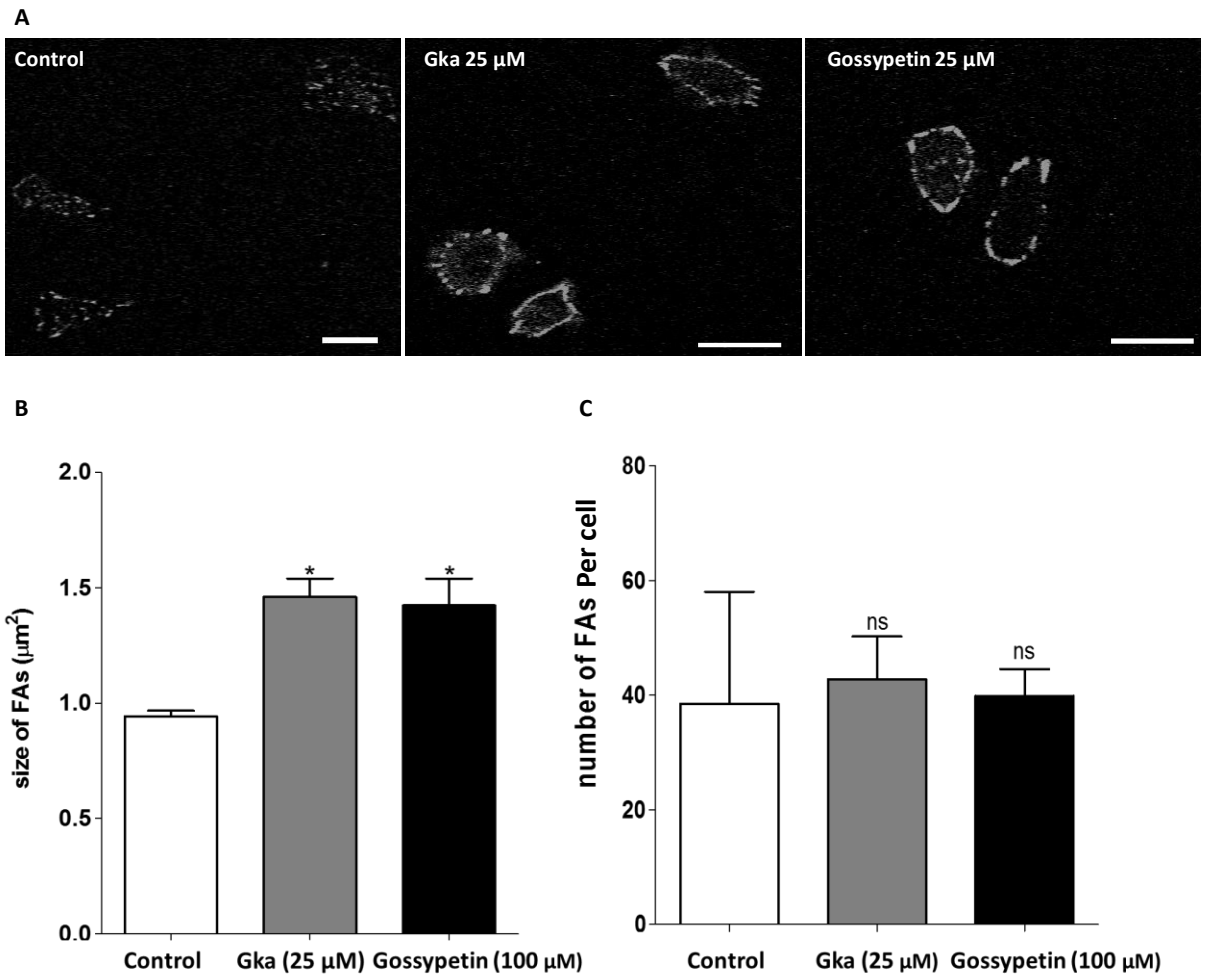

Figure 3.4 Effects of inhibiting SUMOylation on the size and number of FAs in MDA-MB-231 cells. A) Representative images of vinculin containing FAs for control cells (treated with DMSO), 25 µM Ginkgolic acid or 100 µM Gossypetin treated cells. After 2 hours of treatment, cells were fixed, and confocal microscopy was used to take images. Scale bar = 20 µm. B) Quantification analysis showing the mean FA size measurements (C) the mean FA number in control cells compared to 25 µM Ginkgolic acid or 100 µM Gossypetin treated cells. Data was presented as mean ± SEM of three independent experiments, in each experiment a total number of 120 cells were analysed. One-way ANOVA with Tukey's Multiple comparison test was used to evaluate any significance differences between groups (*, ** and *** represent P <0.05, 0.01 and 0.001 respectively).

3.5 Silencing SENP2 or SENP5 significantly reduces cell migration and the turnover of FAs in MDA-MB-231 cells

In order to investigate the role of DeSUMOylation in cancer cell migration, siRNA assay was used to silence the SUMO-associated proteases, SENP2 and SENP5. Wound healing and time lapse cell tracking assays were used to assess the effects of silencing these proteases on the migration of MDA-MB-231 cells. Cells were transfected with non-target siRNA (control), SENP2 siRNA or SENP5 siRNA and 48 hours post-transfection, cells were subjected to wound healing or cell tracking assay. The results from wound healing assay showed a significant reduction in wound closure. The covered area of wound was reduced from 90.18 ± 2.8% in non-target siRNA transfected cells to 54.14 ± 2.66 % in SENP2 siRNA transfected cells ($p<0.001$) or 58.64 ± 1.82% in SENP5 siRNA transfected cells ($p<0.001$). No significant changes in wound closure were observed between SENP2 siRNA and SENP5 siRNA transfected cells (Figure 3.5 (D)).

Time lapse cell tracking was further used to evaluate the effects of silencing these proteases on the migration of MDA-MB-231 cells. The results showed a significant reduction in the speed of these cells when silencing either one of these proteases. The average speed of cells was significantly reduced from 19.01 ± 3.18 µm/h in control cells to 7.5 ± 1.28 µm/h in SENP2 siRNA transfected cells ($p<0.001$) or 5.62 ± 1.16 µm/h in SENP5 siRNA transfected cells ($p<0.001$) (Figure 3.5 (C)).

Similar effects were shown when seeding cells on 1% gelatin or 2 mg/ml collagen coated wells before siRNA treatment. The average speed of control cells on gelatin was 22.12 ± 2.46 µm/h compared to 8.75 ± 0.68 µm/h in SENP2 siRNA transfected cells ($p<0.001$) or 6.29 ± 0.83 µm/h in SENP5 siRNA transfected cells ($p<0.001$). This reduction in speed was also observed in cells seeded on collagen. The average speed of MDA-MB-231 cells on collagen was significantly reduced from 16.74 ± 0.31 µm/h in control cells to 7.47 ± 0.75 µm/h in SENP2 siRNA transfected cells ($p<0.001$) or 9.49 ± 1.66 µm/h in SENP5 siRNA transfected cells ($p<0.001$) (Figure 3.5 (C)).

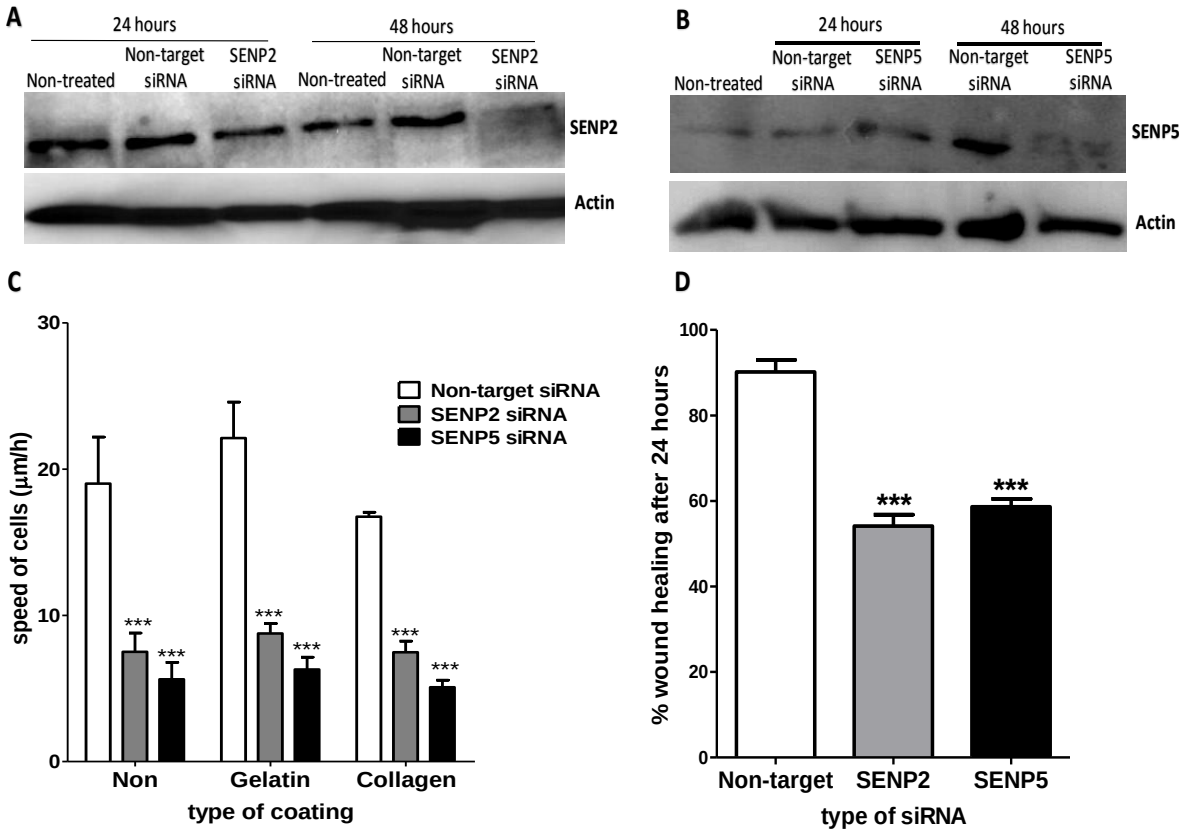

Figure 3.5 Effects of silencing the SUMO-specific proteases, SENP2 or SENP5, on the migration of MDA-MB-231 cells. A) Western blot showing detection of SENP2 or actin in non-transfected cells, Non-target siRNA or SENP2 siRNA transfected cells 24 hours or 48 hours post-transfection. SENP2 was shown to be silenced at 48 hours post-treatment. B) Western blot showing detection of SENP5 or actin in non-transfected cells, Non-target siRNA or SENP5 siRNA transfected cells 24 hours or 48 hours post-transfection. C) Quantification analysis depicting the mean speed measurements in non-target siRNA (control), 35 nM SENP2 siRNA or 35 nM SENP5 siRNA transfected cells on different surfaces. D) Quantification analysis showing the mean wound healing measurements in non-target siRNA (control), 35 nM SENP2 siRNA or 35 nM SENP5 siRNA transfected cells. Data was presented as mean ± SEM of three independent experiments, in each experiment at least 45 cells for each group was analysed. One-way ANOVA with Tukey's Multiple comparison test was used to evaluate any significance differences between groups (*, ** and *** represent P <0.05, 0.01 and 0.001, respectively).

Immunostaining studies were performed to visualise the distribution of SENP2 or SENP5 within cells using confocal microscopy. MDA-MB-231 cells were seeded on coverslips and grown until 80-100% confluency before fixing and subjecting them to immunocytochemistry with SENP2 or SENP5 antibodies. The results showed that SENP5 is mainly localised in the nucleus (Figure 3.6 (B)), whereas SENP2 has a cytoplasmic localisation (Figure 3.6 (A)). The cytoplasmic localisation of SENP2 increases its possibilities to interact with FA-associated proteins, therefore, contributing to their regulation. This has led to the investigation of the possible interaction between SENP2 and FA proteins and the consequences of its silencing on their dynamics.

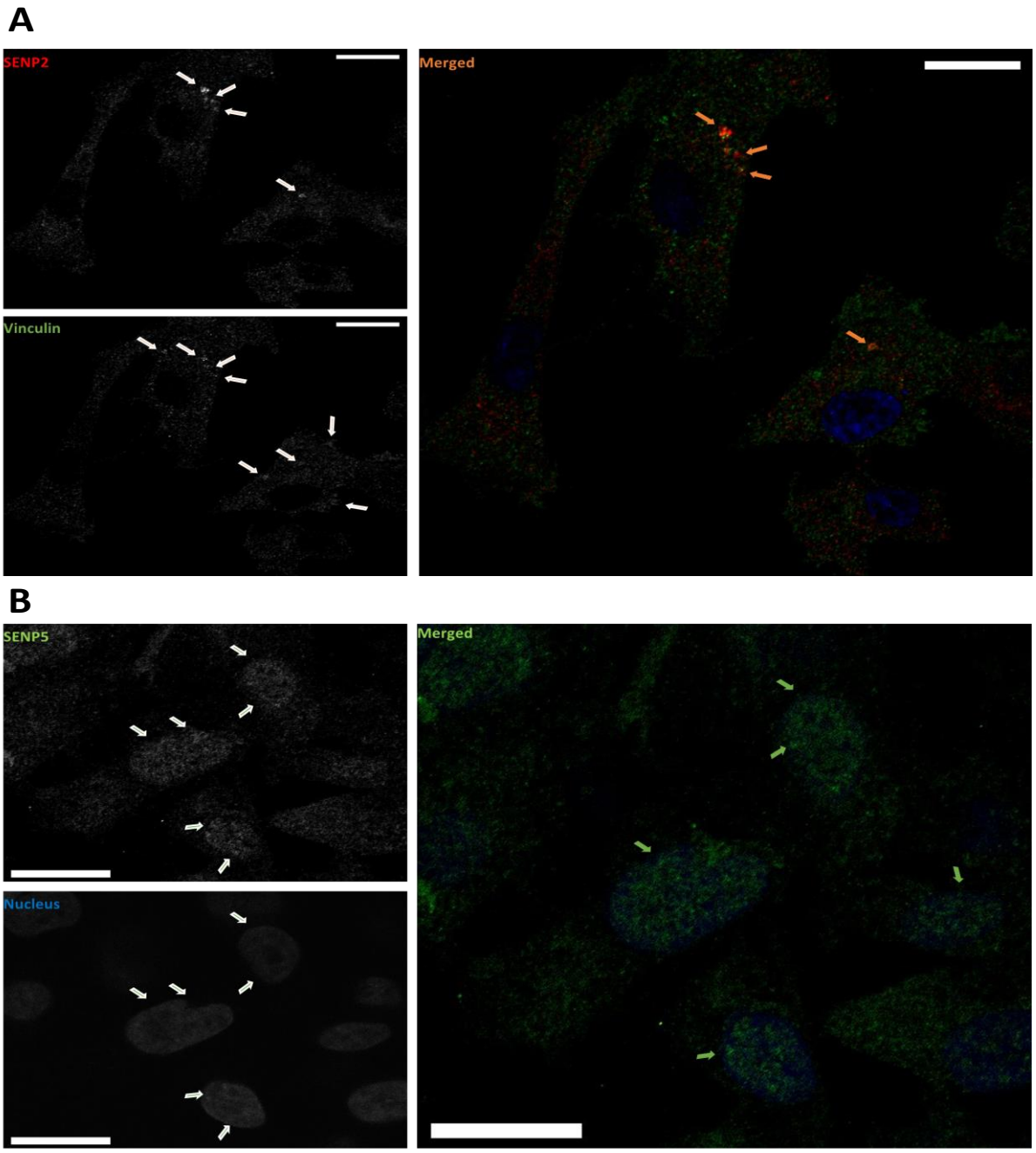

Figure 3.6 Immunostaining of SENP2 with vinculin and SENP5 in MDA-MB-231 cells. Cells were fixed and subjected to immunocytochemistry with SENP2 and vinculin or SENP5 antibodies. A) Confocal microscope Images showing the cytoplasmic distribution of SENP2 and its localisation with vinculin. DAPI was shown as blue. White arrows indicate the expression of SENP2 or vinculin within the cell. Image on the right demonstrates the co-localisation of SENP2 with vinculin (orange arrows) by merging them using Image j software (Scale bar = 20 µm). B) Images showing the expression of SENP5 and its distribution within the cell. DAPI was shown as blue and white arrows indicate the expression of SENP5 within the cell. Image on the right represents a merged image of SENP5 and the nucleus in the cell (green arrows show the localisation of SENP5 in the nucleus) (scale bar = 20 µm). SENP5 was shown to express in these cells and its distribution was mainly in the nucleus.

Co-Immunoprecipitation was used to evaluate whether SENP2 interacts with FA proteins. Anti-SENP2 antibody was mixed with MDA-MB-231 cell lysate over night before incubating with agarose beads to immunoprecipitate SENP2. The interaction of SENP2 with FA proteins was detected by Western Blot with anti-Vinculin, anti-Talin, anti-FAK or anti-paxillin antibodies. All of these FA proteins were detected at their expected sizes in SENP2 Co-IPs indicating a possible involvement of this protease in FAs. Talin was detected at the size of 260 KDa, Vinculin was detected at 130 KDa, FAK was detected at the size of 120 KDa and Paxillin was detected at ~68 KDa (Figure 3.7 (A)). To further confirm this finding, positive and negative controls were used alongside with SENP2 Co-IP. Whole lysate was used as a positive control and nonspecific rabbit IgG Co-IP was used as a negative control. Anti-talin or anti-paxillin antibodies were used in Western Blot to detect talin or paxillin in controls and SENP2 Co-IPs. Bands at the expected size of these proteins were detected in both positive control and SENP2 Co-IPs, while no bands at these sizes were present in the negative control (Figure 3.7 (B)). These findings suggest a possible role of this protease in the regulation of focal adhesion proteins.

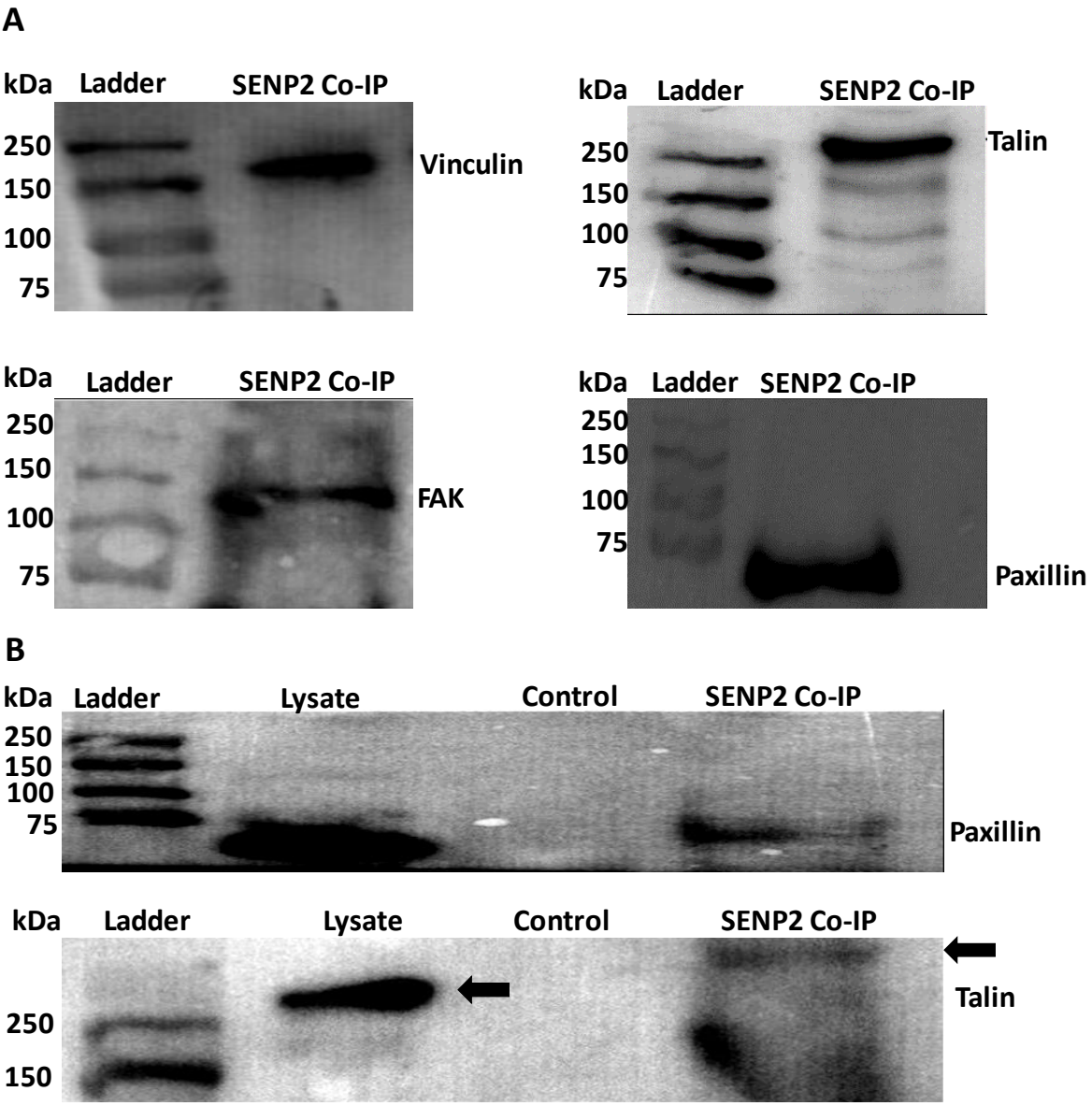

Figure 3.7 SENP2 Co-IP and Western blot showing the detection of different FA-associated proteins in SENP2 Co-IPs in MDA-MB-231 cells. A) SENP2 Co-IP and WB showing that different FA-associated proteins were detected in SENP2 Co-IP. Vinculin was detected at 130 kDa in SENP2 Co-IP, whereas Talin, FAK and paxillin were detected at 250 kDa, 130 kDa and 75 kDa respectively. B) SENP2 Co-IP and WB showing that paxillin and talin were detected in the positive control and SENP2 Co-IP at 75 kDa and 250 kDa respectively, but not in the negative control. In this experiment, cell lysate was used as a positive control (input), while IgG Co-IP was used as a negative control.

To evaluate the effects of silencing SENP2 on the turnover, size and number of FAs, MDA-MB-231 cells were transfected with non-target or SENP2 siRNA before transfection with YFP-vinculin and confocal microscopy was used to monitor the turnover of FAs. The results showed that silencing SENP2 leads to a significantly slower turnover of FAs compared to control. In control cells, the average turnover time of FAs was 38.02 ± 1.29 seconds compared to 53.57 ± 3.45 seconds in SENP2 siRNA transfected cells ($p<0.05$) (Figure 3.8 (B)).

The size of FAs was also affected by knocking down this SUMO-associated protease (Figure 3.8). Results in figure 3.8 (C) show a significant increase in the size of FAs from 0.89 ± 0.05 μm^2 in control cells to 1.33 ± 0.06 μm^2 in SENP2 siRNA transfected cells ($p<0.01$). However, there were no significant effects of silencing SENP2 on the number of vinculin-containing FAs in these cells. The number of FAs in control cells was 89.33± 10.40 compared to 103.7 ± 27.28 in SENP2 siRNA transfected cells ($p<0.648$) (Figure 3.8 (D)).

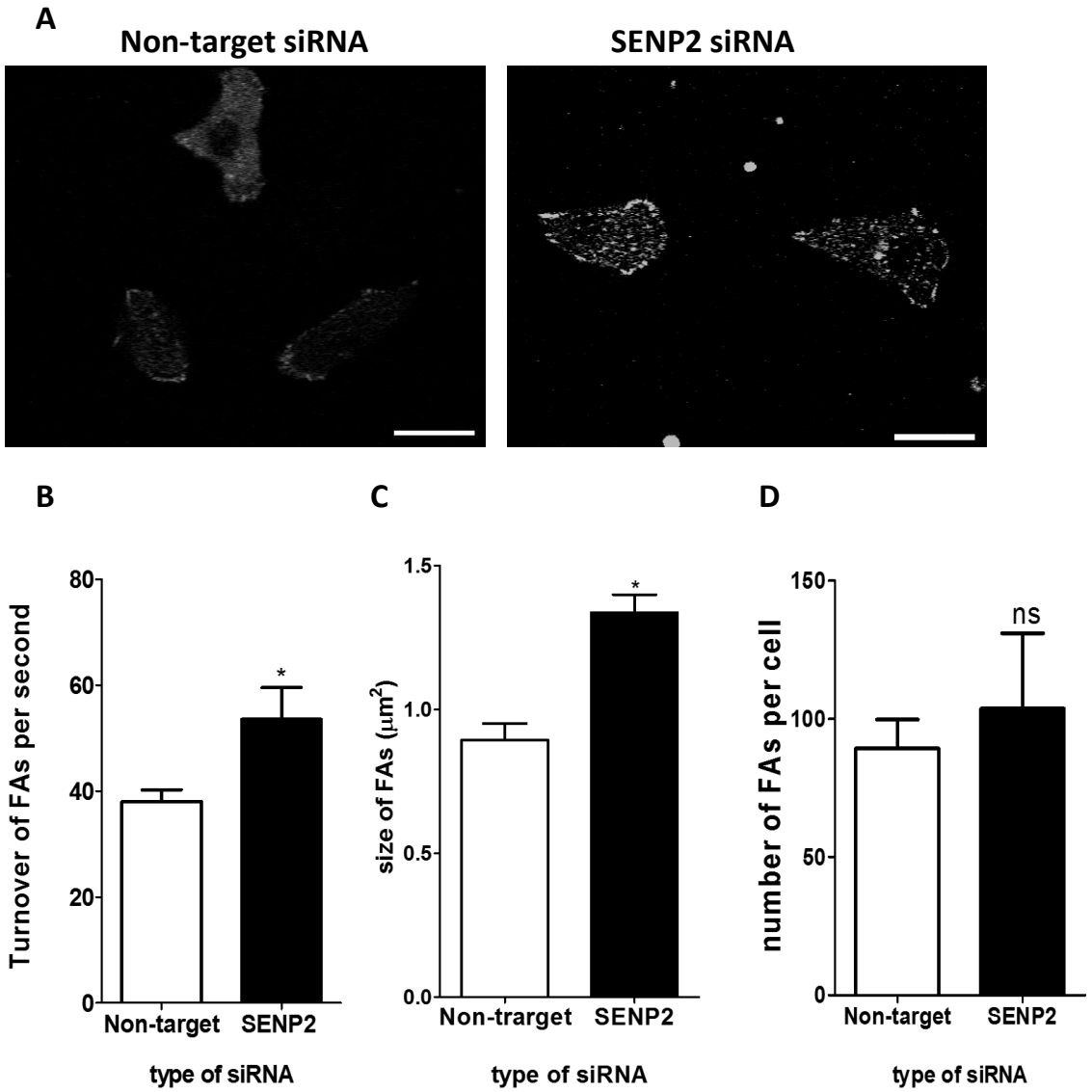

Figure 3.8 Effects of silencing SENP2 on the turnover, size and number of vinculin-containing FAs in MDA-MB-231 cells. Cells were transfected with non-target siRNA (control) or 35 nM SENP2 siRNA and 24 hours post-transfection; cells were transfected with YFP-vinculin and grown for additional 24 hours. Short timelapse movies were generated using confocal microscopy. A) Representative images of vinculin containing FAs for control cells (treated with 35 nM non-target siRNA) or 35 nM SENP2 siRNA treated cells. Scale bar = 20 μm. B) Quantification analysis showing the mean FA turnover measurements (C) the mean FA size (D) the mean FA number in control compared to 35 nM SENP2 siRNA transfected cells. Data was presented as mean ± SEM of three independent experiments, in each experiment a total number of 120 focal adhesions (16 cells) for turnover analyses and at least total number of 60 cells for size and number analyses. T-test was used to evaluate any significance differences between groups (*, ** and *** represent P <0.05, 0.01 and 0.001, respectively).

3.6 Discussion

SUMOylation has been implicated in the regulation of proteins involved in both normal and pathological cellular processes. The expression of SUMO and SUMO-associated proteins has been found to be deregulated in various cancer types and this deregulation is thought to enhance cancer progression and metastasis (Seeler and Dejean, 2017). SUMOylation has previously been reported to be involved in cell migration through modification of proteins that have direct or regulatory roles in cell migration. Cytoskeletal networks provide the tension forces required for cell migration and SUMOylation was shown to regulate their formation by targeting the basic subunits of actin filaments (F-actin) and microtubules (MT), actin and tubulin, respectively (Panse et al., 2004, Hofmann et al., 2009). In addition, it modifies proteins that have a regulatory role in cell migration such as Rac1 GTPase that induce the formation of different actin filament structures such as lamellipodia, filopodia, stress fibres and membrane ruffles (Nobes and Hall, 1995, Castillo-Lluva et al., 2010). Furthermore, SUMOylation has been implicated in the regulation of matrix metalloproteases (MMP), which usually degrade extracellular matrices during cell invasion (Cashman et al., 2014, Lao et al., 2019). However, its roles in cell migration remain poorly appreciated due to the continuous identification of novel SUMO substrates with various functions in cell migration. SUMOylation appears to have a wider role in cell migration, as recent screening studies and SUMOylation prediction tools revealed new SUMOylation targets that exhibit critical roles in cell migration. For example, focal adhesions play a critical role in cell migration and SUMOylation has been reported previously to modify one of the critical FA proteins, FAK, and its SUMOylation was shown to be required for cancer cell migration (Kadaré et al., 2003). Vinculin and talin have critical roles in the formation and

stability of FAs and a recent screening study identified them among SUMO substrates (Xiao et al., 2016). Therefore, investigating the association between SUMOylation and these adhesion sites will expand the current body of knowledge in this field. It will increase our understanding of its roles in cancer cell migration and it could also shed light on targets that could be used to prevent cancer metastasis.

This chapter investigates the effects of inhibiting SUMOylation, using two different SUMOylation inhibitors, or silencing SENP2 on cell migration and the dynamic activities of FAs in MDA-MB-231 cells. Ginkgolic acid (Gka) has been identified as a global SUMOylation inhibitor without affecting ubiquitination. This inhibitor is the most widely used and commercially available SUMOylation inhibitor (Yang et al., 2018). The molecular mechanism and specificity of this natural product compound has been characterised in the literature. This compound was found to bind to the SUMO E1 activating enzyme (SAE) and prevent its interaction with SUMO proteins, thereby disrupting the SUMOylation pathway (Fukuda et al., 2009). The selective activity of this inhibitor as a SUMOylation inhibitor was investigated previously. For instance, introducing a mutant in the SUMO substrate, Nephrin, to prevent its SUMOylation or treating cells with Ginkgolic acid decreased its stability and expression in the membrane (Tossidou et al., 2014). On the other hand, this molecule was found to affect different cellular functions by altering the activity of proteins via mechanisms other than SUMOylation. For example, Gka was found to activate phosphatase 2C (PP2C), which has been implicated in the regulation of various cellular processes including cell growth, apoptosis and stress responses (Ahlemeyer et al., 2001). However, to activate this phosphatase, a high concentration of Gka (500 µM) is necessary, whereas inhibiting

SUMOylation can be achieved using much lower concentrations (Fukuda et al., 2009). In addition, Gka was found to inhibit the acetylation of histones in vitro at concentration of 10 µM (Balasubramanyam et al., 2003). Acetylation of histones is a critical regulatory mechanism that modifies the chromatin structure to allow gene transcription and DNA replication and repair (Roth et al., 2001). However, treating cells with 10-100 µM of Ginkgolic acid has no inhibition effects on histone acetylation, whereas SUMOylation was inhibited by this treatment (Fukuda et al., 2009). Taken together, these findings suggest that Ginkgolic acid is more likely to inhibit SUMOylation at the employed concentration, rather than exhibit non-specific interference with other cellular processes.

In this current study, Gka was used to inhibit SUMOylation in MDA-MB-231 cells. Cell migration assays revealed a significant reduction in the migration of these cells when treated with concentrations 25 µM, 50 µM or 100 µM of this inhibitor. This could indicate the important role of SUMOylation in cancer cell migration. To confirm that this reduction in migration is due to inhibiting SUMOylation and not interventions of Gka with other pathways, another SUMOylation inhibitor, Gossypetin was used and the effects of this inhibitor on the migration of MDA-MB-231 cells were assessed by cell migration assays. Gossypetin (3,5,7,8,3',4'-Hexahydroxyflavone) is an oxygenated flavonoid derivative that has recently been identified to have SUMOylation inhibitory activity (Kim et al., 2013). Treating cells with 100 µM of this inhibitor decreased wound closure significantly. Although it showed SUMOylation inhibitory activity, Gossypetin selective activity and effects on other cellular mechanisms has not been reported yet. Therefore, the effects of this inhibitor on cell migration cannot be linked to SUMOylation with high confidence as the effects of Gka.

Reduction of cell migration in MDA-MB-231 cells when treated with either inhibitors increases the possibility that these effects on their migration is due to inhibition of SUMOylation, not intervention with other processes. The reduction in cell migration when blocking SUMOylation can be explained in different ways. One of them is the involvement of SUMOylation in the regulation of cytoskeletal networks. The driving force of cell motility, actin filaments, are composed of actin polymers that extend toward the plasma membrane. The formation of these cytoskeletal filaments at the edges of migrating cells promotes cell migration by generating the required force to push the plasma membrane forward. Actin has been shown to be a SUMOylation target indicating the involvement of this protein modification system in the regulation of actin filaments and consequently cell migration (Panse et al., 2004, Hofmann et al., 2009). In addition, SUMOylation has been reported to modify critical cytoskeletal regulatory proteins including Rac1 GTPase. This GTPase is involved in the regulation of cell migration by inducing the formation of different actin filament structures such as lamellipodia, filopodia, stress fibres and membrane ruffles (Nobes and Hall, 1995). SUMOylation was reported to be required for stabilising this GTPase in its active state, and this stable active form is required for cell migration and invasion (Castillo-Lluva et al., 2010). Furthermore, Arp2/3 complex is another critical regulator of actin, and it functions by binding to previous actin filaments at the leading edge of the membrane and initiating new branches of these filaments. These newly formed actin filaments push the plasma membrane forward, facilitating cell motility. This complex is composed of Arp2 and Arp3 proteins and five smaller proteins called Arcs (Goley and Welch, 2006). Proteomic studies identified that some components of Arp2/3 complex, particularly Arc35p and Arc40p, can be SUMO modified (Sung et al., 2013). Therefore, the reduction in

cell migration when inhibiting SUMOylation could be caused by the impairment in cytoskeleton network.

The other explanation is the involvement of SUMOylation in the regulation of MMPs. In a recent study, silencing SUMO1 was shown to reduce the migration of fibroblast-like synoviocytes (FLSs) (Lao et al., 2019). The reduced migration of FLSs was linked to impairment in the formation of lamellipodium and reduction in the activity of Rac1. In the same study, they found that knocking down SUMO1 caused a down regulation in the expression of MMP1 and MMP3. In a different study, Ginkgolic acid was found to supress wound healing in breast cancer cells (Hamdoun and Efferth, 2017). In this study it was found that Gka treatment prevented the SUMOylation of NF-κB essential modulator (NEMO) and consequently reduced the activity of the transcription factor NF-κB, which caused a down regulation in metastasis-associated genes including C-X-C chemokine receptor type 4 (CXCR4) and MMP9 (Hamdoun and Efferth, 2017). Thus, the reduction in cell migration when inhibiting SUMOylation could be caused by downregulating these proteases, which in turn reduces cell's ability to invade surrounding microenvironment.

The previous examples indicate a critical role of SUMOylation in different aspects of cell migration. However, it appears that SUMOylation has a wider role in cell migration. SUMOylation could possibly be involved in the regulation of cell migration by regulating FA dynamics. Focal adhesion kinase (FAK) is critical regulator of FAs and cell migration (Ilic et al., 1995). Its phosphorylation, which is induced by the attachment of talin to ECM, is required for its activation (Mitra et al., 2005). SUMOylation was suggested previously to

enhance its auto-phosphorylation (Kadaré et al., 2003). In addition, SUMOylation was found to be involved in its nuclear localisation in non-small cell lung cancer (NSCLC) without effecting its phosphorylation levels. Despite the important role of SUMOylation in its activity, the SUMOylation of this kinase occurs in the nucleus indicating a different function from its roles at FAs (Constanzo et al., 2016). Nevertheless, the implication of SUMOylation in regulating its activity alongside with a proteomic study that identified other key FA proteins, vinculin and talin, (Xiao et al., 2016) as SUMO targets encourages investigating the role of SUMOylation in the regulation of FA dynamics and consequently cell migration.

In this project, two different SUMOylation inhibitors were used to block SUMOylation in MDA-MB-231 cells and a confocal microscope was used to monitor the dynamics of FAs. Treating cells with either inhibitors leads to a significant reduction in the turnover rate of FAs compared to control. In addition, treating cells with Gka or Gossypetin resulted in a significant increase in their size. The slower turnover and increased size of FAs when inhibiting SUMOylation could suggest a critical role of this post-translational modification mechanism in the regulation of FAs. This impairment in FA dynamics could be one of the main causes that led to a reduction in the migration of MDA-MB-231 cells observed in cell migration assays. This impairment could be caused by preventing the SUMO modification of FA proteins. For example, a recent study indicated that the expression of the SUMO E3 ligase, PIASI, induced calpain-mediated cleavage of FAK leading to its disengagement from FAs and translocation to the nucleus. After being translocated into the nucleus, FAK induces the transcriptional activity of various genes involved in cell migration. Silencing this ligase reduced the localisation of FAK into the nucleus and decreased the stability of F-actin fibres

(Constanzo et al., 2016). FAK is important for the turnover of FAs as knocking it down caused a significant increase in the number and size of FAs in fibroblasts and consequently reduced their migration (Ilic et al., 1995). Taken together, these findings support the hypothesis that SUMOylation enhances cell migration by regulating the turnover of FAs. It seems possible that SUMOylation enhances FA turnover by regulating the activity of this kinase, which in turn regulates the recruitment of additional proteins to FAs and the stability of F-actins, thus enhancing cell migration. Calpain-mediated cleavage of FAK was reported previously to enhance the turnover of FAs by inducing the disassembly of existed FAs (Chan et al., 2010) and SUMOylation was found to induce the cleavage of FAK by calpain-2 (Constanzo et al., 2016). Therefore, SUMOylation could enhance FA turnover by inducing the cleavage of FAK and its nuclear translocation. In addition, SUMOylation could target other FAs proteins to regulate the turnover of these adhesion sites.

Protein modification by SUMO proteins is rapidly reversed by SUMO proteases (SENPs) making it an ideal regulatory mechanism in cell migration, which requires rapid and reversible regulation of its associated processes. DeSUMOylation is critical in cell migration as silencing SENPs reduced cell migration in different cancer types (Wang et al., 2013, Ma et al., 2014). The expression of these proteases was shown to be deregulated in different cancer types, and their overexpression is associated with cancer progress and metastasis (Ma et al., 2014, Xu et al., 2011). For instance, overexpression of SENP1 was shown to increase androgen-receptor (AR) activity, and the activity of this receptor is associated with prostate cancer tumorigenesis (Cheng et al., 2004, Kaikkonen et al., 2009). In addition, silencing this protease in pancreatic ductal adenocarcinoma resulted in the disruption of

different cellular functions including cell proliferation and migration (Ma et al., 2014). Furthermore, silencing SENP5 in breast cancer cells reduced their migration and proliferation ability (Cashman et al., 2014). Overexpression of SENP3 in gastric cancer cells enhances their ability to undergo epithelial-to-mesenchymal transition (EMT), which in turn increases their migration capability (Kalluri and Weinberg, 2009). Collectively, these findings indicate the importance of SENPs overexpression in different cancer types. Their overexpression is likely to be involved in the DeSUMOylation of regulatory proteins involved in tumorigenesis and metastasis. However, the expression of a particular SUMO protease, SENP2, has been reported to be reduced in metastatic cancers. The expression of SENP2 was found to be reduced in metastatic bladder cancer cells and re-expressing this protease reduced their migration (Tan et al., 2013). This reduction in cell migration when re-expressing SENP2 indicates that this protease possibly DeSUMOylate proteins associated with cell migration, and DeSUMOylating these proteins reduced their functions. As several FA proteins are possible SUMO substrates, SENP2 could be involved in their regulation. Due to the importance of DeSUMOylation in cancer cell migration, investigating its roles in cell migration and in FA dynamics is one of the main goals of this project.

SENP2 was chosen for this investigation as it has been reported to shuttle between the nucleus and the cytoplasm (Itahana et al., 2006), while the rest of the SUMO proteases were mostly located in the nucleus. In addition, unlike other SUMO specific proteases, the expression of SENP2 was found to be downregulated in different cancer types suggesting a distinct role in cancer progress and metastasis. For example, the expression of SENP2 in bladder cancer samples was downregulated and re-expression of this protease in these cells

was found to decrease cell migration by downregulating the expression of MMP13. This protease was shown to inhibit the translocation of β-catenin to the nucleus, where the later protein activates the transcriptional activity of MMP13, increasing cancer metastasis (Tan et al., 2015). SENP2 could prevent the translocation of FAK to the nucleus via a similar mechanism and consequently reduces cell migration. Taken together, investigating its roles in FA dynamics and cancer cell migration is important. Since SUMOylation enhances FA dynamics, DeSUMOylation by SENP2 could regulate their dynamic differently. Evaluating its effects on FA turnover and cancer cell migration would increase our understanding of the whole picture of SUMOylation roles in these processes. It could also shed light on potential therapeutic target for cancer metastasis intervention.

In this project, the role of SENP2 in FA dynamics and cancer cell migration was investigated. Cell migration assays revealed a significant reduction in the migration of MDA-MB-231 cells when silencing SENP2 or SENP5 compared to control. This finding indicates the important roles for these proteases in cell migration. The critical requirement of these SUMO proteases in cell migration could be explained by two different possibilities. The first explanation could be the requirement of these proteases in the activation of SUMO proteins, therefore, knocking them down disrupted the SUMOylation pathway leading to impairment in various cellular functions including cell migration. The other possibility could be the involvement of these proteases in the De-SUMOylation of key proteins involved in cell migration. Their expression could be required in cell migration to maintain the SUMOylation levels of cell migration-associated proteins for efficient regulation.

The data in this chapter revealed a significant increase in the size and turnover time of FAs when treating cells with SUMOylation inhibitors. Silencing SENP2 was an alternative way to further investigate the involvement of SUMOylation in the regulation of FAs. Western blot revealed that SENP2 is expressed in MDA-MB-231 cells, and immunostaining showed that it is located in the cytoplasm. As SUMOylation was suggested to be involved in the modification of FA proteins, SUMO proteases must interact with these proteins to regulate their SUMOylation levels. Being expressed in the cytoplasm of MDA-MB-231 cells, SENP2 is more likely to interact with FA proteins. Immunostaining studies revealed a cytoplasmic localisation of this protease with vinculin. The localisation of SENP2 with vinculin could suggest a possible role of this protease in the regulation of FAs.

Immunoprecipitation was also used to further investigate whether SENP2 interacts with FA proteins. The data showed an interaction between SENP2 and various FA proteins including talin, vinculin, FAK and paxillin. To confirm this interaction, reversed immunoprecipitation of these proteins was performed, and Western Blot detected the presence of SENP2 in these immunoprecipitations. This interaction indicates that this protease is most likely involved in the regulation of FAs via de-SUMOylating associated proteins. It could regulate the turnover of FAs and cell migration by tightly controlling the level of SUMOylation of associated proteins.

To investigate the possible regulatory role of SENP2 in the dynamic activities of FAs, SENP2 siRNA was used to silence it in MDA-MB-231 cells and a confocal microscope was used to monitor the turnover of FAs. The results showed that silencing SENP2 leads to a significantly slower turnover and an increased size of FAs compared to control. This finding could

indicate that the reduction in cell migration observed in cell migration assays could be due to impairment in FAs turnover. It could also indicate the critical role of this protease in the regulation of FAs. It could be involved in the DeSUMOylation of key FA proteins. On the other hand, it could be simply explained because of its importance in the activation of SUMO proteins leading to SUMO modification of FA proteins.

Taken together, the findings in this chapter indicate a critical role of SUMOylation in the regulation of FA dynamics to enhance cancer cell migration. The use of two different SUMOylation inhibitors increases the possibilities that these effects are the consequences of inhibiting SUMOylation. In addition, using siRNA against SENP2 is another way of evaluating the impact of this post-translational modification system on the dynamics of FAs. Both approaches suggest the requirement of SUMOylation to enhance the turnover of these adhesion sites and consequently cell migration. However, the lack of more detailed characterisation of the specificity and side effects of current SUMOylation inhibitors require alternative ways to further confirm this finding. In addition, as SUMOylation plays important roles in various cellular functions, inhibiting global SUMOylation is not the best way to investigate its direct roles in specific functions such as the turnover of FAs. To overcome these issues, mutagenesis is a powerful technique used to introduce mutations in a specific protein target. Therefore, it can be used to mutate SUMOylation sites in FA proteins to prevent their SUMOylation. Thus, it allows investigating the effects of preventing SUMOylation of specific proteins without effecting global SUMOylation.

4. Identification of a direct role for SUMOylation in FA dynamics through SUMOylation of vinculin.

4.1 Introduction and Hypothesis

The previous chapter demonstrates the critical role of SUMOylation in the dynamics of FAs and cancer cell migration. However, as SUMOylation is involved in a variety of critical cellular processes, the effects of inhibiting SUMOylation on FA turnover and cell migration mean that it could be argued that a disruption of various cellular functions has occurred by inhibiting total SUMOylation. These effects account for the reduced cell migration. In addition, the specificity of the current SUMOylation inhibitors could be doubted as they have been reported to influence the activity of other regulatory mechanisms including the acetylation of histones (Balasubramanyam et al., 2003) and activating phosphatase 2C (PP2C) (Ahlemeyer et al., 2001). Therefore, one aim of this chapter is to be more confident that the impairment in FA dynamics when inhibiting SUMOylation using inhibitors is due to the direct effects on FA proteins rather than the general disruption of SUMOylation on the proteins involved in other cellular processes. SUMOylation has previously been shown to modify a key FA protein (FAK). Focal adhesion kinase (FAK) is one of the SUMO1 targets and its SUMOylation was found to be required for its activity and nuclear translocation (Kadaré et al., 2003). The nuclear translocation of this kinase was suggested to be critical in cancer progression and cell migration (Constanzo et al., 2016). However, the SUMOylation of FAK was found to occur mainly in the nucleus, indicating a distinct function from its role within FA sites (Kadaré et al., 2003).

Nevertheless, the requirement of SUMOylation in FAK functions encourages investigating the role of SUMOylation on other FA proteins within FA sites. Vinculin and talin, important FA proteins, were identified as SUMO substrates in a recent proteomic study (Xiao et al., 2016). Vinculin plays a critical role in anchoring FAs to actin filaments by binding to talin and actin (Carisey et al., 2013). The loss of vinculin in cancer cells reduced the strength of cell adhesion and cell spreading and enhanced cell migration (Coll et al., 1995, Saunders et al., 2006). In addition, silencing the SUMO E3 ligase, PIASI, decreased the localisation of vinculin to FA complexes (Constanzo et al., 2016). Overall, these findings in the literature suggest a critical role of vinculin in the dynamics of FAs and cell migration and that SUMOylation could be involved in the regulation of its activity.

Hypothesis

In this current study, SUMOylation of vinculin was hypothesised to be important for FA dynamics. Additionally, the creation of nonSUMOylatable vinculin by replacing lysine with arginine at SUMO motifs was hypothesised to increase FA turnover time. To test this hypothesis, different steps were taken. Bioinformatic tools were used to predict FA proteins that have SUMOylation motifs. Several FA proteins including vinculin, talin, VASP and FAK were predicted to possess strong SUMOylation consensus motifs. Vinculin was selected to evaluate the possible role of SUMOylation in the regulation of FA dynamics. Then, the interaction between vinculin and SUMO or SUMO-associated enzymes has been investigated using Co-IP and co-localisation studies. Site-directed mutagenesis has been used to substitute the lysine residues with arginine in the SUMOylation consensus motifs that have the highest scores in vinculin in order to prevent its SUMOylation.

Co-immunoprecipitation has been used to assess the interaction between SUMO2/3 and WT or mutated vinculin using anti-GFP and anti-SUMO2 antibodies. A confocal microscope was used to investigate the effects of these mutations on the number, size and the turnover of FAs. It has also been used to track WT or mutated vinculin transfected cells to study the effects of these mutations on the migration of MDA-MB-231 breast cancer cells. Other cancer cells have been used.

4.2 Several FA-associated proteins are shown to have strong SUMOylation consensus motifs and SUMO-interacting motifs (SIMs).

In order to investigate the effects of SUMOylation on FAs, bioinformatic tools including JASSA, GPS-SUMO and SUMOplot were used to identify potential FA-associated SUMOylation targets according to the presence of the SUMOylation consensus motifs (Beauclair et al., 2015). Several FA proteins were predicted to have different SUMOylation consensus motifs and/or SUMO-interacting motifs (SIMs) (Table 4.1). Talin and vinculin were predicted to have a Phosphorylation-dependent SUMOylation motif (PDSM) and a hydrophobic cluster SUMOylation motif (HCSM) respectively (Table 4.1 (A)). In addition, a negatively charged amino acid dependent SUMOylation motif (NDSM) was predicted to be present in FAK, VASP and integrin α_v proteins. SUMOylation consensus motifs were not found in other FA proteins such paxillin, zyxin or α-actinin-1. However, most of these proteins were predicted to have SIMs (Table 4.1 (B)). These later motifs could facilitate their non-covalent interaction with SUMOylated proteins indicating a possible role for SUMOylation in the interaction between FA proteins.

Table 4.1 List of SUMOylation motifs predicted by bioinformatic tools in FA proteins. A) Showing the predicted sites of SUMOylation consensus motifs with high scores in FA proteins. B) Showing the predicted sites of SUMO-interacting motifs (SIMs) in FA proteins.

A

FA protein	Position K	Motif Sequence	Consensus type	JASSA Best PS	GPS-SUMO score
Talin	K841	IKADAEGESDL	Extended PDSM[i]	Low	6.359
	K2445	VKADQDS	Extended PDSM	High	4.358
Vinculin	K80	AFIKVE	HCSM[ii]	High	23.75
	K496	EGKI	Strong inverted[iii]	High	2.348
	K768	AKREVENSEDP	NDSM[iv]	Low	2.378
FAK	K152	VKSDYMLEIAD	NDSM	High	4.273
	K141	EDKP	Inverted	High	1.779
VASP	K252	PKAE	Consensus[v]	High	9.513
	K286	PKDESANQEEP	NDSM	High	10.879
	K348	VKQELLEEVKK	NDSM	High	12.978
	K356	VKKELQKVKEE	NDSM	High	12.462
Integrin α_v	K589	PKLEVSVDSDQ	NDSM	High	6.47

i Phosphorylation-dependent SUMOylation motif (**PDSM**), (ΨKxExxSP).
ii Hydrophobic cluster SUMOylation motif (**HCSM**), (Ψ_3KxE).
iii **Inverted** SUMOylation motif (αxkΨ).
iv Negatively charged amino acid-dependent SUMOylation site (**NDSM**), (Ψ_2Kxαxα$_{2/6}$).
v SUMOylation **consensus** motif, (ΨKxα), where Ψ is a hydrophobic, k lysine, α is an acidic, x is any amino acid.

B

FA protein	Position site	SIM sequence	SIM Type	PS
Talin	AA 397-400	DIIL	SIM Type 4[i]	0.442
	AA 557-560	VVNL	SIM Type β[ii]	0.573
	AA 2078-2081	VVLI	SIM Type β	2.169
Vinculin	AA 134-137	IIRV	SIM Type β	0.272
	AA 244-247	IIRV	SIM Type β	0.272
FAK	AA 267-270	IISV	SIM Type β	0.272
	AA 793-796	VLDL	SIM Type 1[iii]	4.404
	AA 1047-1050	LLDV	SIM Type 1	0.335
α-actinin	AA 129-132	TIIL	SIM Type 4	0.442
Zyxin	AA 523-526	VVAL	SIM Type β	0.573
Actin	AA 102-105	PVLL	SIM Type 4	0.382
	AA 247-250	VITI	SIM Type β	2.256

i SUMO interacting motif 4 (xΨΨΨ), where Ψ is hydrophobic and x is any amino acid.
ii SUMO interacting motif β ({I/L}- {I/L}-x-{I/L/V}).
iii SUMO interacting motif 1 ({I/L/V}-{I/L/V}-x-{I/L/V}).

4.3 Vinculin interacts with SUMO2 and the SUMO-associated enzymes, Ubc9 and SENP2.

Immunostaining studies were performed to investigate the interaction between SUMO2/3 and the FA protein, vinculin, using confocal microscopy. MDA-MB-231 cells were seeded on coverslips and grown until 80-100% confluency before fixing and subjecting them to immunocytochemistry with SUMO2/3 and vinculin antibodies. The results show a cytoplasmic localisation of SUMO2/3 with vinculin (Figure 4.1).

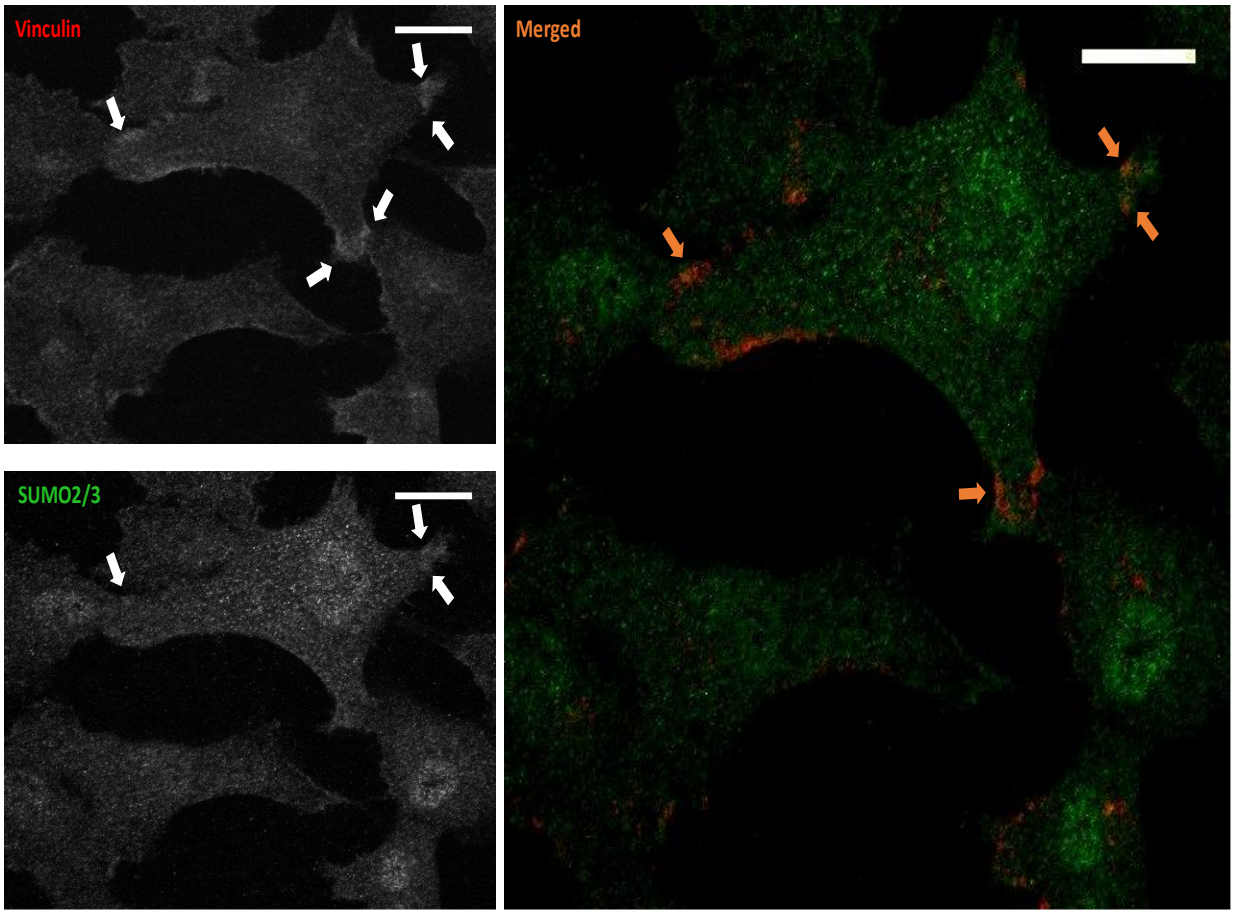

Figure 4.1 Immunostaining of SUMO2/3 and vinculin in MDA-MB-231 cells. Cells were fixed and subjected to immunocytochemistry for SUMO2/3 and vinculin antibodies. Images were taken using a confocal microscope. Vinculin was shown (top left image), while SUMO2/3 was shown (bottom left image) with arrows indicating the distribution of vinculin or SUMO2/3 within the cell. Image on the right demonstrates the co-localisation of SUMO2/3 with vinculin (orange arrow) by merging them using image J (scale bar = 20 μm).

To further support this co-localisation between SUMO2 and vinculin, co-transfection with pAmCyan1-SUMO2 and pZsYellow1-vinculin was used to investigate their possible localisation. MDA-MB-231 cells were co-transfected with both pAmCyan1-SUMO2 and pZsYellow1-vinculin, fixed and confocal microscopy was used to visualise their subcellular distribution (Figure 4.2 (B)). The co-localisation value was analysed using Spearman's (rho) correlation coefficient analysis in ImageJ (Fiji) software. The results show a co-localisation value of 0.556 ± 0.09 between SUMO2 and vinculin (Figure 4.5).

Co-immunoprecipitation was also used to evaluate whether SUMO2 interacts with vinculin. MDA-MB-231 cells were co-transfected with both Ha-SUMO2 and pZsYellow1-vinculin, grown for 24-48 hours before preparing cell lysate. Anti-Ha antibody was mixed with cell lysate overnight before incubating with agarose beads to immunoprecipitate Ha-tagged SUMO2. The interaction between SUMO2 and vinculin was analysed by western blot with anti-GFP antibody. Whole cell lysate was used as a positive control and nonspecific rabbit IgG Co-IP was used as a negative control. Vinculin was detected at 130 kDa in both positive control and Ha Co-IPs, while no bands were present in the negative control (Figure 4.2 (A)). This interaction supports the previous finding in co-localisation studies.

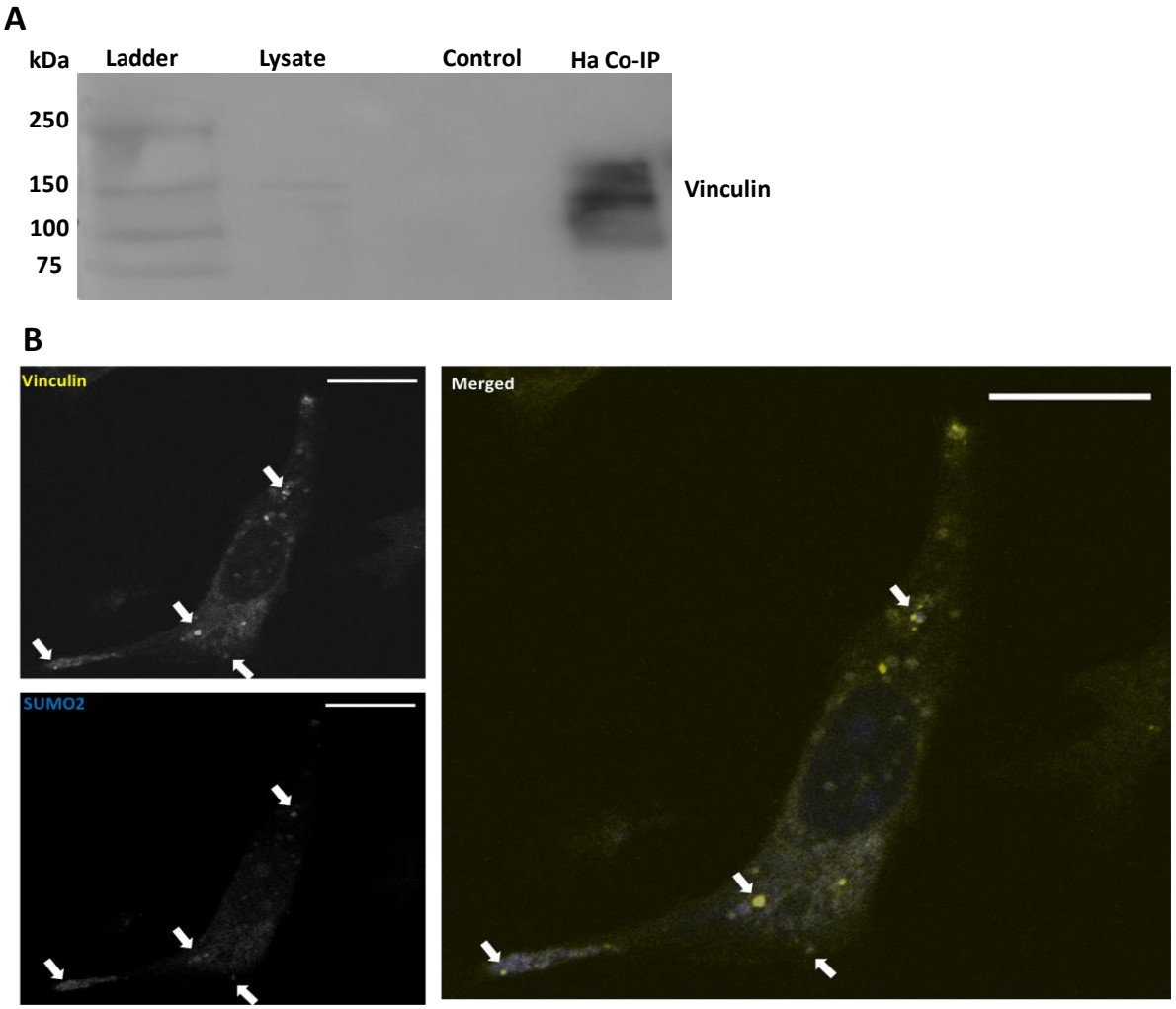

Figure 4.2 SUMO2 interacts with vinculin in MDA-MB-231 cells. A) Ha-SUMO2 IP and Western blotting showing that vinculin protein was detected in Ha-SUMO2 IP at 130 kDa. Total cell lysate was used as a positive control, whereas IgG IP was used as a negative control. B) Confocal microscope images showing the expression of pZsYellow1-vinculin and pAmCyan1-SUMO2 in MDA-MB-231 cells. Cells were transfected with pZsYellow1-vinculin and pAmCyan1-SUMO2, fixed and confocal microscopy was used to take images. Vinculin was shown in top left image, while SUMO2 was shown in bottom left image. Arrows indicate the distribution of vinculin or SUMO2 within the cell. Image on the right demonstrates the co-localisation of SUMO2 with vinculin (white arrows) by merging them using Image J (scale bar = 20 µm).

To further investigate the association between SUMOylation and vinculin, co-localisation studies were performed to investigate the possible interaction between vinculin and the SUMO-associated enzymes, Ubc9 and SENP2. MDA-MB-231 cells were seeded on coverslips and grown until 70% before transfection with pZsYellow1-vinculin. Then, cells were fixed and subjected to immunocytochemistry with Ubc9 antibody. To investigate the association between SENP2 and vinculin, cells were co-transfected with both pAmCyan1-SENP2 and pZsYellow1-vinculin, grown for 24-48 hours before fixing. A confocal microscope was used to visualise the distribution of these proteins within cells and ImageJ (Fiji) software was used to analysis their co-localisation probabilities using Spearman's (rho) correlation coefficient analysis. The results show both a nucleic and cytoplasmic distribution of SENP2 and Ubc9. They also show that Ubc9 is localised with vinculin in the cytoplasm and in the membrane at FA sites (Figure 4.3). The Spearman's (rho) correlation coefficient value of the co-localisation between Ubc9 and vinculin was of 0.63 ± 0.05 (Figure 4.5). In addition, the co-localisation value between SENP2 and vinculin was 0.31 ± 0.03 (Figure 4.5). SENP2 was shown to be localised with vinculin in the cytoplasm, but not at the membrane (Figure 4.4). This localisation between these SUMO-associated proteins and vinculin could further support the possibilities of vinculin as a SUMOylation substrate.

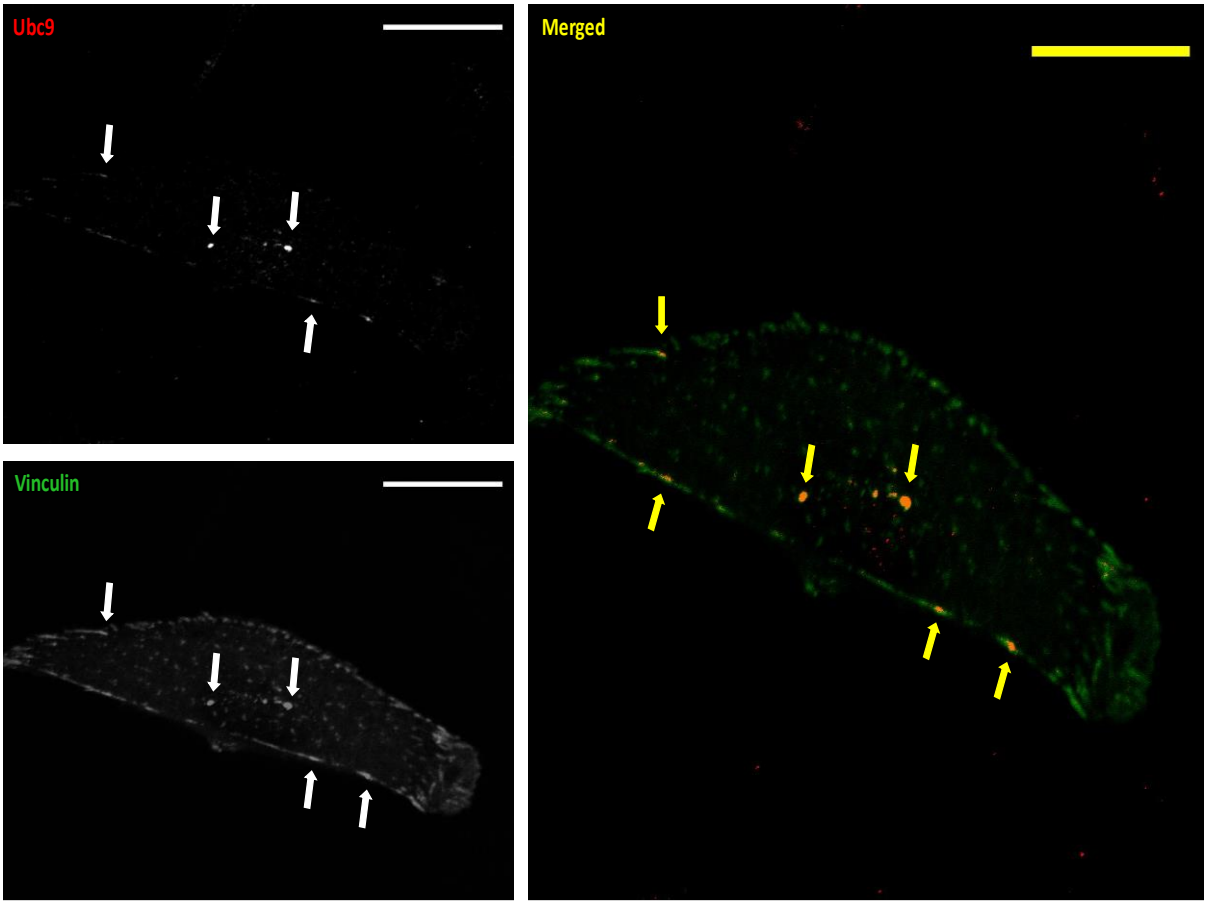

Figure 4.3 Vinculin is localised with the SUMOylation-associated enzyme Ubc9 in MDA-MB-231 cells. Confocal microscope images showing the expression of pZsYellow1-vinculin and immunostaining of Ubc9. Cells were transfected with pZsYellow1-vinculin, fixed and subjected to immunocytochemistry for Ubc9 antibody. Ubc9 was shown as red, while vinculin was shown as green. Arrows indicate the distribution of Ubc9 or vinculin within the cell. Image on the right demonstrates the localisation of Ubc9 with vinculin (yellow arrows show their localisation) by merging them using image J. Scale bar = 20 µm.

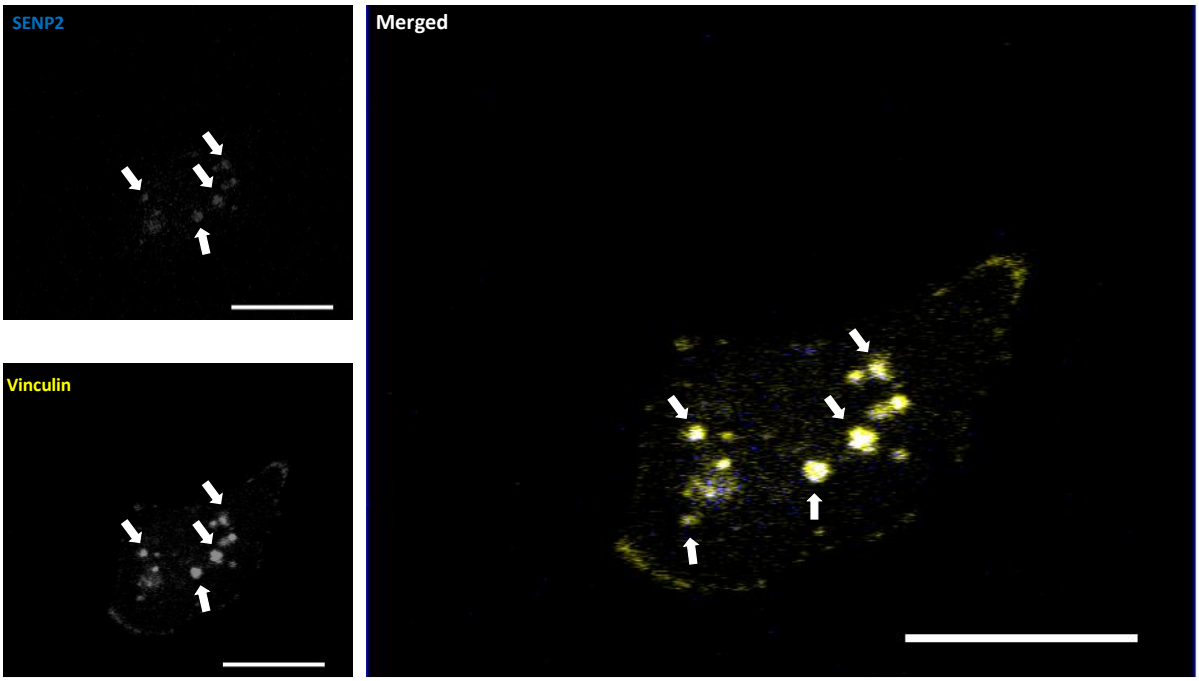

Figure 4.4 Vinculin is localised with the SUMOylation-associated enzyme SENP2 in MDA-MB-231 cells. A) Confocal microscope images showing the expression of pZsYellow1-vinculin and pAmCyan1-SENP2. Cells were co-transfected with pZsYellow1-vinculin and pAmCyan1-SENP2, fixed and confocal microscope was used to take images. SENP2 was shown as blue, while vinculin was shown as yellow. Arrows indicate the distribution of SENP2 or vinculin within the cell. Image on the right demonstrates the co-localisation of SENP2 with vinculin (white arrows show their co-localisation) by merging them using image J. Scale bar = 20 µm.

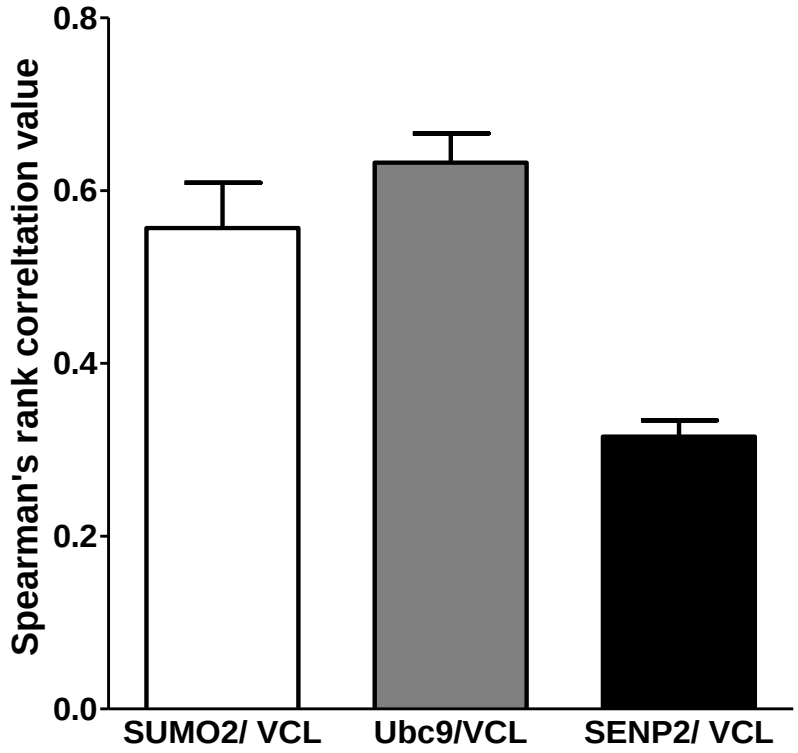

Figure 4.5 Vinculin is colocalised with SUMO2 and SUMO associated enzyme. The graph represents Quantification analysis showing mean spearman's rank correlation values between vinculin (VCL) and SUMO associated proteins, SUMO2, Ubc9 and SENP2. Co-localisation was calculated using spearman rank correlation value with 0 means no co-localisation, whereas 1 means high localisation. Data was presented as mean ± SEM of three independent experiments.

4.4 The lysine 80 (K80) in the amino acid sequence of human vinculin is a strong SUMO site.

As the data in this chapter increases the possibilities of vinculin as a SUMO target, bioinformatic tools were used to identify possible SUMOylation sites in vinculin. Different bioinformatic tools including JASSA, GPS SUMO and SUMOplot predicted the presence of several possible SUMO sites in vinculin with different scores (Table 4.2). One site that has the highest scores in all bioinformatic tools to be a SUMOylation motif is lysine at position 80 (K80). This lysine at position 80 in the amino acid sequence of vinculin was predicted to be in a hydrophobic cluster SUMOylation motif (HCSM). In addition, lysine at position 496 (K496) was shown to have a strong consensus inverted with high score in JASSA. Other possible SUMOylation sites showed the presence of SUMOylation consensus motifs with lower scores than that of K80 and K496. In addition, these tools predicted the presence of SIM interaction motifs at three different sites in this protein (aa 134-137, aa 244-247 and aa 995-998) (Table 4.1 (B)).

In order to identify the regions of K80 and K496 residues in the 3-D fold of vinculin, PyMOL tool was used to visualise its 3-D structure. Unlike K496, lysine at 80 in the amino acid sequence of vinculin is located in the surface of the 3-D structure making it accessible to SUMO proteins binding (Figure 4.6 (B)). Furthermore, multisequence alignment was used to compare the sequences of K80 and K496 SUMOylation consensus motifs in human vinculin with the sequences of these sites in different species. The results show that the amino acid sequence representing the SUMOylation consensus motif at K80 (IKVE) is conserved among different mammalian species, but not the motif at K496 (Figure 4.6 (A)).

Table 4.2 Showing the SUMOylation sites in vinculin. A) List of SUMOylation motifs in vinculin predicted by three separate bioinformatic tools, JASSA, GPS-SUMO and SUMOplot. Direct motifs were highlighted with red, while inverted motifs were highlighted with blue. Scores of predicted sites were presented according to servers scoring systems. K80 showed the highest score in all servers and K496 showed the highest score in inverted motifs in JASSA prediction tool.

Position K	Motif Sequence	Consensus type	JASSA Best PS	GPS-SUMO score	SUMOplot Score	DB Hit
K35	DGKA	Consensus inverted[i]	Low	1.424		
K71	LKRD	Strong consensus[ii]	Low	3.019		2
K80	AFIKVE	HCSM[iii]	High	23.75	0.94	16
K276	DSKL	Strong consensus inverted[iv]	Low	1.216		
K366	AKVE	Consensus[v]	Low	4.139	0.79	
K496	EGKI	Strong consensus inverted	High	2.348	0.67	
K544	AKCD	Consensus	Low	0.757	0.79	
K731	IKKD	Strong consensus	Low	3.532	0.94	1
K768	AKREVENSEDP	NDSM[vi]	Low	2.378	0.79	2
K778	DPKF	Consensus inverted	Low	2.362	0.79	

i Inverted SUMOylation motif (αxkΨ).
ii Strong SUMOylation motif ({I/L/V}kxα).
iii Hydrophobic cluster SUMOylation motif (**HCSM**), (Ψ_3KxE).
iv Strong inverted SUMOylation motif (αxk{I/L/V}).
v SUMOylation consensus motif (Ψkxα).
vi Negatively charged amino acid-dependent SUMOylation site (**NDSM**), (Ψ_2Kxαxα$_{2/6}$).
where Ψ is a hydrophobic, k lysine, α is an acidic, x is any amino acid.

A

Human	KRDMPPAFIKVENACTKLVQ.....VHLEGKIEQA
Chimpanzee	KRDMPPAFIKVENACTKLVQ.....VHLEGKIEQA
Pig	KRDMPPAFIKVENACTKLVQ.....VHLEGKIEQA*
Dog	KRDMPPAFIKVENACTKLVQ.....VHLEGKIEQA
Mouse	KRDMPPAFIKVENACTKLVQ.....VHLEGKIEQA
Chicken	KRDMPPAFIKVENACTKLVR.....VHLEGKIEQA
Xenopus	KRDMPPAFIKVENACAKLVQ.....VNMEGKVEQA
Zebrafish	KRDMPSAFIKVENACAKLVE.....VTLEGKMEQA
Drosophila	QDMPSALHRVEGASQLLEEA.....LKQFTEAVLQ
C. elegans	QDMPPALQRVEGSSKLLEES.....VVDDFADITT

SUMO motif ψKxE

*=K497

K80 motif = isoleucine, lysine, valine, glutamic acid
K496 motif =glycine, lysine, isoleucine/valine/methionine, glutamic acid

B

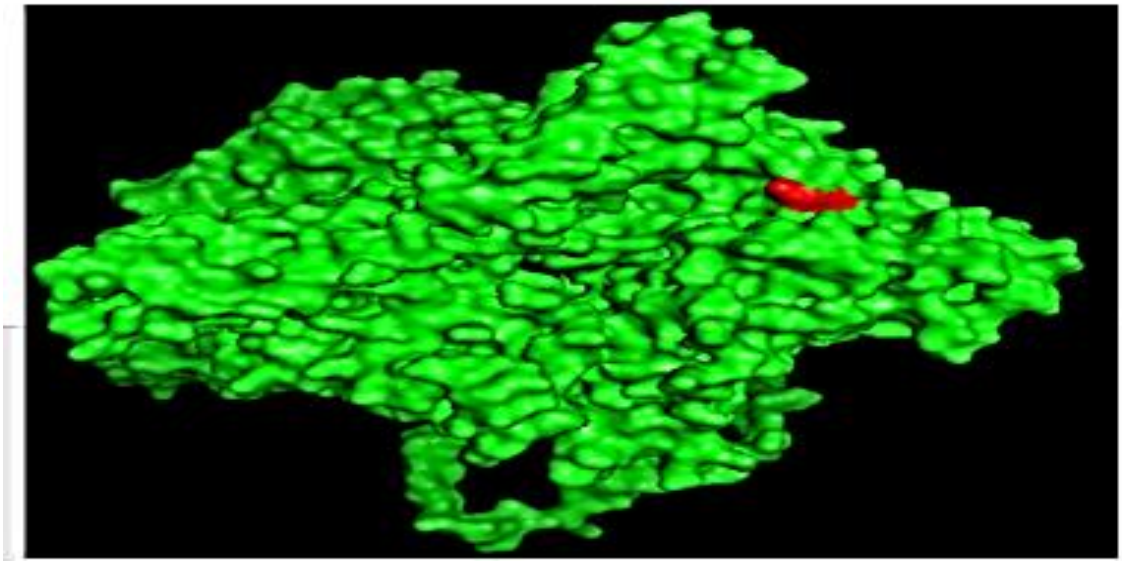

Figure 4.6 Showing the K80 and K496 SUMOylation motifs sites in vinculin. A) Multisequence alignment of the K80 and K496 SUMOylation motifs sequences in human vinculin with these sites in vinculin in different species. Underlined amino acids show the SUMOylation motifs at K80 and K496 (*). Lysine residues (K) were shown as red. The amino acids at the predicted SUMOylation motif at K80 (IKVE) were shown to be conserved among different mammalian species. The isoleucine amino acid at the SUMOylation motif K496 in human vinculin (GKIE) was shown to be non-conserved among different mammalian species. B) Showing the three-dimensional structure of vinculin. K80 (red) is in the surface of vinculin, but not K496.

4.5 The K80R mutation in human vinculin reduces its interaction with SUMO2

Mutagenesis was used to create specific mutations in human vinculin. Individual mutations, K80R or K496R, or combined mutations, K80R/K496R, were created. Co-immunoprecipitation was utilised to investigate the effect of these mutations on vinculin-SUMO2 interaction. MDA-MB-231 cells were co-transfected with both Ha-tagged SUMO2 and WT or mutated vinculin, grown for 24-48 hours before preparing whole cell lysate. Anti-Ha antibody was mixed with cell lysate overnight before incubating with agarose beads to immunoprecipitate Ha-tagged SUMO2. The interaction between SUMO2 and vinculin was analysed by western blot with anti-GFP antibody. Vinculin was detected at 130 kDa in both Ha Co-IPs of WT and mutated vinculin-transfected cells. Interestingly, in Ha Co-IP samples prepared from whole cell lysate of cells transfected with K80R vinculin, there was much less SUMOylated vinculin compared to cells transfected with WT vinculin (Figure 4.7 (B)). Reverse Co-IP was used to further confirm the effect of these mutations on the interaction between SUMO2 and vinculin. Anti-GFP antibody was mixed with cell lysate prepared from cells co-transfected with both Ha-SUMO2 and WT or mutated vinculin. Anti-Ha antibody detected the presence of SUMO2 in all Co-IP samples. Interestingly, there was much less SUMOylated vinculin in samples prepared from cells transfected with either K80R or K80R/K496R mutated vinculin compared to WT or K496R vinculin.

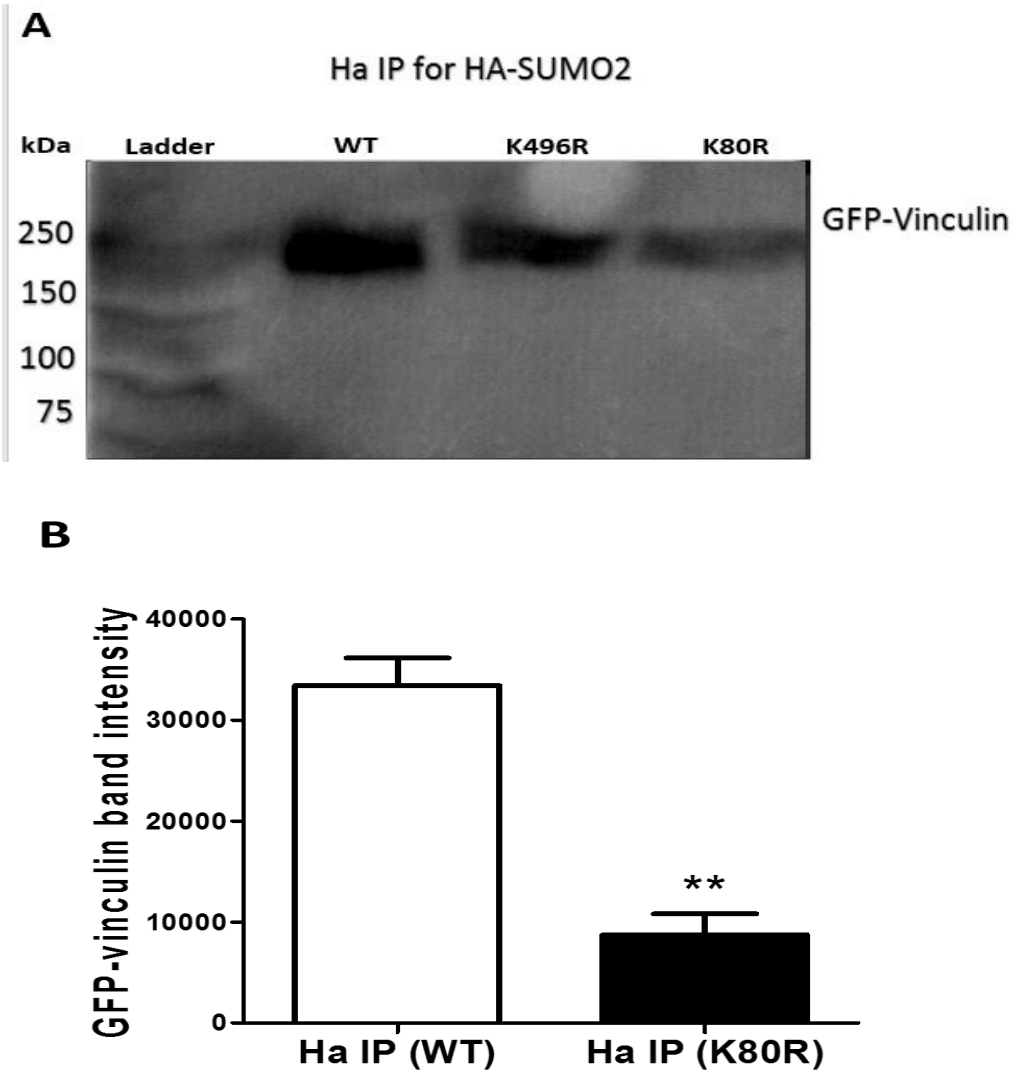

Figure 4.7 Immunoprecipitation and Western blot showing that the K80R mutation in vinculin reduces its interaction with SUMO2. A) HA IP for Ha-SUMO2 and WB showing that less amounts of K80R vinculin molecules was detected in Ha-SUMO2 IP compared to WT or K496R IPs. B) Quantification of band intensity of GFP-vinculin in Ha IPs of cell lysates of WT or K80R transfected cells. Data was presented as mean ± SEM of three independent experiments. T-test with was used to evaluate any significant differences between groups (*, ** and *** represent P <0.05, 0.01 and 0.001 respectively).

4.6 The K80R mutated vinculin significantly increases the size of FAs and leads to a slower turnover and reduces cell migration of MDA-MB-231 cells.

As vinculin was found earlier in this chapter to interact with SUMO and SUMO-associated proteins, this part of this chapter focuses on the effects of this mutation on the dynamic activities of FAs. MDA-MB-231 cells were transfected with WT or mutated vinculin, grown for 24-48 hours and confocal microscopy was used to monitor the dynamics of FAs. The results show that the turnover of vinculin-containing FAs was significantly slower in cells transfected with K80R (Figure 4.8 (C)) or K80R/K496R (Figure 4.8 (D)) mutated vinculin compared to cells transfected with WT (Figure 4.8 (A)) or K496R mutated vinculin (Figure 4.8 (B)). In control cells, the average turnover of FAs was 36.3 ± 1.3 seconds compared to 74.75 ± 6.5 seconds in cells transfected with K80R vinculin ($p<0.001$) and 61.9 ± 0.85 seconds in cells transfected with K80R/K496R vinculin ($p<0.01$) (Figure 4.8 (E)). No significant changes were observed between WT and K496R vinculin transfected cells. No significant changes were observed between K80R and K80R/K496R transfected cells.

The size of FAs was also affected by this mutation. Results in figure 4.9 show a significant increase in the size of FAs from 1.12 ± 0.03 μm^2 in control cells (transfected with WT vinculin) to 1.53 ± 0.10 μm^2 in K80R vinculin transfected cells ($p<0.05$) or 1.48 ± 0.07 μm^2 in K80R/K496R transfected cells ($p<0.05$). No significant changes in the size of FAs were observed between WT and K496R vinculin transfected cells or between K80R and K80R/K496R transfected cells (Figure 4.9 (B)).

However, there were no significant effects of these mutations on the number of vinculin-containing FAs in these cells. The number of FAs in control cells (transfected with WT vinculin) was 34.37 ± 3.05 FAs compared to 32.10 ± 3.2 FAs in K496R vinculin transfected cells, 40.53 ± 7.87 FAs in K80R vinculin transfected cells and 31.57 ± 5.58 FAs in cells transfected with K80R/K496R transfected cells (Figure 4.9 (C)).

Similar effects were shown when seeding cells on 2 mg/ml collagen, 1% gelatin or fibronectin coated wells. The average turnover of FAs in control cells (transfected with WT vinculin) on collagen was 33.26 ± 1.37 seconds compared to 48.26 ± 2.46 seconds in K80R vinculin transfected cells ($p<0.01$) and 50.83 ± 0.98 seconds in K80R/K496R transfected cells ($p<0.001$) (Figure 4.10 (A)). This significantly slower turnover of FAs was also observed in cells seeded on gelatin or fibronectin. The average turnover of FAs in control cells on gelatin was 35 ± 0.67 seconds compared to 47.68 ± 0.50 seconds in K80R vinculin transfected cells ($p<0.01$) and 50.75 ± 2.73 seconds in K80R/k496R transfected cells ($p<0.001$) (Figure 4.10 (B)). In addition, the average turnover of FAs in control cells seeded on fibronectin wells was 35.02 ± 1.5 seconds compared to 49.44 ± 2.42 seconds in K80R vinculin transfected cells ($p<0.01$) and 48.03 ± 0.03 seconds in K80R/K496R transfected cells ($p<0.01$) (Figure 4.10 (C)). No significant changes in the turnover of FAs were observed between WT and K496R vinculin transfected cells or between K80R and K80R/K496R transfected cells on these different coating surfaces (Figure 4.10).

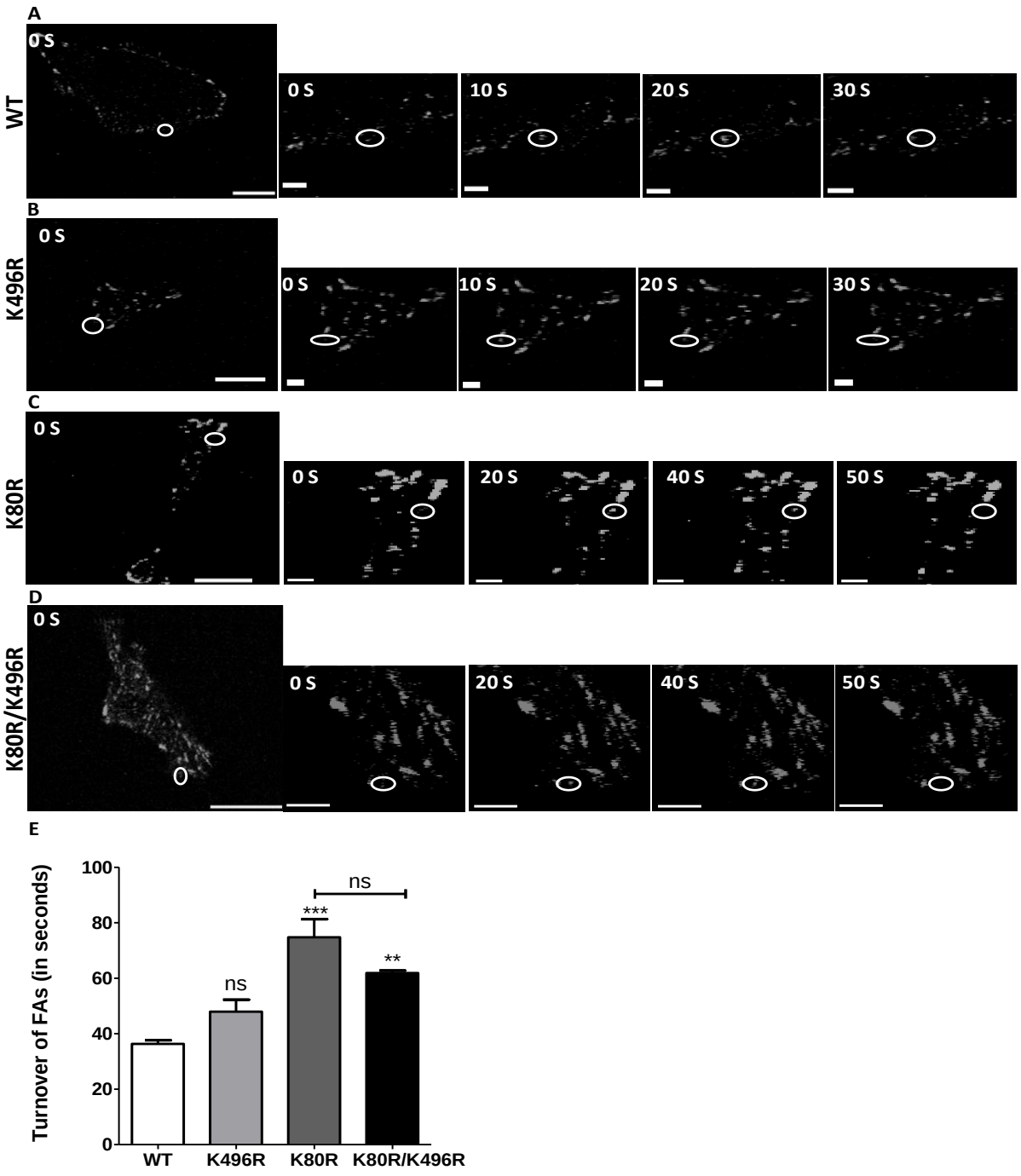

Figure 4.8 The K80R mutation in human vinculin reduces the turnover of FAs in MDA-MB-231 cells. A) Showing the turnover of vinculin-containing FAs in WT transfected cells. B) Showing the turnover of WT vinculin-containing FAs (B) K496R (C) K80R (D) K496R/K80R. Cells were transfected with WT or mutated vinculin, gown for 24-48 hours and live cell imaging was performed using confocal microscope. Images were captured every 10 seconds for 5 minutes, scale bar = 5 µm. White circles demonstrate the dynamic turnover of a single FA starting from appearing to disappearing. D) Quantification analysis shown the mean FA turnover measurements. Data was presented as mean ± SEM of three independent experiments, in each experiment a total number of 300 focal adhesions (35 cells) were analysed. One-way ANOVA with Tukey's Multiple comparison test was used to evaluate any significant differences between groups (*, ** and *** represent P <0.05, 0.01 and 0.001 respectively).

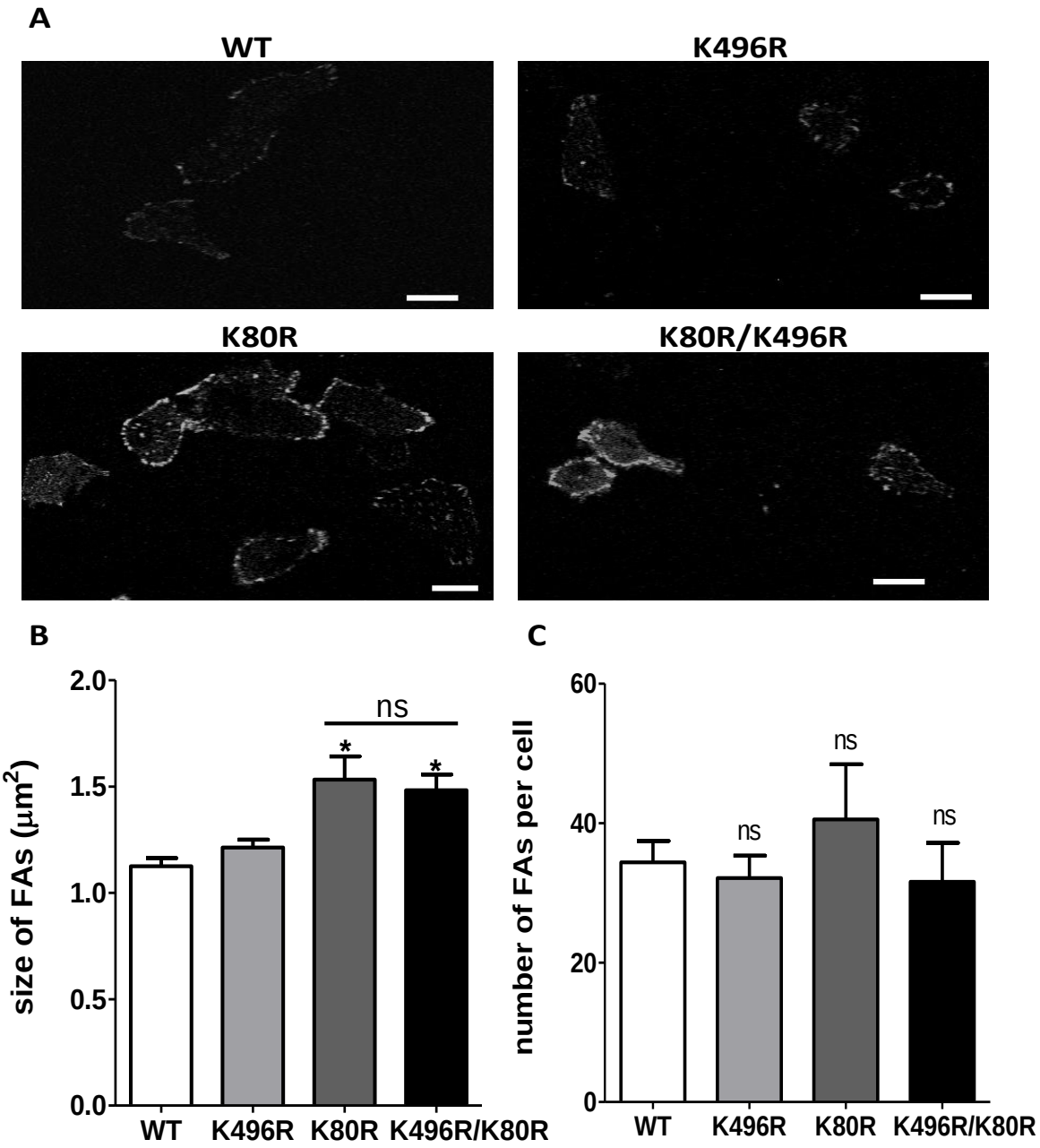

Figure 4.9 Effects of the K80R-vinculin on the size of FAs in MDA-MB-231 cells. A) Representative images of vinculin containing FAs from confocal timelapse movies for control cells (transfected with WT vinculin), K496R-vinculin, K80R-vinculin or K496R/K80R transfected cells. Scale bar = 20 µm. B) A) Quantification analysis shown the mean FA size measurements (C) the mean FA number in control cells (transfected with WT vinculin) compared to K496R, K80R or K496R/K80R vinculin transfected cells. Data was presented as mean ± SEM of three independent experiments, in each experiment a total number of 160 cells were analysed. One-way ANOVA with Tukey's Multiple comparison test was used to evaluate any significant differences between groups (*, ** and *** represent P <0.05, 0.01 and 0.001 respectively).

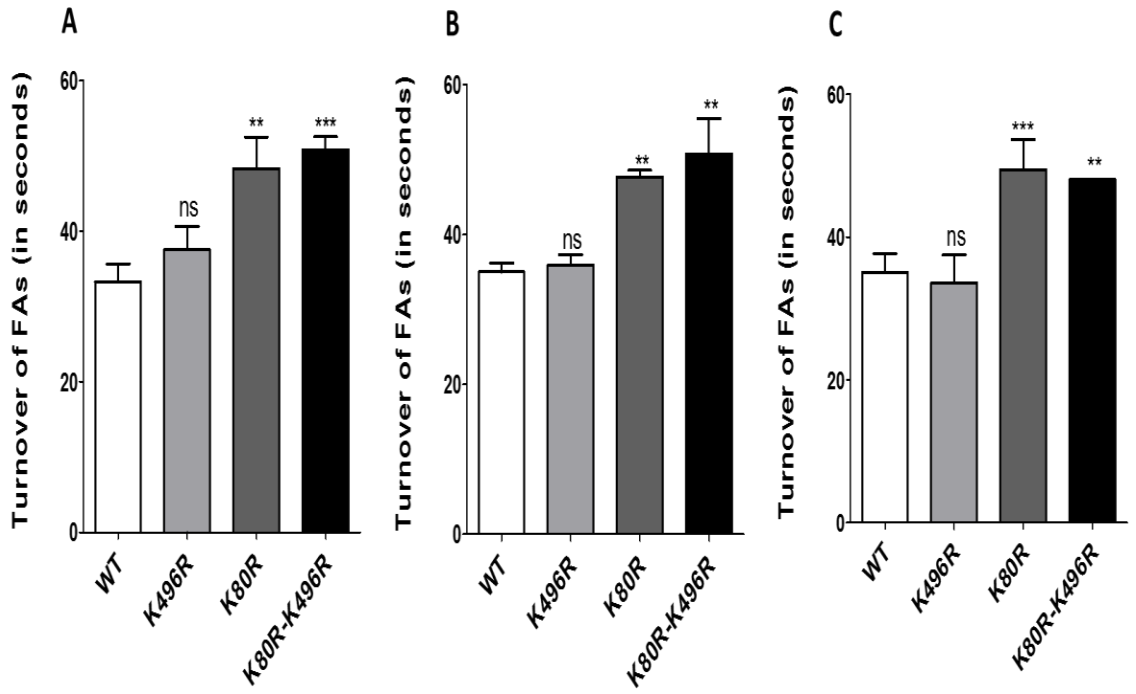

Figure 4.10 Effects of the K80R vinculin mutation on the turnover of FAs in MDA-MB-231 cells on different surfaces. Cells were seeded on collagen, gelatin or fibronectin and grown over night. Then, cells were transfected with WT, K496R, K80R or K496R/K80R vinculin and grown for 24-48 hours. Short timelapse movies were generated using confocal microscopy. A) Quantification analysis shown the mean FA turnover measurements in collagen coated cells (B) gelatin (C) fibronectin in control cells (transfected with WT vinculin) compared to K496R, K80R or K496R/K80R vinculin transfected cells. Data was presented as mean ± SEM of three independent experiments, in each experiment a total number 100 focal adhesions (20 cells) were analysed. One-way ANOVA with Tukey's Multiple comparison test was used to evaluate any significant differences between groups (*, ** and *** represent P <0.05, 0.01 and 0.001 respectively).

Time lapse cell tracking was used to evaluate the effects of K80R mutation on the migration of MDA-MB-231 cells. Cells were transfected with WT or mutated vinculin, grown for 24-48 hours and confocal microscopy was used to capture images of transfected cells every 15 minutes for 24 hours. The results show a significant reduction in the speed of these cells in K80R vinculin transfected cells compared to control cells. The speed of cells was significantly reduced from 16.23 ± 0.82 µm/h in control cells (transfected with WT vinculin) to 9.01 ± 0.62 µm/h in K80R vinculin transfected cells ($p<0.01$) (Figure 4.11 (A)). There were no significant effects of this mutation in vinculin on cell movement directionality or cell proliferation. The average directionality of control cells was 0.1277 ± 0.01447 compared to 0.1259 ± 0.004167 in K80R transfected cells (Figure 4.11 (B)). In addition, no significant effects of the K80R mutation on cell proliferation of MDA-MB-231 cells. The average percentage of proliferated cells was 44.72 ± 3.737 % in control cells compared to 36.25 ± 2.602 % in K80R transfected cells in 8-hour period ($p<0.13$) (Figure 4.11 (C)).

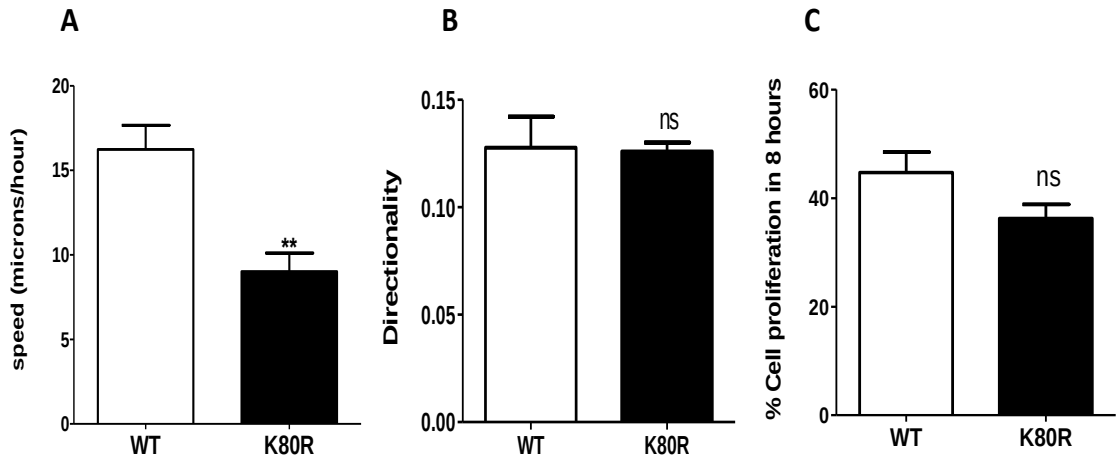

Figure 4.11 Effects of the K80R-vinculin mutation on the migration and proliferation of MDA-MB-231 cells. Cells were transfected with WT or K80R vinculin and grown for 24-48 hours. Confocal microscopy was used to take images of transfected cells every 15 minutes for 24 hours. A) Quantification analysis shown the mean speed measurements (B) mean directionality (C) mean percentage of cell proliferation during a period of 8 hours in WT compared to K80R vinculin transfected cells. Data was presented as mean ± SEM of three independent experiments, in each experiment at least 20 cells were analysed for each group. T-test was used to evaluate any significant differences between groups (*, ** and *** represent P <0.05, 0.01 and 0.001 respectively).

Similar effects were observed when seeding cells on fibronectin, collagen or gelatin coated wells. The average speed of control cells on fibronectin was 25.32 ± 0.56 µm/h compared to 14.77 ± 1.49 µm/h in K80R vinculin transfected cells ($p<0.01$) and 11.41 ± 0.29 µm/h in K80R/K496R vinculin transfected cells ($p<0.001$) (Figure 4.12 (A)). This reduction was also observed in cells seeded on collagen or gelatin coated wells. The average speed of MDA-MB-231 cells on collagen was significantly reduced from 19.37 ± 1.5 µm/h in WT vinculin transfected cells to 11.30 ± 1.5 µm/h in K80R vinculin transfected cells ($p<0.01$) and 9.63 ± 0.55 µm/h in K80R/K496R vinculin transfected cells ($p<0.001$) (Figure 4.12 (B)). In addition, the average speed of these cells on gelatin was significantly reduced from 24.4 ± 2.65 µm/h

in WT vinculin transfected cells to 10.79 ± 0.36 µm/h in K80R vinculin transfected cells ($p<0.01$) and 11.84 ± 1.28 µm/h in K80R/K496R vinculin transfected cells ($p<0.001$) (Figure 4.12 (C)). No significant changes in the speed of MDA-MB-231 cells were observed between WT and K496R vinculin transfected cells or between K80R and K80R/K496R transfected cells on the different coating surfaces (Figure 4.12).

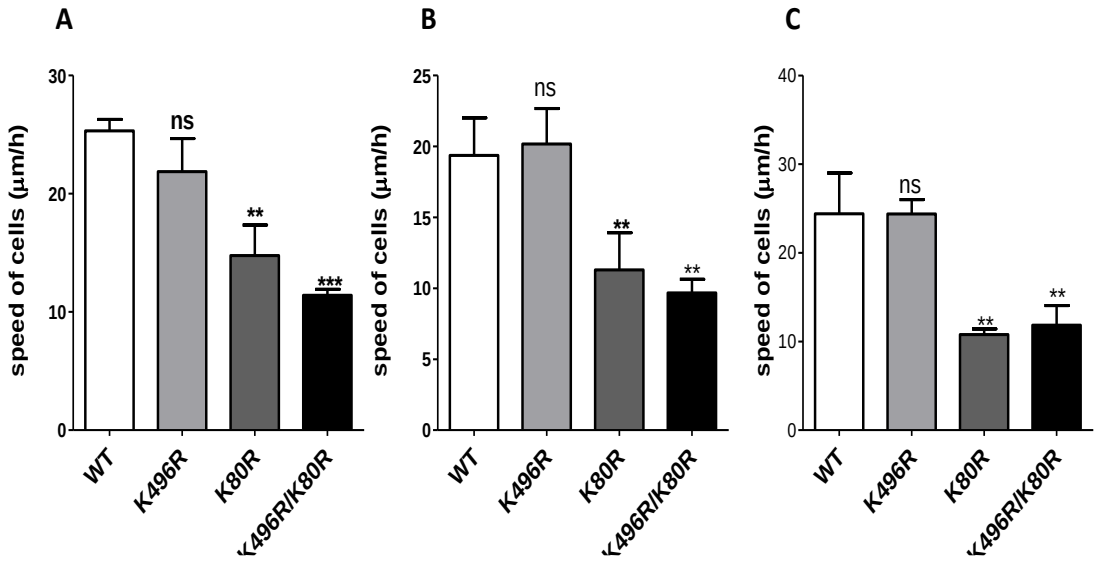

Figure 4.12 Effects of the K80R-vinculin mutation on the speed of MDA-MB-231 cells on different surfaces. Cells were seeded on plastic (non-coated), fibronectin, collagen or gelatin and grown over night. Then, cells were transfected with WT, K496R, K80R or K496R/K80R vinculin and grown for 24-48 hours. Confocal microscopy was used to take images of transfected cells every 15 minutes for 24 hours. A) Quantification analysis shown the mean speed measurements in cells seeded on fibronectin (B) collagen (D) gelatin in control cells (transfected with WT vinculin) compared to mutated-vinculin transfected cells. Data was presented as mean ± SEM of three independent experiments, in each experiment at least 20 cells were analysed for each group. One-way ANOVA with Tukey's Multiple comparison test was used to evaluate any significant differences between groups (*, ** and *** represent P <0.05, 0.01 and 0.001 respectively).

There were no significant effects of the different mutations in vinculin on cell movement directionality on different surfaces. In cells seeded on fibronectin, no significant effects of these different mutations in vinculin on cell directionality were observed. The average directionality of MDA-MB-231 cells on fibronectin was 0.1588 ± 0.02 in WT vinculin transfected cells compared to 0.1682 ± 0.02 in K496R transfected cells, 0.2271 ± 0.004 in K80R vinculin transfected cells and 0.2207 ± 0.018 in K80R/K496R vinculin transfected cells (Figure 4.13 (A)). In addition, the average directionality of control cells on collagen was 0.1815 ± 0.03 compared to 0.1677 ± 0.02 in K496R transfected cells, 0.1610 ± 0.02 in K80R vinculin transfected cells and 0.157 ± 0.02 in K80R/K496R vinculin transfected cells (Figure 4.13 (B)). Furthermore, there were no significant effects of the K80R mutation on cell directionality compared to WT. The average directionality of MDA-MB-231 cells on gelatin was 0.1352 ± 0.01 in WT vinculin transfected cells compared 0.2131 ± 0.01 in K80R vinculin transfected cells and 0.1829 ± 0.03 in K80R/K496R vinculin transfected cells (Figure 4.13 (C)). However, there was a significant increase in cell movement directionality from 0.1130 ± 0.02 in K496R transfected cells to 0.2131 ± 0.01 in K80R vinculin transfected cells on gelatin.

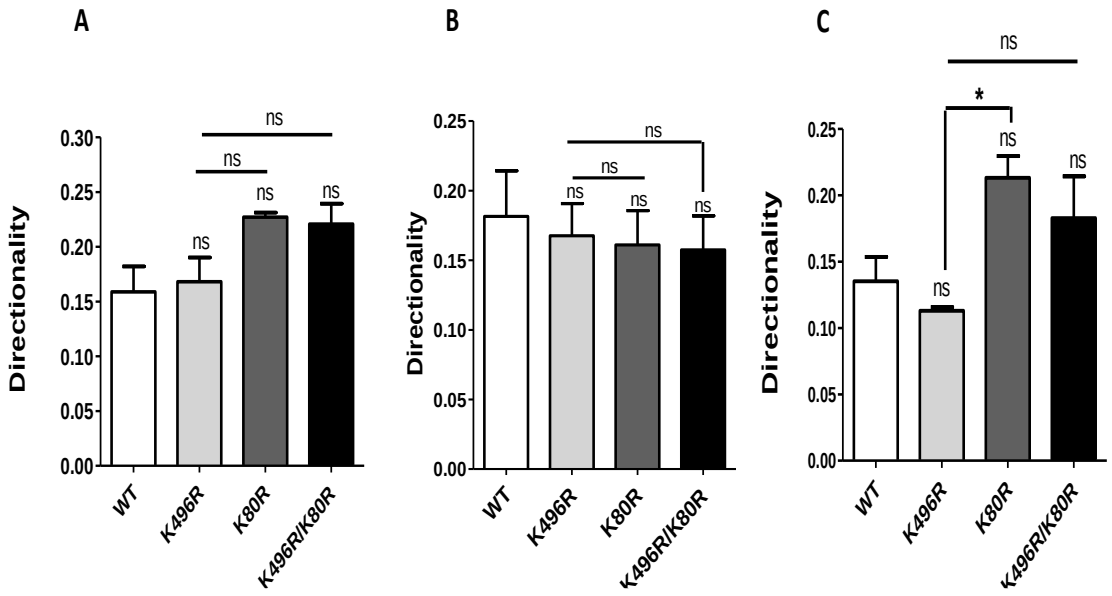

Figure 4.13 Effects of the K80R-vinculin mutation on the directionality of MDA-MB-231 cells on different surfaces. Cells were seeded on plastic collagen, gelatin or fibronectin and grown over night. Then, cells were transfected with WT, K496R, K80R or K496R/K80R vinculin and grown for 24-48 hours. Confocal microscopy was used to take images of transfected cells every 15 minutes for 24 hours. A) Quantification analysis shown the mean directionality measurements in cells seeded on fibronectin (B) collagen (C) gelatin in control cells (transfected with WT vinculin) compared to mutated-vinculin transfected cells. Data was presented as mean ± SEM of three independent experiments. One-way ANOVA with Tukey's Multiple comparison test was used to evaluate any significant differences between groups (*, ** and *** represent P <0.05, 0.01 and 0.001 respectively).

4.7 The K80R mutation in human vinculin significantly increases the size of FAs and leads to a slower FA turnover in different cancer cell lines.

The effects of K80R mutation on the dynamics of FAs and cell migration was also evaluated in different cancer cell lines. The fibrosarcoma cancer cells, HT1080, were transfected with WT or mutated vinculin, grown for 24-48 hours and confocal microscopy was used to monitor the dynamics of FAs. The results show that the turnover of vinculin-containing FAs was significantly slower in cells transfected with K80R vinculin compared to control. In control cells (transfected with WT vinculin), the average turnover of FAs was 36.34 ± 0.38 seconds compared to 52.02 ± 0.93 seconds in cells transfected with K80R vinculin ($p<0.001$) (Figure 4.14 (A)).

The size of FAs was also affected by this mutation. Results in figure 4.15 show a significant increase in the size of FAs from 1.10 ± 0.06 μm^2 in control cells (transfected with WT vinculin) to 1.39 ± 0.03 μm^2 in K80R vinculin transfected cells ($p<0.05$) (Figure 4.15 (B)). However, there were no significant effects of these mutations on the number of vinculin-containing FAs in these cells. The number of FAs in control cells was 87.56 ± 7.73 FAs compared to 100.4 ± 13.33 FAs in K80R vinculin transfected cells (Figure 4.15 (C)).

Time lapse cell tracking was used to evaluate the effects of K80R mutation in vinculin on the migration of HT1080 cells. Cells were transfected with WT or mutated vinculin, grown for 24-48 hours and confocal microscopy was used to take images of transfected cells every 15 minutes for 24 hours. The results show a significant reduction in the speed of these cells when transfected with K80R vinculin compared to WT. The speed of cells was significantly reduced from 15.25 ± 1.67 µm/h in control cells to 8.30 ± 0.79 µm/h in K80R vinculin transfected cells ($p<0.05$) (Figure 4.14 (B)).

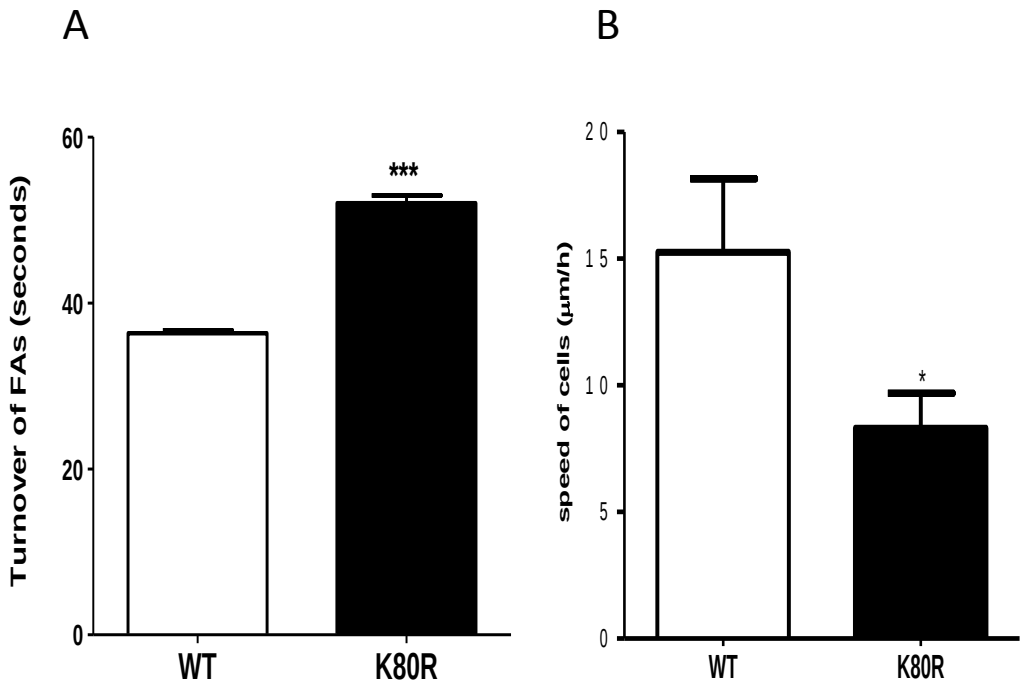

Figure 4.14 Effects of the K80R mutation in human vinculin on the turnover of FAs and cell speed of HT1080 cells. Cells were transfected with WT or K80R vinculin and grown for 24-48 hours. Short timelapse movies to monitor the dynamic activities of FAs were generated using confocal microscopy. Confocal microscopy was also used to take images of transfected cells every 15 minutes for 24 hours to monitor cell speed. A) Quantification analysis shown the mean FA turnover measurements. B) Quantification analysis shown the mean speed measurements in control cells (transfected with WT vinculin) compared to K80R vinculin transfected cells. Data was presented as mean ± SEM of three independent experiments, in each experiment a total number of 140 focal adhesions (18 cells) for turnover were analysed and a total number of 50 for cell speed were analysed. T-test with was used to evaluate any significant differences between groups (*, ** and *** represent P <0.05, 0.01 and 0.001 respectively).

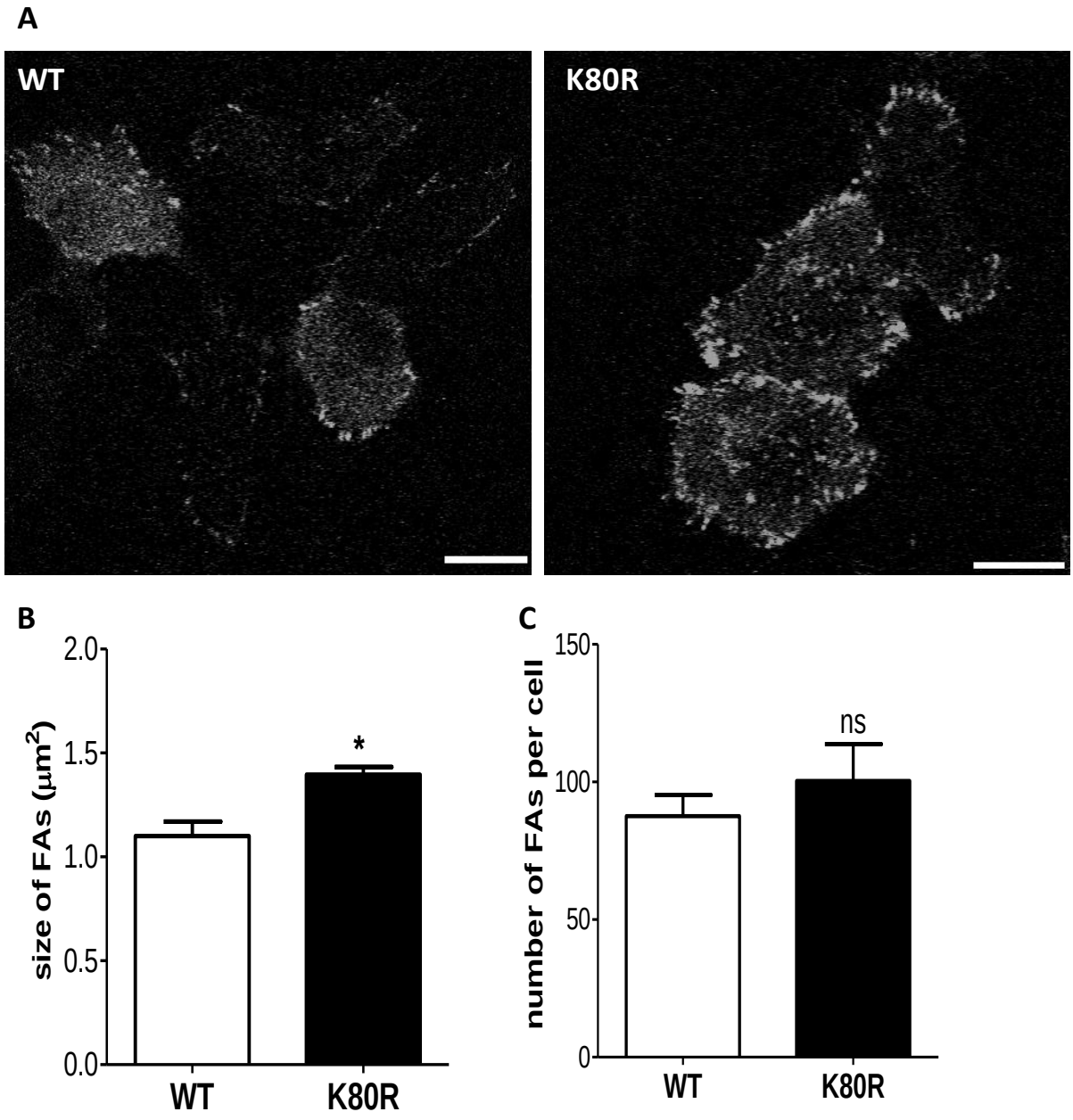

Figure 4.15 Effects of the K80R-vinculin on the size of FAs in HT1080 cells. A) Representative images of vinculin containing FAs in HT1080 cells for control cells (transfected with WT vinculin) or K80R-vinculin transfected cells. Scale bar = 19 µm. B) Quantification analysis shown the mean FA size measurements (C) the mean FA number in control cells (transfected with WT vinculin) compared to K80R vinculin transfected cells. Data was presented as mean ± SEM of three independent experiments, in each experiment a total number of 80 cells were analysed. T-test with was used to evaluate any significant differences between groups (*, ** and *** represent P <0.05, 0.01 and 0.001 respectively).

Then, the effects of K80R mutation on the turnover of FAs was also evaluated in the renal cell adenocarcinoma cells, ACHN. These cells were transfected with WT or mutated vinculin, grown for 24-48 hours and confocal microscopy was used to monitor the dynamics of FAs. The results show that the turnover of vinculin-containing FAs was significantly slower in cells transfected with K80R mutated vinculin compared to control. In control cells (transfected with WT vinculin), the average turnover of FAs was 34.69 ± 0.48 seconds compared to 48.73 ± 0.88 seconds in cells transfected with K80R vinculin ($p<0.001$) (Figure 4.16).

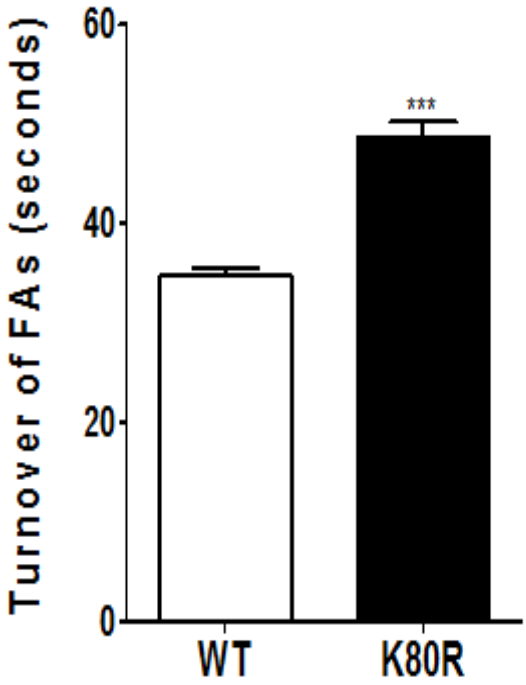

Figure 4.16 Effects of the K80R-vinculin on the turnover of FAs in ACHN cells. Cells were transfected with WT or K80R vinculin and grown for 24-48 hours. Short timelapse movies were generated using confocal microscopy. The graph shows the quantification analysis of the mean FA turnover measurements in control cells (transfected with WT vinculin) compared to K80R vinculin transfected cells. Data was presented as mean ± SEM of three independent experiments, in each experiment a total number of 70 focal adhesions (12 cells) were analysed. T test was used to evaluate any significant differences between groups (*, ** and *** represent P <0.05, 0.01 and 0.001 respectively).

4.8 Discussion

The purpose of this chapter was to investigate the role of SUMOylation on FA dynamics. The findings in the previous chapter suggest an important role of SUMOylation in FA dynamics and cancer cell migration. However, the limitations of using SUMOylation inhibitors to investigate the role of SUMOylation in cellular pathways encourages finding a more specific and alternative approach to support this finding. Although SUMOylation has previously been linked to FAs in the literature, these studies do not reveal a direct role of SUMOylation in the regulation of FA dynamics. For example, the SUMOylation of the FA protein FAK was found to take place in the nucleus, suggesting a distinct role from its functions at the FA complex (Kadaré et al., 2003). In addition, inhibiting general SUMOylation was found to increase the size and turnover time of talin-containing FAs (Huang et al., 2018). However, these effects could be indirect due to the involvement of SUMOylation in various cellular processes and by inhibiting general SUMOylation, multiple processes are disrupted. This leads indirectly to the impairment of FA dynamics. Furthermore, since SUMOylation as a post-translational modification mechanism has been discovered in the last two decades, more SUMO substrates are being identified. For example, vinculin and talin are critical scaffolding FA proteins and they have been identified in a recent proteomic study to be among SUMOylation substrates (Xiao et al., 2016). Therefore, the main aim of this chapter is to investigate the direct effects of SUMOylation on FA dynamics. This was achieved by evaluating the role of SUMOylation in the regulation of FA dynamics through the mutagenesis of individual FA proteins, thus minimising unwanted effects.

In this current study, different approaches were used to investigate the direct effects of SUMOylation in FA dynamics. Identifying potential SUMOylation sites in possible SUMO

targets is important as a part of understanding the impact of SUMOylation on various cellular processes. Several computational tools have been developed to predict the presence of the core SUMOylation motifs in the target protein sequence. These tools facilitate the selection of potential SUMO targets and the best candidate sites for experimental verification. The SUMOplot™ computational tool is one of earliest SUMO prediction tools that predict SUMO conjugating sites in proteins of interest depending on the presence of the SUMOylation core consensus motif in their sequence (Xue et al., 2006). Following that, GPS-SUMO was developed and it is suggested to be one of the best available prediction tools of SUMO sites. This tool has shown a greater prediction accuracy of SUMO sites compared to the other available tools. Besides predicting SUMO conjugating sites, this server also predicts SIM sites, thus increasing its application to predicting SUMO substrates (Zhao et al., 2014). Furthermore, JASSA is another useful prediction tool of potential SUMO sites in proteins and it scores them based on the alignment of more than 877 experimentally validated sites (Beauclair et al., 2015). This server has shown a competitive prediction performance compared to other available prediction tools (Beauclair et al., 2015). In addition, a scoring system for the inverted SUMO consensus motif besides scoring the direct motif is one of the distinct features of this server. The inverted SUMO motif has been reported previously to be SUMOylated (Matic et al., 2010). The inverted motifs achieve lower scores in scoring systems that were designed for the direct SUMO consensus motif (Beauclair et al., 2015). The development of a scoring system that is specific for inverted SUMO motifs could reveal the presence of essential SUMO sites for experimental validation. Furthermore, this SUMO site prediction tool, alongside GPS-SUMO, is the only tool that can predict the presence of SIM sites, which are important in the interaction with SUMOylated

proteins (Zhao et al., 2014). Overall, SUMO prediction tools were shown to be useful in the identification of SUMO sites to investigate the impact of SUMOylation on the target protein functions. For example, FAK was predicted to be SUMOylated at K152 and this site was experimentally verified (Kadaré et al., 2003). In addition, K51 and K195 of Flotillin-1 were predicted to be SUMO conjugating sites and they were experimentally validated (Jang et al., 2019). Furthermore, SUMOplot and JASSA tools predicted the SUMO conjugation to three potential lysine residues in liver kinase B1 (LKB1). The experimental validation of these sites using mutagenesis confirmed the SUMOylation of this kinase at one of these predicted sites, K178 (Zubiete-Franco et al., 2019).

Here, various FA proteins were analysed using bioinformatic tools to identify possible SUMO substrates according to the presence of SUMOylation consensus motifs. The bioinformatic analysis revealed the presence of extended SUMOylation consensus motifs in several FA proteins including vinculin, talin, FAK, VASP, α-actinin, filamin and actin. Some of these motifs were experimentally validated in the literature. Talin was previously identified in our lab to be a SUMO substrate. Talin was detected in SUMO2/3 IPs and Gka treatment reduced SUMOylated talin levels (Huang et al., 2018). Another motif was experimentally validated in FAK at K152 and it was shown to inhibit its SUMOylation and nuclear localisation (Kadaré et al., 2003). Collectively, these extended motifs increase the probability of a protein to be SUMOylated and this could be useful for the prediction of SUMO substrates (Hietakangas et al., 2006). In addition, the presence of these motifs in a protein increases its probability to be a SUMO substrate more than the core SUMOylation consensus alone, which was present in some proteins and was not SUMOylated (Xu et al., 2008). In addition, the presence of

SUMO interacting motifs (SIMs) in various FA proteins could induce their non-covalent interaction with SUMOylated proteins, indicating a possible role of SUMOylation in mediating protein-protein interaction at FA complex. Overall, the presence of multiple SUMO and SIM motifs in various FA proteins suggests the possible role of SUMOylation in their regulation. By modifying them, SUMOylation could regulate their activation, recruitment to FAs or interactions.

SUMOylation was suggested to target clusters of functionally-associated proteins that form cellular structures through covalent and non-covalent interactions (Hendriks and Vertegaal, 2016). SUMOylation has been shown earlier to be involved in the formation of PML nuclear bodies by facilitating the interaction of SUMOylated proteins with associated proteins through SIM motifs. For example, PML is one of the first identified SUMO targets (Boddy et al., 1996). Its SUMOylation was found to be essential for the formation of PML nuclear bodies (Sahin et al., 2014). A previous study by Shen and their colleagues in 2006 identified a SIM motif in this protein beside its SUMOylation motifs. They reported that this motif is required for the formation of PML nuclear bodies (Shen et al., 2006). This could suggest a similar mechanism in the protein modification system in the formation of other protein complexes by modifying target proteins. This modification enhances their binding affinity towards other proteins that possess SIM motifs. This will lead to the recruitment of the required proteins to form complexes. As FAs are formed of multiple proteins and many of these proteins have SUMO consensus motifs and/or SIM motifs, SUMOylation could participate in their formation. The SUMOylation of FAK, talin and vinculin could enhance

their binding affinity towards other proteins, facilitating recruitment of these proteins to form and stabilise FAs.

Vinculin was selected to investigate the role of SUMOylation in the regulation of FAs. Vinculin is a critical protein involved in the development of FAs by linking talin to F-actin fibres (Carisey et al., 2013). After the formation of nascent FAs, vinculin is recruited to FAs where it enhances their stability and maturation through its interaction with multiple FA proteins including talin, α-actinin, paxillin and actin and consequently, it facilitates cell movement (McGregor et al., 1994). The loss of vinculin in cancer cells was found to reduce the strength of cell adhesion and cell spreading, and to enhance cell migration (Coll et al., 1995, Saunders et al., 2006). Vinculin has previously been linked to SUMOylation in the literature. It was identified alongside talin in a proteomic study to be among the SUMO substrates (Xiao et al., 2016). In addition, silencing the SUMO E3 ligase, PIASI, was found to decrease its localisation to FA complexes, thus suggesting a possible role of SUMOylation for its activities at the FA sites (Constanzo et al., 2016). Therefore, the involvement of SUMOylation in its regulation was investigated in this chapter.

Three separate bioinformatic tools predicted the presence of several SUMO motifs in vinculin with different scores. Lysine 80 has the highest score and was predicted to be in an extended SUMO consensus motif (HCSM), whereas lysine 496 was predicted to be in a strong consensus inverted motif. All three tools, JASSA, SUMOplot and GPS SUMO, predicted that the lysine 80 has the highest scores and thus the highest likelihood to be a SUMO conjugating site among all of the FA proteins used in this analysis.

Since conformational changes in vinculin folding are required to promote its interaction with other FA proteins, SUMO attachment to vinculin could be involved in this process. The presence of a K80 site at the surface of the 3-D structure in vinculin makes its accessible to SUMO binding, which in turn may induce structural changes that could reveal binding sites for its interaction partners, leading to the recruitment and activation of vinculin at the FA sites. All of the features of this site increase the possibility that vinculin could be SUMOylated at lysine 80 (K80). These bioinformatic findings suggest that vinculin is a possible SUMO substrate. However, experimental validation is necessary to support this finding and to understand the role of SUMOylation in the functions of this protein.

In order to investigate the association between SUMO and vinculin within the adhesion sites, the interactions between SUMO2/3, which are mainly located in the cytoplasm (Wang and Dasso, 2009), and vinculin has been evaluated using co-localisation and Co-IP studies. Co-localisation studies revealed the localisation of SUMO2 with vinculin at the FA sites, suggesting the presence of SUMO substrates at FA sites. Co-localisation studies also revealed the localisation of two SUMO-associated enzymes, Ubc9 and SENP2, with vinculin. In addition, Co-IP results suggest a possible interaction between SUMO2 and vinculin. These findings could support the possibility that vinculin is a SUMO substrate. Since vinculin is necessary for FA stability and maturation, the SUMOylation of vinculin could regulate their dynamics.

Site directed mutagenesis was used to investigate the possibilities of vinculin as a SUMO substrate and the consequence of inhibiting its SUMOylation on FA dynamics. This method

of investigation is more specific than using SUMOylation inhibitors or silencing SUMO-associated proteins to confirm the regulatory role of SUMOylation in FA dynamics. By expressing the non-SUMOylatable version of vinculin, general SUMOylation is not disrupted, thus allowing for a precise characterisation of SUMOylation's impact on FA dynamics. The interaction between SUMO2 and WT or mutated vinculin was assessed using a Co-IP and FRET assay to validate if these sites are SUMO motifs. The co-immunoprecipitation results revealed the presence of significantly less K80R vinculin molecules in Ha IPs compared to WT or K496R. These findings indicate that lysine 80 in human vinculin is a binding site for SUMO2, but not lysine 496. The K80R mutation in vinculin caused a significant reduction in its interaction with SUMO2. Although there is a significant reduction in the presence of K80R molecules in Ha IPs, there was a low level of K80R mutated vinculin detected in Ha IPs. This could suggest that vinculin could be SUMOylated at multiple sites. Lysine 80 is one of them but not lysine 496. SUMO conjugation to multiple sites in the same substrate has been reported before. For example, the transcription factor Gli-similar 3 (Glis3) has been predicted to have two SUMOylation sites with a high score in the SUMOplot for K224 and K430. Individual mutations showed a reduction in the SUMOylated levels of Glis3 and the combined mutation of both sites abolished all detectable Glis3 SUMOylation (Hoard et al., 2018). Taken together, these findings identify, for the first time, vinculin as a SUMO substrate and that the HCSM motif surrounding lysine 80 is a SUMO2 binding site. Introducing a mutation in this site (K80R) caused a significant loss of SUMOylated vinculin levels in Ha IPs, suggesting that SUMOylating vinculin occurs mainly at this site. In addition, these results could also indicate that SUMOylation is involved in the regulation of vinculin

functions. This non-SUMOylatable version of vinculin provides a great opportunity to investigate the direct effects of SUMOylation on FA dynamics.

To further confirm the Co-IP results, a photo-bleaching FRET assay was used to examine the effects of K80R mutation on the SUMO2-vinculin interaction. Unfortunately, due to the limitations of this approach, the experiment was not successful. The principle of this technique relies on the loss of energy transfer from the donor after bleaching the acceptor, leading to a measurable increase in donor intensity. Although the FRET assay is one of the most common techniques used to study protein-protein interaction, there are several challenges that could affect interpreting the FRET data. One of the main outcomes of this experiment was the low expression of SUMO2. An essential challenge in an photobleaching FRET assay is bleaching the donor during the bursting of the acceptor, leading to an overall reduction in fluorescence intensity. The low expression of SUMO2 increases the consequences of donor bleaching and increases the difficulty to correct the overall intensity reduction. Another reason is the resistance of the acceptor (YFP-vinculin) to bleaching. Thus, the exposure time is increased, which could have greater effects on the donor. In addition, the delay in recording caused by the longer exposure time could cause the movement of the ROIs to being out of focus. Taken together, these effects increase the difficulties of analysing FRET data and this has led to odd values. Therefore, the FRET results were excluded.

To investigate the effects of these mutations on FA dynamics, MDA-MB-231 cells were transfected with WT, K496R, K80R or K80R/K496R vinculin and a confocal microscope was used to monitor their dynamics. Interestingly, the results showed a significant impairment in

FA dynamics in the cells transfected with the non-SUMOylatable version of vinculin (K80R or K80R/K496R) compared to that of WT or K496R transfected cells. The effects of these mutations on the FA dynamics was also observed in different cancer cell lines, including MDA-MB-231 breast cancer cells, HT1080 fibrosarcoma and ACHN renal cell adenocarcinoma cells. Overall, these findings confirm, for the first time, the direct regulatory role of SUMOylation in FA dynamics. By modifying vinculin, SUMOylation regulates the turnover of FAs. The significant increase in FA size and the turnover time in cells that express the non-SUMOylatable vinculin indicates the important role of SUMOylation in the regulation of FA dynamics. The SUMOylation of vinculin could be suggested by this finding to be necessary to enhance the turnover rate of FAs. To investigate whether this impairment of the FA dynamic when expressing the non-SUMOylatable vinculin could have consequences on cell migration, a cell tracking assay performed. The results showed a significant reduction in the cell speed of K80R and the K80R/K496R transfected cells compared to the control. This reduction in their speed was also observed when seeding cells on fibronectin, collagen or gelatine-coated wells, suggesting that SUMOylation regulates cancer cell migration independently of the extracellular matrices. These results demonstrate the important role of SUMOylation in regulating FA dynamics and cancer cell migration. Beside its implications in terms of regulating the different aspects of cell migration, the findings in this chapter identify a novel role for SUMOylation in regulating the turnover of FAs to enhance cancer cell migration.

Taken together, the findings in this chapter demonstrate a novel role for SUMOylation in the regulation of FA dynamics and cancer cell migration. Vinculin was identified as a SUMO

substrate and its SUMOylation at K80 is required for FA turnover and cell migration. Introducing a mutation at this site to prevent its SUMOylation caused a significant reduction in the turnover rate of FAs and cancer cell speed. However, the mechanisms by which the SUMOylation of vinculin affects FA dynamics remain unknown. Since FAs are formed and developed through protein-protein interaction, it can be speculated that SUMOylation could alter protein binding to regulate FA dynamics. Vinculin interacts with different FA proteins including talin, α-actinin, paxillin and actin. The SUMOylation of vinculin could alter its interaction with these proteins. The larger and more stable FAs caused by expressing the non-SUMOylatable vinculin could indicate a more stable interaction between K80R-mutated vinculin and associated FA protein partners due to preventing its SUMOylation. Thus, it can be suggested that SUMOylation enhances FA turnover by altering protein-protein interaction. To evaluate the effects of K80R mutation on its interaction with other FA proteins, protein-protein interaction can be analysed using approaches such as Co-IP and FRET. These approaches could reveal the effects of this mutation on its interaction with other FA binding partners. Therefore, they could facilitate identifying the molecular mechanism by which the SUMOylation of vinculin regulates the FA dynamics.

5. SUMOylation disassociates talin-vinculin interaction to trigger FA disassembly

5.1 Introduction and hypothesis

The findings in the previous chapter clearly identify a novel and direct role for SUMOylation in the regulation of FAs via modifying vinculin at K80 residue. Expressing the non-SUMOylatable version of this protein led to an impairment of the FA dynamics. One of the main functions of SUMOylation is mediating protein-protein interactions (Tatham et al., 2008, Tan et al., 2015). Vinculin is normally localised in the cytoplasm in an auto-inhibitory state caused by the interaction between its head and tail domains (Chorev et al., 2018). Following the formation of early FAs, vinculin is recruited to the adhesion sites and its recruitment to FAs requires conformational changes in its structure that disassociate its head-tail interaction. Its interaction with different FAs proteins including talin, paxillin and α-actinin was reported to be necessary for its activation and localisation to the FA sites (Izard et al., 2004, Ziegler et al., 2006).

The binding of vinculin to α-actinin enhances the binding of the later protein to F-actins, enhancing the overall cross-linking of the actin filaments. This is an important cellular function that enables cells to modify their morphology and to drive cell migration (Ciobanasu et al., 2013). The recruitment of vinculin to FAs was suggested to be induced by its interaction with paxillin. The attachment of integrins to the ECM induces the phosphorylation of paxillin at tyrosine 31 and 118 by FAK/Src kinases, which in turn promotes its interaction with vinculin leading to the recruitment of the later protein to FAs (Pasapera et al., 2010).

Although vinculin was found to interact with phospho-paxillin, vinculin was found to be in an inactive form and their interaction was shown to target vinculin to lower layers of FAs, and consequently prevents vinculin targeting to actin filaments (Case et al., 2015). Its interaction with talin, however, was found to activate and target vinculin to the higher FA layers, thus allowing its engagement with the actin filaments (Case et al., 2015). More importantly, talin's full activation by engagement with the actin-filaments was found in the same study to require the presence of vinculin. Taken together, vinculin interaction with paxillin could target vinculin to FAs, but its interaction with talin is important to activate and engage either proteins to force tractions generated by the actin filaments leading to FAs maturation. This could be supported by the finding that although introducing the A50I mutation in vinculin, which prevents its binding to talin (Cohen et al., 2006), has no effect on its localisation to FAs, expressing this mutated version of vinculin was found to cause a significant reduction in the number and stability of FAs (Diez et al., 2011).

SUMOylation could be involved in the regulation of FAs by mediating its interaction with the FA proteins. The increased size and turnover time of FAs when preventing its SUMOylation could suggest that SUMOylating vinculin at K80 is required to disassociate its interaction with other FA proteins in order to trigger the disassembly of FAs. The K80 in vinculin is located in the D1 domain of the vinculin head (Vh) and is approximate to binding sites for talin and α-actinin (Figure 5.1). Given the fact that vinculin interaction with talin is necessary for FA maturation and given the large size of vinculin-containing FAs in cells expressing the non-SUMOylatable version of vinculin (K80R), SUMOylation could disassociate their interaction to regulate the FA dynamic.

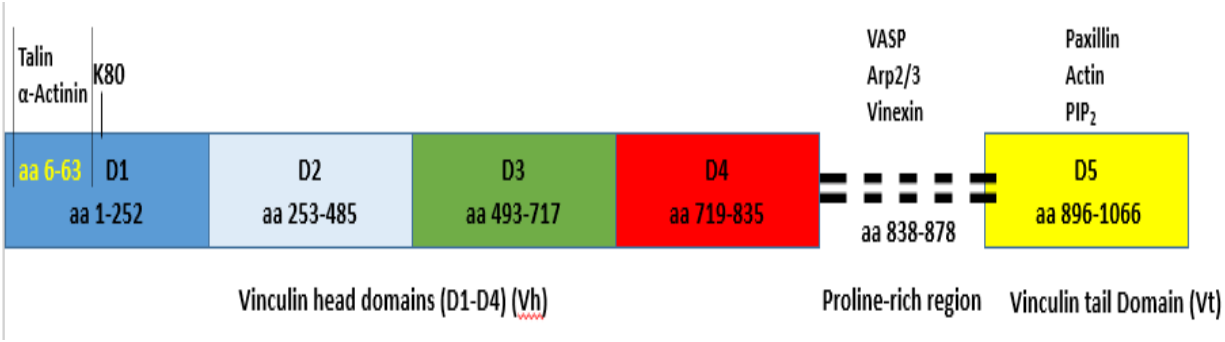

Figure 5.1 Map of vinculin domains and binding sites for its interacting FA partners. Vinculin contains head domain (Vh), which is composed of 4 domains (D1-D4), proline-rich region and tail domain (Vt). The binding sites for several FA proteins are shown. K80 is located in D1 domain, which has binding sites for talin and α-actinin. This diagram is adapted from (Bakolitsa et al., 2004).

Hypothesis

This chapter focuses on identifying the mechanism by which the SUMOylation of vinculin regulates the turnover of FAs. The hypothesis of this chapter is that SUMOylating vinculin alters the protein binding in FAs. One aim of this chapter was to knockout the endogenous vinculin in MDA-MB-231 or HT1080 cells using CRISPR and to re-express WT or mutated vinculin. This technique provides the opportunity to evaluate the precise effects of mutated vinculin on FA dynamics and cell migration without the competition of endogenous vinculin. Another aim of this chapter was to investigate whether SUMOylation could target other FA proteins to regulate the FA dynamic. Ginkgolic acid (Gka) was used to inhibit SUMOylation in K80R vinculin transfected cells to evaluate whether blocking global SUMOylation could have any further effect on the turnover of FAs. The last and main aim of this chapter was to evaluate the effects of the K80R mutation in vinculin on its interaction with talin. The talin-vinculin interaction is important to activate and engage the proteins to force the tractions generated by the actin filaments, leading to FAs maturation (Atherton et al., 2019). Given the importance of their interaction in the development of the adhesion sites, the SUMOylation of vinculin could alter their interaction to regulate the FA dynamics. In order

to investigate the effects of the K80R mutation on their interaction, Co-IP and photobleaching FRET assays were performed. In addition, template based 3D models of vinculin-talin or vinculin-SUMO2 interface were generated by the Reading University bioinformatic server (https://www.reading.ac.uk/bioinf) to demonstrate whether K80 in vinculin is located in the talin binding region in the folding state of vinculin.

5.2 Materials and Methods

5.2.1 Materials

Table 5.1 List of reagents used in Construction of pmCherry-tagged vinculin and CRISPR

Component	Description (catalog No.)
FastDigest NheI restriction enzyme	Restriction enzyme (FD0974), Thermo Scientific
Plasmid Transfection Medium	Transfection medium (sc-108062), Sant Cruz
pmCherry-N1 Vector	Expression Vector (632523), Clontech
Puromycin dihydrochloride, 25 mg	Puromycin Selection (sc-108071), Santa Cruz
UltraCruz® Transfection Reagent	Transfection Reagent (sc-395739), Sant Cruz
Vinculin CRISPR/Cas9 KO Plasmid (h2)	Consists of a pool of three plasmids each encoding the Cas9 nuclease and a vinculin-specific 20 nt guide RNA (gRNA) designed for maximum knockout efficiency (sc-400227-KO-2), Santa Cruz
Vinculin HDR Plasmid (h2)	Consists of a pool of 2-3 plasmids, each containing a homology-directed DNA repair (HDR) template corresponding to the cut sites generated by the vinculin CRISPR/Cas9 KO Plasmid (h2). Each HDR Plasmid inserts a puromycin resistance gene to enable selection of stable knockout (KO) cells and an RFP (Red Fluorescent Protein) gene to visually verify transfection (sc-400227-HDR-2), Santa Cruz

5.2.2 Methods

5.2.2.1 Vinculin knockout with CRISPR

MDA-MB-231 or HT108 cells were seeded in a 6-well plate (3 X 10^5/well) and grown to 40-80% confluency. Cells were maintained in 3 ml of antibiotic-free medium 24 hours before transfection. The transfection mixture was prepared in a sterile hood according to the manufacturer's protocol (Santa Cruz). UltraCruz® Transfection Reagent (10 µl) and a 2 µg of a mixture of vinculin CRISPR/Cas9 KO Plasmid and vinculin HDR Plasmid (h2) were diluted in the transfection medium in separate Eppendorf tubes as described in the following table (table 5.2).

Table 5.2 Procedure of CRISPR preparation

	Tube 1 Diluted plasmids		**Tube 2** Diluted UltraCruz® Transfection Reagent	
Vinculin CRISPR/Cas9 KO and vinculin HDR plasmid	Volume of Plasmids (µl)	Transfection medium (µl)	Volume of UltraCruz® Reagent (µl)	Transfection medium (µl)
Plasmids mixture (200 ng/ µl)	10 µl	140 µl	10 µl	140 µl

Plasmid and transfection reagent solutions were incubated at room temperature for 5 minutes. Then, the Plasmid solution was added gently to the transfection reagent solution and the mixture (total volume = 300 µl) was vortexed immediately before incubating for 20 minutes at room temperature. A fresh antibiotic-free growth medium (3 ml/well) was added to the cells and the entire transfection solution was added dropwise to a well (300 µl/well). Cells were incubated under normal conditions for 24-72 hours. The transfection medium was replaced with normal growth medium 24 hours post-transfection. Successful co-

transfection of vinculin CRISPR/Cas9 KO plasmid and vinculin HDR plasmid is visually confirmed by the detection of RFP via fluorescent microscopy and/or western blot analysis.

Transfected cells were selected with media containing Puromycin. The transfection medium was discarded and a selective medium containing 10 µg/ml Puromycin was added to the cells 48 hours post-transfection. Cells were grown in selective media for 3-5 days before western blot analysis. Successful cell clones were transfected with WT or mutated vinculin to investigate the effects of these mutations on the turnover of FAs and cell migration of MDA-MB-231 or HT1080 cancer cells.

5.2.2.2 Construction of pmCherry-tagged vinculin

In order to construct pmCherry-tagged vinculin, the expression vector pmCherry-N1 was used as a templet in PCR to amplify mCherry. Primers were designed using the Primer3Plus server (http://www.bioinformatics.nl/cgi-bin/primer3plus/primer3plus.cgi) and synthesised by the Sigma Aldrich company. Primers were designed to include a NheI restriction site in the forward primer and SalI in the reverse primer.

Forward primer: (GCGGCTAGCATGGTGAGCAAGGGCGAG), NheI restriction site is highlighted with green.

Reverse primer: (CGCGTCGACCTTGTACAGCTCGTCCATGC), SalI restriction site is highlighted with green.

Reactions and cycling conditions of PCR were as used as described in 2.2.5.3 except the fact that cycles were reduced from 35 to 25 to avoid unwanted mutations in vinculin nucleotide sequence. Then, these same restriction enzymes were used to cut ZsYellow1 in pZsYellow1-tagged vinculin (WT or mutated). After digesting both mCherry PCR products and pZsYellow1-tagged vinculin, products were separated by size using 1% agarose gel electrophoresis. A gel extraction kit (QIAGEN) was used to extract DNA and mCherry was ligated to vinculin plasmids and transformed to E. coli as described in 2.2.5.5 and 2.2.5.6 respectively. Colonies were screened using colony PCR and successful colonies were inoculated in a 10 ml LB broth medium containing 50µg/ml kanamycin. Plasmids were extracted using QIAprep® Miniprep kit (QIAGEN) as described in 2.2.5.7. and confirmed using digestion and transfection before being sent for sequencing.

5.2.2.3 CellLight® Talin-GFP transfection

Cells were seeded in a 12-well plate at a density of $1x10^5$ and allowed to adhere overnight. The desired concentration of Cell Light® Talin-GFP (BacMam 2.0) was calculated to label 40,000 cells with 30 particles per cell (PPC) according to the following equation:

Volume of Cell Light® Reagent (mL) = Number of cells x desired PPC/Cell Light® particles/ ml

For labelling 40,000 cells with 30 PPC = 40,000 * 30 / 1×10^8 = 0.012 ml = 12 µl.

After calculating the desired concentration, the reagent was mixed gently several times and added directly to cells in the complete growth medium. Cells were then incubated overnight at 37°C in 5% CO_2.

5.2.2.4 Photobleaching of the accepter FRET assay

Sterilised cover slips were placed in a 12-well plate and 1 ml of 100% methanol was added to each well for 20 minutes to further sterilise them. After that, methanol was aspirated, and wells were allowed to stand to dry for 30 minutes in a sterilised culture hood before coating with 0.1% gelatin. Then, the gelatin was discarded and the wells were left to dry in the hood for 1 hour and washed with PBS before seeding $2x10^5$ cells in each well and growing them till 40-50% confluency. Following that, the cells were transfected with Cell Light® Talin-GFP (BacMam 2.0) and left in the transfection medium overnight. The next day, the cells were transfected with m-cherry vinculin (WT or mutated) and grown for 24-48 hours. The cells were then washed with PBS and fixed with 1 ml/well of 4% (w/v) paraformaldehyde (PFA) for 15 minutes. PFA was aspirated and cells were washed three times with PBS, 10 minutes each time. Cover slips were then mounted onto glass slides using VECTASHIELD Mounting Medium before sealing the cover slip edges with nail polish and storing at 4°C until the next step. Photo-bleaching FRET assay was performed using confocal microscopy using a 100x oil-immersion objective lens and Nikon confocal system software. Laser channels 488 and 546 were used to take sequential images of GFP-talin (donor) and mCherry-vinculin (acceptor) respectively. Following that, the bleaching area was selected using Polygon selection in the ROI tool and the 488 laser channel was turned off and the 546 laser channel intensity was increased to 100% and was used to burst the

acceptor (mCherry-vinculin) protein (20-30 seconds). Then, the laser settings were returned to their previous settings and sequential images of GFP-talin and mCherry-vinculin were taken again. Image J (Fiji) software was used to calculate the FRET efficiency according to the following equation:

FRET efficiency % = (D_{Post} – D_{Pre}) / D_{Post} x 100

where D_{Post} is the donor fluorescence intensity after bleaching, and D_{Pre} is the donor fluorescence intensity before bleaching.

The intensity of the regions outside the cell were measured before and after bleaching and used to correct the overall reduction in fluorescence intensity.

5.3 The K80R mutation in human vinculin significantly increases the turnover time of FAs and reduces the cell migration in vinculin-knocked out cells.

This part of this chapter focuses on assessing the precise effects of the K80R mutated vinculin on FA dynamic with interruption of endogenous vinculin. CRISPR was used to knock out endogenous vinculin in HT1080 and MDA-MB-231 cancer cells before transfection with K80R vinculin to overcome competition of endogenous vinculin. Cells were transfected with vinculin CRISPR/Cas9 Knockout (KO) Plasmid (h2) and vinculin HDR Plasmid (h2), grown for 48-72 hours before cell selection using puromycin.

Successful vinculin-knockout cell clones were identified using Western blot analysis (Figure 5.2). Successful clones were selected to investigate the effects of the K80R on the turnover

of FAs. Cells were transfected with WT or K80R vinculin, grown for 24-48 hours and short timelapse movies were generated using confocal microscopy. The results show that the turnover of vinculin-containing FAs was significantly slower in vinculin-knockout K80R transfected cells (Figure 5.3 (B)) compared to control (Figure 5.3 (A)) or K80R transfected cells that have endogenous vinculin. In control cells (transfected with WT vinculin), the mean turnover of FAs was 34.70 ± 0.50 seconds compared to 52.02 ± 0.93 seconds in K80R transfected non-CRISPR cells ($p<0.05$) or 59.09 ± 0.95 in K80R transfected vinculin CRISPR-knockout cells ($p<0.01$). A significant increase in the FA turnover time was observed in vinculin CRISPR-knockout K80R transfected cells compared to non-CRISPR K80R transfected cells ($p<0.05$) (Figure 5.3 (C)).

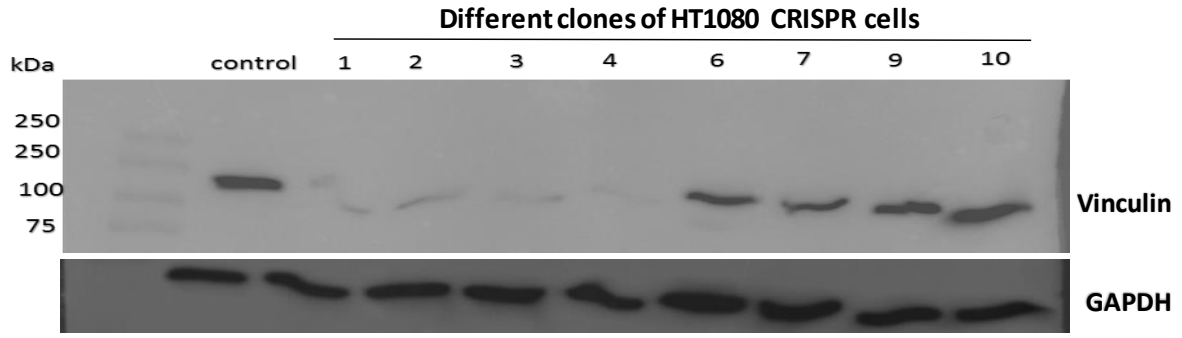

Figure 5.2 Western blot analysis of vinculin knockout using CRISPR in HT1080 cells. Cells were transfected with vinculin CRISPR/Cas9 Knockout (KO) Plasmid (h2) and vinculin HDR Plasmid (h2), grown for 48-72 hours before cell selection using puromycin. Western blotting analysis shown detection of the expression of vinculin or GAPDH in control cells or different clones of vinculin CRISPR/Cas9 Knockout (KO) Plasmid (h2) and vinculin HDR Plasmid (h2) transfected cells. Clones 1-4 are successful knockouts, whereas 6-10 are unsuccessful knockouts.

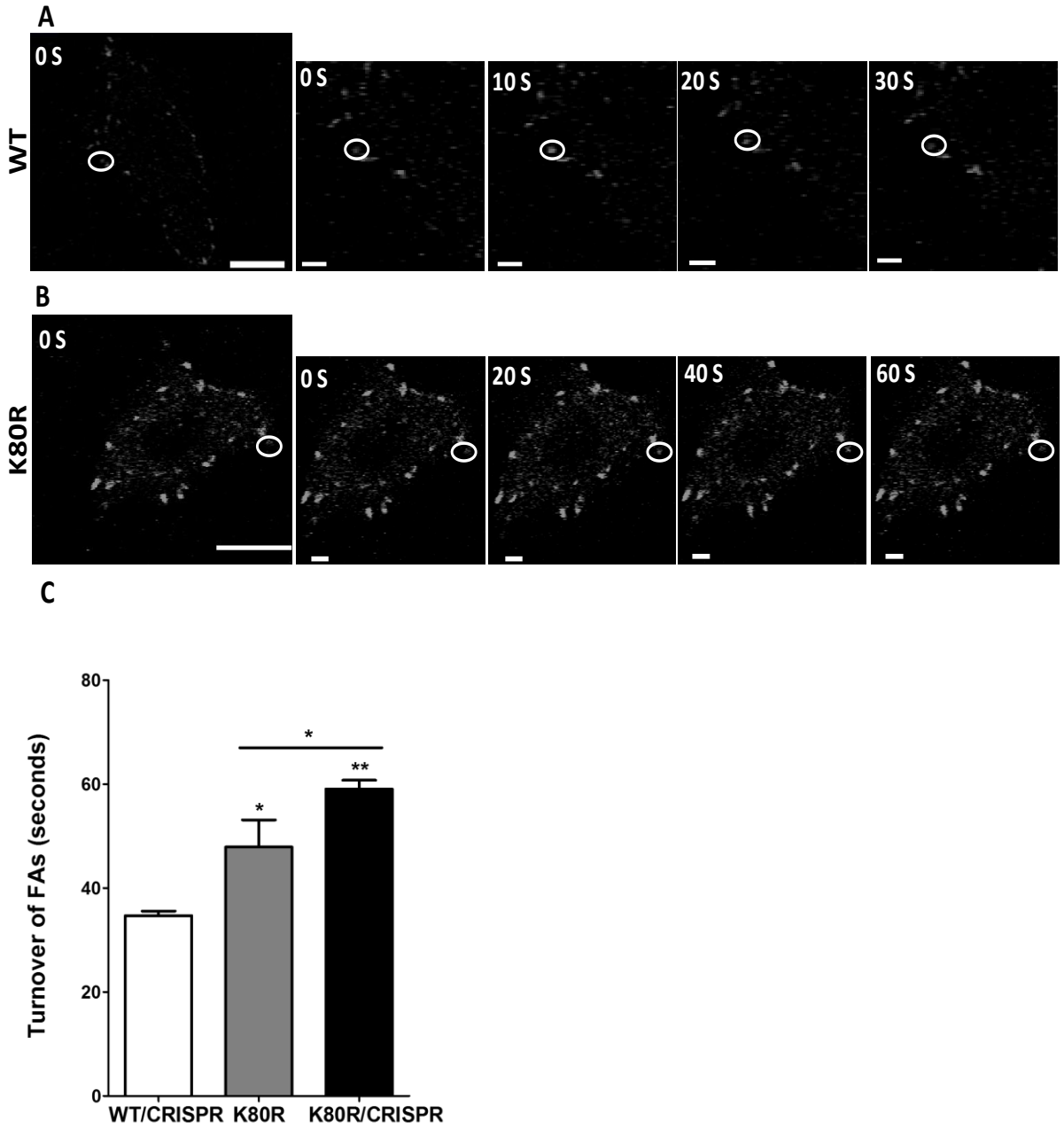

Figure 5.3 Effects of the K80R mutation in human vinculin on the turnover of FAs of vinculin CRISPR-knockout HT1080 cells. A) Representative images taken from timelapse movies of the turnover of WT vinculin containing FAs B) Representative images taken from timelapse movies of the turnover of K80R vinculin containing FAs in vinculin CRISPR-knockout HT1080 cells. Cells were transfected with WT or K80R vinculin, gown for 24-48 hours and live imaging was performed using confocal microscopy. Images were captured every 10 seconds for 5 minutes, scale bar = 5 µm. White circles demonstrate the turnover of a single FA starting from appearing to disappearing. C) Quantification analysis of the mean FA turnover measurements in endogenous vinculin CRISPR-knockout control cells (transfected with WT vinculin) compared to K80R vinculin transfected cells. Data was presented as mean ± SEM of three independent experiments, in each experiment a total number of 150 focal adhesions (27 cells) were analysed. One-way ANOVA with Tukey's Multiple comparison test was used to evaluate any significant differences between groups (*, ** and *** represent P <0.05, 0.01 and 0.001 respectively).

Timelapse cell tracking was used to evaluate the effects of the K80R vinculin on the migration of vinculin CRISPR-knockout HT1080 cells. Cells were transfected with WT or mutated vinculin, grown for 24-48 hours and a confocal microscope was used to take images of transfected cells every 15 minutes for 24 hours. The results show a significant reduction in the speed of K80R vinculin transfected cells compared to control. The speed of cells was significantly reduced from 21.81 ± 2.03 µm/h in WT transfected cells to 13.97 ± 1.5 µm/h in K80R transfected cells. ($p<0.01$) (Figure 5.4 (A)). There were no significant effects of the K80R mutation on cell movement directionality. Cell directionality in control cells was 0.16 ± 0.029 compared to 0.20 ± 0.022 in K80R transfected cells (Figure 5.4 (B)). In addition, there were no significant effects of the K80R mutation on cell proliferation. About 45.09 ± 4.58 % of cells proliferated in WT transfected cells compared to 43.47 ± 1.92 % in a period of 8 hours (Figure 5.4 (C)).

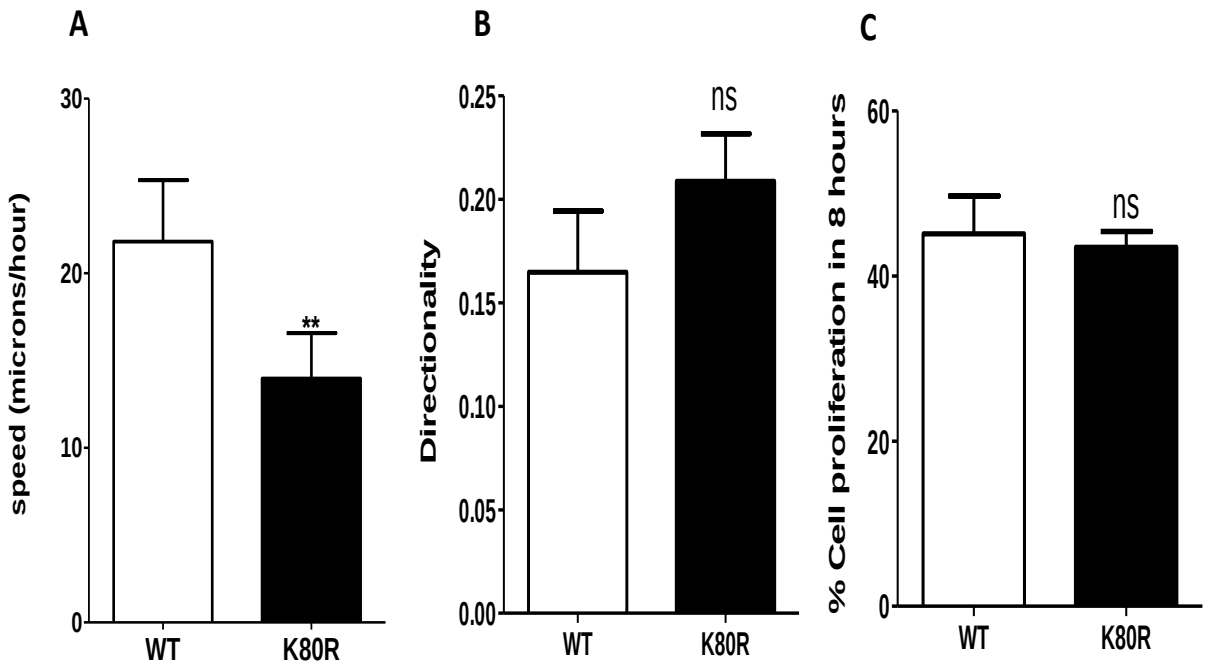

Figure 5.4 Effects of the K80R mutation in human vinculin on the cell migration and proliferation of vinculin CRISPR-knockout HT1080 cells. Cells were transfected with vinculin CRISPR/Cas9 Knockout (KO) Plasmid (h2) and vinculin HDR Plasmid (h2), grown for 48-72 hours before cell selection using puromycin. Cells were then transfected with WT or K80R vinculin and a confocal microscope has been used to track transfected cells every 15 minutes for 24 hours to monitor cell speed. A) Quantification analysis showing the mean speed measurements in vinculin CRISPR-knockout control cells (transfected with WT vinculin) compared to K80R vinculin transfected cells. B) Quantification analysis showing the mean cell movement directionality measurements in vinculin CRISPR-knockout control cells (transfected with WT vinculin) compared to K80R vinculin transfected cells. C) Quantification analysis showing the mean percentage of cell proliferation in 8 hours. Data was presented as mean ± SEM of three independent experiments, in each experiment a total number of 50 cells were analysed. T-test was used to evaluate any significant differences between groups (*, ** and *** represent P <0.05, 0.01 and 0.001 respectively).

5.4 Blocking global SUMOylation has no further effects on the turnover of FAs in vinculin-knockout cells that express the K80R vinculin.

The previous chapters indicate a direct role of SUMOylation in FA dynamics. The results in these chapters showed that either inhibiting global SUMOylation or expressing the non-SUMOylatable vinculin (K80R) caused a significant impairment in their dynamic activities. In addition, different bioinformatic tools predicted the presence of strong SUMO motifs in several FA proteins suggesting a wider role of SUMOylation in their regulation. Therefore, this part of this chapter focusses on the effects of blocking total SUMOylation alongside the K80R vinculin on the turnover of FAs. Vinculin-knocked out MDA-MB-231 cells were transfected with WT or K80R vinculin, grown for 24-48 hours and a confocal microscope was used to monitor the turnover of FAs after treating K80R transfected cells with 25 µM Gka. The results show that the turnover of vinculin-containing FAs was significantly slower in cells transfected with K80R compared to WT vinculin. In control cells (transfected with WT vinculin), the average turnover of FAs was 34.76 ± 0.62 seconds compared to 58.99 ± 2.44 seconds in K80R vinculin transfected cells ($p<0.001$) and 59.4 ± 0.68 seconds in K80R transfected-Gka treated cells ($p<0.001$). However, no significant changes were observed in the turnover of FAs between non-treated and Gka-treated K80R transfected cells (Figure 5.5).

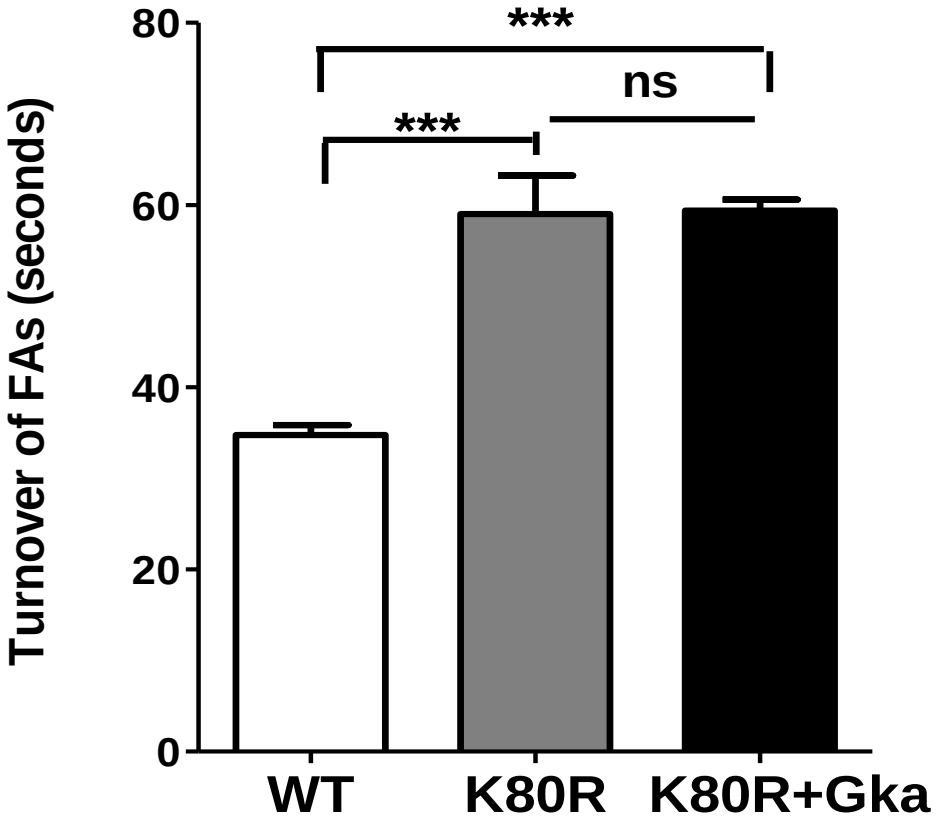

Figure 5.5 Effects of inhibiting SUMOylation on the turnover of FAs in K80R vinculin transfected cells in vinculin CRISPR-knockout MDA-MB-231 cells. Cells were transfected with WT or K80R vinculin and grown for 24-48 hours. Then, cells were treated with DMSO (control) or 25 µM Ginkgolic acid for 2 hours and short timelapse movies were generated using confocal microscopy. The graph shows the quantification analysis of the mean FA turnover measurements in control cells (transfected with WT or K80R vinculin) compared to K80R vinculin transfected Gka treated cells. Data was presented as mean ± SEM of three independent experiments, in each experiment a total number of 150 focal adhesions (24 cells) were analysed. One-way ANOVA with Tukey's Multiple comparison test was used to evaluate any significant differences between groups (*, ** and *** represent P <0.05, 0.01 and 0.001 respectively).

5.5 The K80R mutation in human vinculin enhances its interaction with Talin.

The increase in size and in turnover time of FAs in K80R transfected cells indicates that inhibiting SUMOylation of vinculin at this site enhanced its interaction with other FAs proteins. Since talin is required for the activation of vinculin at FAs, the aims of this part in this chapter was to investigate the effect of this mutation on its interaction with talin.

Co-immunoprecipitation was used to investigate the effects of the K80R mutation in vinculin on its interaction with talin. HT1080 cells were transfected with WT or mutated vinculin and grown for 24-48 hours before preparing whole cell lysate. Anti-GFP antibody was mixed with cell lysates overnight before incubating with agarose beads to immunoprecipitate WT or K80R vinculin. Western blot analysis detected the presence of talin in both GFP Co-IPs prepared from cell lysates of either WT or K80R transfected cells (Figure 5.6 (A)). There were no significant differences in band intensity of talin in K80R vinculin samples compared to WT (Figure 5.6 (B)). Talin band intensity in GFP Co-IPs of K80R transfected cells was 29990 ± 9651 compared to 27550 ± 8438 in GFP Co-IPs of WT transfected cells. Due to the limitations of co-immunoprecipitation, further tests to investigate the effects of K80R mutation on the interaction between vinculin and talin were performed.

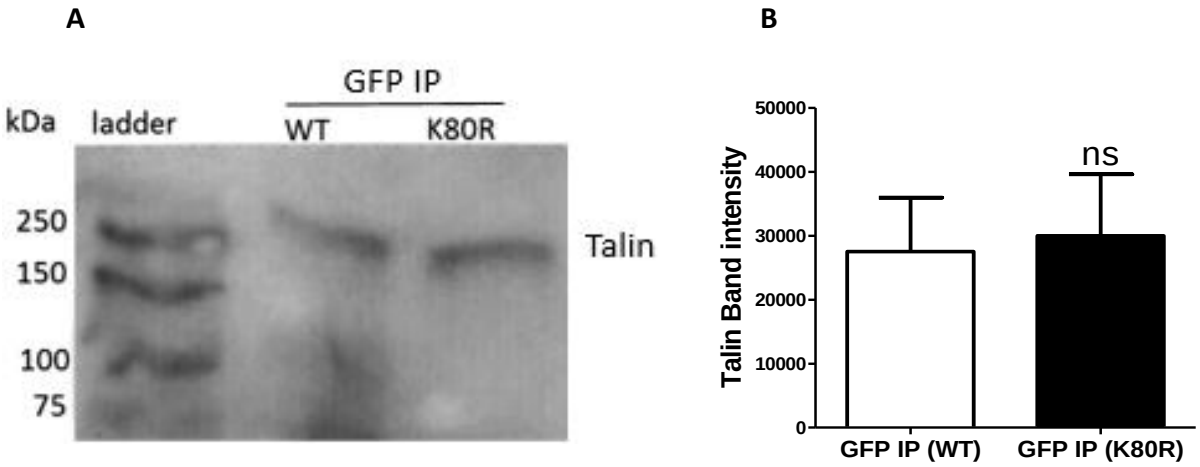

Figure 5.6 Immunoprecipitation and Western blotting showing the K80R-mutated vinculin interaction with talin. A) GFP Co-IP and WB showing talin molecules in GFP Co-IP prepared from lysate of cells transfected with WT or K80R vinculin. B) Quantification of band intensity of talin in GFP Co-IPs of cell lysates of WT or K80R transfected cells.

To further investigate the effects of this mutation on the interaction between vinculin and talin, photo-bleaching FRET assay was performed. MDA-MB-231 cells were transfected with both GFP-talin and m-cherry WT, K496R or K80R vinculin, grown for 48-72 hours before fixing and subjecting them to Photo-bleaching FRET assay using confocal microscopy. Photos of GFP-talin and m-cherry-vinculin were taken before and after bleaching m-cherry-vinculin. ImageJ (Fiji) software was used calculate FRET efficiency of the interaction between vinculin and talin. The results revealed a significant increase in the FRET efficiency of vinculin-talin interaction in K80R transfected cells compared to WT or K496R transfected cells (Figure 5.7). The FRET efficiency increased from 2.97 ± 0.32 % in WT transfected cells to 4.52 ± 0.23 % in K80R transfected cells. This significant increase in FRET efficiency was observed between K496R and K80R transfected cells. In K496R transfected cells, the FRET efficiency was 3.10 ± 0.34 % compared to 4.52 ± 0.23 % in K80R transfected cells ($p<0.02$). No significant changes in FRET efficiency were observed between WT and K496R transfected cells (Figure 5.7 (B)).

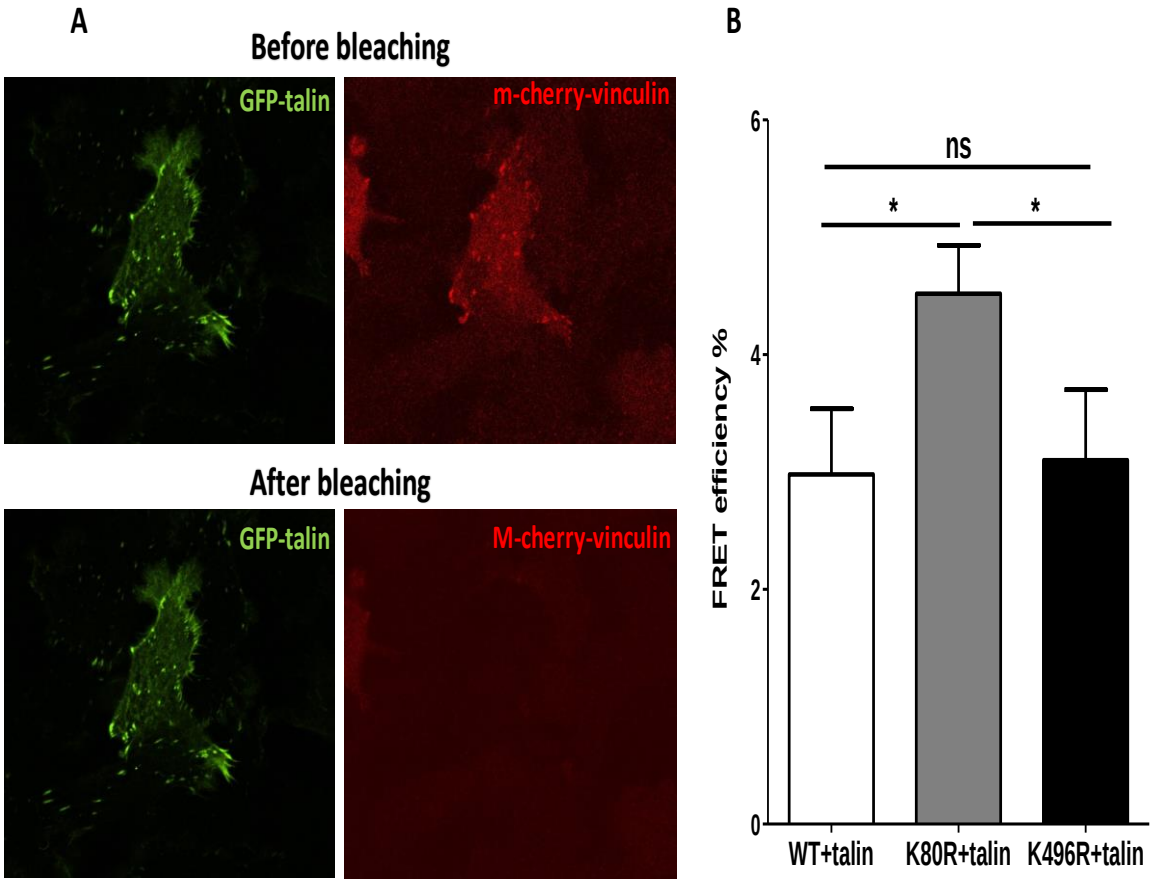

Figure 5.7 Effects of the K80R mutation in vinculin on the interaction between vinculin and talin in MDA-MB-231 cells. Cells were transfected with both GFP-talin and WT, K496R or K80R vinculin, grown for 48-72 hours. Then, cells were fixed and subjected to FRET assay using confocal microscope. A) Representative cells shown GFP-talin and m-cherry-vinculin before and after bleaching. B) Quantification analysis of the mean FRET efficiency measurements in control cells (transfected with WT vinculin) compared to K496R or K80R vinculin transfected cells. Data was presented as mean ± SEM of three independent experiments. One-way ANOVA with Tukey's Multiple comparison test was used to evaluate any significant differences between groups (*, ** and *** represent P <0.05, 0.01 and 0.001 respectively).

To evaluate the importance of the K80 in the interaction between talin and vinculin, IntFOLD server, Reading University, was used to predict the 3D structure of WT or K80R mutated vinculin (with the help of Dr. Liam McGuffin). The predicted models of vinculin showed that the K80R mutation has not caused any structural changes in the folding of this protein. In addition, the K80 residue was found to be located in vinculin N-terminal head domain, which has binding sites for talin. Docking models of talin-vinculin and SUMO2-vinculin interface were generated using this server to investigate whether K80 residue is essential for their interaction. These models showed that talin binding region in vinculin spans residues from 6 to 60, but not K80. However, all the five top ranked models showed that talin binding to vinculin is across K80. SUMO2 binding to this site was shown by these models to interfere with talin binding to vinculin as SUMO2 attachment to K80 was predicted to block talin-vinculin binding pocket (Figure 5.8).

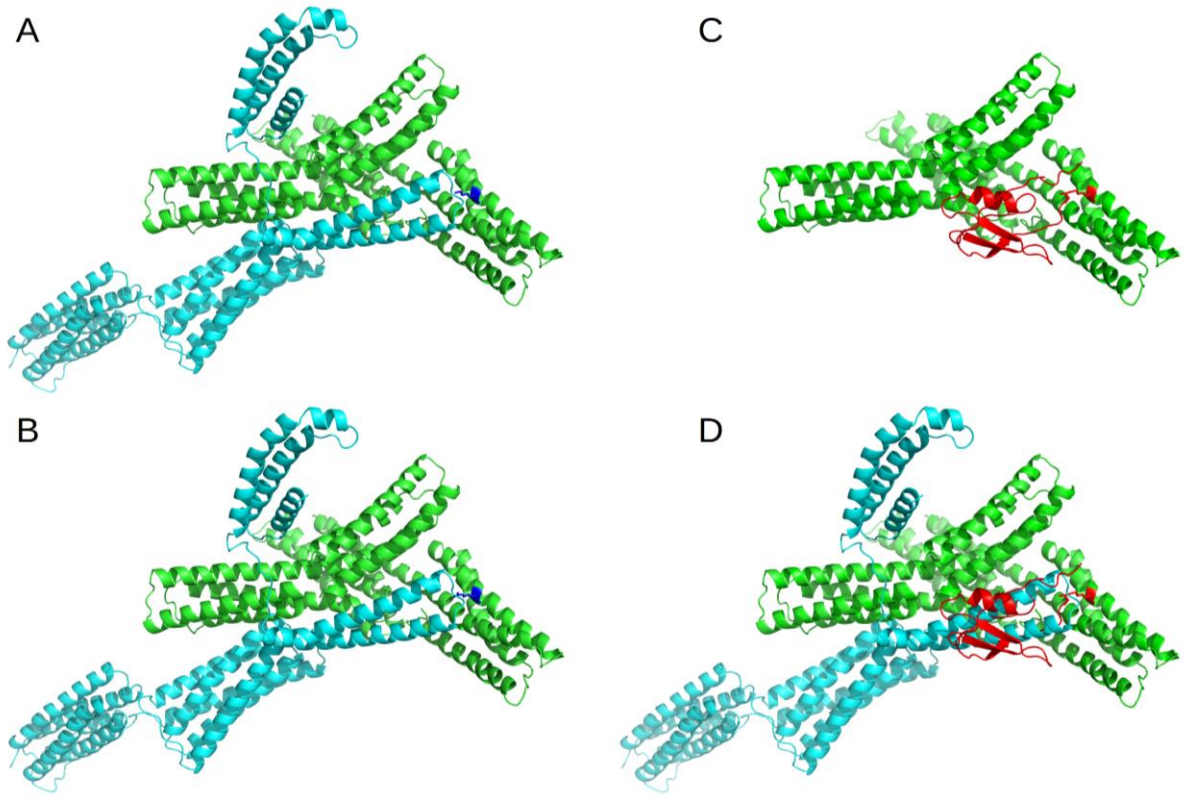

Figure 5.8 Template based models of vinculin-talin and vinculin-SUMO2 interface showing that talin and SUMO2 binding to vinculin is across K80. A) A cartoon representation of vinculin (green)-talin (cyan) interface with K80 residue highlighted in blue. B) A cartoon representation of vinculin (green)-talin (cyan) interface with the replaced lysine with arginine residue at position 80 highlighted in blue. C) A cartoon representation of vinculin (green)-SUMO2 (red) interface with K80 residue highlighted in red. D) A cartoon representation of vinculin (green)-talin (cyan)-SUMO2 (red) interface with K80 residue highlighted in red (Produced using IntFOLD server by Dr. Liam McGuffin).

5.6 Discussion

This chapter focuses on the mechanisms by which the SUMOylation of vinculin regulates the dynamic activities of FAs through modifying vinculin. The CRISPR/Cas9 system occurs naturally in bacteria and archaea as an RNA-based adaptive immune system and it is proven to be useful in editing eukaryotic genomes (Cong et al., 2013). It is a very powerful technique used in research to knockout, insert or edit DNA sequences. Therefore, it facilitates investigating the biological functions of different genes in normal and pathological processes (Jiang et al., 2019). The Cas9 nuclease is guided to its target by about 20 nucleotides that are complementary to the target DNA. In addition, the activity of this nuclease depends on the presence of a protospacer adjacent motif (PAM) sequence in the genome adjacent to the target sequence in the genome (Sternberg et al., 2014, Anders et al., 2014). Although the guide RNA directs Cas9 towards its target, off-target effects are possible and studies have shown that the guide RNA is critical in on-target and off-target effects (Hsu et al., 2013). In addition, off-target effects are suggested to be dependent on the integrity of the double-stranded breaks' (DSBs) repair pathways and they are cell type specific (Duan et al., 2014). Despite its off-target effects, the CRISPR/Cas9 system has proven to be useful in understanding the roles of genes of interest in cellular processes in both normal and pathological conditions. The CRISPR/Cas9 system has been successfully used previously to edit the FA protein, FAK, in order to investigate its role in the DNA damage response in Non-small cell lung cancer (NSCLC) (Tang et al., 2016).

In this project, the CRISPR/Cas9 system was used to knockout the endogenous vinculin in the HT1080 and MDA-MB-231 cells. To increase the specificity of Cas9 towards vinculin, a

smart pool of 3 plasmids, each encoding the Cas9 nuclease and a distinct vinculin-specific 20 nt, guided the RNA. In addition, there was a smart pool of 2-3 plasmids each containing a HDR template corresponding to the cut sites generated by vinculin CRISPR/Cas9 plasmids. Each HDR plasmid inserted a puromycin resistance gene, therefore allowing for the selection of successful knockout cells. The use of the three different vinculin-specific RNA guides and the insertion of puromycin resistance genes in the cut sites increased the efficiency of the vinculin knockout and minimise the defects of endogenous homology-directed DNA repair. The use of smart pools is more efficient and have less off-target effects than using single guide RNA (Hannus et al., 2014). In addition, as off-target effects are suggested to be cell type specific, two different cell lines were used to knockout vinculin. In the vinculin-knockout cells, WT or mutated vinculin was re-expressed to study the effects of mutated vinculin without the interruption of the endogenous vinculin, thus allowing for the investigation of the precise effects of the K80R mutation in vinculin on the turnover of FAs and cell migration. The results showed that expressing the K80R in vinculin-knockout cells caused a minor but a significant reduction in the turnover rate of vinculin-containing FAs in the HT1080 cells compared to K80R vinculin transfected cells that have the endogenous vinculin. On the other hand, in the MDA-MB-231 cells, there were no significant differences in the FA turnover in the vinculin-knockout cells compared to cells that have the endogenous vinculin when expressing the K80R mutated vinculin. This could mean that the competition between the endogenous and K80R mutated vinculin is weak or insufficient to influence FA turnover in these cells. This weak competition may be caused by the overexpression of mutated vinculin. The overexpression of the mutated vinculin could lead to more mutated vinculin molecules in the FA complex than due to the endogenous vinculin.

This finding, alongside the finding in the previous chapter, markedly links vinculin as one of the main targets of SUMOylation for regulating FA dynamic activities. However, several questions remained unanswered, including what the impact of SUMOylating vinculin on its activity at the FAs is and whether SUMOylation has other FA protein targets to regulate their dynamic. Answering these questions will increase our understanding of the role of SUMOylation in regulating FAs. Therefore, one of the main aims of this chapter was to investigate whether SUMOylation could have a wider role in regulating FAs by targeting FA proteins other than vinculin. The finding in the previous chapters indicates that SUMOylation may have multiple targets in FA complexes. Inhibiting global SUMOylation using inhibitors caused a significant impairment in the FA dynamics. Similar effects were observed when expressing the K80R mutated vinculin. In addition, the FA protein, FAK, has been identified as a SUMO target, although its SUMOylation was reported to occur in the nucleus (Constanzo et al., 2016). Furthermore, talin was identified as a SUMO substrate and the turnover of talin-containing FAs was found be significantly reduced by Gka treatment (Huang et al., 2018). Different bioinformatic tools also predicted the presence of extended SUMO and SIM motifs in several FA proteins, thus indicating the wider role of SUMOylation in FAs. Taken together, it was hypothesised that blocking global SUMOylation in cells that express the non-SUMOylatable version of vinculin (K80R) will have further impairment in the turnover of FAs than expressing the mutated vinculin alone. To directly test this hypothesis, Ginkgolic acid (25 µM) was used to inhibit SUMOylation in MDA-MB-231 cells that express the K80R mutated vinculin. Unexpectedly, the results showed that inhibiting the total SUMOylation in K80R vinculin transfected cells has a similar effect on the turnover of vinculin-containing FAs to that of expressing K80R vinculin alone. The similar effects of

Gka treatment on the FA dynamics to that observed when the expressing the K80R mutated vinculin could suggest that vinculin is the main target of SUMOylation at the FAs sites to regulate FA dynamics. This could explain the defects in the FA dynamics upon the treatment of the SUMOylation inhibitors. These inhibitors could inhibit the SUMOylation of vinculin, which in turn leads to impairments in their dynamics. Through modifying vinculin, SUMOylation is most likely to be involved in the regulation of FA turnover to facilitate cell migration. The presence of other potential SUMO targets at the FA sites could conflict with this finding. However, FAs perform multiple functions including sensing the extracellular environment, transmitting traction forces or functioning as signalling hubs for different cellular processes. The SUMOylation of other potential targets at these sites could regulate the different functions. In addition, expressing the non-SUMOylatable vinculin (K80R) resulted in larger and more stable FAs, thus indicating that SUMOylation could be involved in the disassembly of FAs. The SUMOylation of other targets at FAs could be involved in the assembly of FAs by facilitating their recruitment and interaction.

The last aim of this chapter was to examine the consequences of SUMOylating vinculin at K80 on its activity at FAs. Although vinculin interacts with different FA proteins, its interaction with talin was found to be required to activate and target vinculin to higher layers, thus allowing its engagement with actin filaments (Case et al., 2015). The engagement of talin and vinculin to the actin filament enhances the stability and maturation of FAs (Carisey et al., 2013). This could be supported by the finding where expressing the A50I mutated version of vinculin, which prevents its binding to talin (Cohen et al., 2006),

was found to cause a significant reduction in the number and stability of FAs (Diez et al., 2011).

As discussed previously, focal adhesions are formed and progressed through protein-protein interaction. In addition, one of the main functions of SUMOylation is altering the target protein's binding affinity towards its binding partners (Tatham et al., 2008, Tan et al., 2015). The finding in the previous chapter showed that expressing K80R mutated vinculin has led to larger and more stable FAs. Taken together with the fact that the talin-vinculin interaction is necessary for the development and maturation of FAs, SUMOylating vinculin at K80 was hypothesised to trigger the disassembly of maturated FAs by disassociating the talin-vinculin interaction and allowing cells to move. To directly test this hypothesis, the talin-K80R vinculin interaction was assessed using different assays including Co-IP and FRET. Co-IP is one of the most widely used approaches to study protein-protein interactions. The principle of this technique relies on using target protein-specific antibodies to indirectly capture proteins that are bound to the protein of interest. The antigen-antibody complex is precipitated using protein A/G-coated agarose beads (Kaboord and Perr, 2008). The protein of interest interacting candidates can be detected using Western blot analysis, ELISA or mass spectrometry (MS) (Monti et al., 2005). One of the main advantages of Co-IP is the presence of proteins in their native conformation. In addition, it is a relatively inexpensive and straightforward approach that does not require special skills or advanced tools. Different techniques including Western blotting, ELISA or MS can be used following Co-IP to analyse interacting candidates, thus making it a versatile approach for studying protein-protein interaction. It has been previously used to evaluate the effects of SUMOylation

inhibitor treatment on the interaction between talin and SUMO2 (Huang et al., 2018). Although Co-IP is a common approach to studying protein-protein interaction, there are several challenges that could affect identifying protein-protein interaction using this technique. For example, the weak or transient interactions of proteins in dynamic structures such as FAs and actin cytoskeletons can be hard to detect using Co-IP (Lee et al., 2013, Avila et al., 2015). In addition, interacting candidates that can be detected in Co-IP could be caused by the presence of a protein complex of multiple proteins. Therefore, the interacting candidate could be linked to the protein of interest through a modulator protein. Alternatively, a member of a complex may interact with the protein of the interest and lead to the precipitation of the whole complex (Hall, 2005). Other limitations of Co-IP include the availability of primary antibodies, the non-specific binding of IP components and antibody contamination that could reduce the detection efficiency.

In this project, Co-IP was used to evaluate the effects of K80R mutation in human vinculin and its interaction with talin. Although the interaction between talin and vinculin is transient, the K80R mutation was thought to enhance their interaction and therefore, more mutated vinculin molecules would precipitate with talin than WT vinculin. However, the results showed that there were no significant differences in talin band intensity between GFP IPs of either the WT or K80R samples. This could be due to different reasons including the fact that the vinculin-talin interaction is transient, thus making it difficult to quantify their interaction using IP. Another reason could be the loss of protein interaction during the sample preparation and Western blot process. In addition, since talin interacts with both WT

and K80R vinculin, it is difficult to quantify their interaction using Co-IP. Therefore, an alternative way of measuring protein-protein interaction was used in this project.

Fluorescent proteins facilitate the visualisation of the protein's distribution within the cells and this aids in the investigation of protein-protein interaction (Day and Davidson, 2009). One of the ways to study protein-protein interaction is the co-localisation of fluorescent-tagged proteins using high-resolution microscopes such as confocal. The co-localisation between two proteins could indicate their interaction. However, the spatial resolution of these microscopes is around 200 nm due to its dependence on the diffraction limit of light microscopy (Shaw and Ehrhardt, 2013). This could mean that although the two co-localised proteins may appear in the same spot, these proteins could be separated by several proteins. They could be in the same complex or separated by a modulator protein, thus their interaction is not proven by co-localisation. This limitation of the spatial resolution of these microscopes encourages finding another way of studying the protein-protein interaction. One of these ways is using a FRET assay, which depends on the transfer of energy from a fluorescent-tagged donor protein to a fluorescent-tagged acceptor protein. In order for FRET to occur, three main factors are required; the spectral overlap of donor emission and acceptor absorption, the two proteins must be in a very close proximity (<9 nm) and the alignment of the dipole orientation of the proteins. The FRET assay is more specific and highly sensitive compared to Co-IP as it can detect protein interactions where the distance is within 10 nm. It can also visualise the subcellular location of the interaction. However, there are several issues that should be considered when using this approach to study protein-protein interaction. Although the FRET assay is a more common and efficient

way of studying protein-protein interactions than co-localisation and Co-IP studies, several challenges could affect interpreting the FRET data. One of the limitations of FRET is the requirement of conjugating a fluorophore to target protein. These tags could alter the activity or conformation of the proteins of interest. In addition, FRET requires the overexpression of the protein of interest. The overexpression of individual proteins in dynamic structures such as FAs could change the balance of the protein components in the complexes, leading to artificial effects. Another limitation of FRET is the spectral bleed or cross talk between the donor and acceptor fluorescent proteins. This cross talk comes from the fact that all fluorescent proteins absorb and emit photons when subjected to a range of wavelengths rather than at a specific wavelength. This spectral bleed could occur during the excitation of the donor. The acceptor is excited at the same time, thus causing the emission of the acceptor that is not occurring due to FRET. The other type of spectral bleed could occur from the donor emission in the spectrum of the acceptor. These leaks could affect the interpretation of the FRET data analysis (Müller et al., 2013). Adjusting the amount of fluorescent proteins through controlling the gene dosage and using the correct controls was suggested to reduce this bleed (Hecker et al., 2015). One way to detect FRET and to avoid spectral bleed is through measuring the changes in the intensity of the donor before and after the photobleaching of the acceptor. The principle of this technique relies on the loss of energy transfer from the donor after bleaching the acceptor, leading to an increase in donor intensity. One of the challenges in photobleaching is bleaching the donor during the bursting of the acceptor, leading to an overall reduction in fluorescence intensity (Ishikawa-Ankerhold et al., 2012). A correction of this reduction can be achieved by measuring the changes in intensity in the background regions. Another issue that could affect interpreting

the photobleaching FRET data is the movement of ROIs in or out of the focal plane caused by a delay during recording. As photobleaching the acceptor protein may require 20-120 seconds, the longer the time of bursting, the more possible it is for the ROIs to move in or out of the focal plane. Therefore, changes in donor intensity could be caused by this movement instead of the absence of the acceptor protein (JOOSEN et al., 2014). To avoid this, rapid and efficient recording and bleaching is necessary for more accurate results.

Despite the limitations of this approach, FRET provides the opportunity to study the protein-protein interaction at specific cellular compartments. It is one of the highly used approaches to investigate the interactions between FA proteins. For example, it has been used alongside IP to study the interaction between the FA proteins paxillin, vinculin, FAK and Crk-associated substrate (CAS) (Ballestrem et al., 2006). Using these techniques, the authors concluded that FAK, paxillin and CAS were tyrosine phosphorylated at the early FAs and that FAK was found in FRET proximity to CAS and paxillin. In addition, the FRET assay was also used to evaluate the interaction between talin, actin and vinculin in order to investigate the role of surface stiffness on talin tension at FAs (Kumar et al., 2016). In this project, to further confirm the Co-IP results, a photobleaching FRET assay was used to examine the effects of K80R mutation on the talin-vinculin interaction. The results showed that either WT or mutated vinculin were in FRET proximity to talin. Interestingly, a significant increase in the FRET efficiency of talin-K80R vinculin interaction was found compared to that of talin-WT vinculin. This increase in the FRET efficiency clearly indicates that the talin interaction with K80R-mutated vinculin is more stable than its interaction with WT vinculin. The stability of their interaction was due to preventing the SUMO modification of vinculin at K80. The enhanced

stability of the talin-K80R vinculin interaction is probably the main cause of the impairments in the turnover of FAs as seen in cells that express the mutated version of vinculin.

Upon these findings, it can be suggested that SUMOylation regulates the turnover of FAs by disassociating the talin-vinculin interaction. The use of two different techniques increases the confidence of this finding and it clearly indicates SUMOylation as a key regulator of FA dynamics. Preventing vinculin SUMOylation allows the talin-vinculin interaction to last longer, which is responsible for the larger size and slower turnover of FAs in K80R vinculin transfected cells. Although their interaction is critical for the maturation of FAs, talin-vinculin disassociation is required to trigger the disassembly of FAs. During migration through ECM, cells require the continuous disassembly of existing FAs and the assembly of new FAs at new sites. Defects in either of these processes would have a significant influence on the ability of the cell to migrate. A significant question arises from this finding, since K80 in vinculin is not in the talin interaction region, which is how the SUMOylation of vinculin at this site disassociates their interaction. The talin binding region in vinculin was reported previously to span residues 6-63 (Bois et al., 2005). The location of the K80 site outside the talin binding sites in vinculin makes it difficult to understand how the SUMO attachment to vinculin regulates its interaction with talin. The 3-D structure of vinculin could answer this question and explain the involvement of SUMO in controlling their interaction. Although K80 is not in the talin binding region at the sequence level, the folding of vinculin could bring it closer to this region. To test that, the 3-D modelling of the talin-vinculin and SUMO2-vinculin interfaces was performed.

Photobleaching FRET assay and Co-IP experiments are very well-known techniques in determining protein-protein interaction and in this project, FRET revealed an enhanced interaction between K80R mutated vinculin and talin. Structural-based characterisation of the 3D protein structures is equally important for studying protein-protein interactions. It allows researchers to structurally visualise the folding and different functioning domains of proteins. It also facilitates identifying specific regions in protein structures that are critical in their interaction with their binding partners, therefore allowing for the identification of the possible regulatory mechanisms behind the protein interactions. Even though identifying protein 3D structures and interactions experimentally has been established before, the huge advancement in genome sequencing encourages researchers to establish alternative and time saving ways to determine protein structures of the enormously available new sequences (McGuffin et al., 2019). Computational tools provide a cheaper and robust way of predicting protein structures directly from their sequence, facilitating the building of 3D models and investigating their interactions. The development of different computational methods encourages researchers to introduce a unified blind test of the available protein structure prediction methods called the community experiment ''Critical Assessment of Techniques in Structure Prediction'' (CASP). This experiment takes place every 2 years and it aims to compare the performance of available approaches based on their prediction of almost 100 protein structures (Moult et al., 2016). Following this evaluation, a community meeting of the developers took place, allowing them to discuss the performance of the current tools and the latest advancements in this field. The Continuous Automated Model EvaluatiOn (CAMEO) platform provides another and more frequent independent test that evaluates the performance of these methods based on the prediction of known but

unpublished protein structures (Rose et al., 2013, Haas et al., 2018). By providing developers with the accuracy and quality of predicted structures and the possible limitations of their approaches, these experiments have led to a significant advancement in protein structure prediction. The advancement in computational methods that can evaluate the accuracy of the predicted 3D protein models increases the researcher's confidence in structure prediction (Elofsson et al., 2018).

The IntFOLD server at Reading University has gained the attention of being one of the best available computational tools for predicting protein structures, creating 3D models and estimating their quality and predicting protein-protein interactions (McGuffin et al., 2019). Based on the CASP and CAMEO blind assessments, this server has shown competitive performance and it was ranked among the highest available servers for protein structure prediction (Haas et al., 2018). By using this server, Dunwell and their colleagues in 2013 predicted the 3D protein structure of new protein sequences identified in *Drosophila melanogaster* (Dunwell et al., 2013). In addition, Fuller and their colleagues in 2012 used this server to determine the regulatory mechanisms of some mammalian GCKIII (germinal centre kinase III) kinases through structurally predicting the protein-protein interaction (Fuller et al., 2012, Sugden et al., 2013).

Here, this server was used to predict the 3D structure of WT or mutated vinculin, and the obtained models were compared to the published structure of vinculin in the protein data bank (PDB). The predicted models of vinculin showed that the K80R mutation has not caused any structural changes in the folding of this protein. In addition, the K80 residue in

this protein is in the N-terminal head domain, which has binding sites for talin. In order to evaluate the importance of this residue in the talin-vinculin interaction and the consequences of SUMO2 binding, docking models of these interactions based on their structures were generated using this server (with the help of Dr. LiamMcGuffin). The template-based docking models showed that the talin binding region in vinculin spans residues from 6 to 60, but not K80. However, structurally, all of the top five ranked docking models revealed that talin binding to vinculin is across K80. In addition, the docking models of the SUMO2-vinculin interface showed that the attachment of SUMO2 to vinculin at K80 was at the same approximate site as where talin binds. It thus blocks the talin-vinculin binding pocket. Based on these models, SUMO2 attachment to K80 in vinculin disrupts the interaction of the latter protein with talin. By binding to vinculin, SUMO2 blocks the vinculin-conserved region from interacting with talin, causing the disassociation. These structural-based interaction models clearly support the Co-IP and FRET assay results by indicating the importance of SUMO2 binding to vinculin at K80 to disassociate from the talin-vinculin interaction.

Taken together, the finding of this project provides novel evidence that indicates a direct and critical role of SUMOylation in the regulation of FAs and cell migration. Taking advantage of mutagenesis, the FRET assay and the structure prediction of protein-protein interaction, for the first time, the precise mechanism of SUMOylation in the regulation of FAs has been defined. This finding clearly suggests that SUMOylation regulates the disassembly of FAs by the covalent-attachment of SUMO2 to vinculin at K80 to disassociate the talin-vinculin interaction. Talin and vinculin play important roles in the formation and

maturation of FAs. Talin is recruited to early FAs, where it initiates the formation of a linkage between ECM and actin filaments by binding to integrin and actin. This linkage is stabilised by the recruitment of vinculin to the adhesion sites, where it supports the maturation of FAs by binding to talin via its head domains (D1), and to actin through its tail domain (D5) (Bois et al., 2005). This stabilised linkage enables the FAs to bear and transmit higher traction forces between the cytoskeletal fibres and ECM, thus allowing the cells to move through matrices (Carisey et al., 2013). According to the finding of this project, SUMOylation plays a critical role in the regulation of cell migration by triggering the disassembly of existing FAs facilitating cell movement. It triggers the disassembly of maturated FAs by disassociating the talin-vinculin interaction. Talin binds to vinculin in an approximate site to K80 and SUMO2. Binding to this residue disassociates the talin-vinculin interaction and blocks their binding pocket. Introducing a mutation in this site by replacing lysine with arginine to prevent SUMO2 attachment enhances the talin-vinculin interaction. This leads to a larger size and a slower turnover of FAs, in addition to a consequent reduction in cancer cell migration. SUMOylation has shown to be an ideal regulatory mechanism for cell migration, which requires a rapid and reversible regulation of its components. SUMOylation triggers the disassembly of existing FAs by disassociating the talin-vinculin interaction through modifying vinculin. De-SUMOylation could induce the maturation of newly formed early FAs by removing SUMO2 from vinculin, thus allowing for its interaction with talin.

The presence of SUMO motifs in other FA proteins could indicate a distinct and a wider role of SUMOylation in the regulation of FAs apart from its role to trigger the disassembly of the adhesion sites by targeting vinculin. It could be involved in their activation and/or recruitment to FAs by mediating their interactions in the assembly phase of the FAs. However, more studies are required to evaluate the consequences of SUMOylating these proteins on the dynamic activities of FAs.

6. General Discussion

6.1 Future work and perspective

The findings in this project support the hypothesis that SUMOylation promotes cancer cell migration via regulating the turnover of FAs. The SUMO attachment to vinculin is likely to lead to the disassociation of talin-vinculin interaction thus triggering the disassembly of FAs. Since migrating cells require the continuous disassembly of existing mature FAs and assembly of new FAs at new sites to facilitate their movement through the ECM, the involvement of SUMOylation as a regulatory system in this process indicates its potentially critical role in supporting cancer invasiveness and metastasis. Given its important role in cancer cell migration, SUMOylation could be a potential target for therapeutic metastasis intervention. As a regulatory mechanism of various proteins with diverse cellular functions, investigating the possibilities of targeting the SUMO pathway or its substrates for the development of anticancer molecules could lead to the identification of alternative ways to treat cancer or the improvement of current medication. However, more studies are required to determine the applications of targeting this post-translational modification system for developing such treatment.

SUMOylation has gained the attention of been a crucial regulatory mechanism that support cancer growth and metastasis (Seeler and Dejean, 2017). The expression of SUMO and SUMO-associated enzymes have been reported in several studies to be deregulated in various cancers and their deregulation was suggested to drive tumorigenesis and invasiveness (Chen et al., 2011).

Blocking SUMOylation by knocking down the SUMO E1 activating enzyme (SAE) or E2 conjugating enzyme (Ubc9) has resulted in preventing tumour growth in mouse models (Liu et al., 2015). Several studies have reported the implications of SUMOylation in regulating multiple functions in cancer cells including apoptosis, cell proliferation, angiogenesis and metastasis. For example, SUMOylation was suggested to induce cellular senescence and apoptosis by stabilising the tumour suppresser protein, p53 (Ivanschitz et al., 2015). In addition, SUMOylation was shown to regulate Akt-mediated tumorigenesis via regulating Akt activity. The covalent attachment of SUMO1 to this kinase increases its activity, which in turn promotes tumorigenesis, whereas its deSUMOylation by SENP1 reduces its activity (Li et al., 2013). Furthermore, SUMOylation was found to promote cell proliferation of leukemia cell lines by modifying Insulin-like growth factor-1 receptor (IGF-1R) (Zhang et al., 2015). SUMOylation of this receptor leads to its translocation to the nucleus to mediate expression of target genes, some of which induce cell proliferation (Packham et al., 2015). SUMOylation was also identified to support cancer metastasis and protect malignant cancer cells from chemotherapy-induced apoptosis. The higher expression levels of its E2 conjugating enzyme, Ubc9, were shown to drive these processes (Moschos et al., 2007).

The conflicting roles of SUMOylation in cancer cells increase the challenges of its applications in cancer therapy. In addition, the regulatory mechanisms behind its involvement in regulating various functions in cancer cells remain poorly understood. As the further identification of SUMO substrates, some of which may have critical roles in cancer progression and metastasis, addressing the regulatory roles of SUMOylating these proteins could reveal promising therapeutic targets. Although exhibiting conflicting roles in cancer

cells, in most cases, SUMOylation was suggested to enhance cancer progression and metastasis. Although the expression of SUMO and SUMO associated enzymes vary in different cancer types, their expression is upregulated in the majority of cancers (Bellail et al., 2014, Seeler and Dejean, 2017). In addition, the SUMOylation levels were found to be higher in tumours than in surrounding normal tissues (Tomasi et al., 2012). The increased levels of SUMOylation in tumours indicate its importance to aid tumorigenesis. Therefore, investigating its roles in cancer malignancy and metastasis, which is responsible for most cancer-related deaths (Gupta and Massagué, 2006), could lead to the identification of cancer therapeutic targets.

Given its crucial roles in cancer growth and metastasis, targeting SUMOylation for the development of anticancer therapies could be promising. Different steps of the SUMOylation pathway can be targeted. One possible target in this pathway that could be a useful indicator of tumour malignancy and a potential therapeutic target is the SUMO E1 activating enzyme (SAE). The higher expression levels of this enzyme were suggested to enhance cancer malignancy. The malignancy of small lung cancer cells was inhibited and their sensitivity to chemotherapy was enhanced by knocking down this enzyme (Liu et al., 2015). In addition, the expression levels of SAE in Myc-overexpressed breast cancer patients were found to contribute to malignancy stage and survival rate. The low expression levels of this enzyme were described to be associated with improved survival rate and reduced metastasis compared to higher expression levels (Kessler et al., 2012). Myc (c-Myc) is a transcriptional factor that regulates the activity of several genes including genes involved in cell proliferation.

In some cancers, the gene encoding Myc possess a mutation that increase the expression of its encoded protein, which results in upregulation in the expression of target genes leading to cancer progression. Although its overexpression derives carcinogenesis, the activity of this protein was dependent on the enzymatic activity of SAE and knocking down this SUMO-activating enzyme caused synthetic lethality in these cancers (Amente et al., 2012). As SAE is required to activate the SUMO pathway, this finding indicates the importance of enhanced SUMOylation activity in c-Myc-dependent tumorigenesis. In addition, the expression levels of this enzyme could be a useful indicator of malignancy stage in patients with Myc overexpression. Furthermore, SAE could be a potential target for the development of molecular therapy that induce synthetic lethality with mutated Myc in these cancer types.

Small molecules that target this enzyme have been developed including Ginkgolic acid (Fukuda et al., 2009a), kerriamycin B (Fukuda et al., 2009b), and davidiin (Takemoto et al., 2014). These molecules were found to inhibit its interaction with SUMO proteins, thus blocking general SUMOylation. Ginkgolic acid is the most widely used as a total SUMOylation inhibitor and it was found in this project to significantly reduce cancer cell migration. However, due to non-specific side effects and unclear characterisation of these inhibitors, researchers are continuingly screening for natural products or chemically synthesised compounds for more specific targeting. In this regard, three SAE inhibitors were identified recently including tannic acid (Suzawa et al., 2015), compound 21 (Kumar et al., 2013) and ML-792 (He et al., 2017). Among these inhibitors, ML-792 was shown to inhibit the SUMO-SAE intermediate formation by covalently binding to the SAE binding sites in SUMO proteins. This compound was found to inhibit the enzymatic activity of SAE with good

selectivity in Myc-overexpressed cells (He et al., 2017). This inhibitor could have a promising potential for being used or developed as an anticancer drug for Myc-upregulated tumours treatment. However, more characterisation of its specificity and side effects is necessary before testing in clinical trials.

Another potential therapeutic target in the SUMOylation pathway is the SUMO E2 conjugating enzyme (Ubc9), which covalently attaches SUMO proteins to their substrates (Gareau and Lima, 2010). Ubc9 overexpression was reported in different cancer types and its expression is associated with cancer development (Seeler and Dejean, 2017). The expression of this enzyme was shown to increase during the transformation of normal colonic epithelial cells to colon cancer cells. Its expression was also shown to be higher in late-stage melanoma and in tumour breast tissue compared surrounding tissue (Tomasi et al., 2012). The higher expression levels of this enzyme were suggested to increase malignancy and metastasis of melanoma cells and to enhance their resistance to chemotherapy treatment (Moschos et al., 2007). Given its importance in the SUMOylation pathway and its overexpression in most cancers, developing molecule inhibitors targeting this enzyme could be an alternative approach to explore the roles of SUMOylation in cell functions and/or to identify useful compounds with anticancer activity. Several compounds have been reported to inhibit the activity of this enzyme and global SUMOylation including GSK145A (Brandt et al., 2013), 2-D08 (29,39,49-trihydroxyflavone) (Kim et al., 2013) and the gram-positive antibiotic spectomycin B1 (Hirohama et al., 2013). Spectomycin B1 inhibitor was confirmed to have inhibitory effects against SUMOylation by interacting with this enzyme and was reported to inhibit estrogen receptor-mediated cell proliferation in breast

cancer indicating its potential use in treating these tumours (Hirohama et al., 2013). However, characterising current inhibitors against this enzyme stills in early stages and ongoing studies continue to screen for new compounds (Zlotkowski et al., 2017).

The SUMO E3 ligases enhances conjugation of SUMO proteins to their substrates and could be also potential therapeutic targets (Martin et al., 2007). Unlike the sole E1 or E2 enzymes in the SUMOylation pathway, there are several E3 ligases with different substrate specificity. The overexpression of one of these ligases, Ran binding protein 2 (RanBP2), was reported in myeloma (Felix et al., 2009) and small cell lung cancer (Horio et al., 2010). Targeting these enzymes could have a great potential in screening for molecules with anticancer activity. Unlike targeting the E1 or E2 enzymes, which blocks global SUMOylation, targeting an individual E3 ligase will only inhibit the SUMOylation of its specific substrates. This will allow investigating the impact of SUMO modification on the functions of specific targets. In addition, since SUMOylation regulates multiple cellular functions, targeting these enzymes could facilitate evaluating the role of SUMOylation in a specific function without affecting the SUMOylation of proteins involved in other processes. This could indicate that targeting these ligases could be useful for the identification of potential therapeutic targets for the development of anticancer compounds that inhibit the SUMOylation of specific substrates without affecting global SUMOylation. However, no compounds with inhibitory effects against these ligases have been described (Yang et al., 2018).

SUMO-specific proteases (SENPs) represent another potential target for cancer intervention. These proteases have two distinct functions in the SUMO pathway; they cleave the c-termini

in SUMO proteins allowing them to interact with SAE and they deconjugate SUMOs from their targets. DeSUMOylation is important to maintain the SUMOylation levels and the overexpression of SENPs was reported in different cancer types (Xu et al., 2011). The expression of SENP1 was noticed to be upregulated in prostate (Wang et al., 2013) and pancreatic cancers (Ma et al., 2014) and its upregulation enhances their progression and metastasis. Silencing this protease impaired proliferation and migration of these cancer cells. It is expression was also shown to induce androgen receptor (AR)-mediated tumorigenesis in prostate cancer (Kaikkonen et al., 2009) and to upregulate MMP9, which enhances their migration, via de-SUMOylating them (Ma et al., 2014). Unlike SENP1, the expression of SENP2 was observed to be downregulated in bladder tumour tissues (Tan et al., 2013) and in hepatocellular carcinoma (HCC) (Shen et al., 2012), but upregulated in multiple myeloma (Xu et al., 2015). SUMOylation was shown in the first two cancer cells to increase their migration by upregulating MMP13 and overexpression of SENP2 inhibits their migration and invasion by downregulating MMP13. Overexpression of SENP3 and SENP5 was reported in different cancers including gastric cancer (Ren et al., 2014) and breast cancer (Cashman et al., 2014) and their high expression is associated with enhanced malignancy and metastasis. Thus, these proteases could be useful tools for predicting tumour malignancy and survival rate and could be potential targets for cancer therapy. Several SENP1-inhibitors were developed including Triptolide (Huang et al., 2012), Momordin Ic (Wu et al., 2016) and compound 13m (Zhao et al., 2016). These inhibitors were shown to prevent prostate cancer cell growth by downregulating this protease. However, more characterisation of their selective activity and side effects is necessary before testing them in clinical trials for tumour treatment. In addition, novel compounds that target SENP2

have been developed including compound 1, 2, 5-oxadiazole (Kumar et al., 2014), compound 117 and Ebselen (Bernstock et al., 2018). More screening of novel compounds that could have inhibitory effects on SENPs is essential for examining the possibilities of targeting these proteases for cancer treatment.

Taken together, the crucial regulatory role of SUMOylation in various cellular processes in cancer cells makes it an ideal drug discovery target for cancer therapy. The upregulation of SUMO-associated enzymes in tumours can be used to predict the malignancy stage and survival rate of various cancer types. Multiple candidates in the SUMOylation pathway could be used as promising potential therapeutic targets for anticancer drug development. Several molecule inhibitors derived from natural products or synthetic chemicals have been developed to target different steps in the SUMOylation pathway. Some of these inhibitors were reported to have anticancer activities by blocking SUMOylation and were shown to inhibit cancer cell proliferation and cell migration and to induce cell apoptosis. However, the specificity and the molecular mechanisms of these compounds remain poorly understood. In addition, these inhibitors showed a weak or inefficient anticancer activity in multiple cancers and suggested to cause novel side effects in the large scale (Yang et al., 2018). More screening studies are necessary to identify novel SUMOylation inhibitors with good selective activities and detailed characterisation of their molecular mechanisms to evaluate the therapeutic potential of targeting the different SUMO-associated enzymes in cancer intervention.

Although targeting enzymes in the SUMO pathway could be a promising therapeutic strategy for cancer treatment, the main challenge in this regard is the involvement of SUMOylation in various cellular processes in normal and cancer cells. Despite the fact that SUMOylation levels are elevated in tumour cells compared to surrounding tissues, targeting global SUMOylation could lead to severe side effects on signalling pathways in normal cells. Therefore, the development of drugs that could target global SUMOylation could be inefficient for cancer treatment. To overcome this issue, a more specific targeting of SUMOylation components is necessary. One possible way is the development of anticancer drugs that prevent the conjugation of specific isoforms of SUMO proteins. For example, SUMO2/3 isoforms are mainly located in the cytoplasm, where they conjugated to essential proteins involved in cell migration (Wang and Dasso, 2009). Designing drugs that could target these isoforms without affecting SUMO1 protein that regulate nuclear activities could be more specific than targeting general SUMOylation.

Another and more specific SUMO-associated approach that could be used in cancer treatment is targeting specific SUMO substrates. By targeting individual SUMO substrates, general SUMOylation is not affected, and therefore, it could a promising therapeutic strategy for cancer intervention. Identifying essential proteins in cancer progression and metastasis and the development of drugs that could specifically target them to stop their SUMOylation could be more effective with fewer side effects than blocking global SUMOylation. For example, in this project vinculin was identified as a SUMO target and its SUMOylation was found to be important for cell migration. Exploring the effects on inhibiting SUMOylation of other proteins could shed the light on more important proteins

that could be targeted for cancer treatment. For example, various FA proteins have been predicted to be SUMO substrates. By investigating the regulatory roles of SUMOylation in their functions, potential therapeutic targets could be identified. SUMOylation was also reported to regulate different aspects of cancer cell migration by modifying key proteins involved in F-actin cytoskeleton and in matrix degradation. These proteins could be promising therapeutic targets for the development of anticancer drugs.

A promising strategy for the development of anticancer drugs is the development of small molecule inhibitors that could target SUMO substrates and block their SUMOylation. As SUMO proteins conjugate to small regions in their targets, it is more possible to design small molecules that could disrupt their interaction. Identifying specific sites in SUMO substrates facilitates structural based development of small molecules to prevent their interaction with SUMO proteins. Once SUMO binding amino acids in the substrates are identified, databases of small molecules could be screened for compounds that could mimic SUMO binding to this region. The development of small molecules that could have high affinity towards specific targets represent an attractive approach in cancer therapy. This strategy has been used previously to disrupt murine double minute2 (MDM2)-p53 interaction in cancer treatment. The tumour suppresser gene p53 is reported to be inactivated in different cancer types by gene mutations (Feki and Irminger-Finger, 2004) or interaction with the oncoprotein MDM2 (Oliner et al., 1993). The important amino acids in their interaction has been identified using X-ray crystallography and these crystal structures were used to screen for small molecules that could disrupt their interaction (Kussie et al., 1996). One of the identified small molecule inhibitors, MI-219, was shown to mimic the four amino acids (Phe 19, Leu 22, Trp 23 and Leu

26), which represents the MDM2 interacting region in p53 (Kussie et al., 1996). This compound was found to bind to MDM2 with high affinity and prevent its interaction with p53 and was shown to inhibit cancer cell growth in cancer cells that express the WT p53 (Shangary et al., 2008, Ding et al., 2006). This strategy could be implicated in the development of small molecules that could prevent SUMO attachment to specific proteins that are essential in cancer growth and metastasis.

6.2 Future work

Several research lines rise from the findings in this project. The prediction of several potential SUMO substrates at FAs indicate a wider role of SUMOylation in the regulation of different functions of FAs. Mutagenesis could be used to evaluate the effects of their SUMO modification on their recruitment and/or activity in FAs. Since FAs perform multiple cellular functions including sensing the ECM, transmitting tension force and signalling, SUMOylation could involve in the regulation of these functions and determining its roles in these different functions would increase our understanding of its roles in FAs functions.

A future research line could follow this project is investigating the effect of the K80R mutation on metastatic capacity of these cancer cells in animal models. The finding in this project suggests an important role of SUMOylating vinculin at K80 in cancer cell migration in vitro. An important question arises from this finding, which is whether this non-SUMOylatable version of vinculin could have consequences on cell's ability to colonise different organs. Mouse models of metastasis are very important tools that can be used to investigate deferent steps of metastasis. It also provides the opportunity to investigate the

interaction between tumour cells and surrounding microenvironment (Gómez-Cuadrado et al., 2017). There are two different ways of introducing metastatic cancer cells (e.g. MDA-MB-231 cells) expressing the non-SUMOylatable vinculin (K80R) into transplantation mouse models of metastasis. The first way is the intravascular injection of cancer cells in mouse experimental models of metastasis. Injecting cancer cells into different veins leads to the formation of different metastasis. For example, injecting cancer cells into the tail vein leads to the development of lung metastasis, whereas injecting cells into intra-carotid site leads to the formation of brain and bone metastasis (Khanna and Hunter, 2005). These experimental mouse models provide the opportunity to study the effects of K80R mutation in vinculin on different steps of metastasis including cancer cell arrest, extravasation and colonisation of different cancer lines at different regions. Although these models could be useful in determining the impact of vinculin SUMOylation at different steps of metastasis, they do not provide the opportunity to study the initial steps of metastatic cascade including detachment of cells from tumour site, invading surrounding tissues and intravasating circulatory systems. Loss of adhesion is one of the main requirements to initiate metastatic cascade (Friedl and Alexander, 2011) and using these models could not be useful to investigate the impact of this mutation (K80R) on initiation of cancer metastatic. The other way is introducing cancer cells into their primary sites in spontaneous mouse models. These models allow the investigation of all metastatic cascade starting from primary tumour sites to colonisation at secondary sites. Those different mouse models represent great tools to study metastasis of different human cancers. However, a limitation of these models is the lack of adaptive immune system, which was found to contribute to cancer growth and metastasis (Hanahan and Weinberg, 2011). Genetically engineered mouse models could be

useful to overcome the loss of immune system in these models. These models are genetically engineered to overexpress oncogenes and inhibit the expression of tumour suppresser genes to aid tumour growth (Donehower et al., 1992). However, the occurrence of metastasis in these models was reported to be low and does not mimic cancer spread in human (Kabeer et al., 2016, Kersten et al., 2017). Another limitation is the long latency of some cancer types before the formation of metastatic lesions. The resection of primary tumour was suggested to overcome this issue and to initiate cancer metastasis to secondary sites (Doornebal et al., 2013).

Zebrafish models provide the opportunity to overcome the limitations in mouse models and represent an alternative way for studying cancer metastasis of human cancers (Marques et al., 2009, Stoletov and Klemke, 2008, Santhakumar et al., 2012). These models allow investigating metastasis in short period, 48-120 hours, compared to mice models which require six months (Teng et al., 2013). The smaller size of zebrafish and cost-effectiveness allows investigating the effects on metastasis in large cohorts of fish in short period of time, therefore, allowing the robust statistical analysis of these effects. Furthermore, the lack of adaptive immune system in zebrafish larvae as they do not develop adaptive immune system until 14 days post-fertilisation allow the growth and survival of human cancer cells in these larvae without the requirement to supress their immune system that could cause side effects in hosts (Traver et al., 2003).

Another possible research line that could follow the finding in this project is evaluating the effects of K80R mutated vinculin on different functions of FAs. Since FAs transmit traction forces between cytoskeleton and ECM (Tan et al., 2003), the impact of the K80R mutation in

vinculin on the ability of FAs to transmit traction force could be investigated. Polyacrylamide-Traction Force Microscopy (PA-TFM) is common approach to study traction force that can be generated upon adhesion attachment to a substrate (Au - Jerrell and Au - Parekh, 2015). Three-Dimensional Traction Force Quantification (3D-TFM) is another technique that uses 3D matrixes such as agarose, collagen or Matrigel to study cell contractility during migration (Legant et al., 2010). In addition, there are techniques that can measure cell's adhesion strength, which refers to the required force to detach cells from matrixes, including cytodetachment and micropipette aspiration. Single cell force spectroscopy (SCFS) technique could be used to measure the required force for breaking molecular bonds to understand cell adhesion kinetics. Centrifugation Assay is one of the widely used approaches to measure cell adhesion strength. Cells are plated in multiwell plate and centrifuging is used to detach cells. To evaluate adhesion strength, the number of cells before and after centrifuging is quantified by using automated fluorescence analysis (Giacomello et al., 1999). These techniques could be used to evaluate the effects of the K80R mutated vinculin on attachment and detachment of FAs to different matrixes.

Investigating these future research suggestions together with the suggested future works in general discussion is of great importance to further demonstrate the involvement of SUMOylation in cancer progression and metastasis. It will also provide a far more complete understanding of the detailed regulatory roles of SUMOylation in deriving these processes. This could also lead to the identification of promising therapeutic targets and/or the development of anticancer molecules.

7. References

ADAMS, J. M. & CORY, S. 2007. The Bcl-2 apoptotic switch in cancer development and therapy. *Oncogene,* 26**,** 1324-1337.

ADLER, A. S., LIN, M., HORLINGS, H., NUYTEN, D. S. A., VAN DE VIJVER, M. J. & CHANG, H. Y. 2006. Genetic regulators of large-scale transcriptional signatures in cancer. *Nature genetics,* 38**,** 421-430.

ALEXANDER, S., KOEHL, G. E., HIRSCHBERG, M., GEISSLER, E. K. & FRIEDL, P. 2008. Dynamic imaging of cancer growth and invasion: a modified skin-fold chamber model. *Histochem Cell Biol,* 130**,** 1147-54.

AHLEMEYER, B., SELKE, D., SCHAPER, C., KLUMPP, S. & KRIEGLSTEIN, J. 2001. Ginkgolic acids induce neuronal death and activate protein phosphatase type-2C. *European Journal of Pharmacology,* 430**,** 1-7.

ALONSO, A., D'SILVA, S., RAHMAN, M., MELUH, P. B., KEELING, J., MEEDNU, N., HOOPS, H. J. & MILLER, R. K. 2012. The yeast homologue of the microtubule-associated protein Lis1 interacts with the sumoylation machinery and a SUMO-targeted ubiquitin ligase. *Molecular Biology of the Cell,* 23**,** 4552-4566.

ALONSO, A., GREENLEE, M., MATTS, J., KLINE, J., DAVIS, K. J. & MILLER, R. K. 2015. Emerging roles of sumoylation in the regulation of actin, microtubules, intermediate filaments, and septins. *Cytoskeleton,* 72**,** 305-339.

AMENTE, S., LAVADERA, M. L., PALO, G. D. & MAJELLO, B. 2012. SUMO-activating SAE1 transcription is positively regulated by Myc. *American journal of cancer research,* 2**,** 330-334.

ANDERS, C., NIEWOEHNER, O., DUERST, A. & JINEK, M. 2014. Structural basis of PAM-dependent target DNA recognition by the Cas9 endonuclease. *Nature,* 513**,** 569-573.

ATHERTON, P., LAUSECKER, F., CARISEY, A., GILMORE, A., CRITCHLEY, D., BARSUKOV, I. & BALLESTREM, C. 2019. Force-independent interactions of talin and vinculin govern integrin-mediated mechanotransduction. *bioRxiv***,** 629683.

AU - JERRELL, R. J. & AU - PAREKH, A. 2015. Polyacrylamide Gels for Invadopodia and Traction Force Assays on Cancer Cells. *JoVE***,** e52343.

AVILA, J. R., LEE, J. S. & TORII, K. U. 2015. Co-Immunoprecipitation of Membrane-Bound Receptors. *The arabidopsis book,* 13**,** e0180-e0180.

BABA, D., MAITA, N., JEE, J.-G., UCHIMURA, Y., SAITOH, H., SUGASAWA, K., HANAOKA, F., TOCHIO, H., HIROAKI, H. & SHIRAKAWA, M. 2005. Crystal structure of thymine DNA glycosylase conjugated to SUMO-1. *Nature,* 435**,** 979-982.

BAE, S. H., JEONG, J. W., PARK, J. A., KIM, S. H., BAE, M. K., CHOI, S. J. & KIM, K. W. 2004. Sumoylation increases HIF-1alpha stability and its transcriptional activity. *Biochem Biophys Res Commun,* 324**,** 394-400.

BAERISWYL, V. & CHRISTOFORI, G. 2009. The angiogenic switch in carcinogenesis. *Seminars in Cancer Biology,* 19**,** 329-337.

BAILEY, D. & O'HARE, P. 2004. Characterization of the Localization and Proteolytic Activity of the SUMO-specific Protease, SENP1. *Journal of Biological Chemistry,* 279**,** 692-703.

BAKOLITSA, C., COHEN, D. M., BANKSTON, L. A., BOBKOV, A. A., CADWELL, G. W., JENNINGS, L., CRITCHLEY, D. R., CRAIG, S. W. & LIDDINGTON, R. C. 2004. Structural basis for vinculin activation at sites of cell adhesion. *Nature,* 430**,** 583-586.

BALASUBRAMANYAM, K., SWAMINATHAN, V., RANGANATHAN, A. & KUNDU, T. K. 2003. Small Molecule Modulators of Histone Acetyltransferase p300. *Journal of Biological Chemistry,* 278**,** 19134-19140.

BAWA-KHALFE, T. & YEH, E. T. 2010. SUMO Losing Balance: SUMO Proteases Disrupt SUMO Homeostasis to Facilitate Cancer Development and Progression. *Genes Cancer,* 1**,** 748-752.

BEAUCLAIR, G., BRIDIER-NAHMIAS, A., ZAGURY, J.-F., SAÏB, A. & ZAMBORLINI, A. 2015. JASSA: a comprehensive tool for prediction of SUMOylation sites and SIMs. *Bioinformatics,* 31**,** 3483-3491.

BELLAIL, A. C., OLSON, J. J. & HAO, C. 2014. SUMO1 modification stabilizes CDK6 protein and drives the cell cycle and glioblastoma progression. *Nature Communications,* 5**,** 4234.

BELLIS, S. L., MILLER, J. T. & TURNER, C. E. 1995. Characterization of Tyrosine Phosphorylation of Paxillin in Vitro by Focal Adhesion Kinase. *Journal of Biological Chemistry,* 270**,** 17437-17441.

BERNIER-VILLAMOR, V., SAMPSON, D. A., MATUNIS, M. J. & LIMA, C. D. 2002. Structural Basis for E2-Mediated SUMO Conjugation Revealed by a Complex between Ubiquitin-Conjugating Enzyme Ubc9 and RanGAP1. *Cell,* 108**,** 345-356.

BERNSTOCK, J. D., YANG, W., YE, D. G., SHEN, Y., PLUCHINO, S., LEE, Y.-J., HALLENBECK, J. M. & PASCHEN, W. 2018. SUMOylation in brain ischemia: Patterns, targets, and translational implications. *Journal of cerebral blood flow and metabolism : official journal of the International Society of Cerebral Blood Flow and Metabolism,* 38**,** 5-16.

BERTA, M. A., MAZURE, N., HATTAB, M., POUYSSEGUR, J. & BRAHIMI-HORN, M. C. 2007. SUMOylation of hypoxia-inducible factor-1alpha reduces its transcriptional activity. *Biochem Biophys Res Commun,* 360**,** 646-52.

BETTERMANN, K., BENESCH, M., WEIS, S. & HAYBAECK, J. 2012. SUMOylation in carcinogenesis. *Cancer Lett,* 316**,** 113-25.

BLASCO, M. A. 2005. Telomeres and human disease: ageing, cancer and beyond. *Nature Reviews Genetics,* 6**,** 611-622.

BALLESTREM, C., EREZ, N., KIRCHNER, J., KAM, Z., BERSHADSKY, A. & GEIGER, B. 2006. Molecular mapping of tyrosine-phosphorylated proteins in focal adhesions using fluorescence resonance energy transfer. *Journal of Cell Science,* 119**,** 866-875.

BODDY, M. N., HOWE, K., ETKIN, L. D., SOLOMON, E. & FREEMONT, P. S. 1996. PIC 1, a novel ubiquitin-like protein which interacts with the PML component of a multiprotein complex that is disrupted in acute promyelocytic leukaemia. *Oncogene,* 13**,** 971-82.

BOIS, P. R., BORGON, R. A., VONRHEIN, C. & IZARD, T. 2005. Structural dynamics of alpha-actinin-vinculin interactions. *Mol Cell Biol,* 25**,** 6112-22.

BOIS, P. R., O'HARA, B. P., NIETLISPACH, D., KIRKPATRICK, J. & IZARD, T. 2006. The vinculin binding sites of talin and alpha-actinin are sufficient to activate vinculin. *J Biol Chem,* 281**,** 7228-36.

BORREGO-DIAZ, E., KERFF, F., LEE, S. H., FERRON, F., LI, Y. & DOMINGUEZ, R. 2006. Crystal structure of the actin-binding domain of α-actinin 1: Evaluating two competing actin-binding models. *Journal of Structural Biology,* 155**,** 230-238.

BRANDT, M., SZEWCZUK, L. M., ZHANG, H., HONG, X., MCCORMICK, P. M., LEWIS, T. S., GRAHAM, T. I., HUNG, S. T., HARPER-JONES, A. D., KERRIGAN, J. J., WANG, D. Y., DUL, E., HOU, W., HO, T. F., MEEK, T. D., CHEUNG, M. H., JOHANSON, K. O., JONES, C. S., SCHWARTZ, B., KUMAR, S., OLIFF, A. I. & KIRKPATRICK, R. B. 2013. Development of a high-throughput screen to detect inhibitors of TRPS1 sumoylation. *Assay Drug Dev Technol,* 11**,** 308-25.

BRAY, F., FERLAY, J., SOERJOMATARAM, I., SIEGEL, R. L., TORRE, L. A. & JEMAL, A. 2018. Global cancer statistics 2018: GLOBOCAN estimates of incidence and mortality worldwide for 36 cancers in 185 countries. *CA: A Cancer Journal for Clinicians,* 68**,** 394-424.

BRAZIL, D. P., PARK, J. & HEMMINGS, B. A. 2002. PKB binding proteins. Getting in on the Akt. *Cell,* 111**,** 293-303.

BRUDERER, R., TATHAM, M. H., PLECHANOVOVA, A., MATIC, I., GARG, A. K. & HAY, R. T. 2011. Purification and identification of endogenous polySUMO conjugates. *EMBO Rep,* 12**,** 142-8.

BROUSSARD, J. A., WEBB, D. J. & KAVERINA, I. 2008. Asymmetric focal adhesion disassembly in motile cells. *Current Opinion in Cell Biology,* 20**,** 85-90.

BURKHART, D. L. & SAGE, J. 2008. Cellular mechanisms of tumour suppression by the retinoblastoma gene. *Nature Reviews Cancer,* 8**,** 671-682.

BURRIDGE, K. & WENNERBERG, K. 2004. Rho and Rac take center stage. *Cell,* 116**,** 167-79.

CALALB, M. B., POLTE, T. R. & HANKS, S. K. 1995. Tyrosine phosphorylation of focal adhesion kinase at sites in the catalytic domain regulates kinase activity: a role for Src family kinases. *Molecular and Cellular Biology,* 15**,** 954-963.

CAPPADOCIA, L., MASCLE, XAVIER H., BOURDEAU, V., TREMBLAY-BELZILE, S., CHAKER-MARGOT, M., LUSSIER-PRICE, M., WADA, J., SAKAGUCHI, K., AUBRY, M., FERBEYRE, G. & OMICHINSKI, JAMES G. 2015. Structural and Functional Characterization of the Phosphorylation-Dependent Interaction between PML and SUMO1. *Structure,* 23**,** 126-138.

CARBIA-NAGASHIMA, A., GEREZ, J., PEREZ-CASTRO, C., PAEZ-PEREDA, M., SILBERSTEIN, S., STALLA, G. K., HOLSBOER, F. & ARZT, E. 2007. RSUME, a small RWD-containing protein, enhances SUMO conjugation and stabilizes HIF-1alpha during hypoxia. *Cell,* 131**,** 309-23.

CARISEY, A., TSANG, R., GREINER, A. M., NIJENHUIS, N., HEATH, N., NAZGIEWICZ, A., KEMKEMER, R., DERBY, B., SPATZ, J. & BALLESTREM, C. 2013. Vinculin regulates the recruitment and release of core focal adhesion proteins in a force-dependent manner. *Curr Biol,* 23**,** 271-81.

CASE, L. B., BAIRD, M. A., SHTENGEL, G., CAMPBELL, S. L., HESS, H. F., DAVIDSON, M. W. & WATERMAN, C. M. 2015. Molecular mechanism of vinculin activation and nanoscale spatial organization in focal adhesions. *Nat Cell Biol,* 17**,** 880-92.

CASHMAN, R., COHEN, H., BEN-HAMO, R., ZILBERBERG, A. & EFRONI, S. 2014. SENP5 mediates breast cancer invasion via a TGFbetaRI SUMOylation cascade. *Oncotarget,* 5**,** 1071-82.

CASTILLO-LLUVA, S., TATHAM, M. H., JONES, R. C., JAFFRAY, E. G., EDMONDSON, R. D., HAY, R. T. & MALLIRI, A. 2010. SUMOylation of the GTPase Rac1 is required for optimal cell migration. *Nat Cell Biol,* 12**,** 1078-1085.

CHAN, K. T., BENNIN, D. A. & HUTTENLOCHER, A. 2010. Regulation of adhesion dynamics by calpain-mediated proteolysis of focal adhesion kinase (FAK). *J Biol Chem,* 285**,** 11418-26.

CHANG, C.-C., NAIK, MANDAR T., HUANG, Y.-S., JENG, J.-C., LIAO, P.-H., KUO, H.-Y., HO, C.-C., HSIEH, Y.-L., LIN, C.-H., HUANG, N.-J., NAIK, NANDITA M., KUNG, CAMY C. H., LIN, S.-Y., CHEN, R.-H., CHANG, K.-S., HUANG, T.-H. & SHIH, H.-M. 2011. Structural and Functional Roles of Daxx SIM Phosphorylation in SUMO Paralog-Selective Binding and Apoptosis Modulation. *Molecular Cell,* 42**,** 62-74.

CHARRAS, G. & PALUCH, E. 2008. Blebs lead the way: how to migrate without lamellipodia. *Nat Rev Mol Cell Biol,* 9**,** 730-736.

CHEN, S.-F., GONG, C., LUO, M., YAO, H.-R., ZENG, Y.-J. & SU, F.-X. 2011. Ubc9 expression predicts chemoresistance in breast cancer. *Chinese journal of cancer,* 30**,** 638-644.

CHENG, J., KANG, X., ZHANG, S. & YEH, E. T. 2007. SUMO-specific protease 1 is essential for stabilization of HIF1alpha during hypoxia. *Cell,* 131**,** 584-95.

CHENG, J., WANG, D., WANG, Z. & YEH, E. T. H. 2004. SENP1 Enhances Androgen Receptor-Dependent Transcription through Desumoylation of Histone Deacetylase 1. *Molecular and Cellular Biology,* 24**,** 6021-6028.

CHENG, N., CHYTIL, A., SHYR, Y., JOLY, A. & MOSES, H. L. 2008. Transforming Growth Factor-β Signaling–Deficient Fibroblasts Enhance Hepatocyte Growth Factor Signaling in Mammary Carcinoma Cells to Promote Scattering and Invasion. *Molecular Cancer Research,* 6**,** 1521-1533.

CHIU, S.-Y., ASAI, N., COSTANTINI, F. & HSU, W. 2008. SUMO-Specific Protease 2 Is Essential for Modulating p53-Mdm2 in Development of Trophoblast Stem Cell Niches and Lineages. *PLoS Biology,* 6**,** e310.

CHOREV, D. S., VOLBERG, T., LIVNE, A., EISENSTEIN, M., MARTINS, B., KAM, Z., JOCKUSCH, B. M., MEDALIA, O., SHARON, M. & GEIGER, B. 2018. Conformational states during

vinculin unlocking differentially regulate focal adhesion properties. *Scientific Reports,* 8**,** 2693.

CHUPRETA, S., HOLMSTROM, S., SUBRAMANIAN, L. & IÑIGUEZ-LLUHÍ, J. A. 2005. A Small Conserved Surface in SUMO Is the Critical Structural Determinant of Its Transcriptional Inhibitory Properties. *Molecular and Cellular Biology,* 25**,** 4272-4282.

CIECHANOVER, A., HELLER, H., ELIAS, S., HAAS, A. L. & HERSHKO, A. 1980. ATP-dependent conjugation of reticulocyte proteins with the polypeptide required for protein degradation. *Proc Natl Acad Sci U S A,* 77**,** 1365-8.

CIEHANOVER, A., HOD, Y. & HERSHKO, A. 1978. A heat-stable polypeptide component of an ATP-dependent proteolytic system from reticulocytes. *Biochemical and Biophysical Research Communications,* 81**,** 1100-1105.

CIOBANASU, C., FAIVRE, B. & LE CLAINCHE, C. 2013. Integrating actin dynamics, mechanotransduction and integrin activation: the multiple functions of actin binding proteins in focal adhesions. *Eur J Cell Biol,* 92**,** 339-48.

CIOBANASU, C., FAIVRE, B. & LE CLAINCHE, C. 2014. Actomyosin-dependent formation of the mechanosensitive talin–vinculin complex reinforces actin anchoring. *Nature Communications,* 5**,** 3095.

COHEN, D. M., KUTSCHER, B., CHEN, H., MURPHY, D. B. & CRAIG, S. W. 2006. A Conformational Switch in Vinculin Drives Formation and Dynamics of a Talin-Vinculin Complex at Focal Adhesions. *Journal of Biological Chemistry,* 281**,** 16006-16015.

COLL, J. L., BEN-ZE'EV, A., EZZELL, R. M., RODRÍGUEZ FERNÁNDEZ, J. L., BARIBAULT, H., OSHIMA, R. G. & ADAMSON, E. D. 1995. Targeted disruption of vinculin genes in F9 and embryonic stem cells changes cell morphology, adhesion, and locomotion. *Proc Natl Acad Sci U S A,* 92**,** 9161-5.

CONDE, C. & CACERES, A. 2009. Microtubule assembly, organization and dynamics in axons and dendrites. *Nat Rev Neurosci,* 10**,** 319-332.

CONG, L., RAN, F. A., COX, D., LIN, S., BARRETTO, R., HABIB, N., HSU, P. D., WU, X., JIANG, W., MARRAFFINI, L. A. & ZHANG, F. 2013. Multiplex genome engineering using CRISPR/Cas systems. *Science (New York, N.Y.),* 339**,** 819-823.

CONSTANZO, J. D., TANG, K.-J., RINDHE, S., MELEGARI, M., LIU, H., TANG, X., RODRIGUEZ-CANALES, J., WISTUBA, I. & SCAGLIONI, P. P. 2016. PIAS1-FAK Interaction Promotes the Survival and Progression of Non-Small Cell Lung Cancer. *Neoplasia (New York, N.Y.),* 18**,** 282-293.

CORTESIO, C. L., BOATENG, L. R., PIAZZA, T. M., BENNIN, D. A. & HUTTENLOCHER, A. 2011. Calpain-mediated proteolysis of paxillin negatively regulates focal adhesion dynamics and cell migration. *J Biol Chem,* 286**,** 9998-10006.

DAWLATY, M. M., MALUREANU, L., JEGANATHAN, K. B., KAO, E., SUSTMANN, C., TAHK, S., SHUAI, K., GROSSCHEDL, R. & VAN DEURSEN, J. M. 2008. Resolution of Sister Centromeres Requires RanBP2-Mediated SUMOylation of Topoisomerase IIα. *Cell,* 133**,** 103-115.

DAY, R. N. & DAVIDSON, M. W. 2009. The fluorescent protein palette: tools for cellular imaging. *Chemical Society reviews,* 38**,** 2887-2921.

DERAMAUDT, T. B., DUJARDIN, D., NOULET, F., MARTIN, S., VAUCHELLES, R., TAKEDA, K. & RONDÉ, P. 2014. Altering FAK-paxillin interactions reduces adhesion, migration and invasion processes. *PLoS One,* 9**,** e92059.

DERMARDIROSSIAN, C., ROCKLIN, G., SEO, J.-Y. & BOKOCH, G. M. 2006. Phosphorylation of RhoGDI by Src Regulates Rho GTPase Binding and Cytosol-Membrane Cycling. *Molecular Biology of the Cell,* 17**,** 4760-4768.

DESHAIES, R. J. & JOAZEIRO, C. A. 2009. RING domain E3 ubiquitin ligases. *Annu Rev Biochem,* 78**,** 399-434.

DESTERRO, J. M. P., RODRIGUEZ, M. S. & HAY, R. T. 1998. SUMO-1 Modification of IκBα Inhibits NF-κB Activation. *Molecular Cell,* 2**,** 233-239.

DI BACCO, A., OUYANG, J., LEE, H.-Y., CATIC, A., PLOEGH, H. & GILL, G. 2006. The SUMO-Specific Protease SENP5 Is Required for Cell Division. *Molecular and Cellular Biology,* 26**,** 4489-4498.

DIEZ, G., AUERNHEIMER, V., FABRY, B. & GOLDMANN, W. H. 2011. Head/tail interaction of vinculin influences cell mechanical behavior. *Biochem Biophys Res Commun,* 406**,** 85-8.

DING, K., LU, Y., NIKOLOVSKA-COLESKA, Z., WANG, G., QIU, S., SHANGARY, S., GAO, W., QIN, D., STUCKEY, J., KRAJEWSKI, K., ROLLER, P. P. & WANG, S. 2006. Structure-Based Design of Spiro-oxindoles as Potent, Specific Small-Molecule Inhibitors of the MDM2−p53 Interaction. *Journal of Medicinal Chemistry,* 49**,** 3432-3435.

DONEHOWER, L. A., HARVEY, M., SLAGLE, B. L., MCARTHUR, M. J., MONTGOMERY, C. A., BUTEL, J. S. & BRADLEY, A. 1992. Mice deficient for p53 are developmentally normal but susceptible to spontaneous tumours. *Nature,* 356**,** 215-221.

DOORNEBAL, C. W., KLARENBEEK, S., BRAUMULLER, T. M., KLIJN, C. N., CIAMPRICOTTI, M., HAU, C.-S., HOLLMANN, M. W., JONKERS, J. & DE VISSER, K. E. 2013. A Preclinical Mouse Model of Invasive Lobular Breast Cancer Metastasis. *Cancer Research,* 73**,** 353-363.

DOVAS, A. & COUCHMAN, JOHN R. 2005. RhoGDI: multiple functions in the regulation of Rho family GTPase activities. *Biochemical Journal,* 390**,** 1-9.

DRAG, M., MIKOLAJCZYK, J., KRISHNAKUMAR, I. M., HUANG, Z. & SALVESEN, G. S. 2008. Activity profiling of human deSUMOylating enzymes (SENPs) with synthetic substrates suggests an unexpected specificity of two newly characterized members of the family. *Biochem J,* 409**,** 461-9.

DROESCHER, M., CHAUGULE, V. K. & PICHLER, A. 2013. SUMO Rules: Regulatory Concepts and Their Implication in Neurologic Functions. *NeuroMolecular Medicine,* 15**,** 639-660.

DUAN, J., LU, G., XIE, Z., LOU, M., LUO, J., GUO, L. & ZHANG, Y. 2014. Genome-wide identification of CRISPR/Cas9 off-targets in human genome. *Cell research,* 24**,** 1009-1012.

DUNWELL, T. L., MCGUFFIN, L. J., DUNWELL, J. M. & PFEIFER, G. P. 2013. The mysterious presence of a 5-methylcytosine oxidase in the Drosophila genome: possible explanations. *Cell cycle (Georgetown, Tex.),* 12**,** 3357-3365.

EIFLER, K. & VERTEGAAL, A. C. O. 2015. SUMOylation-Mediated Regulation of Cell Cycle Progression and Cancer. *Trends in biochemical sciences,* 40**,** 779-793.

ELOFSSON, A., JOO, K., KEASAR, C. & LEE, J. 2018. Methods for estimation of model accuracy in CASP12. 86 Suppl 1**,** 361-373.

ERIKSSON, J. E., DECHAT, T., GRIN, B., HELFAND, B., MENDEZ, M., PALLARI, H.-M. & GOLDMAN, R. D. 2009. Introducing intermediate filaments: from discovery to disease. *The Journal of Clinical Investigation,* 119**,** 1763-1771.

EVDOKIMOV, E., SHARMA, P., LOCKETT, S. J., LUALDI, M. & KUEHN, M. R. 2008. Loss of SUMO1 in mice affects RanGAP1 localization and formation of PML nuclear bodies, but is not lethal as it can be compensated by SUMO2 or SUMO3. *Journal of Cell Science,* 121**,** 4106-4113.

EZRATTY, E. J., PARTRIDGE, M. A. & GUNDERSEN, G. G. 2005. Microtubule-induced focal adhesion disassembly is mediated by dynamin and focal adhesion kinase. *Nat Cell Biol,* 7**,** 581-590.

FACKLER, O. T. & GROSSE, R. 2008. Cell motility through plasma membrane blebbing. *The Journal of Cell Biology,* 181**,** 879-884.

FANG, S., QIU, J., WU, Z., BAI, T. & GUO, W. 2017. Down-regulation of UBC9 increases the sensitivity of hepatocellular carcinoma to doxorubicin. *Oncotarget,* 8**,** 49783-49795.

FEKI, A. & IRMINGER-FINGER, I. 2004. Mutational spectrum of p53 mutations in primary breast and ovarian tumors. *Critical Reviews in Oncology/Hematology,* 52**,** 103-116.

FELIX, R. S., COLLEONI, G. W. B., CABALLERO, O. L., YAMAMOTO, M., ALMEIDA, M. S. S., ANDRADE, V. C. C., CHAUFFAILLE, M. D. L. L. F., SILVA, W. A. D., BEGNAMI, M. D., SOARES, F. A., SIMPSON, A. J., ZAGO, M. A. & VETTORE, A. L. 2009. SAGE analysis highlights the importance of p53csv, ddx5, mapkapk2 and ranbp2 to multiple myeloma tumorigenesis. *Cancer Letters,* 278**,** 41-48.

FERLAY, J., SOERJOMATARAM, I., DIKSHIT, R., ESER, S., MATHERS, C., REBELO, M., PARKIN, D. M., FORMAN, D. & BRAY, F. 2015. Cancer incidence and mortality worldwide: Sources, methods and major patterns in GLOBOCAN 2012. *International Journal of Cancer,* 136**,** E359-E386.

FIDLER, I. J. 2003. The pathogenesis of cancer metastasis: the 'seed and soil' hypothesis revisited. *Nature Reviews Cancer,* 3**,** 453-458.

FLOTHO, A. & MELCHIOR, F. 2013. Sumoylation: a regulatory protein modification in health and disease. *Annu Rev Biochem,* 82**,** 357-85.

FRANCO, S. J., RODGERS, M. A., PERRIN, B. J., HAN, J., BENNIN, D. A., CRITCHLEY, D. R. & HUTTENLOCHER, A. 2004. Calpain-mediated proteolysis of talin regulates adhesion dynamics. *Nat Cell Biol,* 6**,** 977-83.

FRANKE, W. W., SCHMID, E., OSBORN, M. & WEBER, K. 1978. Different intermediate-sized filaments distinguished by immunofluorescence microscopy. *Proceedings of the National Academy of Sciences of the United States of America,* 75**,** 5034-5038.

FRIEDL, P. & ALEXANDER, S. 2011. Cancer Invasion and the Microenvironment: Plasticity and Reciprocity. *Cell,* 147**,** 992-1009.

FRIEDL, P., BORGMANN, S. & BRÖCKER, E.-B. 2001. Amoeboid leukocyte crawling through extracellular matrix: lessons from the Dictyostelium paradigm of cell movement. *Journal of leukocyte biology,* 70**,** 491-509.

FRIEDL, P. & WEIGELIN, B. 2008. Interstitial leukocyte migration and immune function. *Nat Immunol,* 9**,** 960-9.

FRIEDL, P. & WOLF, K. 2010. Plasticity of cell migration: a multiscale tuning model. *J Cell Biol,* 188**,** 11-9.

FUCHS, E. 1995. Keratins and the Skin. *Annual Review of Cell and Developmental Biology,* 11**,** 123-154.

FUKUDA, I., ITO, A., HIRAI, G., NISHIMURA, S., KAWASAKI, H., SAITOH, H., KIMURA, K.-I., SODEOKA, M. & YOSHIDA, M. 2009a. Ginkgolic Acid Inhibits Protein SUMOylation by Blocking Formation of the E1-SUMO Intermediate. *Chemistry & Biology,* 16**,** 133-140.

FUKUDA, I., ITO, A., URAMOTO, M., SAITOH, H., KAWASAKI, H., OSADA, H. & YOSHIDA, M. 2009b. Kerriamycin B inhibits protein SUMOylation. *The Journal of Antibiotics,* 62**,** 221-224.

FULLER, STEPHEN J., MCGUFFIN, LIAM J., MARSHALL, ANDREW K., GIRALDO, A., PIKKARAINEN, S., CLERK, A. & SUGDEN, PETER H. 2012. A novel non-canonical mechanism of regulation of MST3 (mammalian Sterile20-related kinase 3). *Biochemical Journal,* 442**,** 595-610.

GADEA, G., SANZ-MORENO, V., SELF, A., GODI, A. & MARSHALL, C. J. 2008. DOCK10-Mediated Cdc42 Activation Is Necessary for Amoeboid Invasion of Melanoma Cells. *Current Biology,* 18**,** 1456-1465.

GAL, A., SJOBLOM, T., FEDOROVA, L., IMREH, S., BEUG, H. & MOUSTAKAS, A. 2008. Sustained TGF beta exposure suppresses Smad and non-Smad signalling in mammary epithelial cells, leading to EMT and inhibition of growth arrest and apoptosis. *Oncogene,* 27**,** 1218-30.

GAO, C., HO, C.-C., REINEKE, E., LAM, M., CHENG, X., STANYA, K. J., LIU, Y., CHAKRABORTY, S., SHIH, H.-M. & KAO, H.-Y. 2008. Histone Deacetylase 7 Promotes PML Sumoylation and Is Essential for PML Nuclear Body Formation. *Molecular and Cellular Biology,* 28**,** 5658-5667.

GAREAU, J. R. & LIMA, C. D. 2010. The SUMO pathway: emerging mechanisms that shape specificity, conjugation and recognition. *Nature reviews. Molecular cell biology,* 11**,** 861-871.

GEIGER, B. & YAMADA, K. M. 2011. Molecular Architecture and Function of Matrix Adhesions. *Cold Spring Harbor Perspectives in Biology,* 3.

GEISS-FRIEDLANDER, R. & MELCHIOR, F. 2007. Concepts in sumoylation: a decade on. *Nat Rev Mol Cell Biol,* 8**,** 947-56.

GIANNONI, E., BIANCHINI, F., CALORINI, L. & CHIARUGI, P. 2011. Cancer associated fibroblasts exploit reactive oxygen species through a proinflammatory signature leading to epithelial mesenchymal transition and stemness. *Antioxid Redox Signal,* 14**,** 2361-71.

GIACOMELLO, E., NEUMAYER, J., COLOMBATTI, A. P. R. & PERRIS, R. 1999. Centrifugal Assay for Fluorescence-Based Cell Adhesion Adapted to the Analysis of Ex Vivo Cells and Capable of Determining Relative Binding Strengths. *BioTechniques,* 26**,** 758-62, 764.

GOLEBIOWSKI, F., MATIC, I., TATHAM, M. H., COLE, C., YIN, Y., NAKAMURA, A., COX, J., BARTON, G. J., MANN, M. & HAY, R. T. 2009. System-wide changes to SUMO modifications in response to heat shock. *Sci Signal,* 2**,** ra24.

GOLEY, E. D. & WELCH, M. D. 2006. The ARP2/3 complex: an actin nucleator comes of age. *Nat Rev Mol Cell Biol,* 7**,** 713-726.

GÓMEZ-CUADRADO, L., TRACEY, N., MA, R., QIAN, B. & BRUNTON, V. G. 2017. Mouse models of metastasis: progress and prospects. *Disease models & mechanisms,* 10**,** 1061-1074.

GONG, L., MILLAS, S., MAUL, G. G. & YEH, E. T. H. 2000. Differential Regulation of Sentrinized Proteins by a Novel Sentrin-specific Protease. *Journal of Biological Chemistry,* 275**,** 3355-3359.

GRÉGOIRE, S. & YANG, X.-J. 2005. Association with Class IIa Histone Deacetylases Upregulates the Sumoylation of MEF2 Transcription Factors. *Molecular and Cellular Biology,* 25**,** 2273-2287.

GRINNELL, F. 2003. Fibroblast biology in three-dimensional collagen matrices. *Trends Cell Biol,* 13**,** 264-9.

GUERVILLY, J.-H., TAKEDACHI, A., NAIM, V., SCAGLIONE, S., CHAWHAN, C., LOVERA, Y., DESPRAS, E., KURAOKA, I., KANNOUCHE, P., ROSSELLI, F. & GAILLARD, P.-HENRI L. 2015. The SLX4 Complex Is a SUMO E3 Ligase that Impacts on Replication Stress Outcome and Genome Stability. *Molecular Cell,* 57**,** 123-137.

GUMBINER, B. M. 1996. Cell adhesion: the molecular basis of tissue architecture and morphogenesis. *Cell,* 84**,** 345-57.

GUO, L., GIASSON, B. I., GLAVIS-BLOOM, A., BREWER, M. D., SHORTER, J., GITLER, A. D. & YANG, X. 2014. A cellular system that degrades misfolded proteins and protects against neurodegeneration. *Molecular cell,* 55**,** 15-30.

GUPTA, G. P. & MASSAGUÉ, J. 2006. Cancer Metastasis: Building a Framework. *Cell,* 127**,** 679-695.

HAAS, J., BARBATO, A., BEHRINGER, D., STUDER, G., ROTH, S., BERTONI, M., MOSTAGUIR, K., GUMIENNY, R. & SCHWEDE, T. 2018. Continuous Automated Model EvaluatiOn (CAMEO) complementing the critical assessment of structure prediction in CASP12. *Proteins,* 86 Suppl 1**,** 387-398.

HAMADI, A., BOUALI, M., DONTENWILL, M., STOECKEL, H., TAKEDA, K. & RONDÉ, P. 2005. Regulation of focal adhesion dynamics and disassembly by phosphorylation of FAK at tyrosine 397. *Journal of Cell Science,* 118**,** 4415-4425.

HAMDOUN, S. & EFFERTH, T. 2017. Ginkgolic acids inhibit migration in breast cancer cells by inhibition of NEMO sumoylation and NF-κB activity. *Oncotarget,* 8**,** 35103-35115.

HAN, Y., HUANG, C., SUN, X., XIANG, B., WANG, M., YEH, E. T. H., CHEN, Y., LI, H., SHI, G., CANG, H., SUN, Y., WANG, J., WANG, W., GAO, F. & YI, J. 2010. SENP3-mediated De-conjugation of SUMO2/3 from Promyelocytic Leukemia Is Correlated with Accelerated Cell Proliferation under Mild Oxidative Stress. *Journal of Biological Chemistry,* 285**,** 12906-12915.

HANAHAN, D. & WEINBERG, R. A. 2000. The Hallmarks of Cancer. *Cell,* 100**,** 57-70.

HANAHAN, D. & WEINBERG, ROBERT A. 2011. Hallmarks of Cancer: The Next Generation. *Cell,* 144**,** 646-674.

HANNICH, J. T., LEWIS, A., KROETZ, M. B., LI, S.-J., HEIDE, H., EMILI, A. & HOCHSTRASSER, M. 2005. Defining the SUMO-modified Proteome by Multiple Approaches in Saccharomyces cerevisiae. *Journal of Biological Chemistry,* 280**,** 4102-4110.

HANNUS, M., BEITZINGER, M., ENGELMANN, J. C., WEICKERT, M.-T., SPANG, R., HANNUS, S. & MEISTER, G. 2014. siPools: highly complex but accurately defined siRNA pools eliminate off-target effects. *Nucleic acids research,* 42**,** 8049-8061.

HE, X., RICEBERG, J., SOUCY, T., KOENIG, E., MINISSALE, J., GALLERY, M., BERNARD, H., YANG, X., LIAO, H., RABINO, C., SHAH, P., XEGA, K., YAN, Z.-H., SINTCHAK, M., BRADLEY, J., XU, H., DUFFEY, M., ENGLAND, D., MIZUTANI, H., HU, Z., GUO, J., CHAU, R., DICK, L. R., BROWNELL, J. E., NEWCOMB, J., LANGSTON, S., LIGHTCAP, E. S., BENCE, N. & PULUKURI, S. M. 2017. Probing the roles of SUMOylation in cancer cell biology by using a selective SAE inhibitor. *Nature Chemical Biology,* 13**,** 1164-1171.

HECKER, C.-M., RABILLER, M., HAGLUND, K., BAYER, P. & DIKIC, I. 2006. Specification of SUMO1- and SUMO2-interacting Motifs. *Journal of Biological Chemistry,* 281**,** 16117-16127.

HECKER, A., WALLMEROTH, N., PETER, S., BLATT, M. R., HARTER, K. & GREFEN, C. 2015. Binary 2in1 Vectors Improve in Planta (Co)localization and Dynamic Protein Interaction Studies. *Plant Physiology,* 168**,** 776-787.

HEGERFELDT, Y., TUSCH, M., BROCKER, E. B. & FRIEDL, P. 2002. Collective cell movement in primary melanoma explants: plasticity of cell-cell interaction, beta1-integrin function, and migration strategies. *Cancer Res,* 62**,** 2125-30.

HENDRIKS, I. A., D'SOUZA, R. C., YANG, B., VERLAAN-DE VRIES, M., MANN, M. & VERTEGAAL, A. C. 2014. Uncovering global SUMOylation signaling networks in a site-specific manner. *Nat Struct Mol Biol,* 21**,** 927-36.

HENDRIKS, I. A. & VERTEGAAL, A. C. 2016. A comprehensive compilation of SUMO proteomics. *Nat Rev Mol Cell Biol,* 17**,** 581-95.

HICKEY, C. M., WILSON, N. R. & HOCHSTRASSER, M. 2012. Function and regulation of SUMO proteases. *Nat Rev Mol Cell Biol,* 13**,** 755-66.

HIETAKANGAS, V., ANCKAR, J., BLOMSTER, H. A., FUJIMOTO, M., PALVIMO, J. J., NAKAI, A. & SISTONEN, L. 2006. PDSM, a motif for phosphorylation-dependent SUMO modification. *Proceedings of the National Academy of Sciences of the United States of America,* 103**,** 45-50.

HIROHAMA, M., KUMAR, A., FUKUDA, I., MATSUOKA, S., IGARASHI, Y., SAITOH, H., TAKAGI, M., SHIN-YA, K., HONDA, K., KONDOH, Y., SAITO, T., NAKAO, Y., OSADA, H., ZHANG, K. Y. J., YOSHIDA, M. & ITO, A. 2013. Spectomycin B1 as a Novel SUMOylation Inhibitor That Directly Binds to SUMO E2. *ACS Chemical Biology,* 8**,** 2635-2642.

HIROKAWA, N., NODA, Y., TANAKA, Y. & NIWA, S. 2009. Kinesin superfamily motor proteins and intracellular transport. *Nat Rev Mol Cell Biol,* 10**,** 682-96.

HOARD, T., YANG, X., JETTEN, A. & ZERUTH, G. 2018. PIAS-family proteins negatively regulate Glis3 transactivation function through SUMO modification in pancreatic β cells. *Heliyon,* 4**,** e00709.

HOFMANN, W. A., ARDUINI, A., NICOL, S. M., CAMACHO, C. J., LESSARD, J. L., FULLER-PACE, F. V. & DE LANEROLLE, P. 2009. SUMOylation of nuclear actin. *The Journal of Cell Biology,* 186**,** 193-200.

HOFFMANN, B. & SCHÄFER, C. 2010. Filopodial focal complexes direct adhesion and force generation towards filopodia outgrowth. *Cell Adh Migr,* 4**,** 190-3.

HOLLIER, B. G., TINNIRELLO, A. A., WERDEN, S. J., EVANS, K. W., TAUBE, J. H., SARKAR, T. R., SPHYRIS, N., SHARIATI, M., KUMAR, S. V., BATTULA, V. L., HERSCHKOWITZ, J. I., GUERRA, R., CHANG, J. T., MIURA, N., ROSEN, J. M. & MANI, S. A. 2013. FOXC2 expression links epithelial-mesenchymal transition and stem cell properties in breast cancer. *Cancer Res,* 73**,** 1981-92.

HORIO, Y., OSADA, H., SHIMIZU, J., OGAWA, S., HIDA, T. & SEKIDO, Y. 2010. Relationship of mRNA expressions of RanBP2 and topoisomerase II isoforms to cytotoxicity of amrubicin in human lung cancer cell lines. *Cancer Chemotherapy and Pharmacology,* 66**,** 237-243.

HORTON, E. R., BYRON, A., ASKARI, J. A., NG, D. H. J., MILLON-FRÉMILLON, A., ROBERTSON, J., KOPER, E. J., PAUL, N. R., WARWOOD, S., KNIGHT, D., HUMPHRIES, J. D. & HUMPHRIES, M. J. 2015. Definition of a consensus integrin adhesome and its dynamics during adhesion complex assembly and disassembly. *Nat Cell Biol,* 17**,** 1577-1587.

HSU, P. D., SCOTT, D. A., WEINSTEIN, J. A., RAN, F. A., KONERMANN, S., AGARWALA, V., LI, Y., FINE, E. J., WU, X., SHALEM, O., CRADICK, T. J., MARRAFFINI, L. A., BAO, G. & ZHANG, F. 2013. DNA targeting specificity of RNA-guided Cas9 nucleases. *Nature Biotechnology,* 31**,** 827-832.

HU, Y.-L., LU, S., SZETO, K. W., SUN, J., WANG, Y., LASHERAS, J. C. & CHIEN, S. 2014. FAK and paxillin dynamics at focal adhesions in the protrusions of migrating cells. *Scientific Reports,* 4**,** 6024.

HUANG, Z., BARKER, D., GIBBINS, J. M. & DASH, P. R. 2018. Talin is a substrate for SUMOylation in migrating cancer cells. *Experimental cell research,* 370**,** 417-425.

HUANG, C., HAN, Y., WANG, Y., SUN, X., YAN, S., YEH, E. T. H., CHEN, Y., CANG, H., LI, H., SHI, G., CHENG, J., TANG, X. & YI, J. 2009. SENP3 is responsible for HIF-1 transactivation under mild oxidative stress via p300 de-SUMOylation. *The EMBO Journal,* 28**,** 2748-2762.

HUANG, E. J. & REICHARDT, L. F. 2003. Trk Receptors: Roles in Neuronal Signal Transduction. *Annual Review of Biochemistry,* 72**,** 609-642.

HUANG, W., HE, T., CHAI, C., YANG, Y., ZHENG, Y., ZHOU, P., QIAO, X., ZHANG, B., LIU, Z., WANG, J., SHI, C., LEI, L., GAO, K., LI, H., ZHONG, S., YAO, L., HUANG, M.-E. & LEI, M. 2012. Triptolide inhibits the proliferation of prostate cancer cells and down-regulates SUMO-specific protease 1 expression. *PloS one,* 7**,** e37693-e37693.

HUSNJAK, K., KEITEN-SCHMITZ, J. & MULLER, S. 2016. Identification and Characterization of SUMO-SIM Interactions. *Methods Mol Biol,* 1475**,** 79-98.

ILIC, D., FURUTA, Y., KANAZAWA, S., TAKEDA, N., SOBUE, K., NAKATSUJI, N., NOMURA, S., FUJIMOTO, J., OKADA, M. & YAMAMOTO, T. 1995. Reduced cell motility and enhanced focal adhesion contact formation in cells from FAK-deficient mice. *Nature,* 377**,** 539-44.

INAMURA, K., SHIMOJI, T., NINOMIYA, H., HIRAMATSU, M., OKUI, M., SATOH, Y., OKUMURA, S., NAKAGAWA, K., NODA, T., FUKAYAMA, M. & ISHIKAWA, Y. 2007. A metastatic signature in entire lung adenocarcinomas irrespective of morphological heterogeneity. *Human Pathology,* 38**,** 702-709.

ISHIKAWA-ANKERHOLD, H. C., ANKERHOLD, R. & DRUMMEN, G. P. C. 2012. Advanced fluorescence microscopy techniques--FRAP, FLIP, FLAP, FRET and FLIM. *Molecules (Basel, Switzerland),* 17**,** 4047-4132.

ITAHANA, Y., YEH, E. T. H. & ZHANG, Y. 2006. Nucleocytoplasmic Shuttling Modulates Activity and Ubiquitination-Dependent Turnover of SUMO-Specific Protease 2. *Molecular and Cellular Biology,* 26**,** 4675-4689.

IVANSCHITZ, L., TAKAHASHI, Y., JOLLIVET, F., AYRAULT, O., LE BRAS, M. & DE THÉ, H. 2015. PML IV/ARF interaction enhances p53 SUMO-1 conjugation, activation, and senescence. *Proceedings of the National Academy of Sciences,* 112**,** 14278-14283.

IZARD, T., EVANS, G., BORGON, R. A., RUSH, C. L., BRICOGNE, G. & BOIS, P. R. 2004. Vinculin activation by talin through helical bundle conversion. *Nature,* 427**,** 171-5.

JACKSON, S. P. & DUROCHER, D. 2013. Regulation of DNA damage responses by ubiquitin and SUMO. *Mol Cell,* 49**,** 795-807.

JAIN, D. & COOPER, J. P. 2010. Telomeric Strategies: Means to an End. *Annual Review of Genetics,* 44**,** 243-269.

JANG, D., KWON, H., CHOI, M., LEE, J. & PAK, Y. 2019. Sumoylation of Flotillin-1 promotes EMT in metastatic prostate cancer by suppressing Snail degradation. *Oncogene,* 38**,** 3248-3260.

JIANG, C., MENG, L., YANG, B. & LUO, X. 2019. Application of CRISPR/Cas9 gene editing technique in the study of cancer treatment. *Clinical Genetics,* 0.

JASPERSEN, S. L. & WINEY, M. 2004. THE BUDDING YEAST SPINDLE POLE BODY: Structure, Duplication, and Function. *Annual Review of Cell and Developmental Biology,* 20**,** 1-28.

JIANG, M., CHIU, S. Y. & HSU, W. 2011. SUMO-specific protease 2 in Mdm2-mediated regulation of p53. *Cell Death Differ,* 18**,** 1005-15.

JOHNSON, E. S. & GUPTA, A. A. 2001. An E3-like Factor that Promotes SUMO Conjugation to the Yeast Septins. *Cell,* 106**,** 735-744.

JOOSEN, L., HINK, M. A., GADELLA JR., T. W. J. & GOEDHART, J. 2014. Effect of fixation procedures on the fluorescence lifetimes of Aequorea victoria derived fluorescent proteins. *Journal of Microscopy,* 256**,** 166-176.

KABEER, F., BEVERLY, L. J., DARRASSE-JÈZE, G. & PODSYPANINA, K. 2016. Methods to Study Metastasis in Genetically Modified Mice. *Cold Spring Harbor Protocols,* 2016**,** pdb.top069948.

KABOORD, B. & PERR, M. 2008. Isolation of proteins and protein complexes by immunoprecipitation. *Methods Mol Biol,* 424**,** 349-64.

KADARÉ, G., TOUTANT, M., FORMSTECHER, E., CORVOL, J.-C., CARNAUD, M., BOUTTERIN, M.-C. & GIRAULT, J.-A. 2003. PIAS1-mediated Sumoylation of Focal Adhesion Kinase Activates Its Autophosphorylationn. *Journal of Biological Chemistry,* 278**,** 47434-47440.

KAGEY, M. H., MELHUISH, T. A. & WOTTON, D. 2003. The Polycomb Protein Pc2 Is a SUMO E3. *Cell,* 113**,** 127-137.

KAIKKONEN, S., JAASKELAINEN, T., KARVONEN, U., RYTINKI, M. M., MAKKONEN, H., GIOELI, D., PASCHAL, B. M. & PALVIMO, J. J. 2009. SUMO-specific protease 1 (SENP1) reverses the hormone-augmented SUMOylation of androgen receptor and modulates gene responses in prostate cancer cells. *Mol Endocrinol,* 23**,** 292-307.

KALLURI, R. & WEINBERG, R. A. 2009. The basics of epithelial-mesenchymal transition. *J Clin Invest,* 119**,** 1420-8.

KANCHANAWONG, P., SHTENGEL, G., PASAPERA, A. M., RAMKO, E. B., DAVIDSON, M. W., HESS, H. F. & WATERMAN, C. M. 2010. Nanoscale architecture of integrin-based cell adhesions. *Nature,* 468**,** 580-584.

KAVERINA, I., KRYLYSHKINA, O. & SMALL, J. V. 1999. Microtubule Targeting of Substrate Contacts Promotes Their Relaxation and Dissociation. *The Journal of Cell Biology,* 146**,** 1033-1044.

KELLER, R. 2005. Cell migration during gastrulation. *Curr Opin Cell Biol,* 17**,** 533-41.

KEREN, K., PINCUS, Z., ALLEN, G. M., BARNHART, E. L., MARRIOTT, G., MOGILNER, A. & THERIOT, J. A. 2008. Mechanism of shape determination in motile cells. *Nature,* 453**,** 475-80.

KERSTEN, K., DE VISSER, K. E., VAN MILTENBURG, M. H. & JONKERS, J. 2017. Genetically engineered mouse models in oncology research and cancer medicine. *EMBO molecular medicine,* 9**,** 137-153.

KESSLER, J. D., KAHLE, K. T., SUN, T., MEERBREY, K. L., SCHLABACH, M. R., SCHMITT, E. M., SKINNER, S. O., XU, Q., LI, M. Z., HARTMAN, Z. C., RAO, M., YU, P., DOMINGUEZ-VIDANA, R., LIANG, A. C., SOLIMINI, N. L., BERNARDI, R. J., YU, B., HSU, T., GOLDING, I., LUO, J., OSBORNE, C. K., CREIGHTON, C. J., HILSENBECK, S. G., SCHIFF, R., SHAW, C. A., ELLEDGE, S. J. & WESTBROOK, T. F. 2012. A SUMOylation-dependent transcriptional subprogram is required for Myc-driven tumorigenesis. *Science (New York, N.Y.),* 335**,** 348-353.

KHANNA, C. & HUNTER, K. 2005. Modeling metastasis in vivo. *Carcinogenesis,* 26**,** 513-523.

KHO, C., LEE, A., JEONG, D., OH, J. G., CHAANINE, A. H., KIZANA, E., PARK, W. J. & HAJJAR, R. J. 2011. SUMO1-dependent modulation of SERCA2a in heart failure. *Nature,* 477**,** 601-5.

KIM, K. I., BAEK, S. H., JEON, Y.-J., NISHIMORI, S., SUZUKI, T., UCHIDA, S., SHIMBARA, N., SAITOH, H., TANAKA, K. & CHUNG, C. H. 2000. A New SUMO-1-specific Protease, SUSP1, That Is Highly Expressed in Reproductive Organs. *Journal of Biological Chemistry,* 275**,** 14102-14106.

KIM, Y. S., NAGY, K., KEYSER, S. & SCHNEEKLOTH, J. S., JR. 2013. An electrophoretic mobility shift assay identifies a mechanistically unique inhibitor of protein sumoylation. *Chemistry & biology,* 20**,** 604-613.

KNIPSCHEER, P., FLOTHO, A., KLUG, H., OLSEN, J. V., VAN DIJK, W. J., FISH, A., JOHNSON, E. S., MANN, M., SIXMA, T. K. & PICHLER, A. 2008. Ubc9 sumoylation regulates SUMO target discrimination. *Mol Cell,* 31**,** 371-82.

KORNBERG, L., EARP, H. S., PARSONS, J. T., SCHALLER, M. & JULIANO, R. L. 1992. Cell adhesion or integrin clustering increases phosphorylation of a focal adhesion-associated tyrosine kinase. *J Biol Chem,* 267**,** 23439-42.

KRYLYSHKINA, O., KAVERINA, I., KRANEWITTER, W., STEFFEN, W., ALONSO, M. C., CROSS, R. A. & SMALL, J. V. 2002. Modulation of substrate adhesion dynamics via microtubule targeting requires kinesin-1. *J Cell Biol,* 156**,** 349-59.

KUMAR, A., OUYANG, M., VAN DEN DRIES, K., MCGHEE, E. J., TANAKA, K., ANDERSON, M. D., GROISMAN, A., GOULT, B. T., ANDERSON, K. I. & SCHWARTZ, M. A. 2016. Talin

tension sensor reveals novel features of focal adhesion force transmission and mechanosensitivity. *The Journal of Cell Biology,* 213**,** 371-383.

KUMAR, A., ITO, A., HIROHAMA, M., YOSHIDA, M. & ZHANG, K. Y. J. 2013. Identification of Sumoylation Activating Enzyme 1 Inhibitors by Structure-Based Virtual Screening. *Journal of Chemical Information and Modeling,* 53**,** 809-820.

KUMAR, A., ITO, A., TAKEMOTO, M., YOSHIDA, M. & ZHANG, K. Y. J. 2014. Identification of 1,2,5-Oxadiazoles as a New Class of SENP2 Inhibitors Using Structure Based Virtual Screening. *Journal of Chemical Information and Modeling,* 54**,** 870-880.

KUSSIE, P. H., GORINA, S., MARECHAL, V., ELENBAAS, B., MOREAU, J., LEVINE, A. J. & PAVLETICH, N. P. 1996. Structure of the MDM2 Oncoprotein Bound to the p53 Tumor Suppressor Transactivation Domain. *Science,* 274**,** 948-953.

LALLEMAND-BREITENBACH, V., JEANNE, M., BENHENDA, S., NASR, R., LEI, M., PERES, L., ZHOU, J., ZHU, J., RAUGHT, B. & DE THE, H. 2008. Arsenic degrades PML or PML-RAR[alpha] through a SUMO-triggered RNF4/ubiquitin-mediated pathway. *Nat Cell Biol,* 10**,** 547-555.

LAMMERMANN, T., BADER, B. L., MONKLEY, S. J., WORBS, T., WEDLICH-SOLDNER, R., HIRSCH, K., KELLER, M., FORSTER, R., CRITCHLEY, D. R., FASSLER, R. & SIXT, M. 2008. Rapid leukocyte migration by integrin-independent flowing and squeezing. *Nature,* 453**,** 51-5.

LAO, M., ZHAN, Z., LI, N., XU, S., SHI, M., ZOU, Y., HUANG, M., ZENG, S., LIANG, L. & XU, H. 2019. Role of small ubiquitin-like modifier proteins-1 (SUMO-1) in regulating migration and invasion of fibroblast-like synoviocytes from patients with rheumatoid arthritis. *Experimental Cell Research,* 375**,** 52-61.

LAUFFENBURGER, D. A. & HORWITZ, A. F. 1996. Cell Migration: A Physically Integrated Molecular Process. *Cell,* 84**,** 359-369.

LAUKAITIS, C. M., WEBB, D. J., DONAIS, K. & HORWITZ, A. F. 2001. Differential dynamics of alpha 5 integrin, paxillin, and alpha-actinin during formation and disassembly of adhesions in migrating cells. *J Cell Biol,* 153**,** 1427-40.

LE, S., HU, X., YAO, M., CHEN, H., YU, M., XU, X., NAKAZAWA, N., MARGADANT, F. M., SHEETZ, M. P. & YAN, J. 2017. Mechanotransmission and Mechanosensing of Human alpha-Actinin 1. *Cell Reports,* 21**,** 2714-2723.

LEE, J.-S. & THORGEIRSSON, S. S. 2004. Genome-scale profiling of gene expression in hepatocellular carcinoma: Classification, survival prediction, and identification of therapeutic targets. *Gastroenterology,* 127**,** S51-S55.

LEE, H.-W., KYUNG, T., YOO, J., KIM, T., CHUNG, C., RYU, J. Y., LEE, H., PARK, K., LEE, S., JONES, W. D., LIM, D.-S., HYEON, C., DO HEO, W. & YOON, T.-Y. 2013. Real-time single-molecule co-immunoprecipitation analyses reveal cancer-specific Ras signalling dynamics. *Nature Communications,* 4**,** 1505.

LEGANT, W. R., MILLER, J. S., BLAKELY, B. L., COHEN, D. M., GENIN, G. M. & CHEN, C. S. 2010. Measurement of mechanical tractions exerted by cells in three-dimensional matrices. *Nature Methods,* 7**,** 969-971.

LEU, T. H. & MAA, M. C. 2002. Tyr-863 phosphorylation enhances focal adhesion kinase autophosphorylation at Tyr-397. *Oncogene,* 21**,** 6992-7000.

LI, H., NIU, H., PENG, Y., WANG, J. & HE, P. 2013a. Ubc9 promotes invasion and metastasis of lung cancer cells. *Oncol Rep,* 29**,** 1588-94.

LI, J., XU, Y., LONG, X. D., WANG, W., JIAO, H. K., MEI, Z., YIN, Q. Q., MA, L. N., ZHOU, A. W., WANG, L. S., YAO, M., XIA, Q. & CHEN, G. Q. 2014. Cbx4 governs HIF-1alpha to potentiate angiogenesis of hepatocellular carcinoma by its SUMO E3 ligase activity. *Cancer Cell,* 25**,** 118-31.

LI, R., WEI, J., JIANG, C., LIU, D., DENG, L., ZHANG, K. & WANG, P. 2013. Akt SUMOylation Regulates Cell Proliferation and Tumorigenesis. *Cancer Research,* 73**,** 5742-5753.

LI, Y. & YANG, D.-Q. 2010. The ATM Inhibitor KU-55933 Suppresses Cell Proliferation and Induces Apoptosis by Blocking Akt In Cancer Cells with Overactivated Akt. *Molecular Cancer Therapeutics,* 9**,** 113-125.

LIANG, Z., YANG, Y., HE, Y., YANG, P., WANG, X., HE, G., ZHANG, P., ZHU, H., XU, N., ZHAO, X. & LIANG, S. 2017. SUMOylation of IQGAP1 promotes the development of colorectal cancer. *Cancer Letters,* 411**,** 90-99.

LIU, J., ZHANG, D., LUO, W., YU, Y., YU, J., LI, J., ZHANG, X., ZHANG, B., CHEN, J., WU, X.-R., ROSAS-ACOSTA, G. & HUANG, C. 2011. X-linked Inhibitor of Apoptosis Protein (XIAP) Mediates Cancer Cell Motility via Rho GDP Dissociation Inhibitor (RhoGDI)-dependent Regulation of the Cytoskeleton. *Journal of Biological Chemistry,* 286**,** 15630-15640.

LIU, X., XU, Y., PANG, Z., GUO, F., QIN, Q., YIN, T., SANG, Y., FENG, C., LI, X., JIANG, L., SHU, P. & WANG, Y. 2015. Knockdown of SUMO-activating enzyme subunit 2 (SAE2) suppresses cancer malignancy and enhances chemotherapy sensitivity in small cell lung cancer. *Journal of hematology & oncology,* 8**,** 67-67.

LIU, S., CALDERWOOD, D. A. & GINSBERG, M. H. 2000. Integrin cytoplasmic domain-binding proteins. *J Cell Sci,* 113 (Pt 20)**,** 3563-71.

LOFTUS, L. T., GALA, R., YANG, T., JESSICK, V. J., ASHLEY, M. D., ORDONEZ, A., THOMPSON, S. J., SIMON, R. P. & MELLER, R. 2009. Sumo-2/3-ylation following in vitro modeled ischemia is reduced in delayed ischemic tolerance. *Brain research,* 1272**,** 71-80.

LOIS, L. M. & LIMA, C. D. 2005. Structures of the SUMO E1 provide mechanistic insights into SUMO activation and E2 recruitment to E1. *The EMBO Journal,* 24**,** 439-451.

LU, X., OLSEN, S. K., CAPILI, A. D., CISAR, J. S., LIMA, C. D. & TAN, D. S. 2010. Designed semisynthetic protein inhibitors of Ub/Ubl E1 activating enzymes. *J Am Chem Soc,* 132**,** 1748-9.

LOWE, S. W., CEPERO, E. & EVAN, G. 2004. Intrinsic tumour suppression. *Nature,* 432**,** 307-315.

MA, C., WU, B., HUANG, X., YUAN, Z., NONG, K., DONG, B., BAI, Y., ZHU, H., WANG, W. & AI, K. 2014. SUMO-specific protease 1 regulates pancreatic cancer cell proliferation and invasion by targeting MMP-9. *Tumor Biology,* 35**,** 12729-12735.

MADSEN, C. D. & SAHAI, E. 2010. Cancer dissemination--lessons from leukocytes. *Dev Cell,* 19**,** 13-26.

MAHAJAN, R., DELPHIN, C., GUAN, T., GERACE, L. & MELCHIOR, F. 1997. A small ubiquitin-related polypeptide involved in targeting RanGAP1 to nuclear pore complex protein RanBP2. *Cell,* 88**,** 97-107.

MANFREDI, J. J. 2010. The Mdm2-p53 relationship evolves: Mdm2 swings both ways as an oncogene and a tumor suppressor. *Genes & development,* 24**,** 1580-1589.

MANNING, B. D. & CANTLEY, L. C. 2007. AKT/PKB signaling: navigating downstream. *Cell,* 129**,** 1261-74.

MARQUES, I. J., WEISS, F. U., VLECKEN, D. H., NITSCHE, C., BAKKERS, J., LAGENDIJK, A. K., PARTECKE, L. I., HEIDECKE, C.-D., LERCH, M. M. & BAGOWSKI, C. P. 2009. Metastatic behaviour of primary human tumours in a zebrafish xenotransplantation model. *BMC Cancer,* 9**,** 128.

MARTIN, S., WILKINSON, K. A., NISHIMUNE, A. & HENLEY, J. M. 2007. Emerging extranuclear roles of protein SUMOylation in neuronal function and dysfunction. *Nature reviews. Neuroscience,* 8**,** 948-959.

MARTIN, K. H., SLACK, J. K., BOERNER, S. A., MARTIN, C. C. & PARSONS, J. T. 2002. Integrin connections map: to infinity and beyond. *Science,* 296**,** 1652-3.

MATIC, I., SCHIMMEL, J., HENDRIKS, I. A., VAN SANTEN, M. A., VAN DE RIJKE, F., VAN DAM, H., GNAD, F., MANN, M. & VERTEGAAL, A. C. O. 2010. Site-Specific Identification of SUMO-2 Targets in Cells Reveals an Inverted SUMOylation Motif and a Hydrophobic Cluster SUMOylation Motif. *Molecular Cell,* 39**,** 641-652.

MATIC, I., VAN HAGEN, M., SCHIMMEL, J., MACEK, B., OGG, S. C., TATHAM, M. H., HAY, R. T., LAMOND, A. I., MANN, M. & VERTEGAAL, A. C. 2008. In vivo identification of human small ubiquitin-like modifier polymerization sites by high accuracy mass spectrometry and an in vitro to in vivo strategy. *Mol Cell Proteomics,* 7**,** 132-44.

MATUNIS, M. J., COUTAVAS, E. & BLOBEL, G. 1996. A novel ubiquitin-like modification modulates the partitioning of the Ran-GTPase-activating protein RanGAP1 between the cytosol and the nuclear pore complex. *The Journal of cell biology,* 135**,** 1457-1470.

MCGREGOR, A., BLANCHARD, A. D., ROWE, A. J. & CRITCHLEY, D. R. 1994. Identification of the vinculin-binding site in the cytoskeletal protein alpha-actinin. *Biochem J,* 301 (Pt 1)**,** 225-33.

MCGUFFIN, L. J., ADIYAMAN, R., MAGHRABI, A. H. A., SHUID, A. N., BRACKENRIDGE, D. A., NEALON, J. O. & PHILOMINA, L. S. 2019. IntFOLD: an integrated web resource for high performance protein structure and function prediction. *Nucleic acids research,* 47**,** W408-W413.

MELUH, P. B. & KOSHLAND, D. 1995. Evidence that the MIF2 gene of Saccharomyces cerevisiae encodes a centromere protein with homology to the mammalian centromere protein CENP-C. *Mol Biol Cell,* 6**,** 793-807.

MERRILL, J. C., MELHUISH, T. A., KAGEY, M. H., YANG, S.-H., SHARROCKS, A. D. & WOTTON, D. 2010. A Role for Non-Covalent SUMO Interaction Motifs in Pc2/CBX4 E3 Activity. *PLoS ONE,* 5**,** e8794.

MINTY, A., DUMONT, X., KAGHAD, M. & CAPUT, D. 2000. Covalent Modification of p73α by SUMO-1: TWO-HYBRID SCREENING WITH p73 IDENTIFIES NOVEL SUMO-1-INTERACTING PROTEINS AND A SUMO-1 INTERACTION MOTIF. *Journal of Biological Chemistry,* 275**,** 36316-36323.

MITCHISON, T. J. & CRAMER, L. P. 1996. Actin-based cell motility and cell locomotion. *Cell,* 84**,** 371-9.

MITRA, S. K., HANSON, D. A. & SCHLAEPFER, D. D. 2005. Focal adhesion kinase: in command and control of cell motility. *Nat Rev Mol Cell Biol,* 6**,** 56-68.

MOORE, S. W., ROCA-CUSACHS, P. & SHEETZ, M. P. 2010. Stretchy proteins on stretchy substrates: the important elements of integrin-mediated rigidity sensing. *Dev Cell,* 19**,** 194-206.

MONTI, M., ORRU, S., PAGNOZZI, D. & PUCCI, P. 2005. Interaction proteomics. *Biosci Rep,* 25**,** 45-56.

MOREL, A.-P., LIÈVRE, M., THOMAS, C., HINKAL, G., ANSIEAU, S. & PUISIEUX, A. 2008. Generation of Breast Cancer Stem Cells through Epithelial-Mesenchymal Transition. *PLoS ONE,* 3**,** e2888.

MORITA, Y., KANEI-ISHII, C., NOMURA, T. & ISHII, S. 2005. TRAF7 Sequesters c-Myb to the Cytoplasm by Stimulating Its Sumoylation. *Molecular Biology of the Cell,* 16**,** 5433-5444.

MOSCHOS, S. J., SMITH, A. P., MANDIC, M., ATHANASSIOU, C., WATSON-HURST, K., JUKIC, D. M., EDINGTON, H. D., KIRKWOOD, J. M. & BECKER, D. 2007. SAGE and antibody array analysis of melanoma-infiltrated lymph nodes: identification of Ubc9 as an important molecule in advanced-stage melanomas. *Oncogene,* 26**,** 4216-4225.

MOSER, M., LEGATE, K. R., ZENT, R. & FÄSSLER, R. 2009. The Tail of Integrins, Talin, and Kindlins. *Science,* 324**,** 895-899.

MOULT, J., FIDELIS, K., KRYSHTAFOVYCH, A., SCHWEDE, T. & TRAMONTANO, A. 2016. Critical assessment of methods of protein structure prediction: Progress and new directions in round XI. *Proteins,* 84 Suppl 1**,** 4-14.

MUKHOPADHYAY, D. & DASSO, M. 2007. Modification in reverse: the SUMO proteases. *Trends Biochem Sci,* 32**,** 286-95.

MÜLLER, S., MATUNIS, M. J. & DEJEAN, A. 1998. Conjugation with the ubiquitin-related modifier SUMO-1 regulates the partitioning of PML within the nucleus. *The EMBO Journal,* 17**,** 61-70.

MÜLLER, S. M., GALLIARDT, H., SCHNEIDER, J., BARISAS, B. G. & SEIDEL, T. 2013. Quantification of Förster resonance energy transfer by monitoring sensitized emission in living plant cells. *Frontiers in plant science,* 4**,** 413-413.

NACERDDINE, K., LEHEMBRE, F., BHAUMIK, M., ARTUS, J., COHEN-TANNOUDJI, M., BABINET, C., PANDOLFI, P. P. & DEJEAN, A. 2005. The SUMO Pathway Is Essential for Nuclear Integrity and Chromosome Segregation in Mice. *Developmental Cell,* 9**,** 769-779.

NISHIDA, N., MIMORI, K., YOKOBORI, T., SUDO, T., TANAKA, F., SHIBATA, K., ISHII, H., DOKI, Y. & MORI, M. 2011. FOXC2 is a Novel Prognostic Factor in Human Esophageal Squamous Cell Carcinoma. *Annals of Surgical Oncology,* 18**,** 535-542.

NISHIDA, T., TANAKA, H. & YASUDA, H. 2000. A novel mammalian Smt3-specific isopeptidase 1 (SMT3IP1) localized in the nucleolus at interphase. *Eur J Biochem,* 267**,** 6423-7.

NOBES, C. D. & HALL, A. 1995. Rho, Rac, and Cdc42 GTPases regulate the assembly of multimolecular focal complexes associated with actin stress fibers, lamellipodia, and filopodia. *Cell,* 81**,** 53-62.

OKEGAWA, T., PONG, R. C., LI, Y. & HSIEH, J. T. 2004. The role of cell adhesion molecule in cancer progression and its application in cancer therapy. *Acta Biochim Pol,* 51**,** 445-57.

OKURA, T., GONG, L., KAMITANI, T., WADA, T., OKURA, I., WEI, C. F., CHANG, H. M. & YEH, E. T. 1996. Protection against Fas/APO-1- and tumor necrosis factor-mediated cell death by a novel protein, sentrin. *The Journal of Immunology,* 157**,** 4277-4281.

OLINER, J. D., PIETENPOL, J. A., THIAGALINGAM, S., GYURIS, J., KINZLER, K. W. & VOGELSTEIN, B. 1993. Oncoprotein MDM2 conceals the activation domain of tumour suppressor p53. *Nature,* 362**,** 857-860.

OLSEN, S. K., CAPILI, A. D., LU, X., TAN, D. S. & LIMA, C. D. 2010. Active site remodelling accompanies thioester bond formation in the SUMO E1. *Nature,* 463**,** 906-12.

OUYANG, J., GARNER, E., HALLET, A., NGUYEN, H. D., RICKMAN, K. A., GILL, G., SMOGORZEWSKA, A. & ZOU, L. 2015. Noncovalent interactions with SUMO and ubiquitin orchestrate distinct functions of the SLX4 complex in genome maintenance. *Mol Cell,* 57**,** 108-22.

PACKHAM, S., WARSITO, D., LIN, Y., SADI, S., KARLSSON, R., SEHAT, B. & LARSSON, O. 2015. Nuclear translocation of IGF-1R via p150Glued and an importin-β/RanBP2-dependent pathway in cancer cells. *Oncogene,* 34**,** 2227-2238.

PANSE, V. G., HARDELAND, U., WERNER, T., KUSTER, B. & HURT, E. 2004. A Proteome-wide Approach Identifies Sumoylated Substrate Proteins in Yeast. *Journal of Biological Chemistry,* 279**,** 41346-41351.

PARSONS, J. T., HORWITZ, A. R. & SCHWARTZ, M. A. 2010. Cell adhesion: integrating cytoskeletal dynamics and cellular tension. *Nat Rev Mol Cell Biol,* 11**,** 633-43.

PASAPERA, A. M., SCHNEIDER, I. C., RERICHA, E., SCHLAEPFER, D. D. & WATERMAN, C. M. 2010. Myosin II activity regulates vinculin recruitment to focal adhesions through FAK-mediated paxillin phosphorylation. *The Journal of Cell Biology,* 188**,** 877-890.

PATERSON, H. F., SELF, A. J., GARRETT, M. D., JUST, I., AKTORIES, K. & HALL, A. 1990. Microinjection of recombinant p21rho induces rapid changes in cell morphology. *The Journal of Cell Biology,* 111**,** 1001-1007.

PICHLER, A., GAST, A., SEELER, J. S., DEJEAN, A. & MELCHIOR, F. 2002. The Nucleoporin RanBP2 Has SUMO1 E3 Ligase Activity. *Cell,* 108**,** 109-120.

PICHLER, A., KNIPSCHEER, P., OBERHOFER, E., VAN DIJK, W. J., KORNER, R., OLSEN, J. V., JENTSCH, S., MELCHIOR, F. & SIXMA, T. K. 2005. SUMO modification of the ubiquitin-conjugating enzyme E2-25K. *Nat Struct Mol Biol,* 12**,** 264-9.

PICKART, C. M. 2001. Mechanisms underlying ubiquitination. *Annu Rev Biochem,* 70**,** 503-33.

PRICE, L. S., LANGESLAG, M., KLOOSTER, J. P. T., HORDIJK, P. L., JALINK, K. & COLLARD, J. G. 2003. Calcium Signaling Regulates Translocation and Activation of Rac. *Journal of Biological Chemistry,* 278**,** 39413-39421.

PRUDDEN, J., PEBERNARD, S., RAFFA, G., SLAVIN, D. A., PERRY, J. J. P., TAINER, J. A., MCGOWAN, C. H. & BODDY, M. N. 2007. SUMO-targeted ubiquitin ligases in genome stability. *The EMBO Journal,* 26**,** 4089-4101.

REN, Y. H., LIU, K. J., WANG, M., YU, Y. N., YANG, K., CHEN, Q., YU, B., WANG, W., LI, Q. W., WANG, J., HOU, Z. Y., FANG, J. Y., YEH, E. T., YANG, J. & YI, J. 2014. De-SUMOylation of FOXC2 by SENP3 promotes the epithelial-mesenchymal transition in gastric cancer cells. *Oncotarget,* 5**,** 7093-104.

REVERTER, D. & LIMA, C. D. 2006. Structural basis for SENP2 protease interactions with SUMO precursors and conjugated substrates. *Nat Struct Mol Biol,* 13**,** 1060-8.

RIDLEY, A. J. & HALL, A. 1992. The small GTP-binding protein rho regulates the assembly of focal adhesions and actin stress fibers in response to growth factors. *Cell,* 70**,** 389-399.

RODRIGUEZ, M. S., DARGEMONT, C. & HAY, R. T. 2001. SUMO-1 Conjugation in Vivo Requires Both a Consensus Modification Motif and Nuclear Targeting. *Journal of Biological Chemistry,* 276**,** 12654-12659.

ROSAS-ACOSTA, G., RUSSELL, W. K., DEYRIEUX, A., RUSSELL, D. H. & WILSON, V. G. 2005. A Universal Strategy for Proteomic Studies of SUMO and Other Ubiquitin-like Modifiers. *Molecular & Cellular Proteomics,* 4**,** 56-72.

ROSE, P. W., BI, C., BLUHM, W. F., CHRISTIE, C. H., DIMITROPOULOS, D., DUTTA, S., GREEN, R. K., GOODSELL, D. S., PRLIC, A., QUESADA, M., QUINN, G. B., RAMOS, A. G., WESTBROOK, J. D., YOUNG, J., ZARDECKI, C., BERMAN, H. M. & BOURNE, P. E. 2013. The RCSB Protein Data Bank: new resources for research and education. *Nucleic acids research,* 41**,** D475-D482.

ROTH, S. Y., DENU, J. M. & ALLIS, C. D. 2001. Histone acetyltransferases. *Annu Rev Biochem,* 70**,** 81-120.

SABEH, F., OTA, I., HOLMBECK, K., BIRKEDAL-HANSEN, H., SOLOWAY, P., BALBIN, M., LOPEZ-OTIN, C., SHAPIRO, S., INADA, M., KRANE, S., ALLEN, E., CHUNG, D. & WEISS, S. J. 2004. Tumor cell traffic through the extracellular matrix is controlled by the

membrane-anchored collagenase MT1-MMP. *The Journal of Cell Biology,* 167**,** 769-781.

SACHDEV, S., BRUHN, L., SIEBER, H., PICHLER, A., MELCHIOR, F. & GROSSCHEDL, R. 2001. PIASy, a nuclear matrix–associated SUMO E3 ligase, represses LEF1 activity by sequestration into nuclear bodies. *Genes & Development,* 15**,** 3088-3103.

SAHIN, U., DE THÉ, H. & LALLEMAND-BREITENBACH, V. 2014. PML nuclear bodies: assembly and oxidative stress-sensitive sumoylation. *Nucleus (Austin, Tex.),* 5**,** 499-507.

SAITOH, H. & HINCHEY, J. 2000. Functional heterogeneity of small ubiquitin-related protein modifiers SUMO-1 versus SUMO-2/3. *J Biol Chem,* 275**,** 6252-8.

SANTHAKUMAR, K., JUDSON, E. C., ELKS, P. M., MCKEE, S., ELWORTHY, S., VAN ROOIJEN, E., WALMSLEY, S. S., RENSHAW, S. A., CROSS, S. S. & VAN EEDEN, F. J. M. 2012. A Zebrafish Model to Study and Therapeutically Manipulate Hypoxia Signaling in Tumorigenesis. *Cancer Research,* 72**,** 4017-4027.

SAUNDERS, R. M., HOLT, M. R., JENNINGS, L., SUTTON, D. H., BARSUKOV, I. L., BOBKOV, A., LIDDINGTON, R. C., ADAMSON, E. A., DUNN, G. A. & CRITCHLEY, D. R. 2006. Role of vinculin in regulating focal adhesion turnover. *European Journal of Cell Biology,* 85**,** 487-500.

SCHALLER, M. D., HILDEBRAND, J. D. & PARSONS, J. T. 1999. Complex formation with focal adhesion kinase: A mechanism to regulate activity and subcellular localization of Src kinases. *Mol Biol Cell,* 10**,** 3489-505.

SCHMIDT, S. & FRIEDL, P. 2009. Interstitial cell migration: integrin-dependent and alternative adhesion mechanisms. *Cell and Tissue Research,* 339**,** 83.

SCHMIDT, D. & MÜLLER, S. 2002. Members of the PIAS family act as SUMO ligases for c-Jun and p53 and repress p53 activity. *Proceedings of the National Academy of Sciences,* 99**,** 2872-2877.

SCHULMAN, B. A. & HARPER, J. W. 2009. Ubiquitin-like protein activation by E1 enzymes: the apex for downstream signalling pathways. *Nature reviews. Molecular cell biology,* 10**,** 319-331.

SEELER, J.-S. & DEJEAN, A. 2017. SUMO and the robustness of cancer. *Nature Reviews Cancer,* 17**,** 184-197.

SEMENZA, G. L. 2003. Angiogenesis in ischemic and neoplastic disorders. *Annu Rev Med,* 54**,** 17-28.

SHANGARY, S., QIN, D., MCEACHERN, D., LIU, M., MILLER, R. S., QIU, S., NIKOLOVSKA-COLESKA, Z., DING, K., WANG, G., CHEN, J., BERNARD, D., ZHANG, J., LU, Y., GU, Q., SHAH, R. B., PIENTA, K. J., LING, X., KANG, S., GUO, M., SUN, Y., YANG, D. & WANG, S. 2008. Temporal activation of p53 by a specific MDM2 inhibitor is selectively toxic to tumors and leads to complete tumor growth inhibition. *Proceedings of the National Academy of Sciences,* 105**,** 3933-3938.

SHARMA, P., YAMADA, S., LUALDI, M., DASSO, M. & KUEHN, MICHAEL R. 2013. Senp1 Is Essential for Desumoylating Sumo1-Modified Proteins but Dispensable for Sumo2 and Sumo3 Deconjugation in the Mouse Embryo. *Cell Reports,* 3**,** 1640-1650.

SHAW, S. L. & EHRHARDT, D. W. 2013. Smaller, Faster, Brighter: Advances in Optical Imaging of Living Plant Cells. *Annual Review of Plant Biology,* 64**,** 351-375.

SHEN, H. J., ZHU, H. Y., YANG, C. & JI, F. 2012. SENP2 regulates hepatocellular carcinoma cell growth by modulating the stability of beta-catenin. *Asian Pac J Cancer Prev,* 13**,** 3583-7.

SHEN, L. N., DONG, C., LIU, H., NAISMITH, J. H. & HAY, R. T. 2006. The structure of SENP1–SUMO-2 complex suggests a structural basis for discrimination between SUMO paralogues during processing. *Biochemical Journal,* 397**,** 279-288.

SHEN, L. N., GEOFFROY, M. C., JAFFRAY, E. G. & HAY, R. T. 2009. Characterization of SENP7, a SUMO-2/3-specific isopeptidase. *Biochem J,* 421**,** 223-30.

SHEN, T. H., LIN, H.-K., SCAGLIONI, P. P., YUNG, T. M. & PANDOLFI, P. P. 2006. The mechanisms of PML-nuclear body formation. *Molecular cell,* 24**,** 331-339.

SHEN, Z., PARDINGTON-PURTYMUN, P. E., COMEAUX, J. C., MOYZIS, R. K. & CHEN, D. J. 1996. Associations of UBE2I with RAD52, UBL1, p53, and RAD51 Proteins in a Yeast Two-Hybrid System. *Genomics,* 37**,** 183-186.

SHIMA, H., SUZUKI, H., SUN, J., KONO, K., SHI, L., KINOMURA, A., HORIKOSHI, Y., IKURA, T., IKURA, M., KANAAR, R., IGARASHI, K., SAITOH, H., KURUMIZAKA, H. & TASHIRO, S. 2013. Activation of the SUMO modification system is required for the accumulation of RAD51 at sites of DNA damage. *Journal of Cell Science,* 126**,** 5284-5292.

SJÖBLOM, B., SALMAZO, A. & DJINOVIĆ-CARUGO, K. 2008. α-Actinin structure and regulation. *Cellular and Molecular Life Sciences,* 65**,** 2688.

SMITH, L. A., ARANDA-ESPINOZA, H., HAUN, J. B., DEMBO, M. & HAMMER, D. A. 2007. Neutrophil traction stresses are concentrated in the uropod during migration. *Biophys J,* 92**,** L58-60.

SOLDATI, T. & SCHLIWA, M. 2006. Powering membrane traffic in endocytosis and recycling. *Nature Reviews Molecular Cell Biology,* 7**,** 897-908.

SONG, J., DURRIN, L. K., WILKINSON, T. A., KRONTIRIS, T. G. & CHEN, Y. 2004. Identification of a SUMO-binding motif that recognizes SUMO-modified proteins. *Proceedings of the National Academy of Sciences of the United States of America,* 101**,** 14373-14378.

STEEG, P. S. 2016. Targeting metastasis. *Nature Reviews Cancer,* 16**,** 201-218.

STERNBERG, S. H., REDDING, S., JINEK, M., GREENE, E. C. & DOUDNA, J. A. 2014. DNA interrogation by the CRISPR RNA-guided endonuclease Cas9. *Nature,* 507**,** 62-67.

STOLETOV, K. & KLEMKE, R. 2008. Catch of the day: zebrafish as a human cancer model. *Oncogene,* 27**,** 4509-4520.

STOSSEL, T. P. 1993. On the crawling of animal cells. *Science,* 260**,** 1086-94.

SUBRAMANIAM, S., SIXT, K. M., BARROW, R. & SNYDER, S. H. 2009. Rhes, a Striatal Specific Protein, Mediates Mutant-Huntingtin Cytotoxicity. *Science,* 324**,** 1327-1330.

SUGDEN, PETER H., MCGUFFIN, LIAM J. & CLERK, A. 2013. SOcK, MiSTs, MASK and STicKs: the GCKIII (germinal centre kinase III) kinases and their heterologous protein–protein interactions. *Biochemical Journal,* 454**,** 13-30.

SUN, H., LEVERSON, J. D. & HUNTER, T. 2007. Conserved function of RNF4 family proteins in eukaryotes: targeting a ubiquitin ligase to SUMOylated proteins. *The EMBO Journal,* 26**,** 4102-4112.

SUNG, M.-K., LIM, G., YI, D.-G., CHANG, Y. J., YANG, E. B., LEE, K. & HUH, W.-K. 2013. Genome-wide bimolecular fluorescence complementation analysis of SUMO interactome in yeast. *Genome Research,* 23**,** 736-746.

SUZAWA, M., MIRANDA, D. A., RAMOS, K. A., ANG, K. K. H., FAIVRE, E. J., WILSON, C. G., CABONI, L., ARKIN, M. R., KIM, Y.-S., FLETTERICK, R. J., DIAZ, A., SCHNEEKLOTH, J. S. & INGRAHAM, H. A. 2015. A gene-expression screen identifies a non-toxic sumoylation inhibitor that mimics SUMO-less human LRH-1 in liver. *eLife,* 4**,** e09003.

TAKADA, Y., YE, X. & SIMON, S. 2007. The integrins. *Genome Biol,* 8**,** 215.

TAKAHASHI, K., ROCHFORD, C. D. P. & NEUMANN, H. 2005. Clearance of apoptotic neurons without inflammation by microglial triggering receptor expressed on myeloid cells-2. *The Journal of experimental medicine,* 201**,** 647-657.

TAKEMOTO, M., KAWAMURA, Y., HIROHAMA, M., YAMAGUCHI, Y., HANDA, H., SAITOH, H., NAKAO, Y., KAWADA, M., KHALID, K., KOSHINO, H., KIMURA, K.-I., ITO, A. & YOSHIDA, M. 2014. Inhibition of protein SUMOylation by davidiin, an ellagitannin from Davidia involucrata. *The Journal of Antibiotics,* 67**,** 335-338.

TAN, J. L., TIEN, J., PIRONE, D. M., GRAY, D. S., BHADRIRAJU, K. & CHEN, C. S. 2003. Cells lying on a bed of microneedles: an approach to isolate mechanical force. *Proceedings of the National Academy of Sciences of the United States of America,* 100**,** 1484-1489.

TAN, M. Y., MU, X. Y., LIU, B., WANG, Y., BAO, E. D., QIU, J. X. & FAN, Y. 2013. SUMO-specific protease 2 suppresses cell migration and invasion through inhibiting the expression of MMP13 in bladder cancer cells. *Cell Physiol Biochem,* 32**,** 542-8.

TAN, M., GONG, H., WANG, J., TAO, L., XU, D., BAO, E., LIU, Z. & QIU, J. 2015. SENP2 regulates MMP13 expression in a bladder cancer cell line through SUMOylation of TBL1/TBLR1. *Scientific reports,* 5**,** 13996-13996.

TANG, X., ZHENG, X., QI, Y., ZHANG, D., CHENG, Y., TANG, A., VOYTAS, D. F. & ZHANG, Y. 2016. A Single Transcript CRISPR-Cas9 System for Efficient Genome Editing in Plants. *Mol Plant,* 9**,** 1088-91.

TATHAM, M. H., GEOFFROY, M.-C., SHEN, L., PLECHANOVOVA, A., HATTERSLEY, N., JAFFRAY, E. G., PALVIMO, J. J. & HAY, R. T. 2008. RNF4 is a poly-SUMO-specific E3 ubiquitin ligase required for arsenic-induced PML degradation. *Nat Cell Biol,* 10**,** 538-546.

TENG, Y., XIE, X., WALKER, S., WHITE, D. T., MUMM, J. S. & COWELL, J. K. 2013. Evaluating human cancer cell metastasis in zebrafish. *BMC cancer,* 13**,** 453-453.

TOMASI, M. L., TOMASI, I., RAMANI, K., PASCALE, R. M., XU, J., GIORDANO, P., MATO, J. M. & LU, S. C. 2012. S-adenosyl methionine regulates ubiquitin-conjugating enzyme 9 protein expression and sumoylation in murine liver and human cancers. *Hepatology (Baltimore, Md.),* 56**,** 982-993.

TRAVER, D., PAW, B. H., POSS, K. D., PENBERTHY, W. T., LIN, S. & ZON, L. I. 2003. Transplantation and in vivo imaging of multilineage engraftment in zebrafish bloodless mutants. *Nature Immunology,* 4**,** 1238-1246.

TAM, W. L. & WEINBERG, R. A. 2013. The epigenetics of epithelial-mesenchymal plasticity in cancer. *Nat Med,* 19**,** 1438-49.

TAN, M., GONG, H., WANG, J., TAO, L., XU, D., BAO, E., LIU, Z. & QIU, J. 2015. SENP2 regulates MMP13 expression in a bladder cancer cell line through SUMOylation of TBL1/TBLR1. *Scientific reports,* 5**,** 13996-13996.

TAN, M. Y., MU, X. Y., LIU, B., WANG, Y., BAO, E. D., QIU, J. X. & FAN, Y. 2013. SUMO-specific protease 2 suppresses cell migration and invasion through inhibiting the expression of MMP13 in bladder cancer cells. *Cell Physiol Biochem,* 32**,** 542-8.

TANAKA, K., NISHIDE, J., OKAZAKI, K., KATO, H., NIWA, O., NAKAGAWA, T., MATSUDA, H., KAWAMUKAI, M. & MURAKAMI, Y. 1999. Characterization of a fission yeast SUMO-1 homologue, pmt3p, required for multiple nuclear events, including the control of telomere length and chromosome segregation. *Mol Cell Biol,* 19**,** 8660-72.

TANG, Z., HECKER, C. M., SCHESCHONKA, A. & BETZ, H. 2008. Protein interactions in the sumoylation cascade: lessons from X-ray structures. *FEBS J,* 275**,** 3003-15.

TATHAM, M. H., JAFFRAY, E., VAUGHAN, O. A., DESTERRO, J. M., BOTTING, C. H., NAISMITH, J. H. & HAY, R. T. 2001. Polymeric chains of SUMO-2 and SUMO-3 are conjugated to protein substrates by SAE1/SAE2 and Ubc9. *J Biol Chem,* 276**,** 35368-74.

THIERY, J. P. 2002. Epithelial-mesenchymal transitions in tumour progression. *Nat Rev Cancer,* 2**,** 442-54.

TOZLUOGLU, M., KARACA, E., NUSSINOV, R. & HALILOGLU, T. 2010. A mechanistic view of the role of E3 in sumoylation. *PLoS Comput Biol,* 6.

TOSSIDOU, I., HIMMELSEHER, E., TENG, B., HALLER, H. & SCHIFFER, M. 2014. SUMOylation determines turnover and localization of nephrin at the plasma membrane. *Kidney Int,* 86**,** 1161-73.

ULRICH, H. D. 2005. Mutual interactions between the SUMO and ubiquitin systems: a plea of no contest. *Trends in Cell Biology,* 15**,** 525-532.

UZUNOVA, K., GÖTTSCHE, K., MITEVA, M., WEISSHAAR, S. R., GLANEMANN, C., SCHNELLHARDT, M., NIESSEN, M., SCHEEL, H., HOFMANN, K., JOHNSON, E. S., PRAEFCKE, G. J. K. & DOHMEN, R. J. 2007. Ubiquitin-dependent Proteolytic Control of SUMO Conjugates. *Journal of Biological Chemistry,* 282**,** 34167-34175.

VALIRON, O., CAUDRON, N. & JOB, D. 2001. Microtubule dynamics. *Cellular and Molecular Life Sciences CMLS,* 58**,** 2069-2084.

VAN DER FLIER, A. & SONNENBERG, A. 2001. Function and interactions of integrins. *Cell and Tissue Research,* 305**,** 285-298.

VAUGHAN, R. B. & TRINKAUS, J. P. 1966. Movements of epithelial cell sheets in vitro. *J Cell Sci,* 1**,** 407-13.

WANG, L., WANSLEEBEN, C., ZHAO, S., MIAO, P., PASCHEN, W. & YANG, W. 2014. SUMO2 is essential while SUMO3 is dispensable for mouse embryonic development. *EMBO Reports,* 15**,** 878-885.

WANG, Q., XIA, N., LI, T., XU, Y., ZOU, Y., ZUO, Y., FAN, Q., BAWA-KHALFE, T., YEH, E. T. & CHENG, J. 2013. SUMO-specific protease 1 promotes prostate cancer progression and metastasis. *Oncogene,* 32**,** 2493-8.

WANG, Y. & DASSO, M. 2009. SUMOylation and deSUMOylation at a glance. *Journal of Cell Science,* 122**,** 4249-4252.

WEBB, D. J., DONAIS, K., WHITMORE, L. A., THOMAS, S. M., TURNER, C. E., PARSONS, J. T. & HORWITZ, A. F. 2004. FAK-Src signalling through paxillin, ERK and MLCK regulates adhesion disassembly. *Nat Cell Biol,* 6**,** 154-161.

WEBB, D. J., WEBB, D. J., PARSONS, J. T. & HORWITZ, A. F. 2002. Adhesion assembly, disassembly and turnover in migrating cells - Over and over and over again. *Nature cell biology,* 4**,** E97-E100.

WEI, W., YANG, P., PANG, J., ZHANG, S., WANG, Y., WANG, M. H., DONG, Z., SHE, J. X. & WANG, C. Y. 2008. A stress-dependent SUMO4 sumoylation of its substrate proteins. *Biochem Biophys Res Commun,* 375**,** 454-9.

WERNER, A., FLOTHO, A. & MELCHIOR, F. 2012. The RanBP2/RanGAP1∗SUMO1/Ubc9 Complex Is a Multisubunit SUMO E3 Ligase. *Molecular Cell,* 46**,** 287-298.

WHITTAKER, C. A., BERGERON, K. F., WHITTLE, J., BRANDHORST, B. P., BURKE, R. D. & HYNES, R. O. 2006. The echinoderm adhesome. *Dev Biol,* 300**,** 252-66.

WILKINSON, K. A. & HENLEY, J. M. 2010. Mechanisms, regulation and consequences of protein SUMOylation. *Biochem J,* 428**,** 133-45.

WOLF, K. & FRIEDL, P. 2011. Extracellular matrix determinants of proteolytic and non-proteolytic cell migration. *Trends Cell Biol,* 21**,** 736-44.

WOLF, K., MAZO, I., LEUNG, H., ENGELKE, K., VON ANDRIAN, U. H., DERYUGINA, E. I., STRONGIN, A. Y., BROCKER, E. B. & FRIEDL, P. 2003. Compensation mechanism in tumor cell migration: mesenchymal-amoeboid transition after blocking of pericellular proteolysis. *J Cell Biol,* 160**,** 267-77.

WOOD, C. K., TURNER, C. E., JACKSON, P. & CRITCHLEY, D. R. 1994. Characterisation of the paxillin-binding site and the C-terminal focal adhesion targeting sequence in vinculin. *Journal of Cell Science,* 107**,** 709-717.

WU, J., LEI, H., ZHANG, J., CHEN, X., TANG, C., WANG, W., XU, H., XIAO, W., GU, W. & WU, Y. 2016. Momordin Ic, a new natural SENP1 inhibitor, inhibits prostate cancer cell proliferation. *Oncotarget,* 7**,** 58995-59005.

WYCKOFF, J. B., PINNER, S. E., GSCHMEISSNER, S., CONDEELIS, J. S. & SAHAI, E. 2006. ROCK- and myosin-dependent matrix deformation enables protease-independent tumor-cell invasion in vivo. *Curr Biol,* 16**,** 1515-23.

XIAO, Y., POLLACK, D., ANDRUSIER, M., LEVY, A., CALLAWAY, M., NIEVES, E., REDDI, P. & VIGODNER, M. 2016. Identification of cell-specific targets of sumoylation during mouse spermatogenesis. *Reproduction (Cambridge, England),* 151**,** 149-166.

XING, Z., CHEN, H. C., NOWLEN, J. K., TAYLOR, S. J., SHALLOWAY, D. & GUAN, J. L. 1994. Direct interaction of v-Src with the focal adhesion kinase mediated by the Src SH2 domain. *Mol Biol Cell,* 5**,** 413-21.

XU, J., HE, Y., QIANG, B., YUAN, J., PENG, X. & PAN, X. M. 2008. A novel method for high accuracy sumoylation site prediction from protein sequences. *BMC Bioinformatics,* 9**,** 8.

XU, J., SUN, H.-Y., XIAO, F.-J., WANG, H., YANG, Y., WANG, L., GAO, C.-J., GUO, Z.-K., WU, C.-T. & WANG, L.-S. 2015. SENP1 inhibition induces apoptosis and growth arrest of multiple myeloma cells through modulation of NF-κB signaling. *Biochemical and Biophysical Research Communications,* 460**,** 409-415.

XU, Y., LI, J., ZUO, Y., DENG, J., WANG, L. S. & CHEN, G. Q. 2011. SUMO-specific protease 1 regulates the in vitro and in vivo growth of colon cancer cells with the upregulated expression of CDK inhibitors. *Cancer Lett,* 309**,** 78-84.

XUE, Y., ZHOU, F., FU, C., XU, Y. & YAO, X. 2006. SUMOsp: a web server for sumoylation site prediction. *Nucleic Acids Research,* 34**,** W254-W257.

YANG, S.-H., GALANIS, A., WITTY, J. & SHARROCKS, A. D. 2006. An extended consensus motif enhances the specificity of substrate modification by SUMO. *The EMBO Journal,* 25**,** 5083-5093.

YANG, W., SHENG, H., WARNER, D. S. & PASCHEN, W. 2008. Transient global cerebral ischemia induces a massive increase in protein sumoylation. *J Cereb Blood Flow Metab,* 28**,** 269-79.

YANG, Y., HE, Y., WANG, X., LIANG, Z., HE, G., ZHANG, P., ZHU, H., XU, N. & LIANG, S. 2017. Protein SUMOylation modification and its associations with disease. *Open biology,* 7**,** 170167.

YANG, Y., XIA, Z., WANG, X., ZHAO, X., SHENG, Z., YE, Y., HE, G., ZHOU, L., ZHU, H., XU, N. & LIANG, S. 2018. Small-Molecule Inhibitors Targeting Protein SUMOylation as Novel Anticancer Compounds. *Mol Pharmacol,* 94**,** 885-894.

YEH, E. T. 2009. SUMOylation and De-SUMOylation: wrestling with life's processes. *J Biol Chem,* 284**,** 8223-7.

YU, J., ZHANG, D., LIU, J., LI, J., YU, Y., WU, X.-R. & HUANG, C. 2012. RhoGDI SUMOylation at Lys-138 Increases Its Binding Activity to Rho GTPase and Its Inhibiting Cancer Cell Motility. *Journal of Biological Chemistry,* 287**,** 13752-13760.

YU, Y. H., CHEN, H. A., CHEN, P. S., CHENG, Y. J., HSU, W. H., CHANG, Y. W., CHEN, Y. H., JAN, Y., HSIAO, M., CHANG, T. Y., LIU, Y. H., JENG, Y. M., WU, C. H., HUANG, M. T., SU, Y. H., HUNG, M. C., CHIEN, M. H., CHEN, C. Y., KUO, M. L. & SU, J. L. 2013. MiR-520h-mediated FOXC2 regulation is critical for inhibition of lung cancer progression by resveratrol. *Oncogene,* 32**,** 431-443.

ZHANG, H., SAITOH, H. & MATUNIS, M. J. 2002. Enzymes of the SUMO modification pathway localize to filaments of the nuclear pore complex. *Mol Cell Biol,* 22**,** 6498-508.

ZHANG, J., HUANG, F.-F., WU, D.-S., LI, W.-J., ZHAN, H.-E., PENG, M.-Y., FANG, P., CAO, P.-F., ZHANG, M.-M., ZENG, H. & CHEN, F.-P. 2015. SUMOylation of insulin-like growth factor 1 receptor, promotes proliferation in acute myeloid leukemia. *Cancer Letters,* 357**,** 297-306.

ZHAO, Q., XIE, Y., ZHENG, Y., JIANG, S., LIU, W., MU, W., LIU, Z., ZHAO, Y., XUE, Y. & REN, J. 2014. GPS-SUMO: a tool for the prediction of sumoylation sites and SUMO-interaction motifs. *Nucleic Acids Research,* 42**,** W325-W330.

ZHAO, X. & BLOBEL, G. 2005. A SUMO ligase is part of a nuclear multiprotein complex that affects DNA repair and chromosomal organization. *Proceedings of the National Academy of Sciences of the United States of America,* 102**,** 4777-4782.

ZHAO, Y., WANG, Z., ZHANG, J. & ZHOU, H. 2016. Identification of SENP1 inhibitors through in silico screening and rational drug design. *European Journal of Medicinal Chemistry,* 122**,** 178-184.

ZHU, J., ZHU, S., GUZZO, C. M., ELLIS, N. A., SUNG, K. S., CHOI, C. Y. & MATUNIS, M. J. 2008. Small Ubiquitin-related Modifier (SUMO) Binding Determines Substrate Recognition and Paralog-selective SUMO Modification. *Journal of Biological Chemistry,* 283**,** 29405-29415.

ZIEGLER, W. H., LIDDINGTON, R. C. & CRITCHLEY, D. R. 2006. The structure and regulation of vinculin. *Trends Cell Biol,* 16**,** 453-60.

ZIEGLER, WOLFGANG H., GINGRAS, ALEX R., CRITCHLEY, DAVID R. & EMSLEY, J. 2008. Integrin connections to the cytoskeleton through talin and vinculin. *Biochemical Society Transactions,* 36**,** 235-239.

ZLOTKOWSKI, K., HEWITT, W. M., SINNIAH, R. S., TROPEA, J. E., NEEDLE, D., LOUNTOS, G. T., BARCHI, J. J., JR., WAUGH, D. S. & SCHNEEKLOTH, J. S., JR. 2017. A Small-Molecule Microarray Approach for the Identification of E2 Enzyme Inhibitors in Ubiquitin-Like Conjugation Pathways. *SLAS discovery : advancing life sciences R & D,* 22**,** 760-766.

ZUBIETE-FRANCO, I., GARCÍA-RODRÍGUEZ, J. L., LOPITZ-OTSOA, F., SERRANO-MACIA, M., SIMON, J., FERNÁNDEZ-TUSSY, P., BARBIER-TORRES, L., FERNÁNDEZ-RAMOS, D., GUTIÉRREZ-DE-JUAN, V., LÓPEZ DE DAVALILLO, S., CARLEVARIS, O., BEGUIRISTAIN GÓMEZ, A., VILLA, E., CALVISI, D., MARTÍN, C., BERRA, E., ASPICHUETA, P., BERAZA,

N., VARELA-REY, M., ÁVILA, M., RODRÍGUEZ, M. S., MATO, J. M., DÍAZ-MORENO, I., DÍAZ-QUINTANA, A., DELGADO, T. C. & MARTÍNEZ-CHANTAR, M. L. 2019. SUMOylation regulates LKB1 localization and its oncogenic activity in liver cancer. *EBioMedicine,* 40**,** 406-421.